ON THE DETAILED FLOW STRUCTURE AND THE CORRESPONDING DAMAGE TO TEST SPECIMENS IN A CAVITATING VENTURI

Marion John Robinson

A dissertation submitted in partial fulfillment
of the requirements for the degree of
Doctor of Philosophy in the
University of Michigan
1965

Doctoral Committee:
Professor Frederick G. Hammitt, Chairman
Associate Professor William P. Graebel
Associate Professor Terry Kammash
Professor William Kerr
Professor Clarence A. Siebert
Professor George L. West

ACKNOWLEDGMENTS

The author would like to acknowledge the financial support of The National Aeronautics and Space Administration under Grant NsG-39-60 which provided the bulk of the equipment for this work.

The guidance and assistance of Professor F. G. Hammitt during the term of this investigation is gratefully appreciated.

The loan of the Linear Proficorder by the manufacturer, Micrometrical Division, The Bendix Corporation of Ann Arbor, to the University, and the cooperation of the Mechanical Engineering Department and Professor L. V. Colwell during its use is gratefully appreciated.

Also, many thanks are due the numerous fellow candidates and research assistants who worked on this grant for their valuable assistance and helpful suggestions.

Finally, thanks are due my wonderful wife, Sonja, for the beneficial environment which she created during the period during which this dissertation was conducted.

TABLE OF CONTENTS

LIST OF TABLES

LIST OF FIGURES

Figure

Page

Figure Page

Figure Page

Figure Page

Figure Page

NOMENCLATURE

A	Area
AcI, AcImp	Acoustic impedance
Al (2)*	Aluminum
As Rec'd	As received (material condition, 60% cold-worked)
BHN	Brinell hardness
CbZr (CbZr)*	Columbium-1% zirconium
cn (cn)*	Copper-nickel alloy
cs (1)*	Carbon steel
cu (cu)*	Copper
cz (cz)*	Copper-zinc alloy (brass)
D, d	Diameter
E	Elastic modulus
El, %El	Percent elongation
ESE	Engineering strain energy
F	Degrees Fahrenheit
fps	Feet per second
g	Conversion unit
Hi. Ht. Trt.	Highest heat treatment or annealing temperature
l	Length
L. Ht. Trt.	Lowest heat treatment or annealing temperature

MDP	Mean depth of penetration
MHD	Magnetohydrodynamic
Mo-1/2Ti (E)*	Molybedenum and titanium alloy
ni (ni)*	Nickel
p	Pressure
P	Load or force
ppm	Parts per million
pps	Pictures per second
%RA	Percent reduction of area
SS (ss)*	Stainless steel
STP	Standard temperature and pressure
t	Subscript denoting values at venturi throat
Ta-10w (A)*	Tantalum and tungsten alloy
Ta-8w-2Hf (B)*	Tantalum, tungsten and hafnium alloy
TBS	True breaking stress
TS	Tensile strength
TSE	True strain energy
V	Velocity, volume
v	Subscript denoting vapor properties, velocity
YS	Yield strength
ε_t	True strain
ρ	Density
σ_c	Cavitation number
σ_t	True stress

*Symbols and numbers in brackets indicate designation stamped on test specimens for material identification.

CHAPTER I

INTRODUCTION AND LITERATURE SURVEY

A. Introduction

For the past two hundred years, the phenomenon of cavitation has been known and the accompanying losses of component performance and the material damage done to the cavitating fluid enclosure or liner has been of considerable importance to the furtherance of scientific and technological progress in the fluid machinery field for approximately sixty-five years. This phenomenon has been the subject of numerous investigations and contributions to a partial understanding of this phenomenon have been made by many people. However, controversies and disagreement as to the actual basic mechanisms of damage which are inflicted by the cavitating flow regime still exist at this time and probably will for some time into the future. Comparatively little is known even today about the prediction of damage by a cavitating flow regime other than in a few specific and simplified systems that have been carefully investigated.

In the earliest considerations of the cavitation phenomenon the primary fluid of importance was water, as this was the basic fluid used in fluid machinery until recent times. At the present, however, liquid metals, cryogenics, organics and other fluids have come into prime

consideration as working fluids, in heat transfer systems, various process systems, as working fluids in thermodynamic cycles, etc. With the advent of liquid metals as heat transfer fluids for nuclear reactor power plants, and as working fluids in various power generating plants especially, at present, those for space vehicles, the prediction of cavitation performance and damage in a variety of fluid-material environments and at various temperatures becomes of great importance. The high developmental costs for the component machinery, and the difficult handling problems encountered with liquid metals, makes the full scale component testing and the materials-screening programs, which have had to be used in many cases, highly undesirable and very costly. In addition, the desire to design very high-performance components, as for space vehicle power plants, requires that the fluid handling components utilize higher velocity flows and minimum suppression heads so that they may have to operate under some degree of cavitation to obtain optimum weight to power performance. In addition, long unattended life is desired for many such units. Thus it becomes increasingly more important to define precisely the method of attack of the cavitation flow regime and to determine those physical and mechanical properties of materials which are important in resisting attack. Once this goal is accomplished it will be possible to intelligently choose and/or develop materials for these purposes, and permit more aggressive and still reliable designs to be made. The current investigation sheds more light on the basic damage mechanisms and helps in determining a relationship between measurable mechanical properties of materials,

and their resistance to cavitation damage in a variety of fluids. In order to gain some constructive insight into the complex damage mechanisms of cavitating flow, it is necessary that the laboratory test conditions match as closely as possible the actual operating conditions of fluid-handling machines. However, certain compromises become necessary for reasons such as budgetary requirements, flexibility for the handling of multiple and differing test specimens, ability to handle different test fluids under differing conditions of velocity, temperature, pressure, gas content, etc., and to obtain reproducible results which are susceptible to analysis, both in terms of knowledge of the flow regime and of the test materials properties. With these requirements in mind the closed loop cavitating venturi test section facility was selected for the present investigation. This system lends itself well to the requirements of multiple test specimen insertion, temperature and velocity variation and control, susceptibility of results to careful analysis, and very close similarity to flow-induced cavitation in actual field equipment.

B. Summary Review of Cavitation Literature

The concept of cavitation was first postulated by Leonhard Euler in 1754 in his theory on hydraulic turbines.[1] However, the major early analyses of importance were those by Rayleigh[2] and Besant.[3] Shortly thereafter the accompanying loss of component performances and the destructive action of cavitation were discovered by many of other early investigators of fluid handling machinery such as with propellors,[4,5] and turbines.[6] In the 1930's, the laboratory testing of

materials for their resistance to cavitation damage came into wide use and several different means of such testing were developed. Schroeter,[7] in 1932, used a constricted-tube type of water tunnel to produce cavitation, the extent and intensity of which could be controlled, and made to occur in a region where a test specimen could be inserted. Gaines,[8] in 1932, and Kerr,[9] in 1937, first used the vibratory method of cavitation testing. Other investigators have used devices as a high velocity liquid jet impinging on multiple test specimens mounted on a rotating disk* (Hobbs),[10] and a rotating disk with through-holes which is rotated in a chamber of fluid to produce cavitation on the disk downstream of the holes (Rasmussen).[11]

To the present time, each of the above-mentioned laboratory tests has received considerable attention from several investigators in the cavitation field and there are several current materials-screening programs underway throughout the world.

With the advent of cavitation damage testing in the laboratory and the resulting interpretation of results in order to rank materials as to their relative resistance to cavitation damage, many investigators postulated the physical properties of materials of significance in their susceptibility to cavitation damage. Schroeter[7] presented a correlation of his data with Brinell Hardness and other early investigators, such as Boetcher,[12] and Mousson,[13] postulated surface hardening

---

*It has long been known that the damage caused by an impinging jet resembled cavitation damage, but only recently has the connection become reasonably clear.

effects, fatigue failures (due to the pounding of the surface with many impacts from the collapsing bubbles), and showed results of slip lines in the material surfaces resulting from the cavitation action. Since then, many investigators have put forward their results in terms of a correlation with a single mechanical property of the materials tested. The list of investigators in this category is too lengthy to list. Several of these have shown correlations with hardness, yield strength and tensile strength.

The actual mode of the material attack by the cavitation flow regime has also been the subject of numerous hypotheses. Classically, it has been assumed that shock waves from bubble implosions impinge on adjacent solid structures.[14,etc.] Under ideal fluid assumptions, in an incompressible fluid with an empty bubble, and assuming spherical symmetry, infinitely high pressures at the mathematical point of bubble collapse can result. Recent theoretical studies by Hickling and Plesset,[41] and by Ivany,[42] in our own laboratory, throw doubt on the likelihood of this mechanism in that it was shown in both cases that if the bubble collapse center remains stationary (which of ccurse it would not in detail, being perturbed by the nearness of the solid member to be damaged), the pressures applied to the wall would in general not reach damaging magnitudes. Damaging pressures could be created, however, by bubble rebounds, which have been observed by Ivany[42] and others. More recently, evidence of the possible importance of non-spherical collapses resulting in a central liquid jet which impacts on the material has accrued. This mode of collapse was first suggested by

deHaller and Ackeret,[15] and Suverov.[16] Recent evidence to support its significance has been furnished by Naude and Ellis,[17] Shutler and Mesler,[18] and Benjamin and Ellis.[19]

Fatigue failure due to the repeated exposure to forces resulting from either of the already discussed mechanisms has been proposed by many investigators.[9,11,13,15,20,21,22,23,24,25,26,28,etc.] Direct failure due to the imposition of sufficiently high forces from either of the above mechanisms has been postulated by many[17,18,19,26,28,etc.] (undoubtedly, both fatigue and cratering failure occur in most real cases to differing extents, depending on the intensity of the cavitation).

Since corrosion is often present with cavitation, the interrelation has been discussed by many, assuming that the combined action creates damage more readily than either separately.[27,28,29,30,31,etc.]

Other less probable theories have also been advanced in the past as chemical disassociation of the liquid producing very reactive fluid corrosion, etc.[32]

The above impressive list of possible mechanisms is an indication of the very complex nature of the cavitation phenomena and serves to illustrate that an attempt to understand the mechanism of attack must include an attempt to isolate the particular mechanism which is under investigation, although this cannot be done rigorously, or completely, in any system.

C. Material Selection Criterion

In light of the above-mentioned modes of attack and in view of the high emphasis of earlier work on the mechanical aspect of the cavitation damage, most of the materials for the present investigation have been chosen for the following reasons:

1. Low susceptibility to chemical attack (corrosion) in the fluid environment in which they are to be tested.
2. Wide range of mechanical properties so that the existence of a possible material properties correlation could be tested.
3. Flexibility of the material state (i.e., ability to be cold-worked) so that the same material could be examined in different states, i.e., several materials were tested in three different heat treatment states so that variations on grain size, mechanical properties as strain energy, tensile strength, etc. could be examined on the same material.

Since in the very early stages of the investigation it was noted that the available materials mechanical property data in manufacturers' handbooks, engineering handbooks, etc. gave wide variations (order of ± 25%) in the reported properties for supposedly the same alloys and materials, a program was initiated to measure the applicable mechanical properties of the particular materials used from the same piece of stock from which the test specimens for the analysis were to be made and at the actual test temperature. This has been done in all but a very few cases where sufficient material was not available. The results of the complete material property tests are reported in detail elsewhere,[39] and the pertinent data only are reproduced herein.

D. Flow Regime Investigation

The investigation of the cavitating flow behavior and the resulting damage was conducted in three main phases. First, the effects of small changes in degree of cavitation, velocity, pressure, specimen orientation to flow, etc., on the final results were examined. Then, high-speed movies of the flow and an electrical probe technique, to be described later, were utilized to obtain detailed information on the actual flow pattern existing, and thus to help interpret the observed damage. Also envisioned was the determination of a bubble size spectrum to be compared with the subsequent pit size spectrum on the test specimens. The final phase consisted of constant duration cavitation damage tests on many different materials with the flow, temperature and gas content and other cavitation parameters kept the same. In all cases, more than one specimen of a material was tested for statistical interpretation of the data. The specimens so exposed were examined in detail, as described later.

CHAPTER II

EXPERIMENTAL APPARATUS AND PROCEDURES

The two venturi test facilities used in the present investigation have been described in complete detail in an earlier report.[33] However, the pertinent equipment and modifications utilized in this investigation will be summarized below for convenience.

A. Water Test Facility

This facility is a multiple-venturi closed-loop system with a maximum capability of four test venturis in a parallel combination. It includes equipment for deaerating and purifying the water, and has been designed for operation with a minimum of operator attention. The maximum venturi throat velocity obtainable is slightly in excess of 200 feet per second. Figure 1 is a schematic drawing of this facility, and Figures 2 and 3 respectively are photographs of the facility and of a venturi test section. The general operational procedure for testing specimens in this facility was to run three such venturis in parallel with three specimens in each venturi so that nine specimens were tested at one time, under identical flow conditions.

B. Mercury Test Facility

This facility is a single-venturi closed-loop system which was operated with mercury at room temperature for this particular

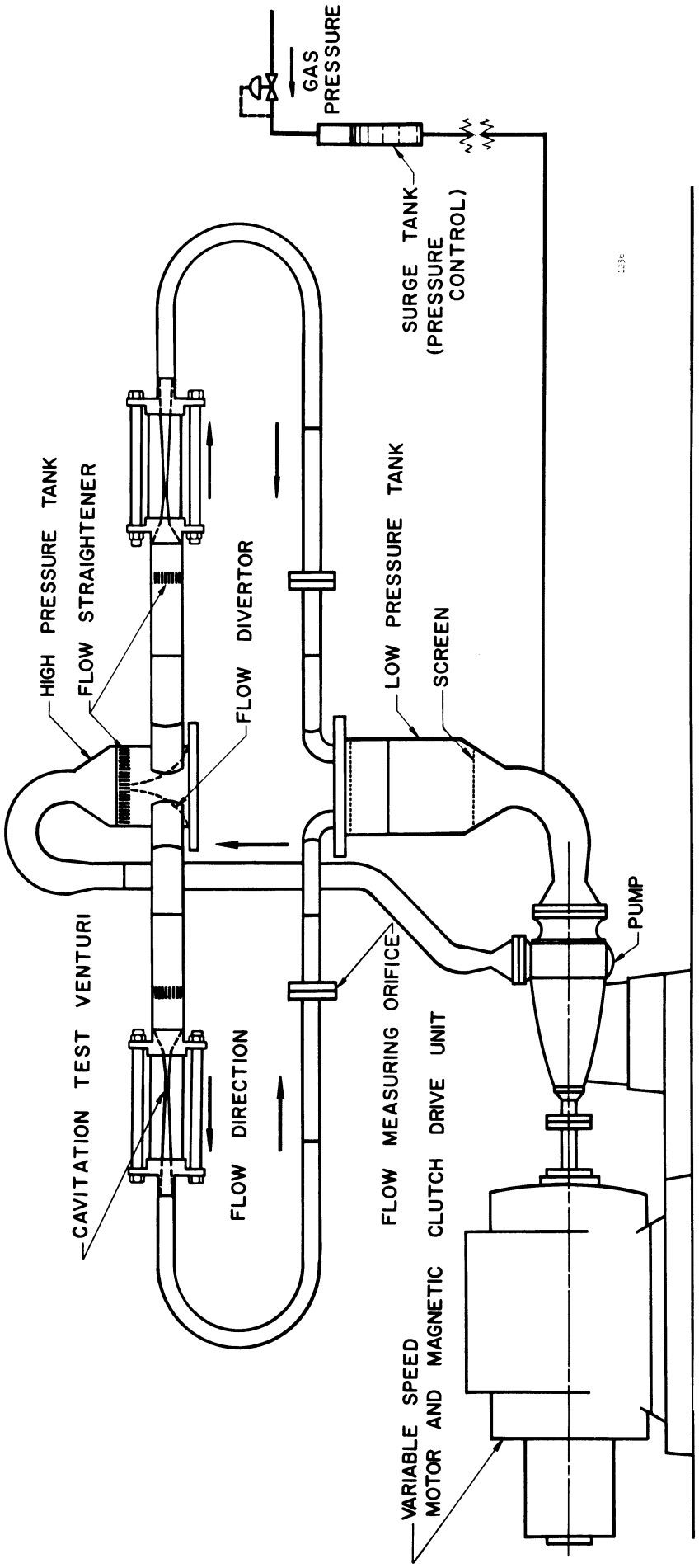

Fig. 1.--Schematic of water cavitation damage facility (only two of the four loops are shown).

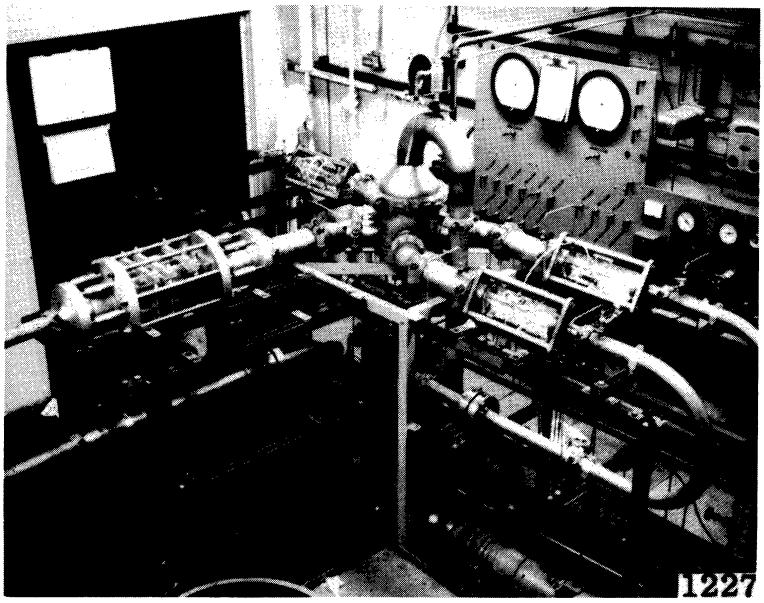

Fig. 2.--Photograph of water cavitation damage, closed loop, venturi facility.

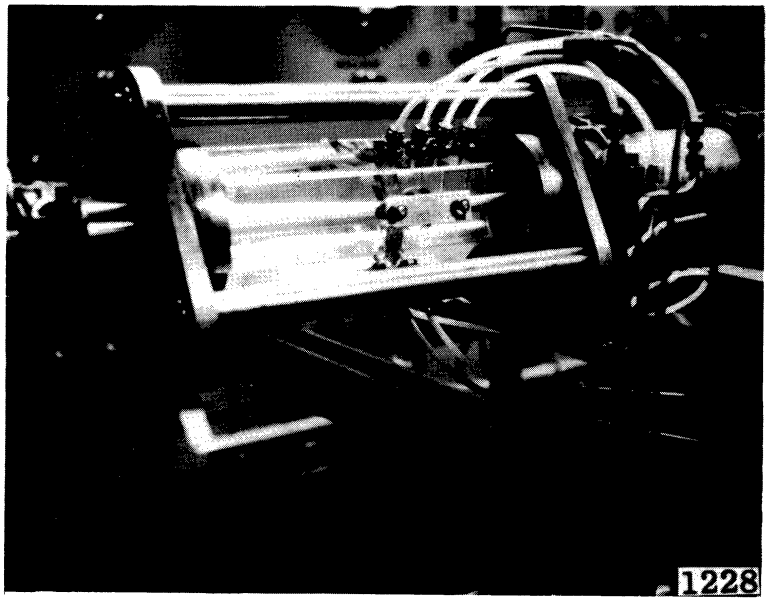

Fig. 3.--Photograph of a typical plexiglas test venturi installed in the water loop.

investigation. For the general damage correlation two specimens were run at the same time, and of the same material. The effects of specimen insertion geometry, and number of test specimens in a single venturi were also studied in this venturi, to be described later. A schematic drawing of the facility is shown in Figure 4, and a photograph which includes the heater section for higher temperature operation (not included in the present study), is shown in Figure 5. In this photograph the top half of the heater sections have been removed to facilitate the viewing of the loop components.

C. Test Specimens

The damage test specimens are thin flat plates with tapered ends. The nominal dimensions are 1/16" wide by 5/8" high by 3/4" long. They are inserted into the walls of the diffuser portion of the venturi with suitable specimen holders so that the longest dimension is parallel to the fluid flow and only about 0.200" of the test specimen height is submerged in the fluid. Figure 6 (a) is a schematic drawing of a typical specimen.

D. Damage Test Venturis

All of the cavitation damage tests have been conducted in venturis with identical flow paths, although the number and respective orientation of the test specimen insertion has been varied. The nominal flow path dimensions are shown in Figure 6, along with the variations of venturi-specimen geometry. All of the damage tests in the water facility were conducted in a venturi arrangement as Figure 6 (c), the venturi

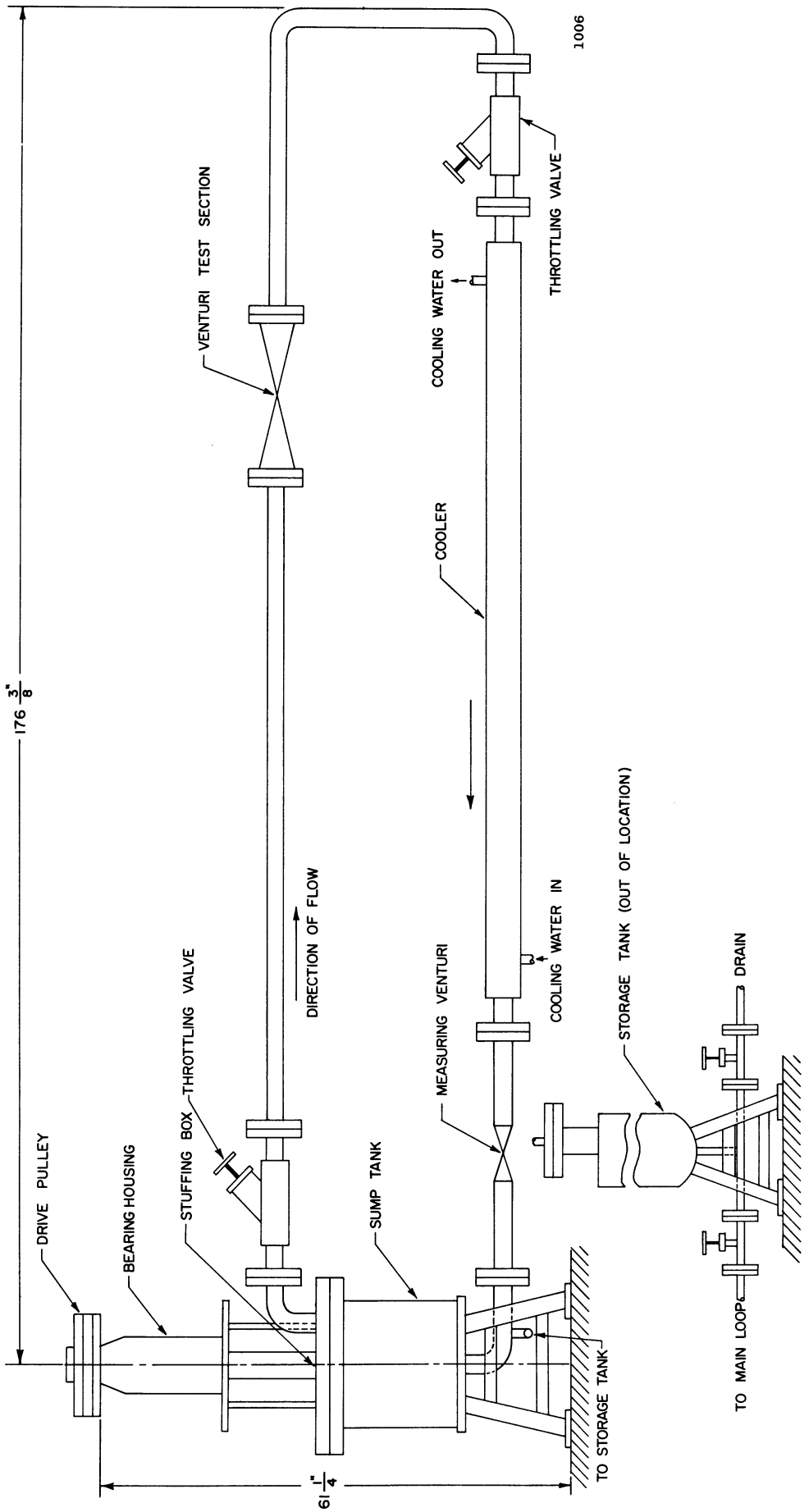

Fig. 4.--Schematic drawing of overall mercury facility layout.

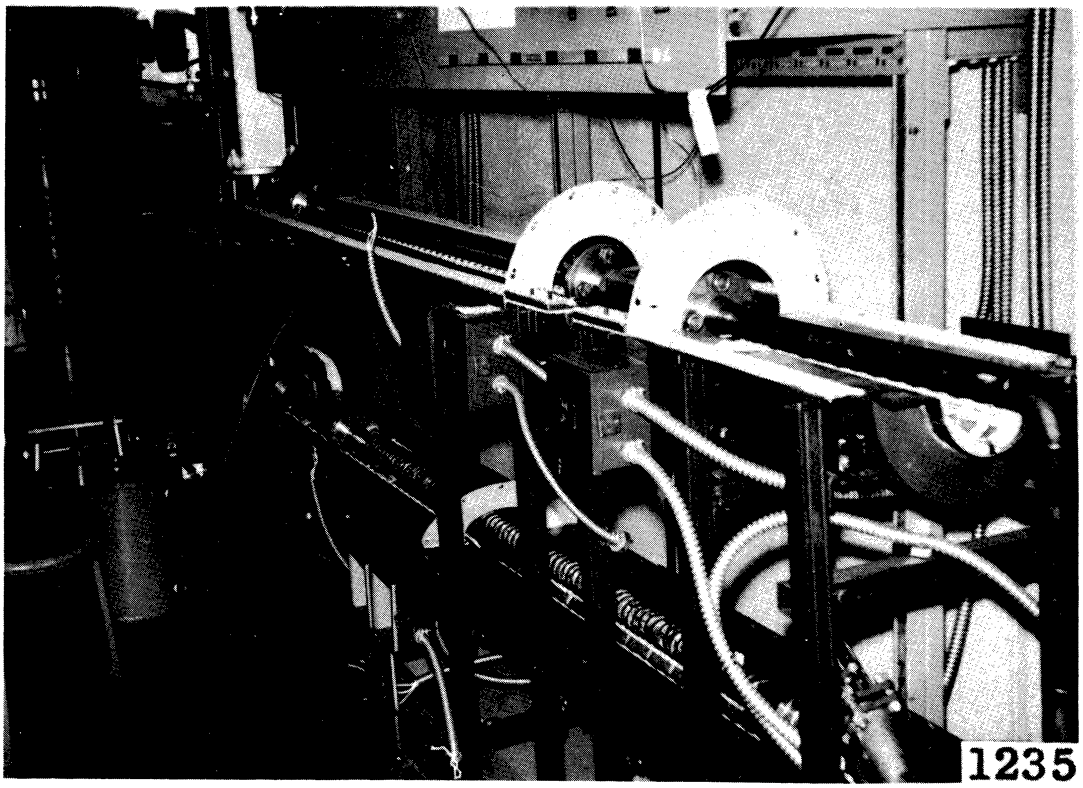

Fig. 5.--Photograph of mercury facility with top half of heater sections removed.

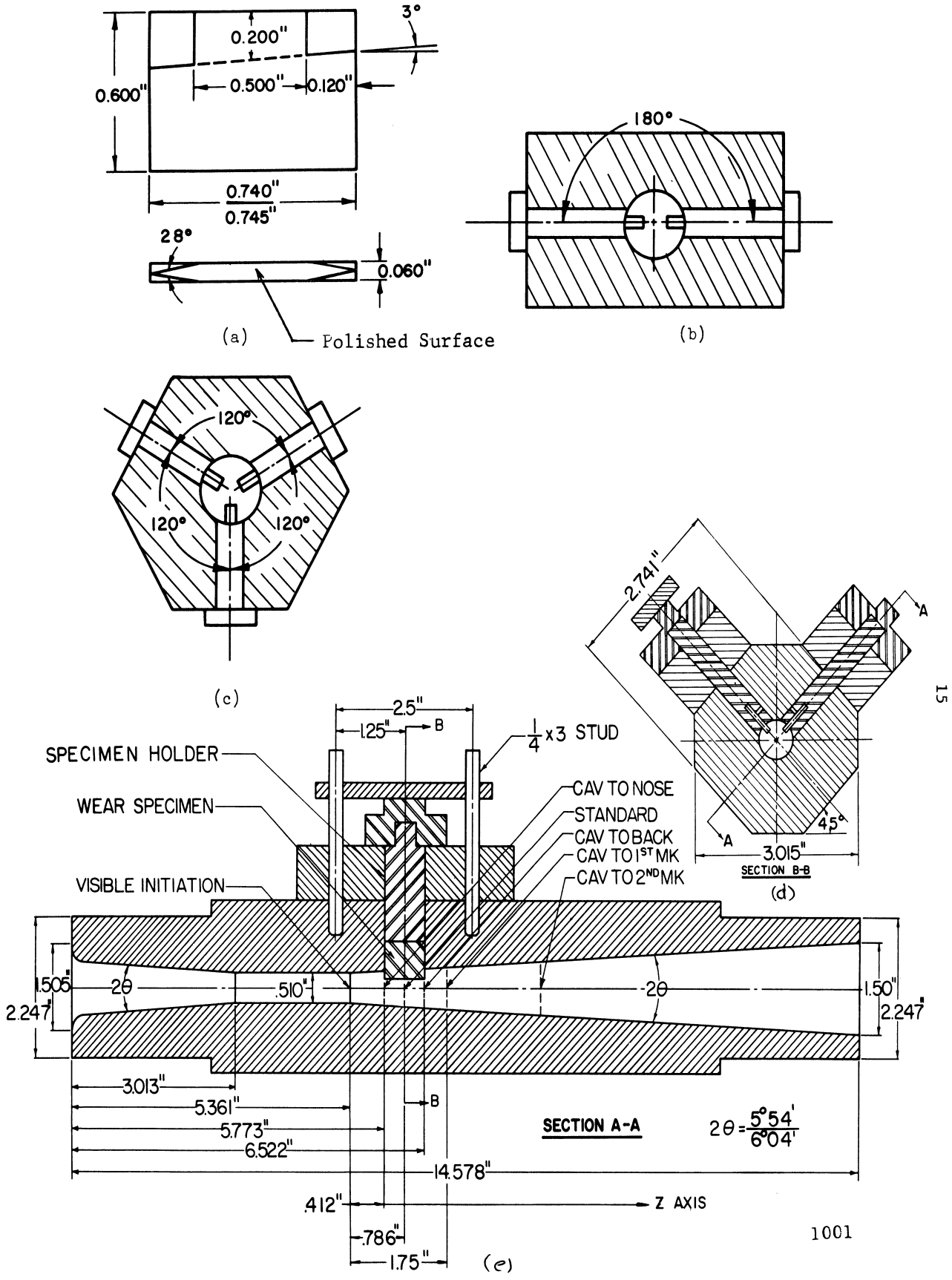

Fig. 6.--Schematic drawing of the damage test venturis showing nominal flow passage, axial specimen location, cavitation termination points, and (a) test specimen dimensions, (b) two specimen symmetrical arrangement for mercury, (c) three specimen symmetrical arrangement for water, (d) two specimen unsymmetrical arrangement for earlier mercury tests.

being constructed from plexiglas, while all of the damage tests in the mercury facility were conducted in a stainless steel venturi as shown in Figure 6 (b). Comparisons of damage between venturi arrangements (b) and (d) were made in mercury and between (c) and (d) in water in order to be able to observe the specimen orientation effect and thus be able to compare the mercury and water results. It would have been preferable to use identical venturis and test specimen geometries throughout. However, cost and time limitations did not permit the fabrication of the required numbers of venturis (with the differing end attachments required for the two loops), so that existing equipment was used. Arrangements (b) and (c) have a symmetrical flow path with specimens inserted, and arrangement (d) is nonsymmetrical.

E. Associated Experimental Apparatus and Techniques

1. Pressure Profile Measurements

A special pressure tapped venturi was modified to enable use in either of the two closed-loop facilities described earlier in this report. It is essentially identical to the damage venturis in the water loop although the ends were turned down to fit the mercury loop venturi holders and special adaptors then made to enable use again in the water loop. A schematic drawing of this venturi is shown in Figure 7, indicating the location of the pressure tap points, a typical pressure tap dimension and the possible specimen insertion ports. The flow path dimensions are identical to the ones used for the damage studies. Figure 8 is a schematic drawing of the special plexiglas specimen-holder

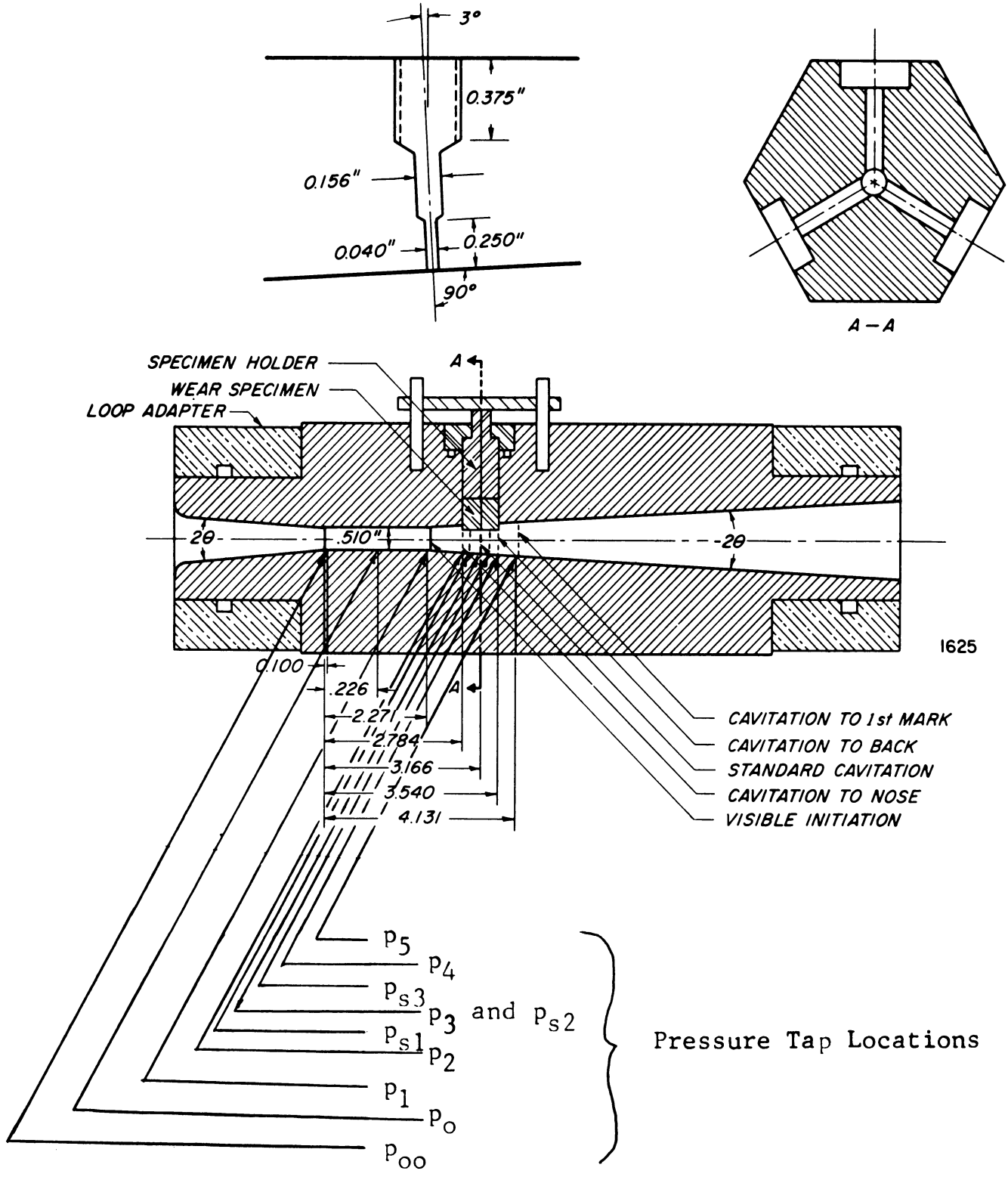

Fig. 7.--Cross section schematic drawing of damage venturi as modified for pressure profile measurements.

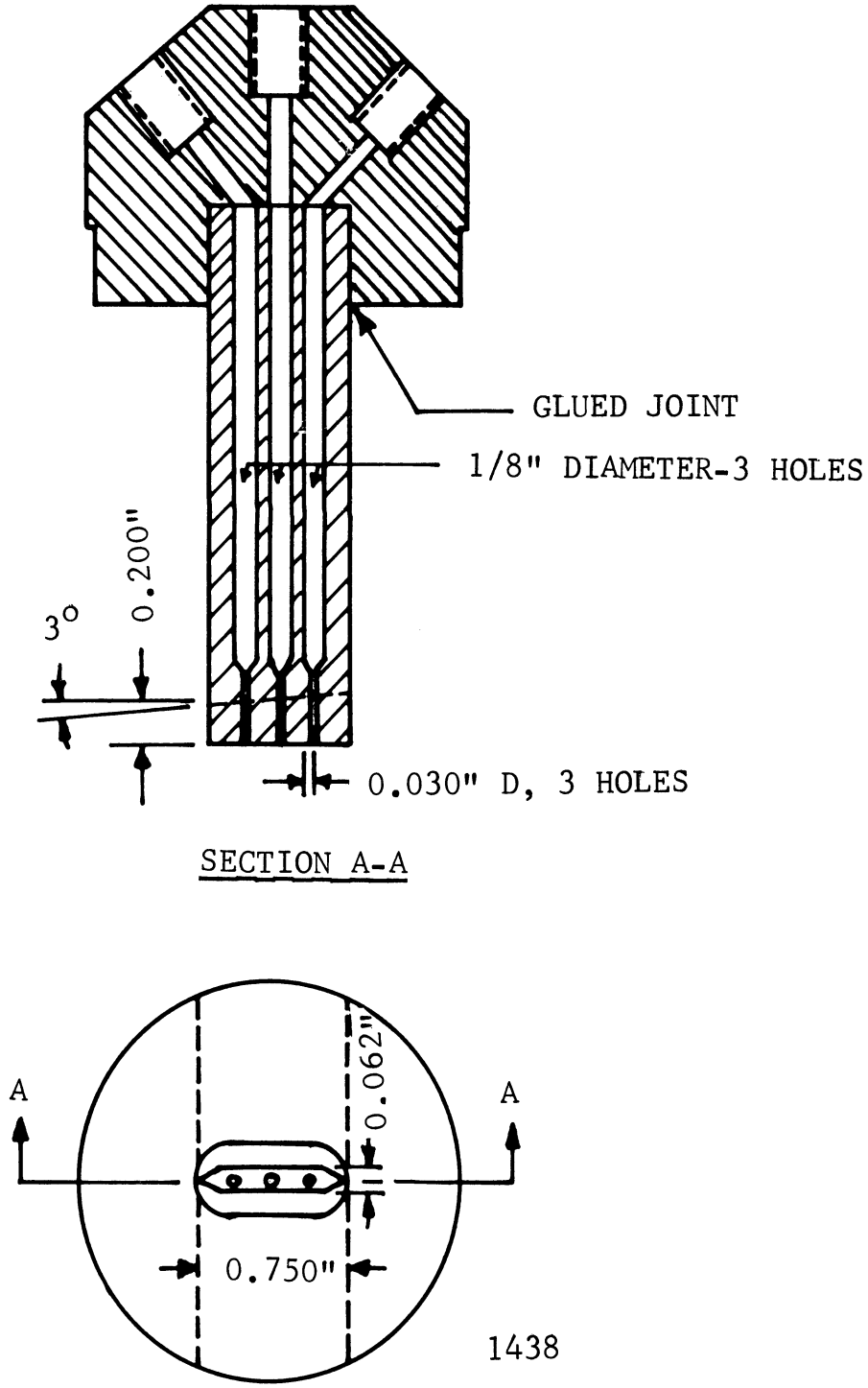

Fig. 8.--Schematic drawing of plexiglas specimen-holder combination for measuring pressures on specimen face.

combination used to measure the actual pressures existing on the test specimen polished surface in conjunction with the axial pressure profile measurements. There are three pressure taps located on the polished surface, symmetrically located in an axial direction. With this system it was possible to utilize either one, two or three specimen insertion geometries by filling the other ports with flush inserts. Also, it was possible to visually observe the cavitation cloud on the surface between the pressure taps in order to verify the methods used for setting the degree of cavitation (extent of cavitating cloud). A photograph of this apparatus is shown in Figure 9.

2. High-Speed Photography

Due to the opacity of the mercury it is impossible to observe the flow around the cavitation damage test specimens as can be done in the water loop. However, the mercury provides an advantage in that any activity observed in an opaque fluid through a transparent wall must be occurring adjacent to that wall, whereas in water, a transparent fluid, the precise location of an event is not so easily established. Hence, a device was designed and fabricated to allow viewing of the polished surface (labelled in Figure 6) of a transparent test specimen through the specimen, i.e., from the back. This device is a specimen and holder combination of plexiglas, suitably polished, so that the underside of the surface of the test specimen can be viewed through the plexiglas holder (Figure 10). The plexiglas test specimen polished surface to mercury interface (Figure 6 [a]) can be viewed quite clearly, and in fact all of the high-speed movies have been taken through a device of

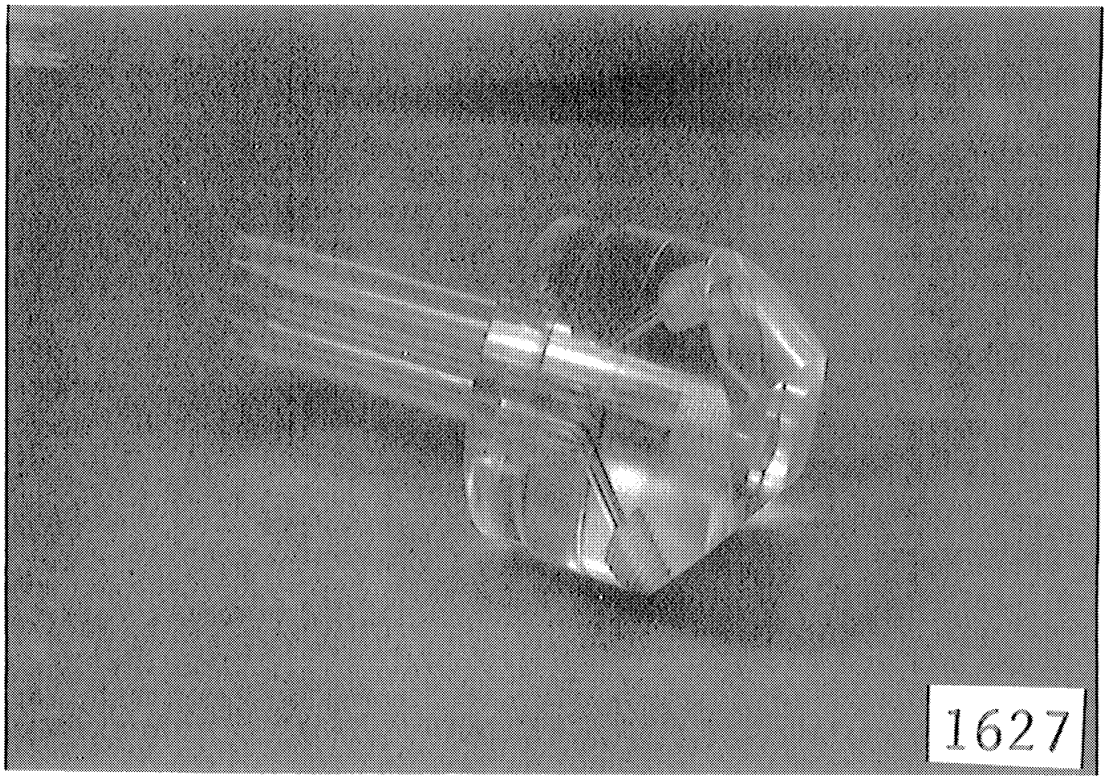

Fig. 9.- Photograph of plexiglas specimen-holder combination for pressure measurements.

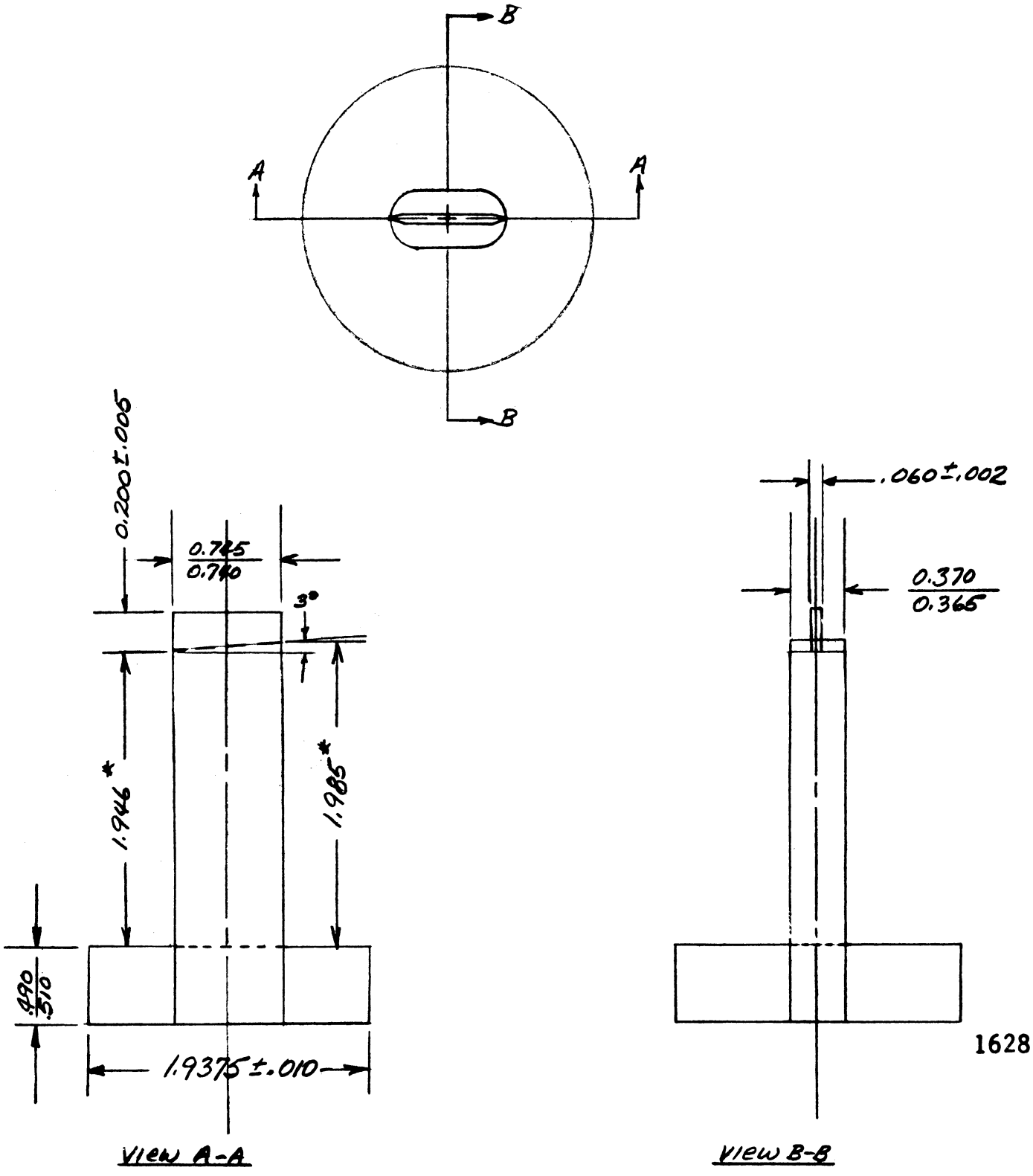

Fig. 10.--Schematic drawing of transparent specimen-holder combination for high-speed photography.

this kind. The first feasibility model was not contoured to match the inside tapered curvature of the venturi. After the photographic technique was demonstrated, however, a subsequent model, contoured to match the inside surface of the venturi, was constructed. It was necessary to use two pieces, glued together. After many trials, this was accomplished with no loss of clarity to the view. After a time in the cavitating mercury field, mercury penetrated the glued interface so that a replacement unit was necessary. Special adaptors were required to seal the unit into place in all three types of venturis (water test venturis and mercury, plexiglas and stainless steel, test venturis). Figure 11 shows the adaptors and the transparent test specimen. Figure 11 (c) shows a grid of lines on paper at the location which would ordinarily constitute the mercury-test specimen interface, serving to illustrate the clarity of the view obtained and the field of view for the pictures in the following sections.

Figure 12 (a) is a photograph of the plexiglas venturi with both of the special plexiglas specimen-holder combinations installed. In this manner it was possible to record the pressures on the surface, the extent of the cavitating cloud (degree of cavitation), and the high-speed movies simultaneously. In Figure 12 (b) is the same photograph with the Fastax camera, camera control unit, flash holder and pressure measuring manifold in place. A 1:1 image to actual view was obtained with this set-up. Any further enlargement of the image was prevented by the camera lens to subject distance required to allow the direction of sufficient light onto the mercury-specimen interface.

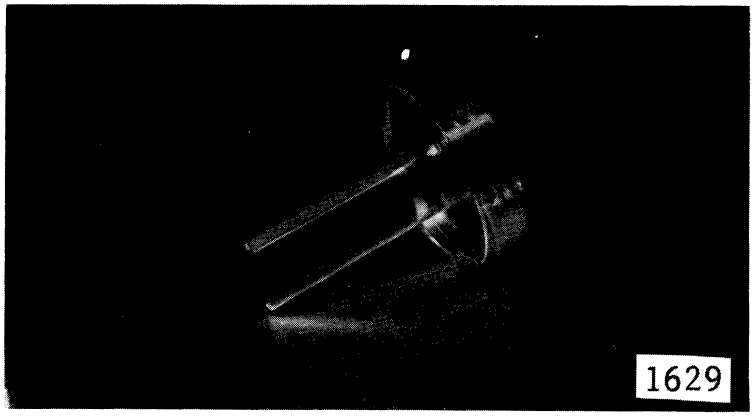

(a)

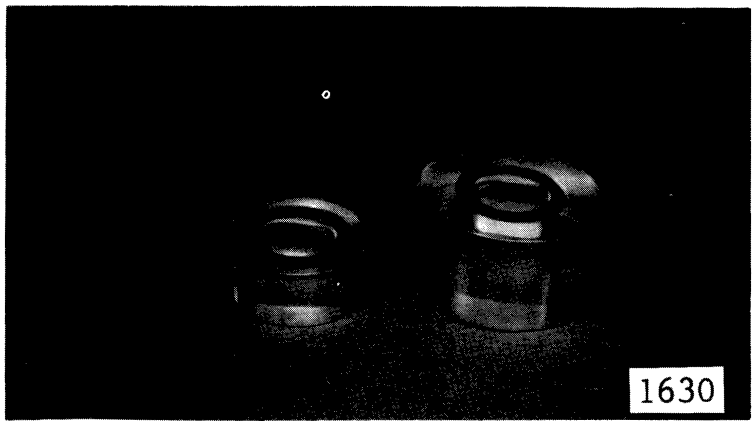

(b)

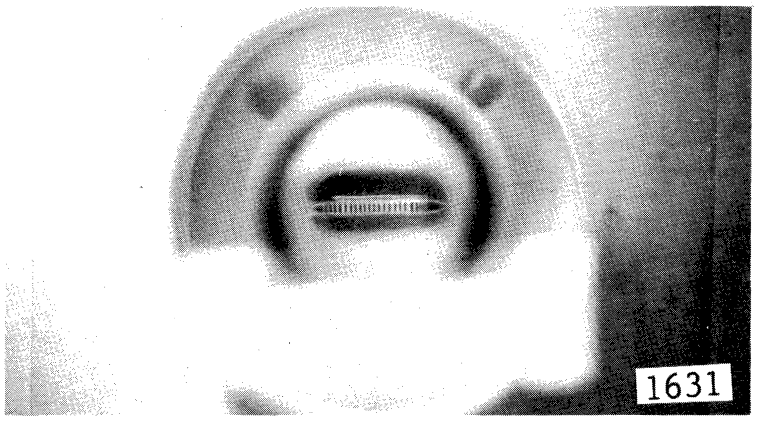

(c)

Fig. 11.--(a) Photograph of the transparent photographic specimen-holder combination, (b) adaptors for different venturis, (c) view through this unit illustrating view obtained in high-speed motion pictures.

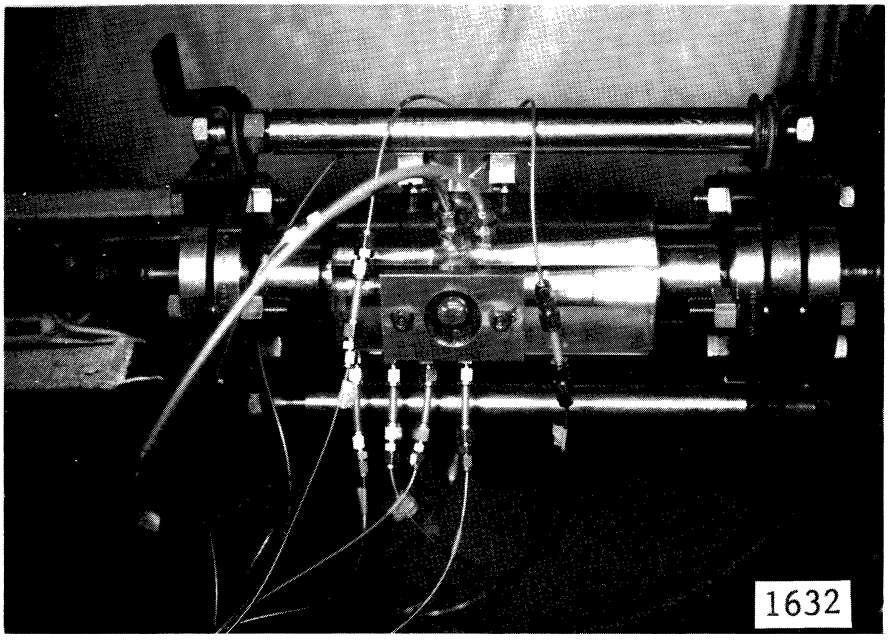

(a)

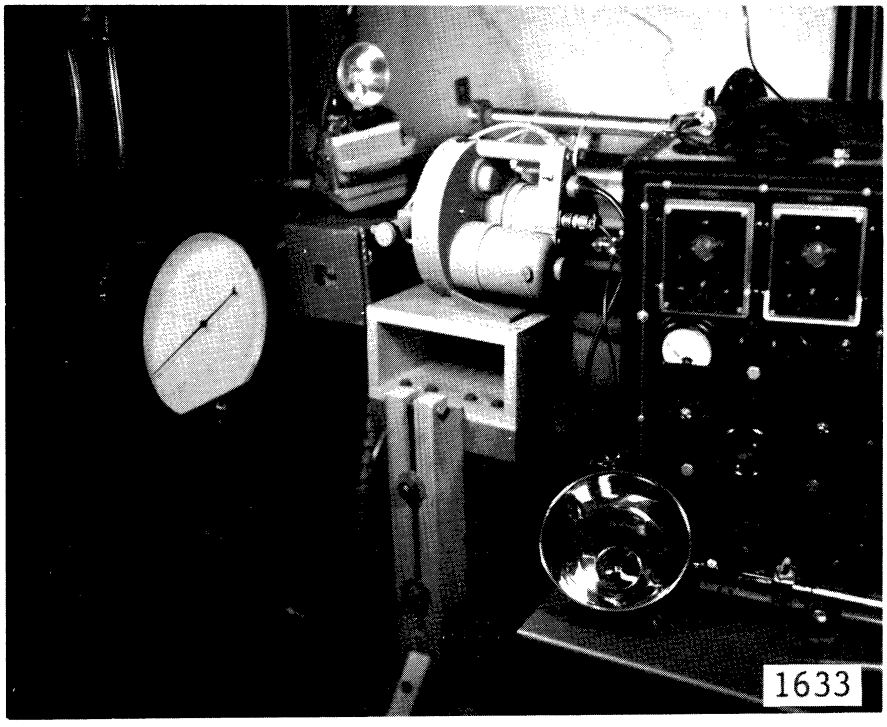

(b)

Fig. 12.--(a) Photograph of mercury loop plexiglas venturi with photo and pressure measurement test specimens installed, and (b) camera set-up and pressure measuring equipment.

With this arrangement high-speed motion pictures were taken at a framing rate of 16,000 pictures per second with two different frame exposure times. The first light source used was a Sylvania FF-33 Flood Flash Lamp in a 6" hemispherical reflector. In this case framing was controlled by the rotating prism in the Fastax camera, and the corresponding exposure time per frame was on the order of 21 microseconds. The second light source used was an Edgerton, Germerhausen and Grier, Type 501 High-Speed Stroboscope, which was synchronized with the camera to give an exposure time of 1.2 microseconds per frame. In this latter case the maximum framing rate was limited by the maximum flashing rate of the light source to about 8,000 frames per second.

3. Electrical Probe Technique

It was observed from the high-speed movies that, in some cases, the mercury appeared to lift free of the specimen surface, recontacting the surface further downstream. A rather unique method of further investigating this phenomenon was developed, which consists of electrically measuring the physical contact between the mercury and specimen surface using a plexiglas test specimen-holder combination, somewhat similar to those already described. Figure 13 is a schematic drawing of the apparatus and Figure 14 is a photograph.

Three 0.019" wires pass through the holder, terminating flush with the surface of the test specimen, and located at three axial positions on the surface. These wires are sealed with glue to prevent mercury leakage. A good visual observation of the surface can still be made through the holder, so that the extent of the cavitation zone on the surface can be noted.

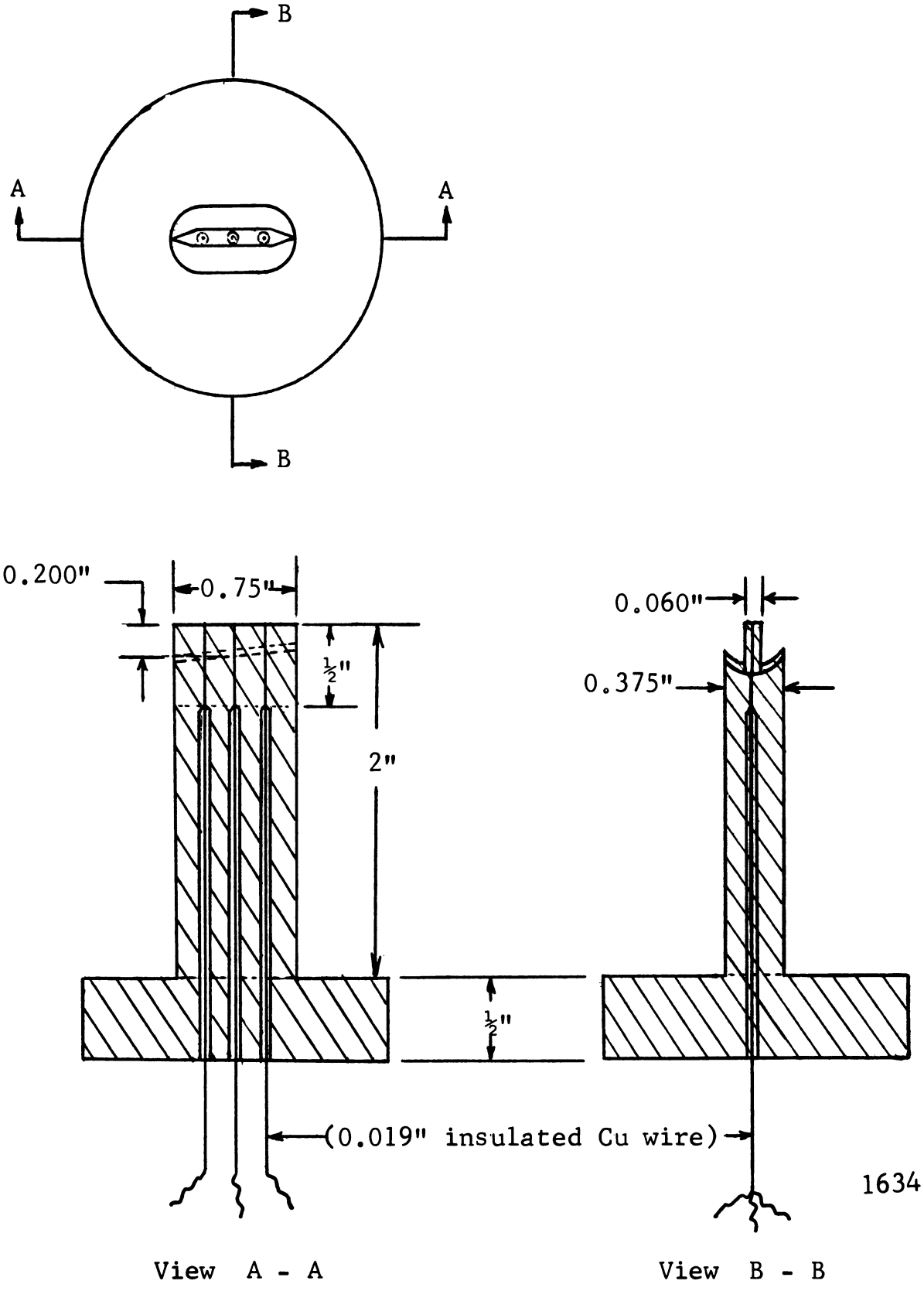

Fig. 13.--Schematic drawing of plexiglas electrode specimen-holder assembly for contact measurements.

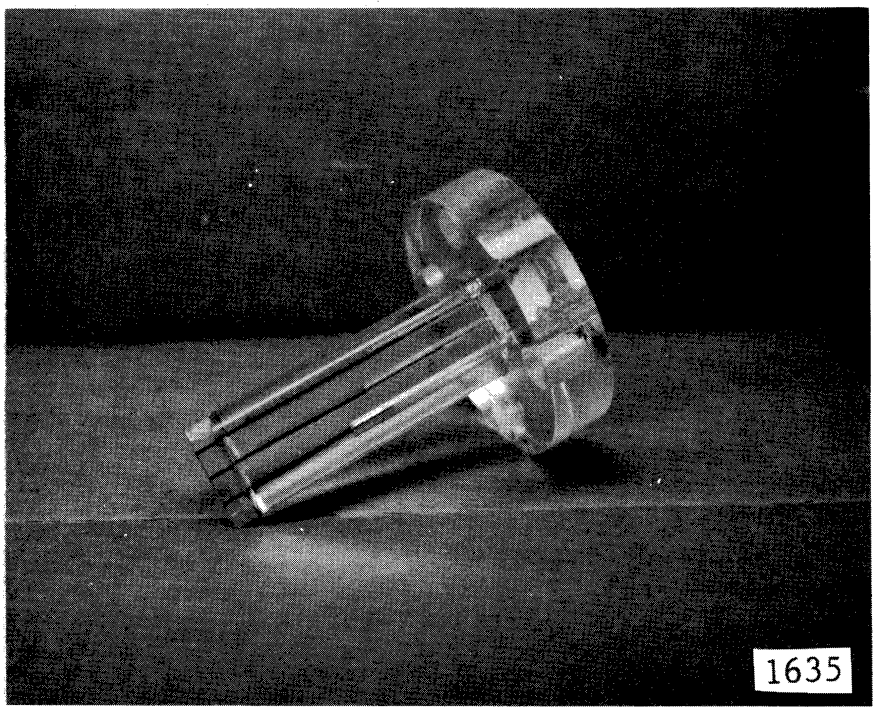

(a)

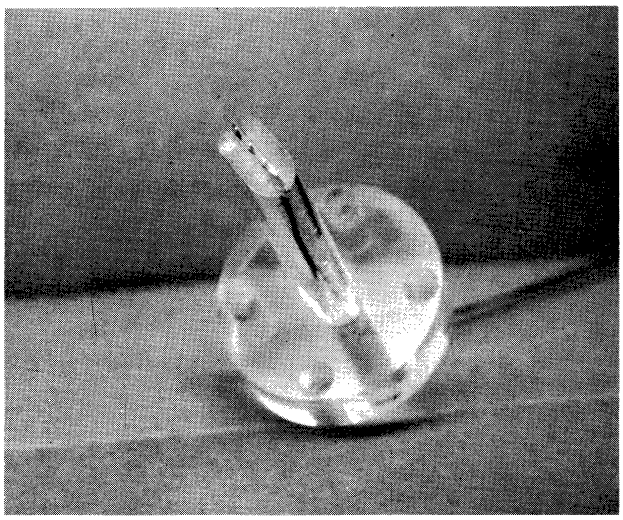

(b)

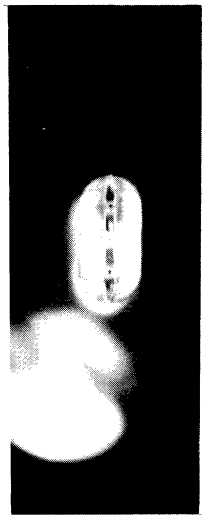

(c)

Fig. 14.--Photographs of the electrode specimen-holder combination, (a) side view showing wires in holder, (b) angle view showing wire termination points, (c) end view showing axial location of termination points.

Figure 15 (a) shows the preliminary electrical circuit used to establish the feasibility of the technique. A 6 volt, 200 ma lamp was used in series with a 6 volt battery to give a visual indication of mercury contact with the wires. Oscilloscope output was taken from the lamp terminals. An improved circuit, Figure 15 (b), was later used to monitor all three probe positions at the same time, using the lamps. Also, any two could be connected to the dual beam oscilloscope (Tetronix 502A), for instantaneous comparison. The transformer in the circuit is used only for visual monitoring of the cavitation condition via the lamps, as the output has a strong 60 cycle component. The battery circuit is used only for data taking, to conserve battery life.

The circuit in Figure 15 (b) was not optimum as there was interference between the oscilloscope outputs from the different probes, to be explained in detail later. To avoid this, a combination of the two circuits, Figure 15 (a) and (b) was finally used and proved to be quite satisfactory. Each oscilloscope beam trace was then from an independent circuit and battery. Figure 16 is a photograph of this experimental set-up.

4. Damage Specimen Examination

In general, test specimen preparation and post-test examination were conducted as follows:

1. Metallographic polish performed on the flat surface parallel to the venturi centerline ("polished surface" labelled in Figure 6). Typical before-exposure photomicrographs and roughness profiles of this surface are shown and described in the next section.

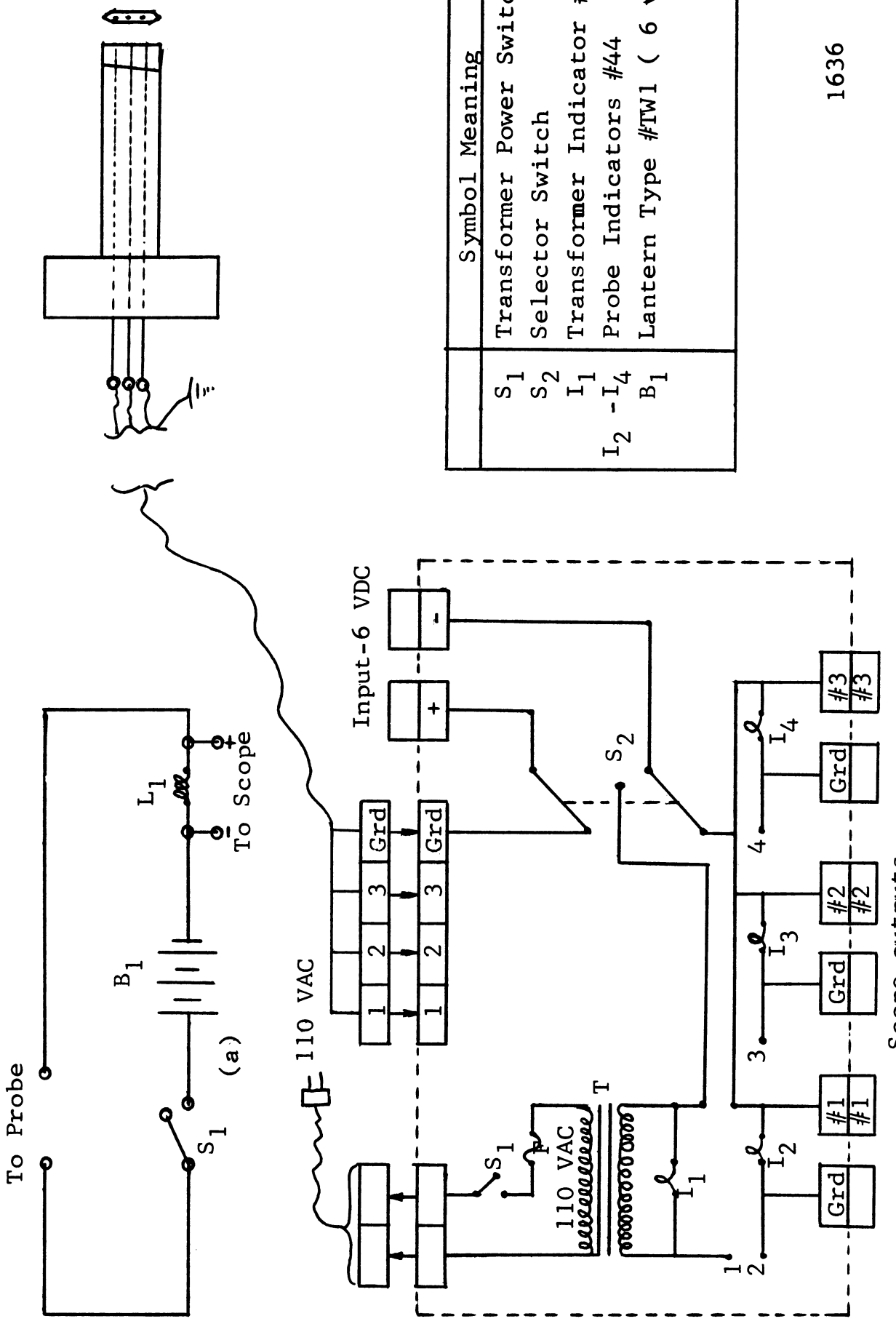

Fig. 15.--(a) Single channel, (b) three-channel mercury contact indicator circuit.

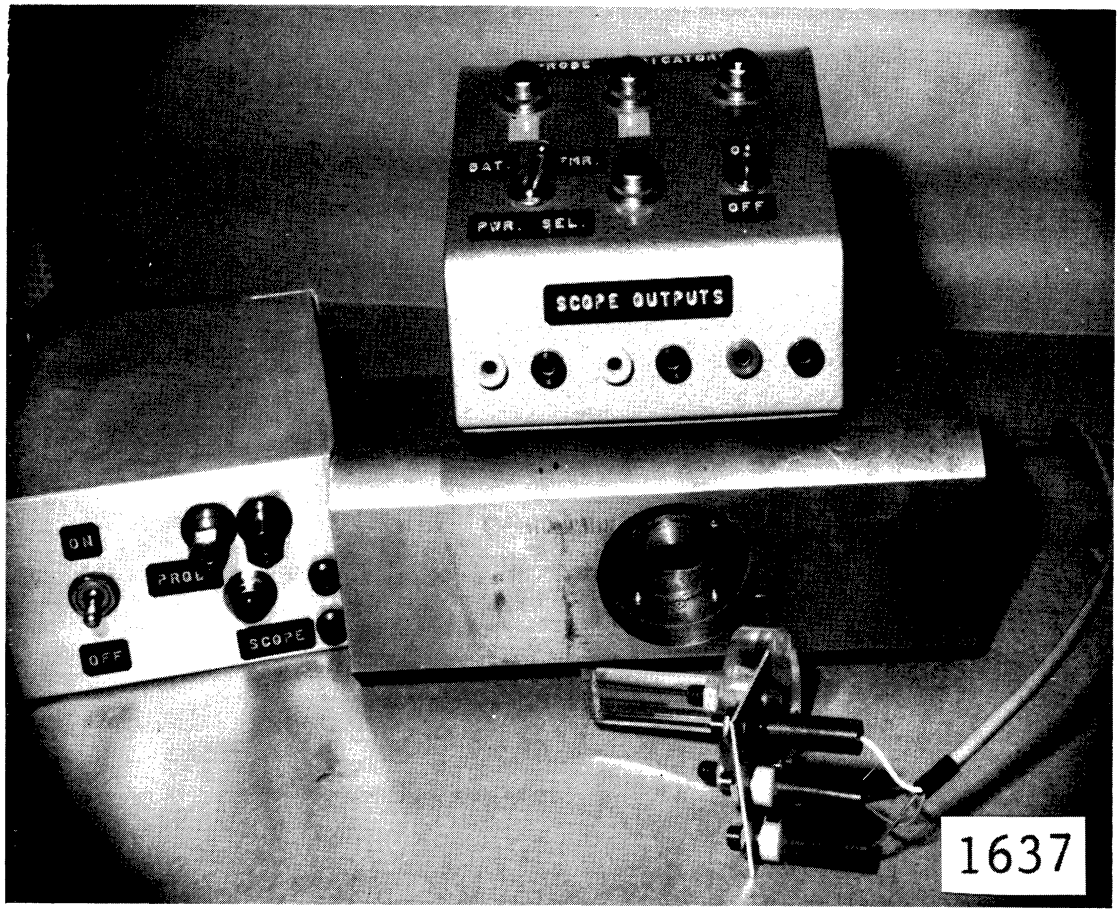

Fig. 16.--Photograph of electrode specimen-holder, stainless steel venturi center section (no test specimens in place), boxes containing circuitry.

2. Initial specimen weight recorded to a precision of 10^{-5} grams on electronic balance.
3. Original surface pits and imperfections examined at 100X under microscope and tabulated into several size categories by two observers.
4. Photomicrographs taken, in some cases, of full surface at 40X, and selected areas of probable damage at 100X before exposure.
5. After exposure to cavitation of selected condition and duration items (2), (3) and (4) repeated.
6. After (5) in the mercury runs only the specimens were baked at a temperature of 500°F for a period of 5 hours in a vacuum chamber in order to remove any mercury on the surfaces that was not removed by the normal cleaning operation in N-Heptane. Experience showed that this was necessary. By this process, as explained below, it was possible to determine the existence of possible chemical attack or chemical corrosion as opposed to purely mechanical damage. A few materials exhibited large weight gains after cavitation but before baking, and large weight losses after baking. This was taken to be an indication of the existence during the cavitation test of chemical formation of amalgamations, etc. However, most materials exhibited very small weight changes after baking due primarily to vaporization and removal of mercury droplets from the surfaces.
7. Selected areas of typical cavitation damage were photographed at several magnifications and detailed proficorder traces made in

several cases. The results of these investigations will be described in a later section.

8. In a few cases, metallographic cross-section through typical damaged areas were performed.

5. Fluid Purity Observations and Operating Conditions

a. Water Conditions

The water used in these tests was normal tap water at a temperature of 80°F ± 10°F, with a nominal total gas content of 2.5 ± .5 percent by volume at STP as determined by Van Slyke measurements, and an impurity content of 8.0 ± 0.5 grains per gallon (about 140 ± 10 ppm solids), as measured by an RDE4 Solubridge and VSO216 Dip Cell manufactured by Industrial Instruments in New Jersey.

b. Mercury Conditions

The mercury installed in the cavitation damage facility for these tests was triple-distilled laboratory grade mercury, at a temperature of 75°F ± 5°F, with an entrained gas content of $\sim$ 0.2 ppm by mass as determined by a modified Van Slyke apparatus, and a water vapor content below 10 to 15 ppm by mass. The required instrumentation was designed and developed in this laboratory.

During the investigation, it was noted that sealing water used in the pump had contaminated the mercury to about 500 ppm by mass. Subsequently, a means of measuring the water content of the mercury was developed. The water was removed from the mercury by operating the loop for a prolonged period at 500°F. Henceforth, the tests were conducted

in "dry" mercury (established by the sensitivity limitation of the instrument to be less than 15 ppm by mass, and probably zero).

CHAPTER III

CAVITATING FLOW STRUCTURE IN VENTURI

The cavitating flow structure in the venturis used in this investigation has been experimentally observed in three different ways. In each case the observation has included the effects of velocity, degree of cavitation, and the number and orientation of the test specimens. The following three sections describe these methods, and the possible relation between the variation of the above-mentioned parameters and the observed damage.

A. Measurement of Venturi Pressure Profiles

1. General

Axial wall pressure profiles have been used in this laboratory for investigations of scale effects in the flow[34] and currently an extensive effort is being made to examine the scale effects phenomenon of cavitating flow.[35] However, the walls of the venturi were smooth during these measurements and no test specimens were inserted. Since the test specimens projecting into the venturi constitute significant obstructions, it is presumed that the local pressures seen by the test specimens will not be the same as the wall pressure at that point. Hence, a test specimen assembly was fabricated in order to measure the

actual pressures existing on the test specimen polished surface at the same time as conventional wall pressure profiles were measured. The equipment for this has already been described.

2. Motivation

The motivation for conducting this particular type of measurement stems from two considerations. First, it was necessary to know the actual pressures or pressure gradients existing on the test specimen surfaces to be able to compare the observed bubble size and number distribution, to be obtained photographically, with observed pitting and theoretical treatments of forces imposed on the surface by bubble collapse. Secondly, it was desired to determine the local flow environmental changes produced by variations of velocity, degree of cavitation (see Appendix A for definitions of degrees of cavitation), and number and geometry of test specimen insertion, since the comparison of the mercury and water damage depends on knowing this relationship.

3. Data Reduction

The pressure profile data has been normalized by dividing the observed pressure above vapor pressure ("suppression pressure") by the kinetic pressure at the appropriate flow conditions, i.e.,

$$P_{norm.} = \frac{p - p_v}{\rho v_t^2/2g}$$

where

$p_{norm.}$ = the normalized pressure

p = the observed or measured pressure

p_v = the fluid vapor pressure

v_t = the mean venturi throat velocity

ρ = the liquid density

When this method of normalization (i.e., not a true normalization, since the maximum values exceed 1.0) is used, the minimum value of normalized pressure is the conventional cavitation number, σ_c, i.e.,

$$\sigma_c = \frac{p_{min} - p_v}{\rho v_t^2/2g}$$

The data reduction was facilitated by the use of a computer program written for the IBM 7090 facility, described in Appendix B.

4. Velocity and Number of Test Specimen Effects

Lichtman[36] (rotating disk), Hobbs[10] (jet or droplet impacting device), and Knapp[24] (ogive in a water tunnel), all reported a considerable effect of velocity upon damage rate. It is the author's opinion that the existence of such an effect, not observed previously in general in the venturi arrangements herein used,[37] and the small dependence of damage on velocity noted in this investigation, i.e., a very large increase in damaging capabilities of a particular laboratory or field device with velocity, is due indirectly to the effect of velocity on the location, pressure environment, and distribution of the cavitating bubble cloud produced by the device. Thus it is not evident that there can be a generally applicable, simplified velocity effect "law" as, e.g., Damage Rate $\propto V^n$ as previously suggested.[10,24,36] In many systems, when velocity is increased, the system pressures and pressure

gradients, influencing the violence of bubble collapse, are increased. In addition, the departure from classical scaling laws involving fluid flow parameters can also be produced by these changes in velocity, and thus indirectly influence damage. Finally, the presently undefined mode of attack and material failure from the cavitation flow regime could be influenced indirectly in some presently unknown manner by a change in velocity through a change in intensity of cavitation attack. If, as described later, the intensity level of the cavitation flow regime is such that the forces resulting have the effect of producing a fatigue failure of the material, then an increase in velocity could produce an increase in intensity of cavitation level which would in turn influence the relative importance of failure mechanisms and cause proportionately more damage by single blow failure, cratering, e.g. This would also apply to change of fluid, as discussed later.

In the present case, it is believed that the major effect of velocity upon damage is due to the increase of collapse pressure and/or the increase in pressure gradient in the collapse region of the cavitation cloud due to an increase in velocity. In the particular venturi system used in this investigation, the degree of cavitation is variable and several such "degrees" are defined in Appendix A. For the less developed conditions as "visible initiation," a substantial portion of the specimen, somewhat downstream of the collapse region of the apparent cavitation cloud, is under pressures considerably higher than vapor pressure. Thus these pressures influencing the collapse of the larger bubbles which do most of the damage are proportional to velocity squared.

Conversely, for the well-developed cavitation conditions, the entire specimen is under pressures near vapor pressure, regardless of the velocity. As expected, the damage shows a maximum when plotted against degree of cavitation, since the numbers of bubbles increase as the cavitation condition becomes more fully developed, but the pressure differential causing collapse decreases. The maximum cavitation condition for damage ("standard cavitation," Appendix A) was selected for this investigation.

Consideration of Figures 17 through 26 illustrates the applicability of the above-described effect of velocity on damage. Normalized static pressure profiles reduced, as previously described, from the same venturi in mercury and in water, are shown.

From these profiles, it is observed that the pressures on the test specimen surface are slightly lower than the wall pressures measured at the same axial location. For the well-developed cavitation conditions the wall pressure adjacent to the nose of the specimen is apparently increased by a kinetic component of the flow due to the flow pattern around the specimen. It can also be observed that the pressure gradient on the specimen surface decreases as the degree of cavitation is increased towards the more fully developed condition, where the entire surface of the specimen is under pressure only slightly in excess of vapor pressure.

The normalized profiles for different velocities are almost identical (Figures 17, 18, 21, 22, 23). Hence, the actual pressure differentials above vapor pressure on the surface are higher for the higher

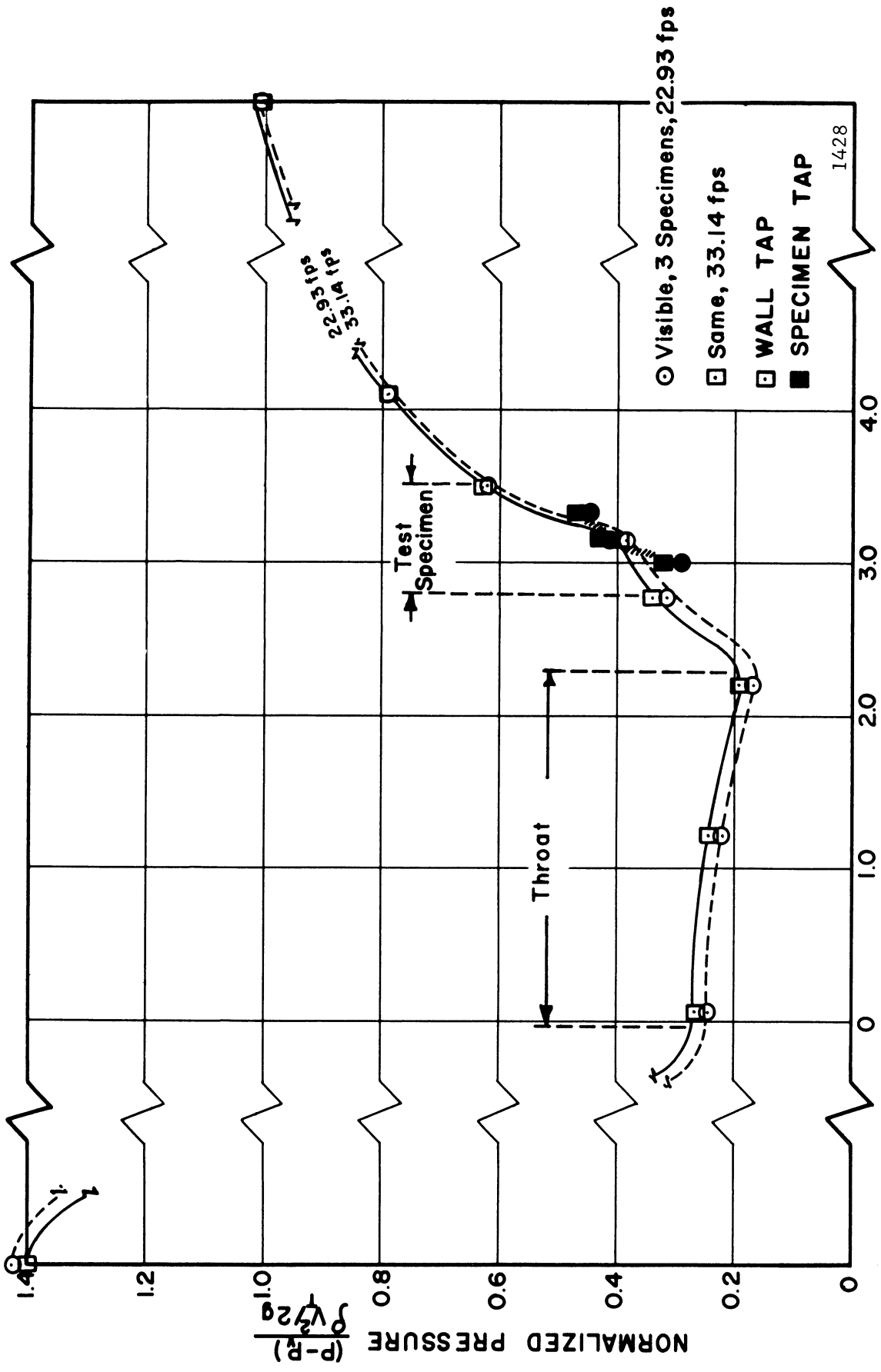

Fig. 17.--Normalized pressure profile for "visible initiation" with three specimens in "dry" mercury at various velocities.

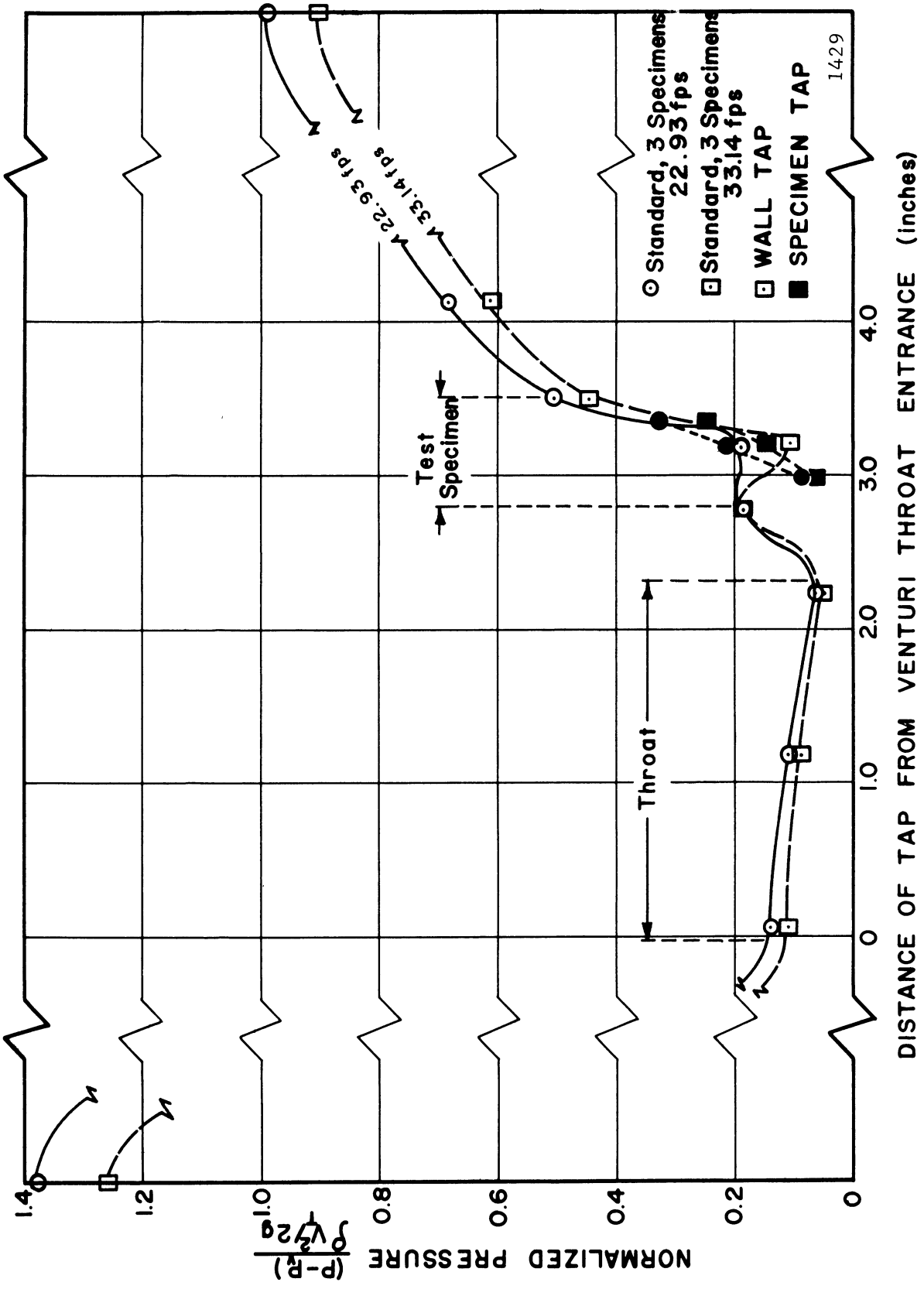

Fig. 18.- Normalized pressure profile for "standard cavitation" with three specimens in "dry" mercury at various velocities.

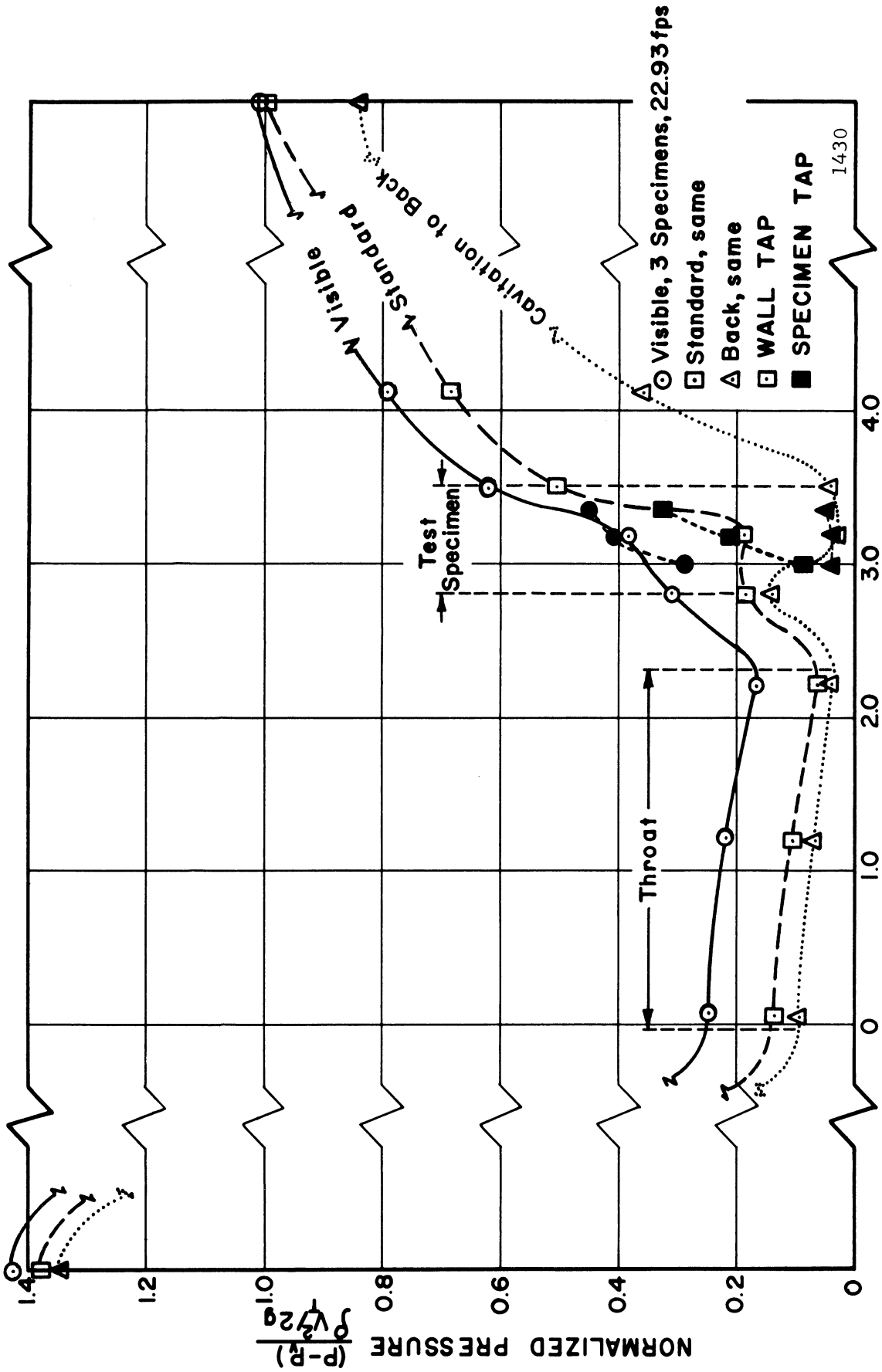

Fig. 19.--Normalized pressure profile for velocity of 22.9 ft./sec., in "dry" mercury, with three specimens at various cavitation conditions.

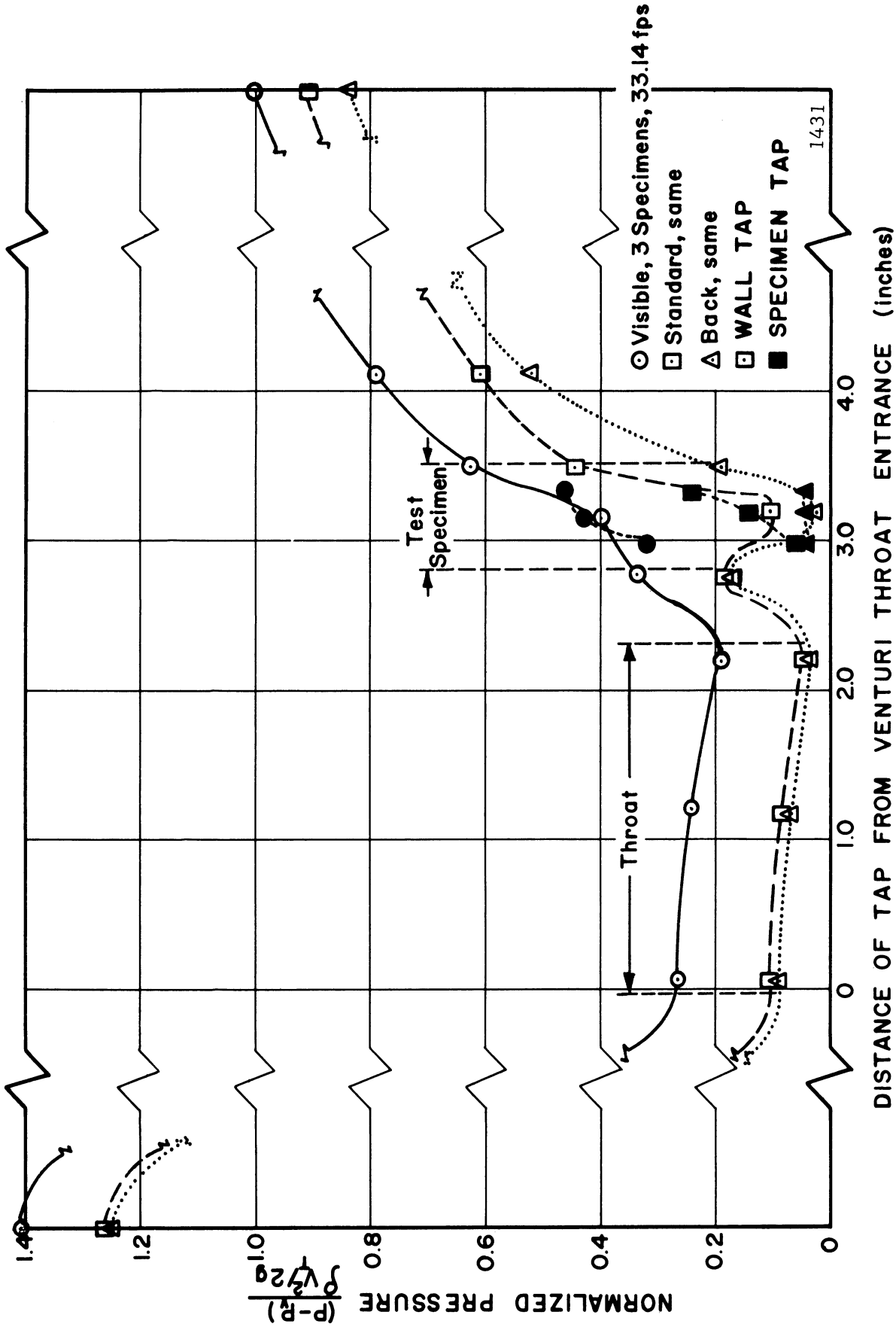

Fig. 20.--Normalized pressure profile for velocity of 33.1 ft./sec. with three specimens in "dry" mercury at various cavitation conditions.

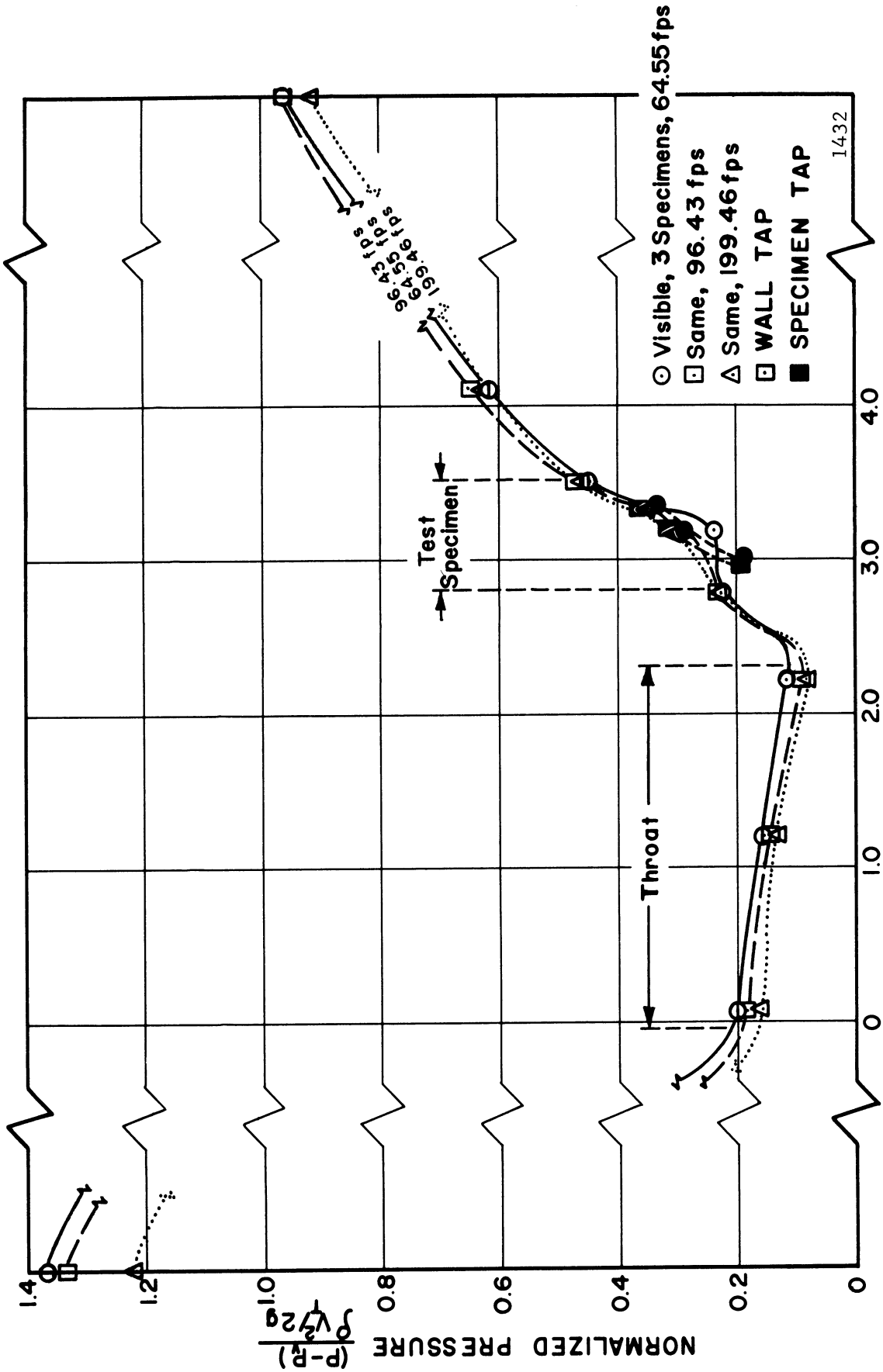

Fig. 21.--Normalized pressure profiles for "visible initiation," three specimens in water, at various velocities.

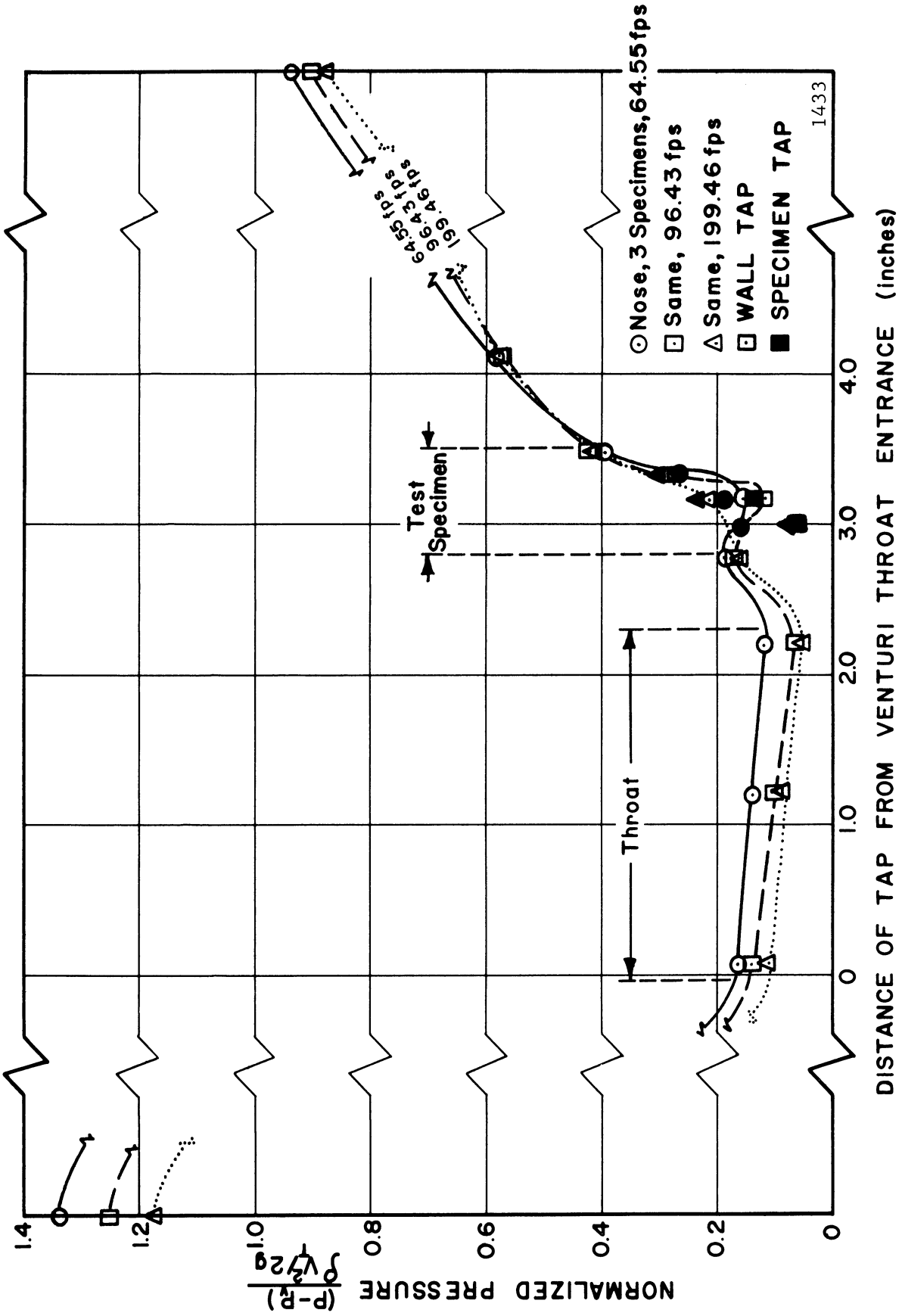

Fig. 22.--Normalized pressure profile for cavitation to nose" with three specimens in water at various velocities.

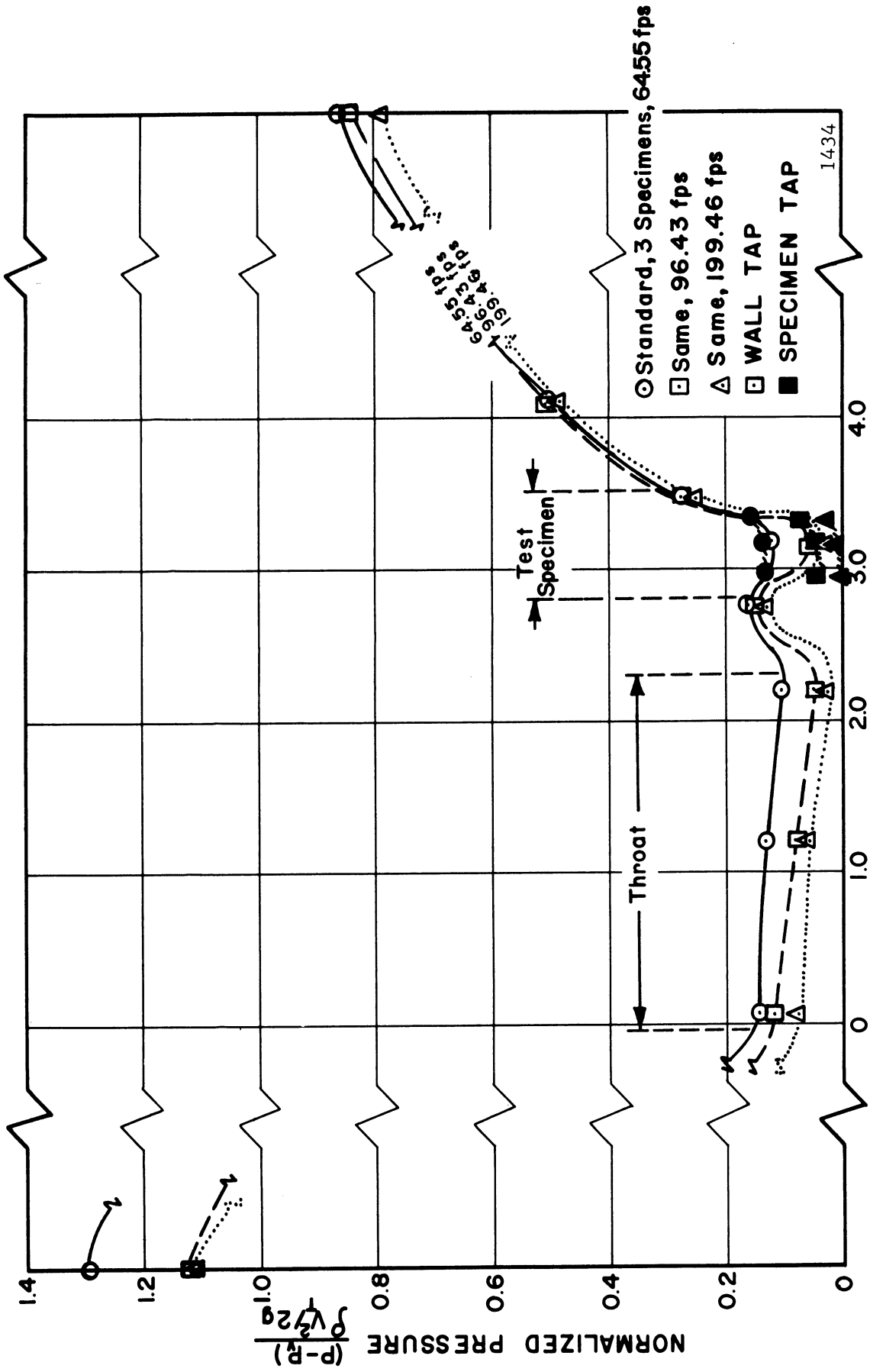

Fig. 23.--Normalized pressure profile for "standard cavitation" with three specimens in water at various velocities.

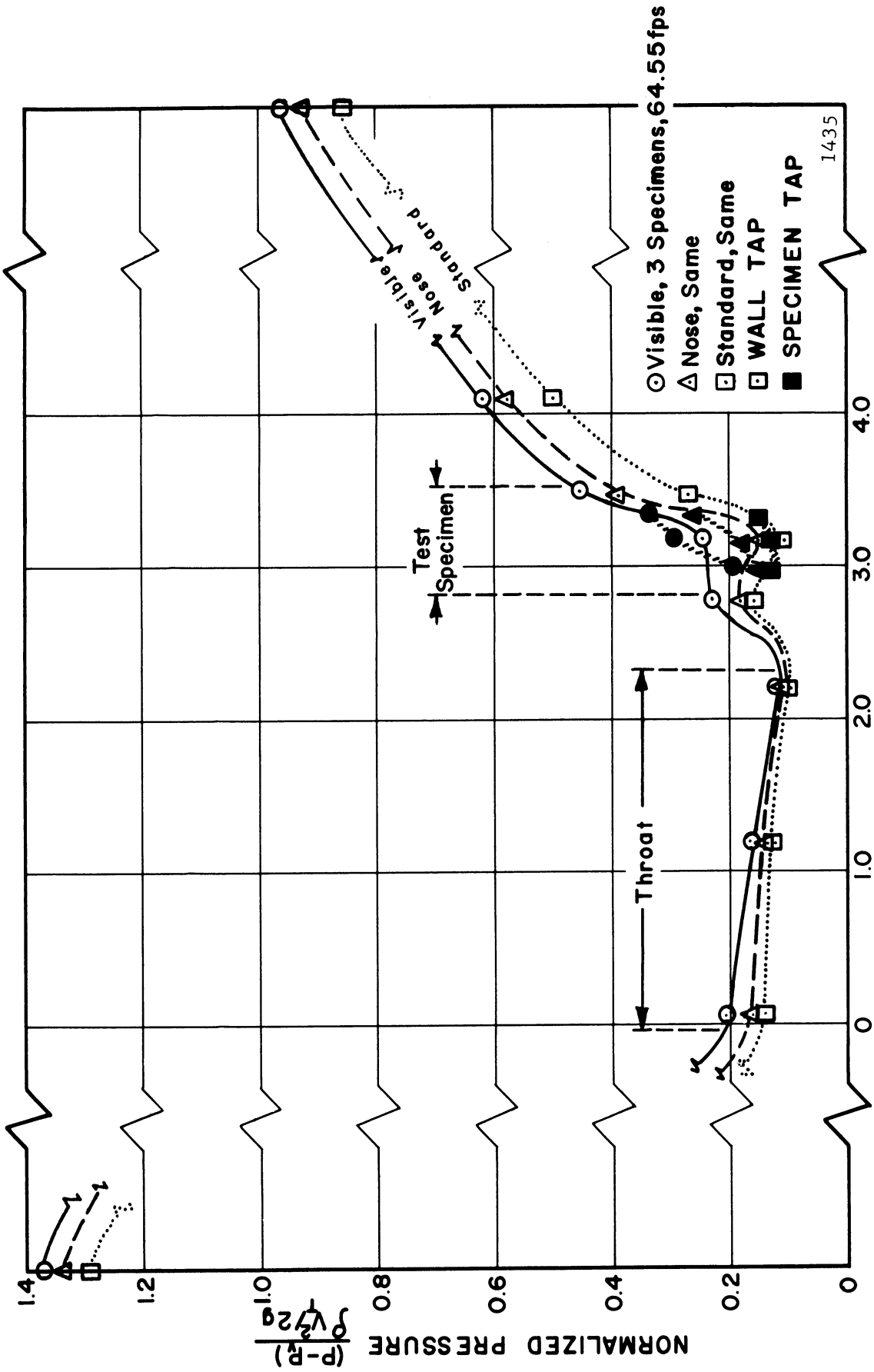

Fig. 24.--Normalized pressure profile for 64.5 ft./sec. with three specimens in water at various cavitation conditions.

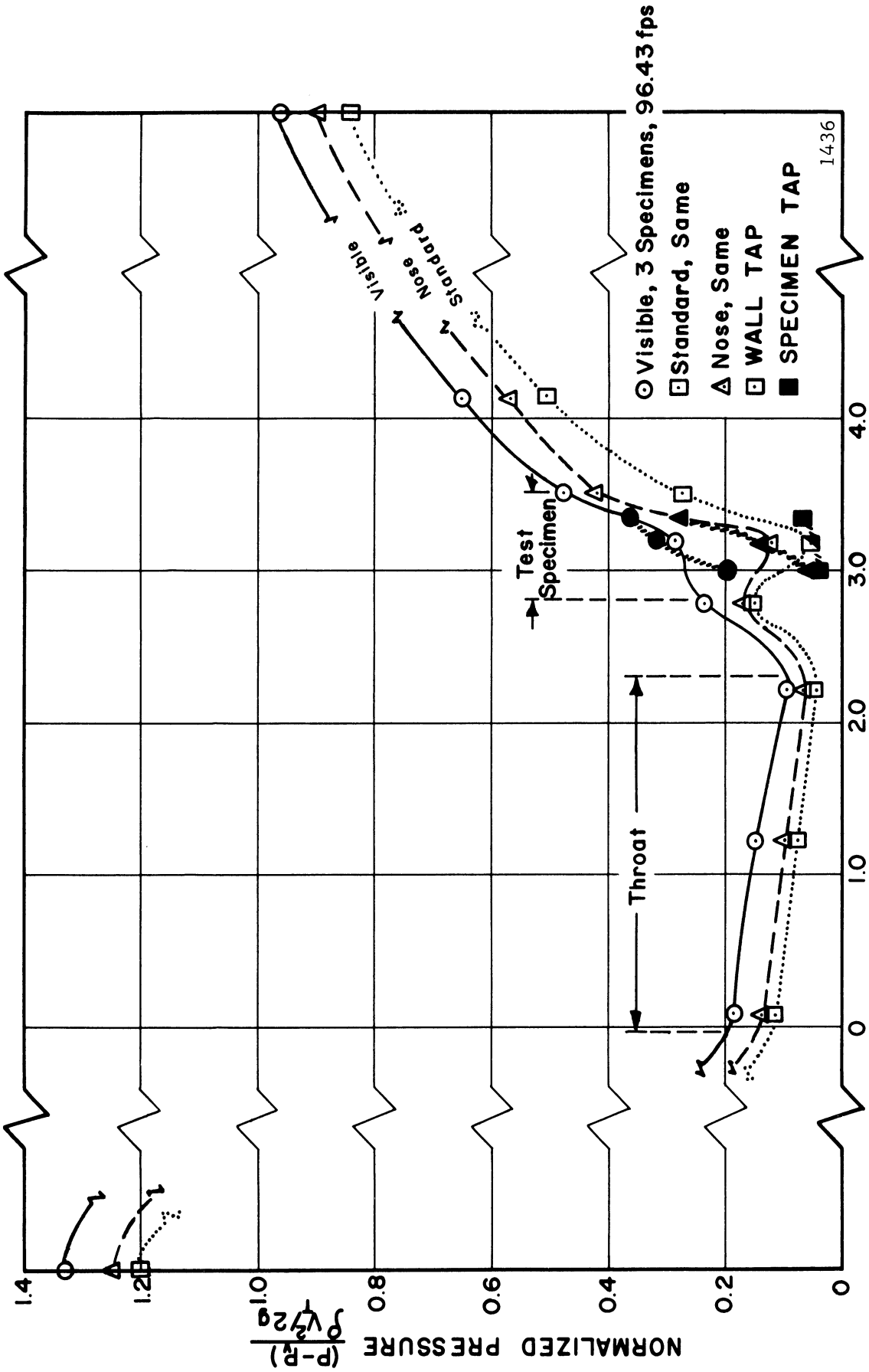

Fig. 25.--Normalized pressure profile for 96.4 ft./sec. with three specimens in water at various cavitation conditions.

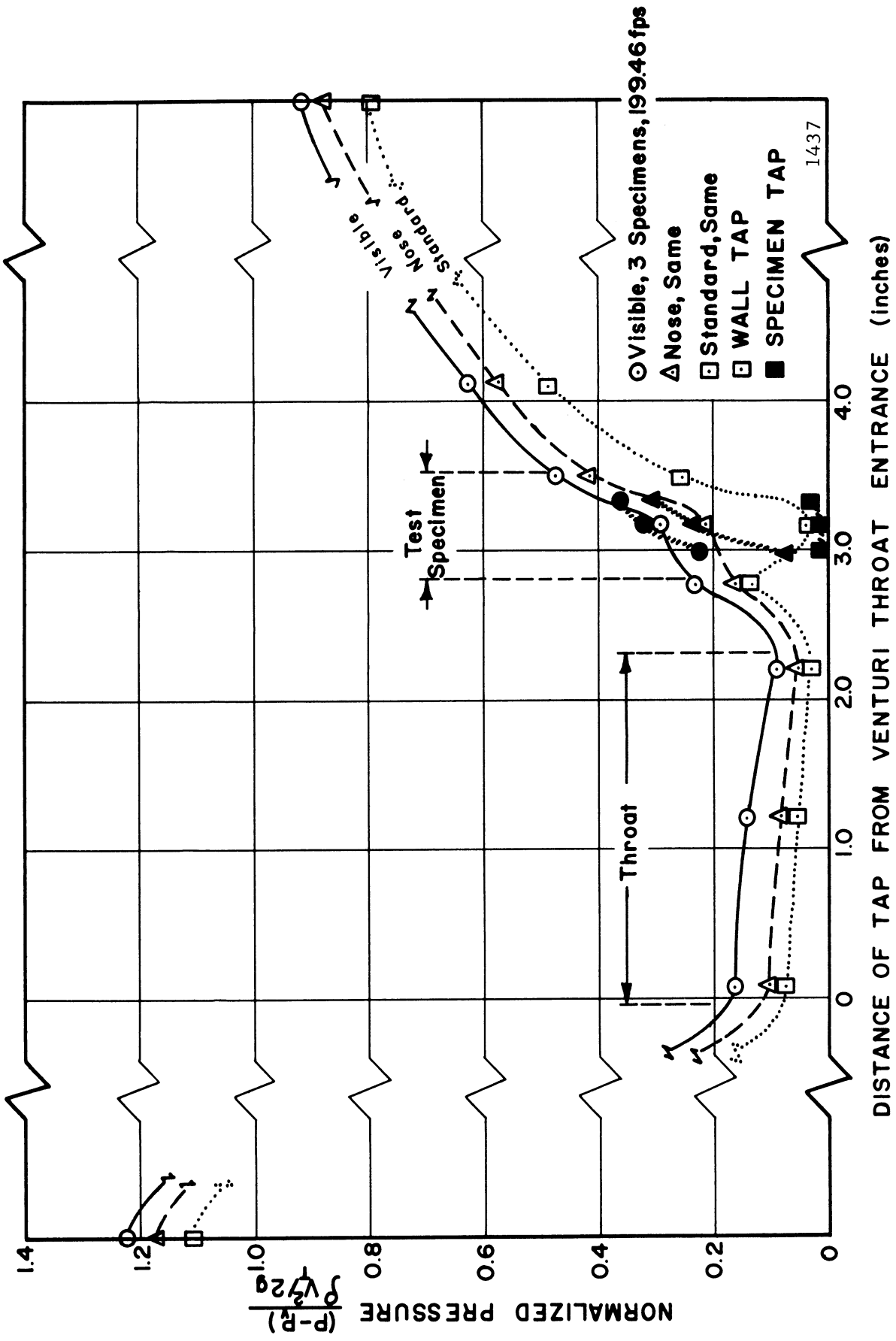

Fig. 26.--Normalized pressure profile for 199.5 ft./sec. with three specimens in water at various cavitation conditions.

velocities approximately according to the square of the velocity. This differential becomes substantial for the less-developed cavitation conditions. The measured specimen surface pressures minus vapor pressure for mercury and for water and for three specimens in the venturi, with a variation in velocity, are shown in Table 1, illustrating the foregoing comments.

Figure 27, reproduced from a previous investigation from this system,[37] shows the actual effects of degree of cavitation on the observed damage for different materials, at different velocities, in both water and mercury. The ordinate values, $MDP/MDP_{max.}$, are normalized values (simply divided by the maximum) of the damage received at the different conditions. The damage data for all materials is reported as mean depth of penetration (MDP), which is a "specific volume loss," i.e., the weight loss is divided by the total exposed area and density of the specimen so as to make the comparison of damage received by all materials directly and correctly comparable. An important observation apparent from this plot is that the maximum damaging condition for mercury is "standard cavitation," where the cavitation cloud on the surface appears to end at the center of the specimen, while the most damaging for water is also "standard cavitation," however, the cavitation cloud here appears to end at the tail of the specimen. As discussed in more detail later, it is believed that these two conditions are similar, in that bubbles are thought to exist in the mercury at a small distance above the surface, and are not visible due to the opacity of the mercury. Although the same terms are used to describe the cavitation

TABLE 1

ACTUAL PRESSURE ABOVE VAPOR PRESSURE ON TEST SPECIMEN SURFACE FOR STANDARD CAVITATION IN MERCURY AND WATER

Fluid	Velocity Ft./Sec.	No. of Specs.	Spec. Tap No.	Pressure (psi) Run No.1	Run No.2	Run No.3
Water 54°F	64	3	1	3.9	4.4	3.0
			2	4.2	4.5	3.4
			3	4.6	5.0	3.9
Water 54°F	97	3	1	2.6	2.6	2.4
			2	3.4	2.9	2.9
			3	4.9	4.3	3.3
Water 75°F	200	3	1	4.0	3.9	3.5
			2	5.5	5.2	5.2
			3	11.7	7.1	6.2
"Dry" Mercury 75°F	23	3	1	3.5	4.7	3.6
			2	9.2	11.0	10.0
			3	15.1	16.0	15.2
"Dry" Mercury 88°F	34	3	1	5.3	7.0	6.5
			2	11.5	17.5	13.8
			3	19.1	29.3	25.5
"Dry" Mercury 120°F	46	3	1	12.1	9.1	8.7
			2	9.4	9.8	8.2
			3	14.7	16.3	16.6
"Wet" Mercury 75°F	23	3	1	9.7	11.1	9.7
			2	15.5	15.8	15.4
			3	21.6	22.1	21.5
"Wet" Mercury 88°F	34	3	1	3.3	3.1	3.0
			2	11.4	12.2	11.0
			3	31.1	31.3	29.3
"Wet" Mercury 115°F	46	3	1	8.3	3.5	4.8
			2	20.6	16.0	15.0
			3	58.8	30.5	51.8
"Dry" Mercury 78°F	34	2 (180°)	1	1.7	1.7	
			2	4.9	1.7	
			3	9.5	5.3	

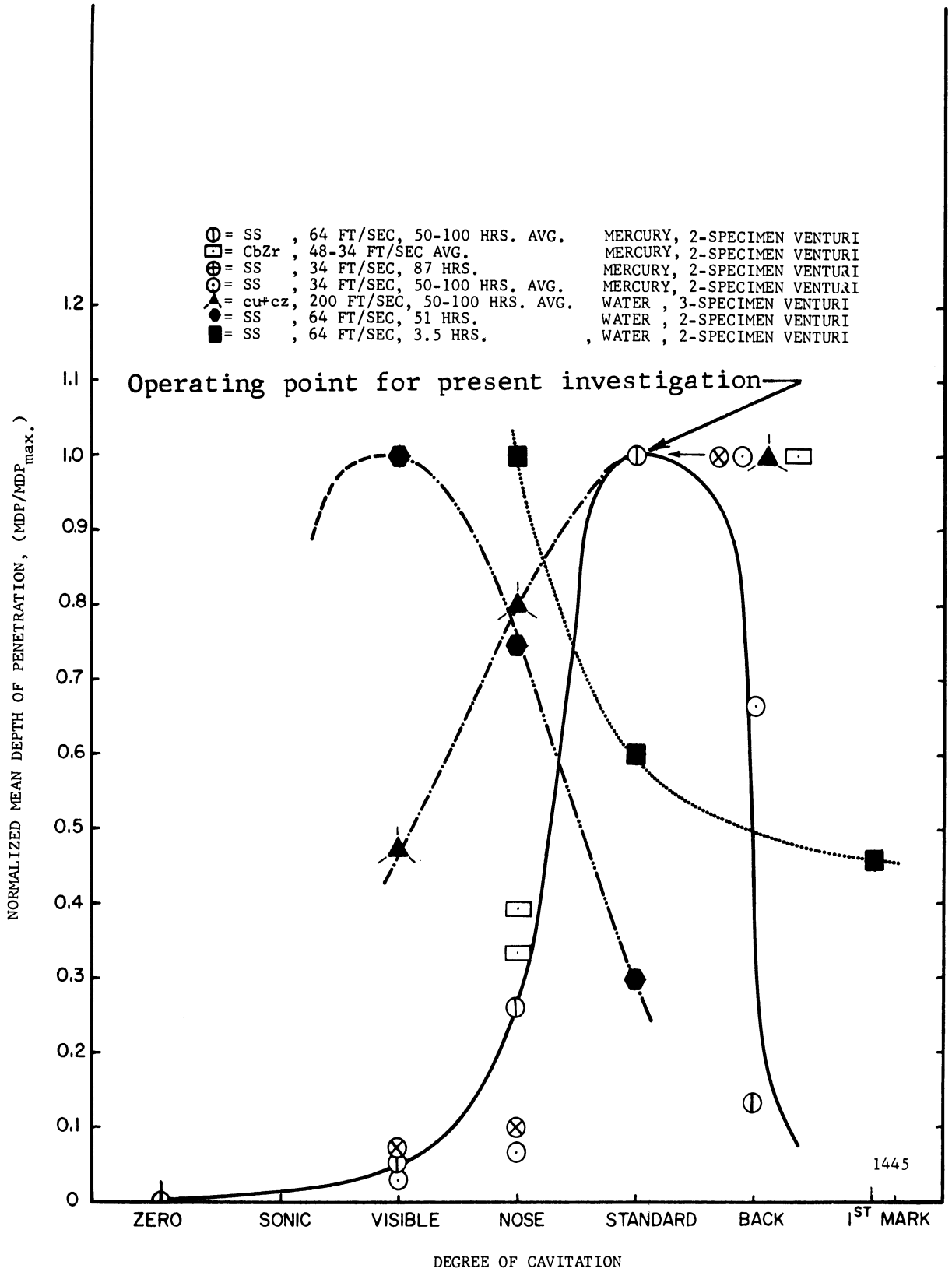

Fig. 27.--(MDP/MDP_{max}) versus cavitation condition for various materials in mercury and water.

conditions in water and mercury, the corresponding visual flow patterns are not identical. Detailed visual descriptions and cross-correlations between water and mercury are given in Appendix A.

The pressure profile examination of the effects of one, two, and three specimen insertion geometry has been made. Figures 28, 29, and 30 show the results for water at three velocities and "standard cavitation." A corresponding examination was made, Figures 31 through 34, in mercury at two velocities and two cavitation conditions, "visible initiation" and "standard cavitation." The latter condition in both cases was selected for the damage correlation with mechanical properties, presented later.

In general, it is observed that the magnitude of the pressures on the test specimen surface is increased as the number of test specimens is increased for a given velocity and cavitation condition. It has been previously observed[37] that the maximum damage occurs with a less-developed cavitation condition for mercury than for water (Figure 27). An examination of the pressure profile plots shows that the pressure gradient on the test specimen surface is very similar when a comparison is made between mercury at 34 feet per second, "standard cavitation," and water at 97 feet per second, "cavitation to nose." Similarly, "standard cavitation" in water compares closely to "cavitation to back" in mercury in the velocity range used and with the same number of test specimens. However, an examination of the actual pressures above vapor pressure, as listed in Table 1, shows that the magnitude of the pressures are quite a bit higher in mercury. Also, it is evident from

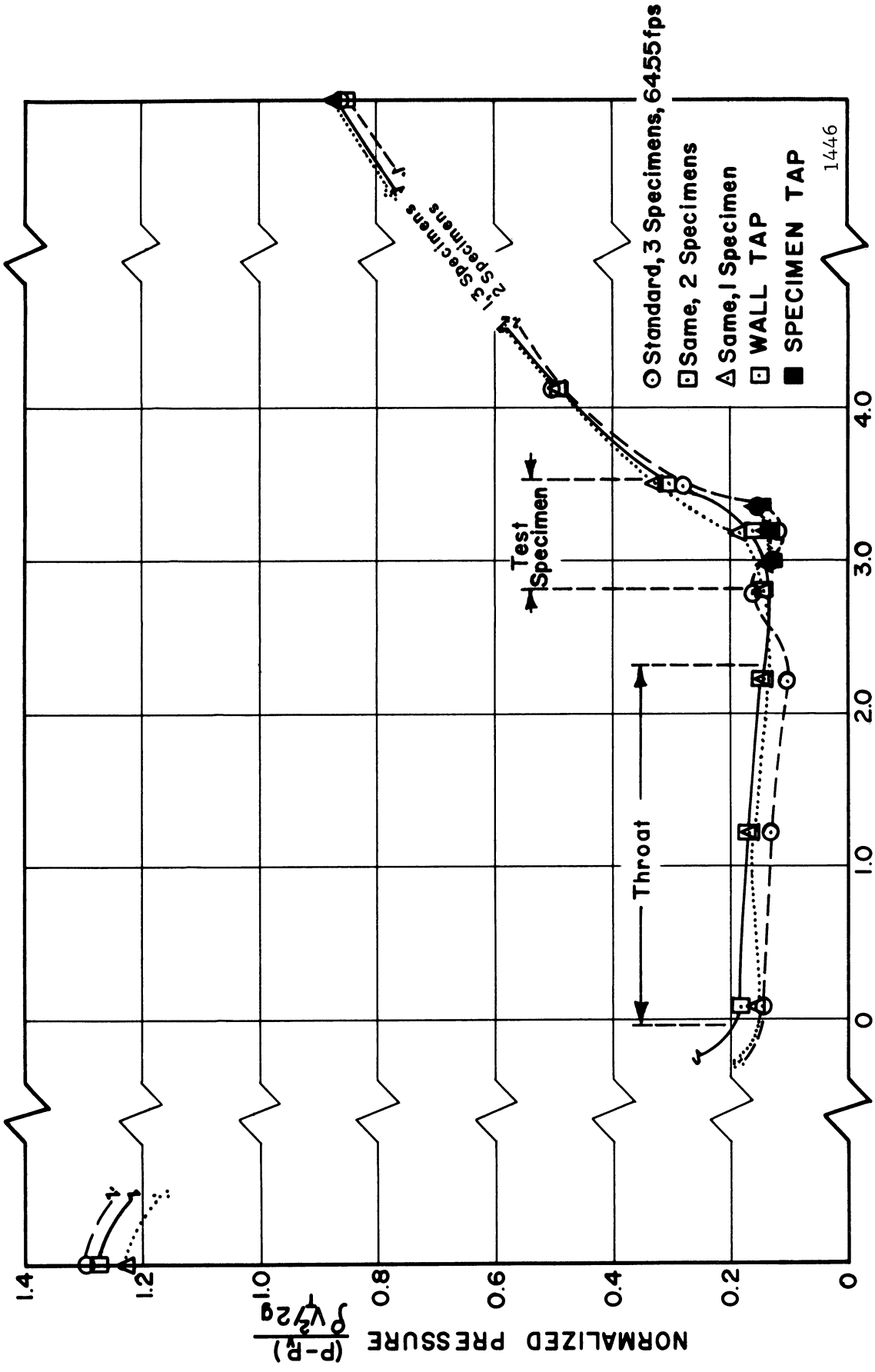

Fig. 28.--Normalized pressure profile for velocity of 64.5 ft./sec. for "standard cavitation" in water with one, two and three specimens.

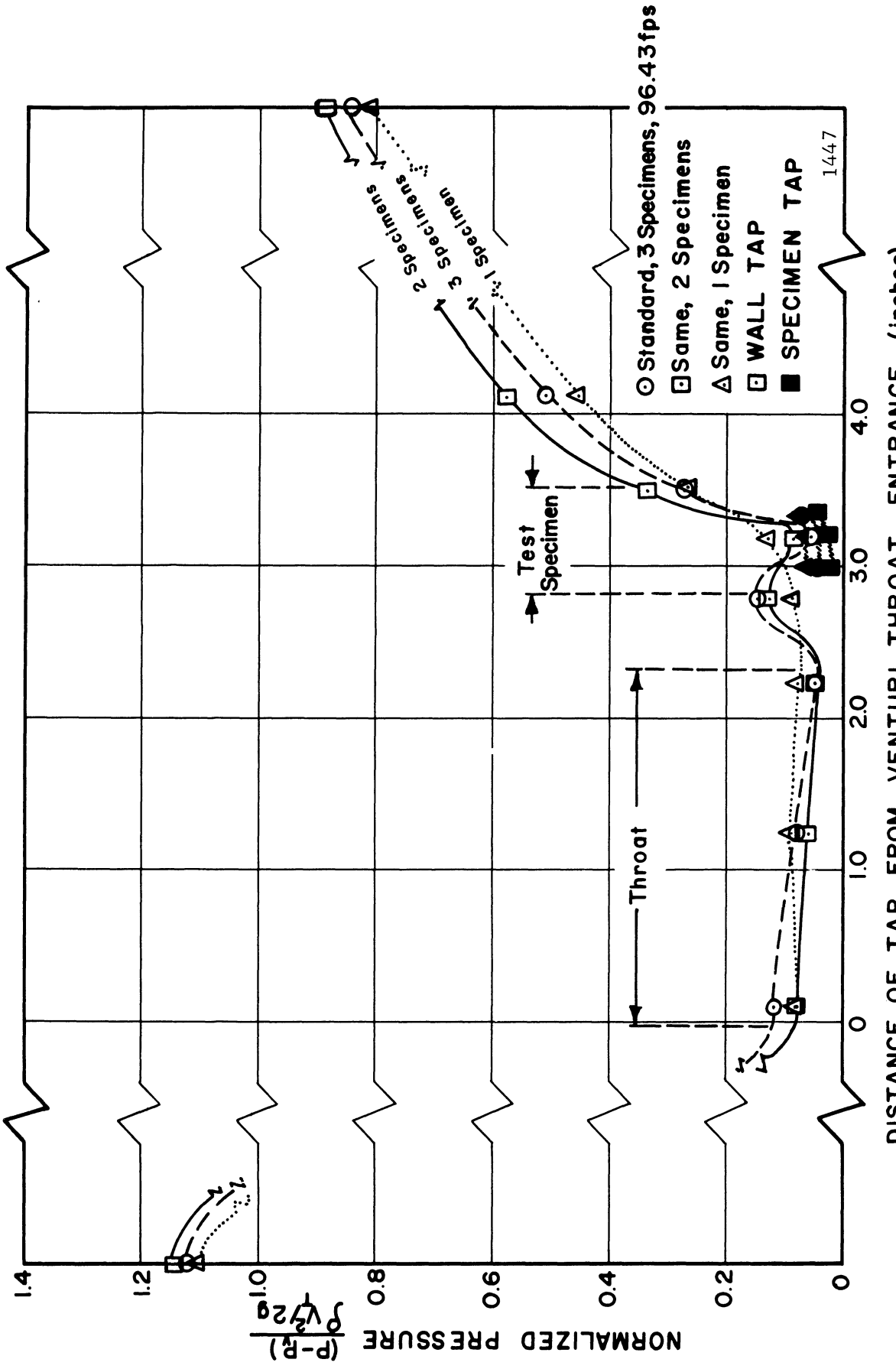

Fig. 29.--Normalized pressure profile for velocity of 96.4 ft./sec. for "standard cavitation" in water with one, two and three specimens.

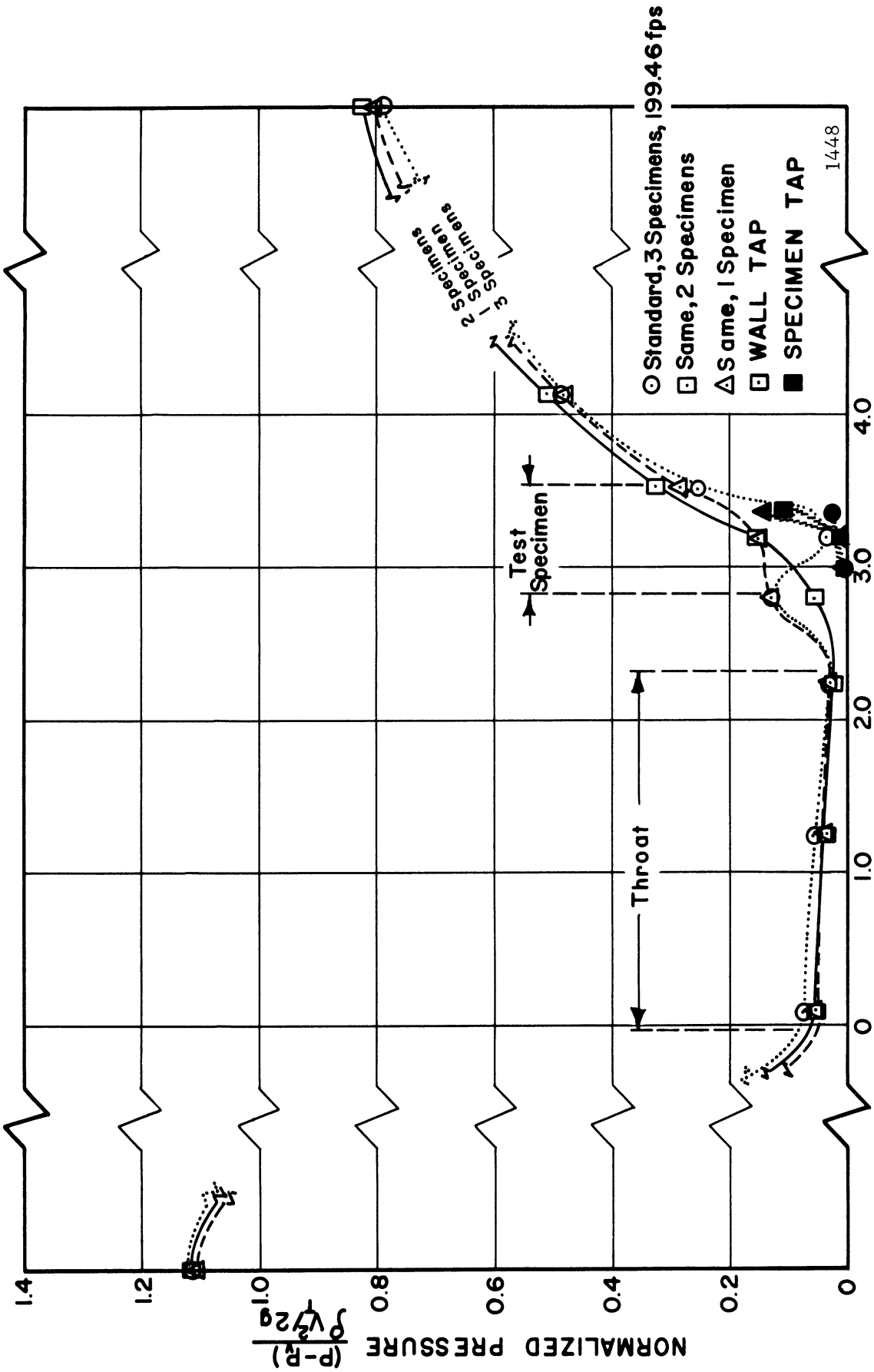

Fig. 30.--Normalized pressure profile for velocity of 199.5 ft./sec. for "standard cavitation" in water with one, two and three specimens.

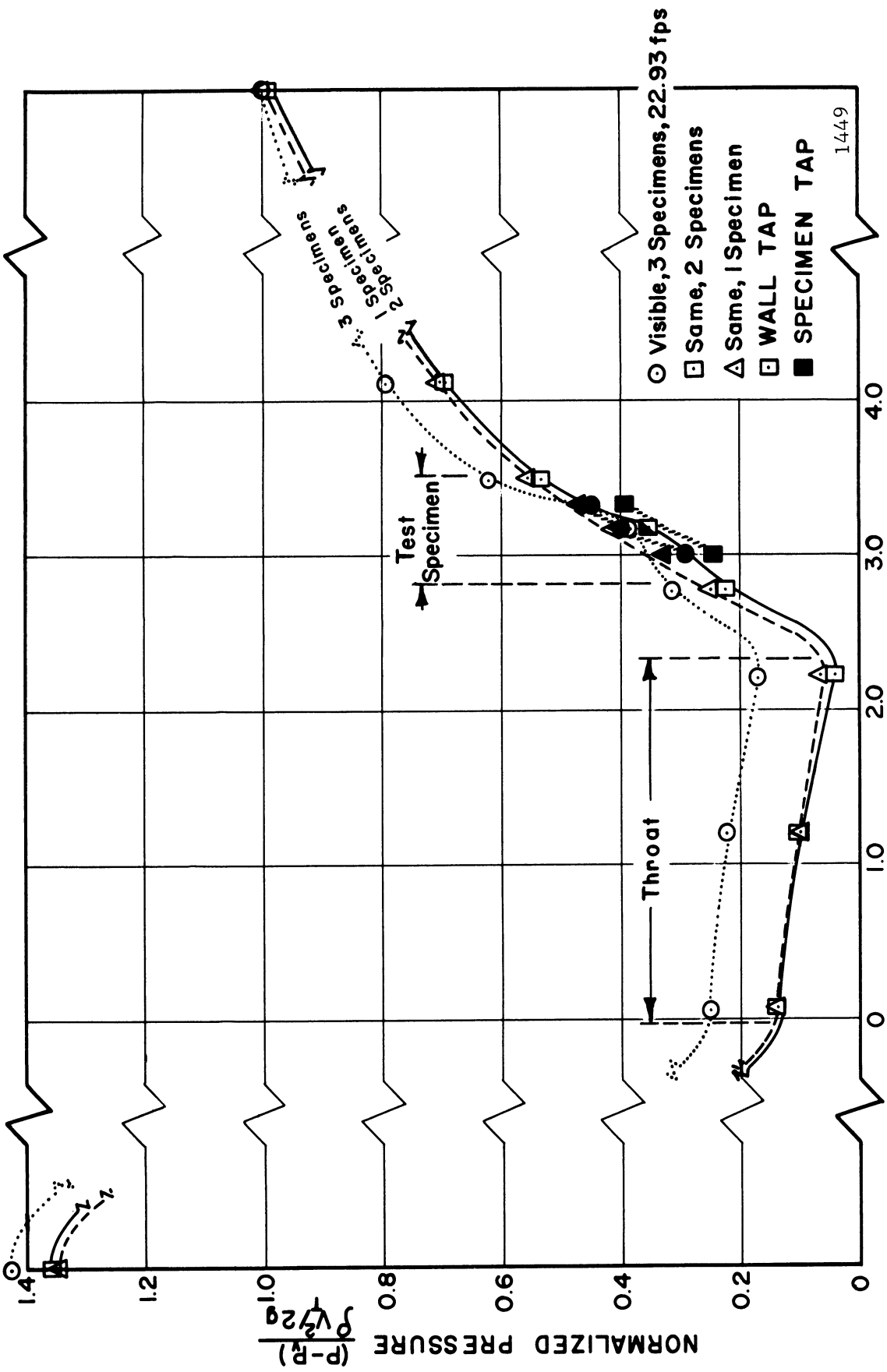

Fig. 31.--Normalized pressure profile for velocity of 22.9 ft./sec. for "visible initiation" in "dry" mercury with one, two and three specimens.

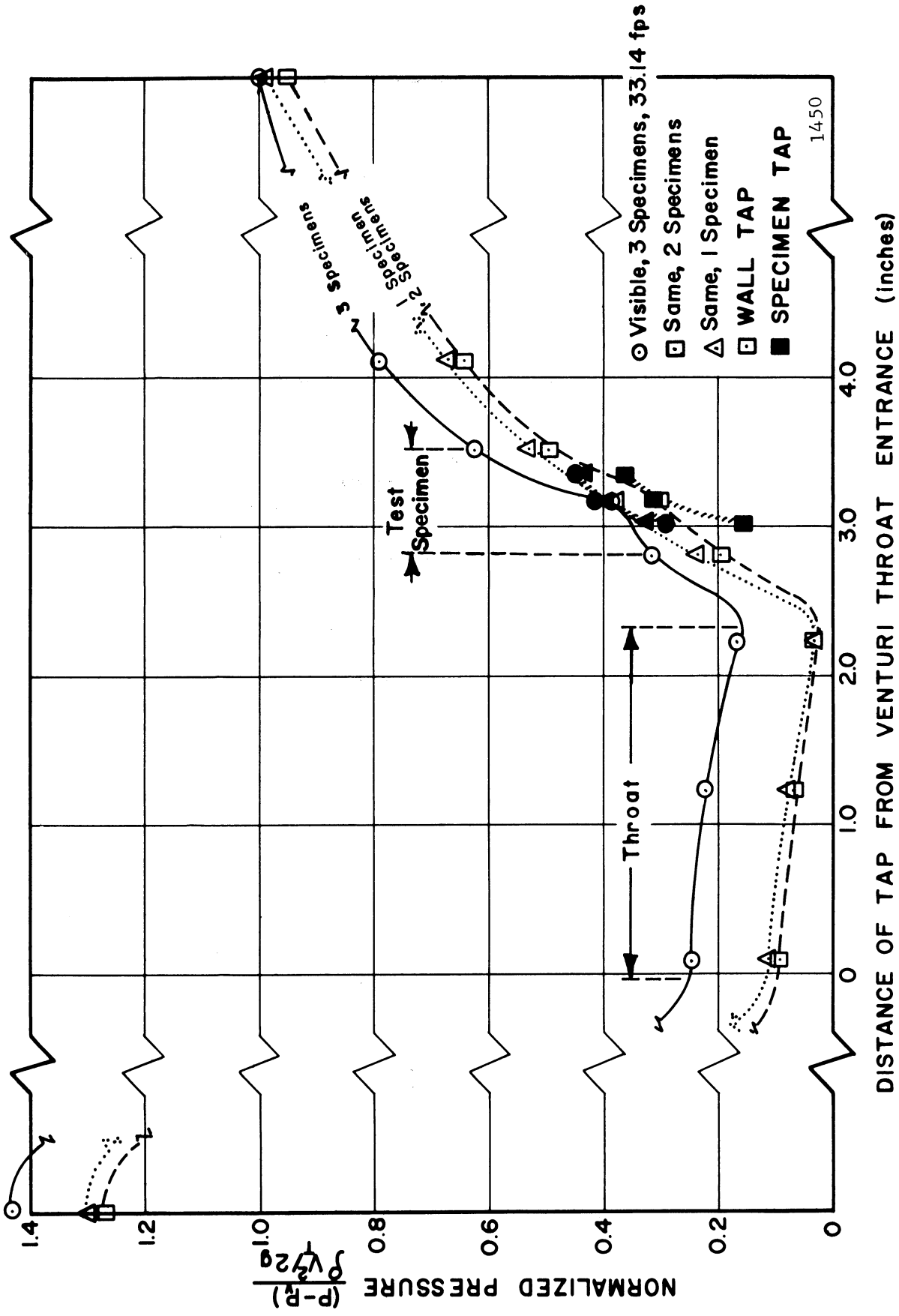

Fig. 32.--Normalized pressure profile for velocity of 33.1 ft./sec. for "visible initiation" in "dry" mercury with one, two and three specimens.

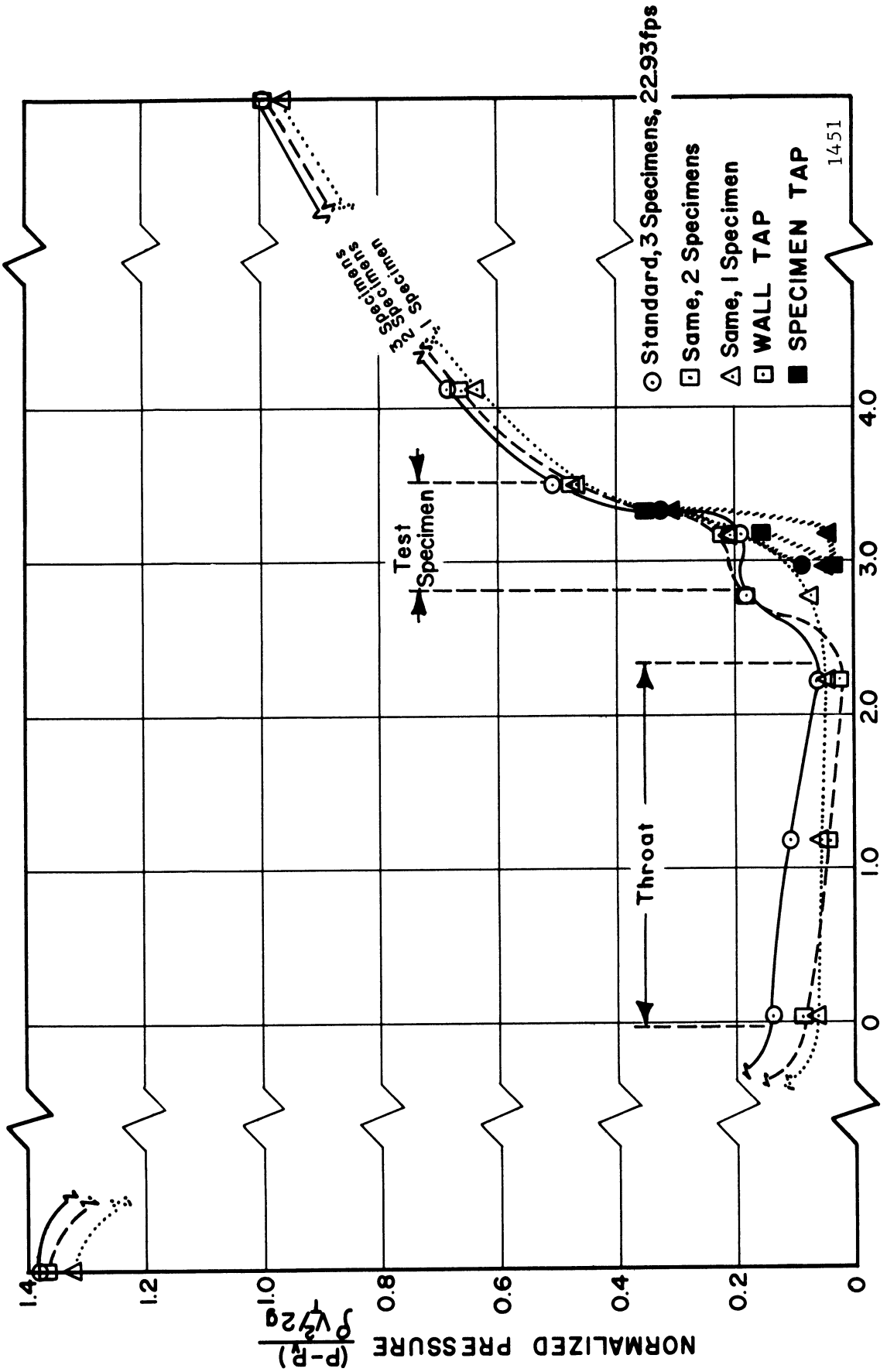

Fig. 33.--Normalized pressure profile for velocity of 22.9 ft./sec. for "standard cavitation" in "dry" mercury with one, two and three specimens.

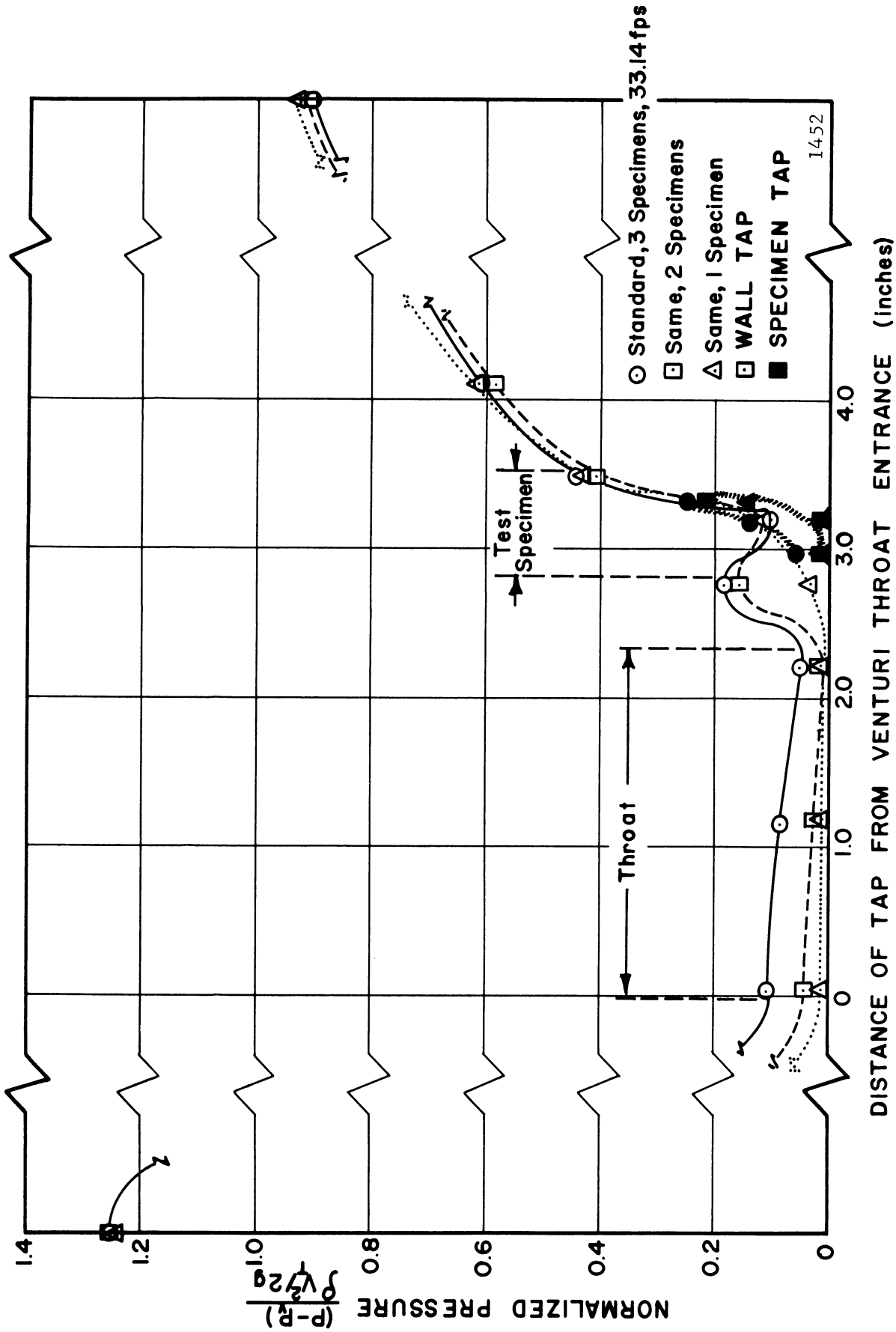

Fig. 34.--Normalized pressure profile for velocity of 33.1 ft./sec. for "standard cavitation" in "dry" mercury with one, two and three specimens.

Table 1 that the actual pressure above vapor pressure gradient on the surface for the mercury, two specimen symmetrical arrangement at 34 feet per second is almost identical to that for the water three specimen symmetrical arrangement at 200 feet per second. Still, the damage obtained in mercury on most materials is about the same as that obtained in water, thus, with regard to the above statements, indicating a similar cavitating situation in mercury.

Previous work done to measure the extent of the cavitation regime with test specimens in the venturi via void fraction techniques[38] has shown that the apparent visual termination of the cavitation cloud on the test specimen surface does coincide with the point of maximum fluid void. However, a closer examination of the appropriate data, Figure 35 (reproduced from the above reference), shows that there is a fair amount of void present in the mercury out to the end of the specimen for "standard cavitation" in mercury, where the visual termination is at the center. This tends to confirm the earlier statements as to the existence of bubbles above the specimen surface over the downstream half of the surface.

B. High-Speed Photography of Cavitation Regime

1. General

In a highly transient phenomenon such as cavitating flow of the type under examination, it is impossible to observe any detail at normal visual speeds. In addition, for complicated flow situations, such as this test-specimen and venturi combination, no reasonably complete

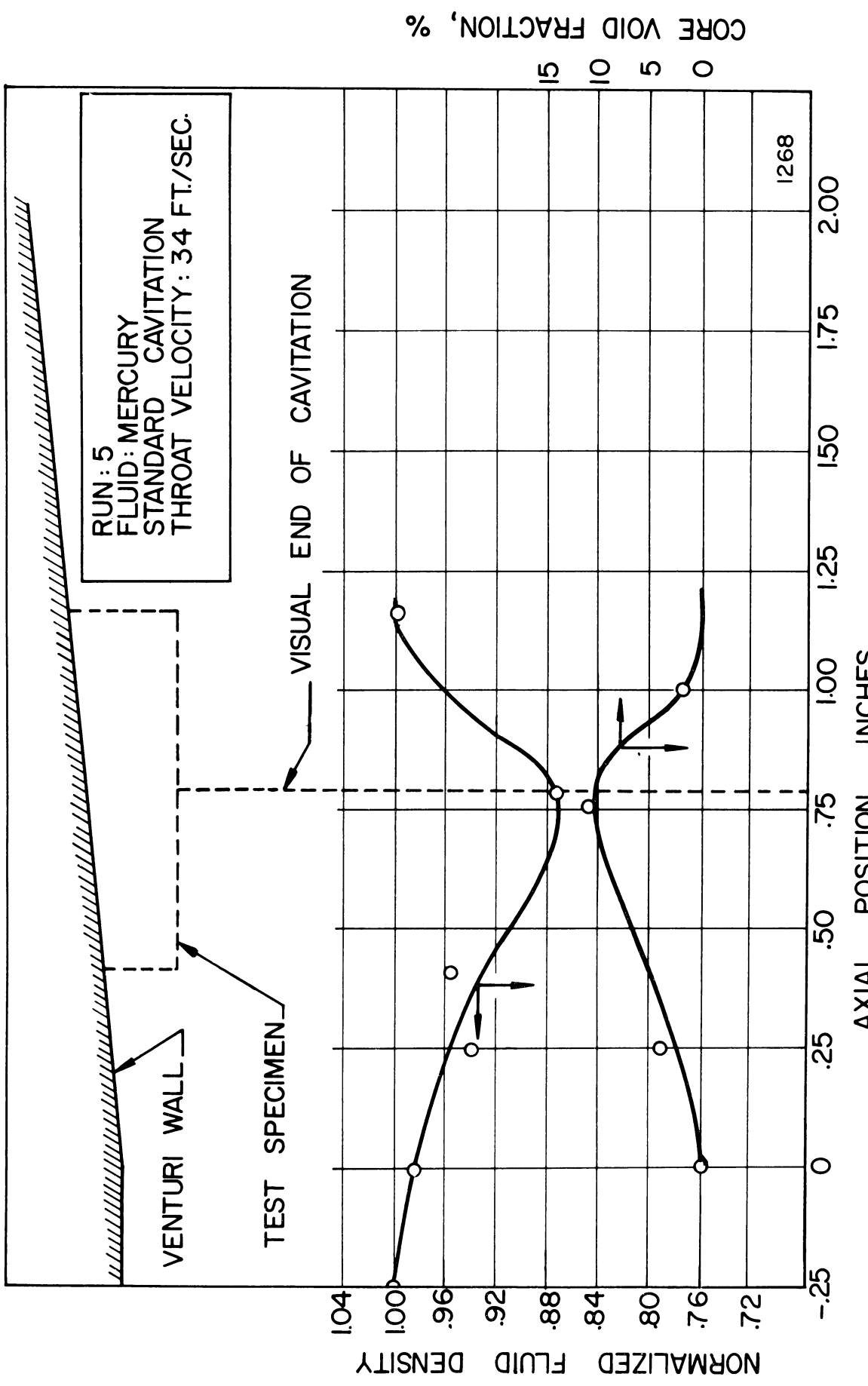

Fig. 35.--Normalized fluid density and core void fraction vs. centerline axial position for "standard cavitation" in mercury at a throat velocity of 34 ft./sec.

theoretical treatment is currently possible. Thus, high-speed photography becomes a very useful technique for detailed understanding of the flow patterns. The goal thereof is to observe the flow regime at normal visual speeds, including hopefully the collapse of cavitation bubbles and the corresponding surface damage. Due to the very transient nature of this phenomenon and the obtainable equipment, however, this has not been fully possible.

2. Motivation

Many theoretical treatments and theories have been advanced concerning the pressures and forces produced by the collapsing cavitation bubbles. Also, it has been postulated that a spectrum of bubbles exist, and that this is related to the size spectrum of the pits produced on the damaged surface.[40] It was hoped to be able to photograph the flow and visually determine the size spectrum of bubbles that came into contact with the test specimen surface. This spectrum of bubbles could then be related to the spectrum of pits that are observed on the damage specimens. Due to its opacity, mercury seems to offer an especially good opportunity for such a study.

The photographic technique, however, was attempted both in water and mercury, and as expected, it proved difficult to obtain suitable information in the water system. In the mercury system, however, the technique worked well. The specimen surface to mercury interface was clearly observed, and the only bubbles that appear on the film are those in direct contact, in some period of their life history, with the test specimen surface. It was not possible to record the number and size

spectrum of the bubbles in contact with the surface, for the particular experimental set-up considered. However, some indication as to the size and number ranges were obtained. It is not meant to imply that necessarily only those bubbles in direct contact with the surface are responsible for the damage. In fact, the observations have not shown this to be the case, as is discussed later.

Two of the more prominent hypotheses regarding the bubble implosion and the resulting surface damage are: (1) the spherically symmetric collapse model[2] leading to the imposition of shock waves on the surface, either during the initial collapse, or more probably, according to recent theoretical studies,[41,42,43] during a subsequent rebound, and (2) the liquid jet impact model where the bubble collapses in a non-spherical-symmetric manner such that a jet of fluid pierces the bubble in the later stages of collapse, impacting on the surface.[17] Both experimental[17,18,42] and theoretical[19] evidence now indicate that such a collapse model does in fact occur, although perhaps not in all cases.

Recent theoretical studies[41,42,43] indicate that the bubbles must be very close to the surface if the forces produced are to be of a damaging magnitude, and then only rebounds would be damaging.*

3. Qualitative Observations

The high-speed movies of the mercury cavitation cloud indicate that the local cavitation induced by the specimens themselves is of

---

*This is assuming that the center of collapse is stationary during collapse, whereas actually the bubble would,[19,44,45] at least to some extent, migrate toward the surface during collapse. In addition, the close proximity of the surface would obviously prevent a symmetrical collapse.

primary importance with respect to the damage received. This has become apparent in the water venturi tests where the complete cavitation cloud can be observed,[40] but until now was only a postulation for the mercury tests. A cavitation region appears to initiate on the nose of the test specimen and extend downstream along the specimen to a point determined by the back pressure at venturi outlet. The visual termination has been fixed at the axial center of the test specimen for this portion of the study ("standard cavitation"). A more or less stationary "void" is attached to the nose of the specimen from which individual bubbles detach and are swept downstream with the fluid. The high-speed motion picture observations have shown an oscillation in the apparent ending point of the cloud. However, no fixed frequency has been found. The attachment of a cavity at the nose of the specimen, and the subsequent detachment of bubbles from it, has been verified by the electrode specimen tests described later.

Typical sequential photographs from the high-speed motion pictures for the two-specimen symmetrical venturi arrangement are presented in Figures 36, 37, 38 and 39. It is observed that the cavitation cloud consists of two separate wakes trailing downstream along the surface near either edge and also a wake along either radial side of the specimen. Only the very edge of this cloud is visible in the photographs, i.e., the side nearest the wall of the venturi, as the rest is obscured by the opaque mercury. The pattern of pitting damage on the test specimens matches the observed cavitation cloud pattern in that the heaviest concentration of pitting lies on the polished surface along the edges

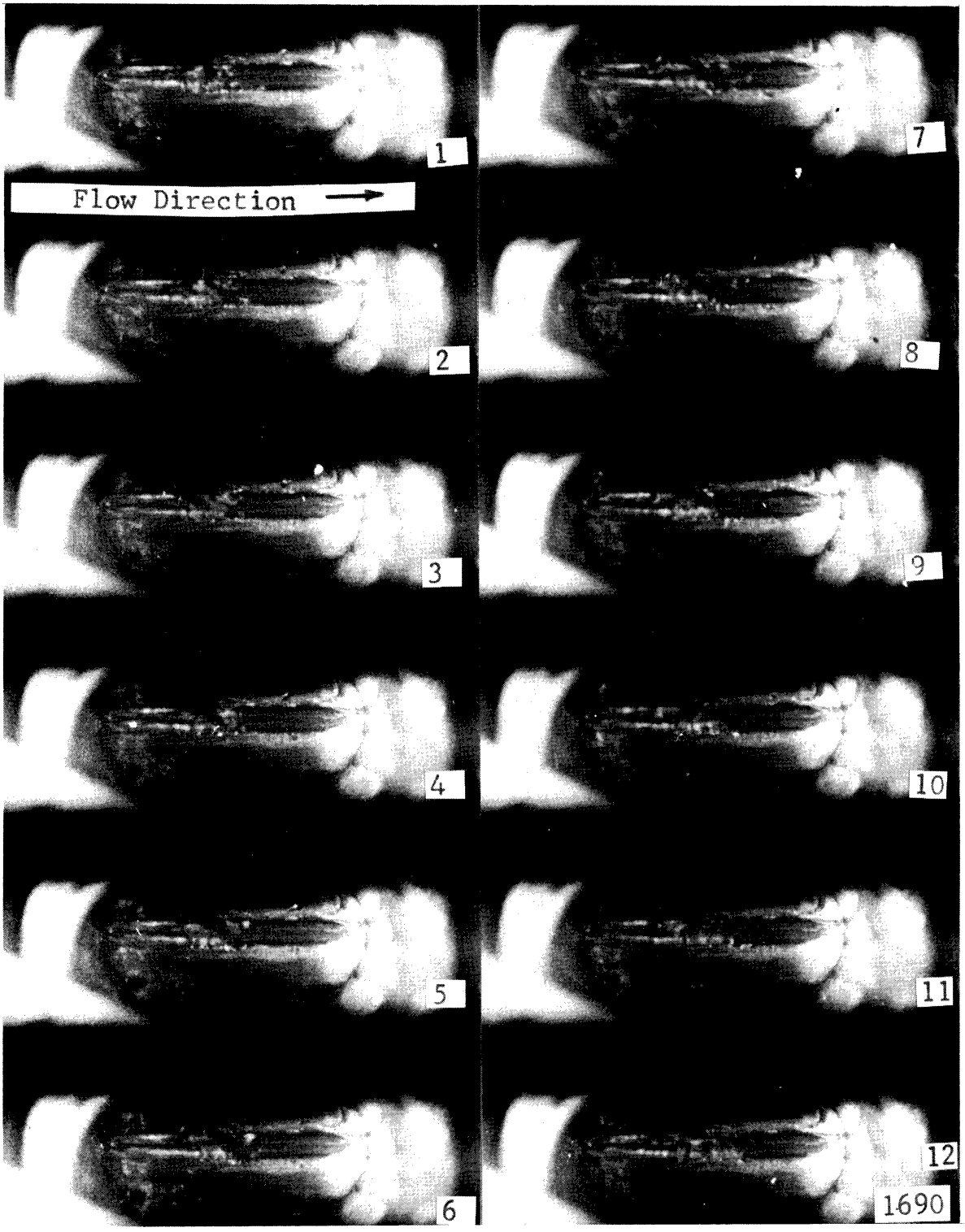

Fig. 36.--Typical sequence of pictures of cavitating flow on specimen surface in mercury at 34 ft./sec., exposure time per frame = 39 microseconds, time between frames = 116 microseconds (8,650 pps), Reel #19, for two specimen symmetrical arrangement, "standard cavitation."

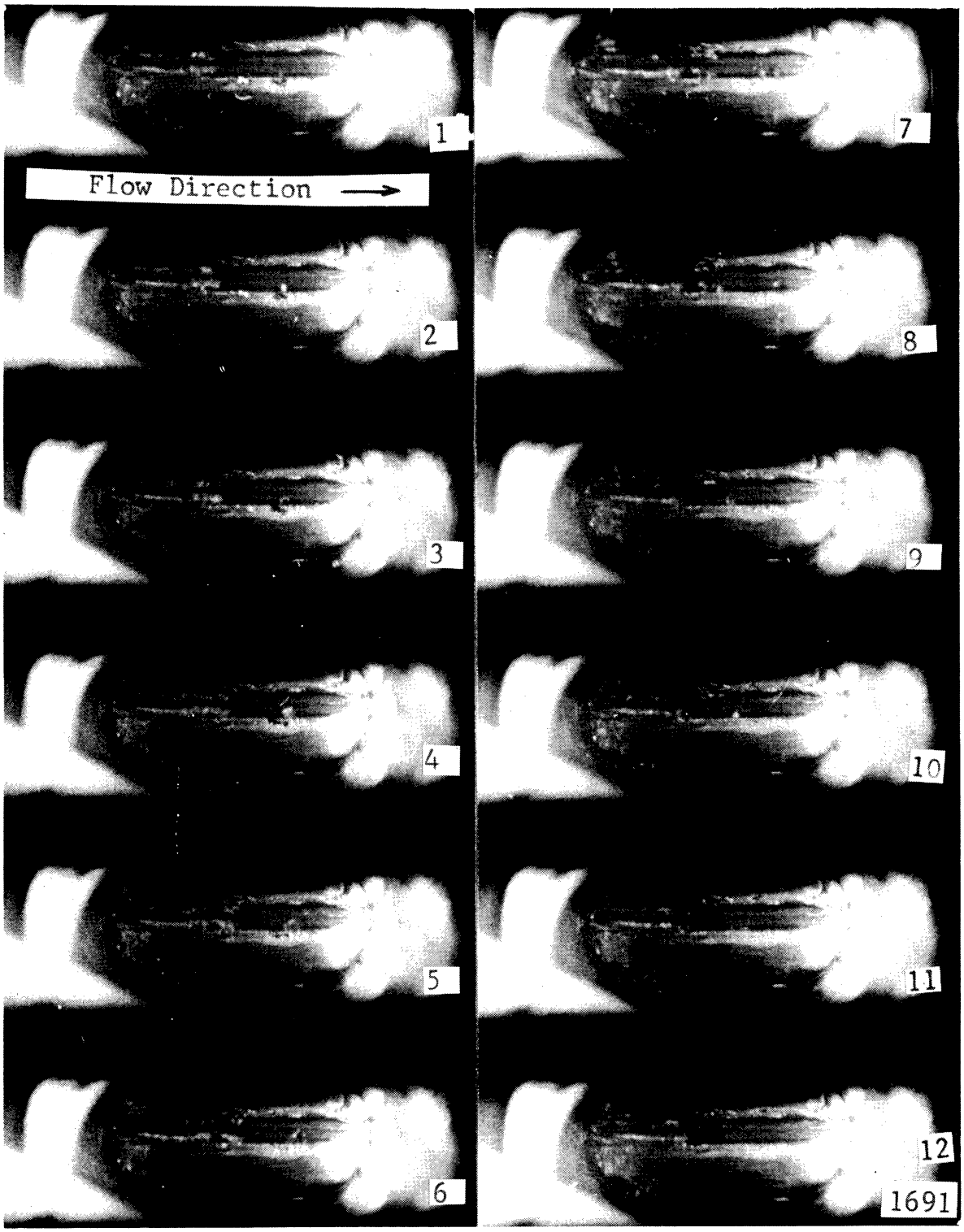

Fig. 37.--Typical sequence of pictures of cavitating flow on specimen surface in mercury at 34 ft./sec., exposure time per frame = 26 microseconds, time between frames = 79 microseconds (12,700 pps), Reel #19, for two specimen symmetrical arrangement, "standard cavitation."

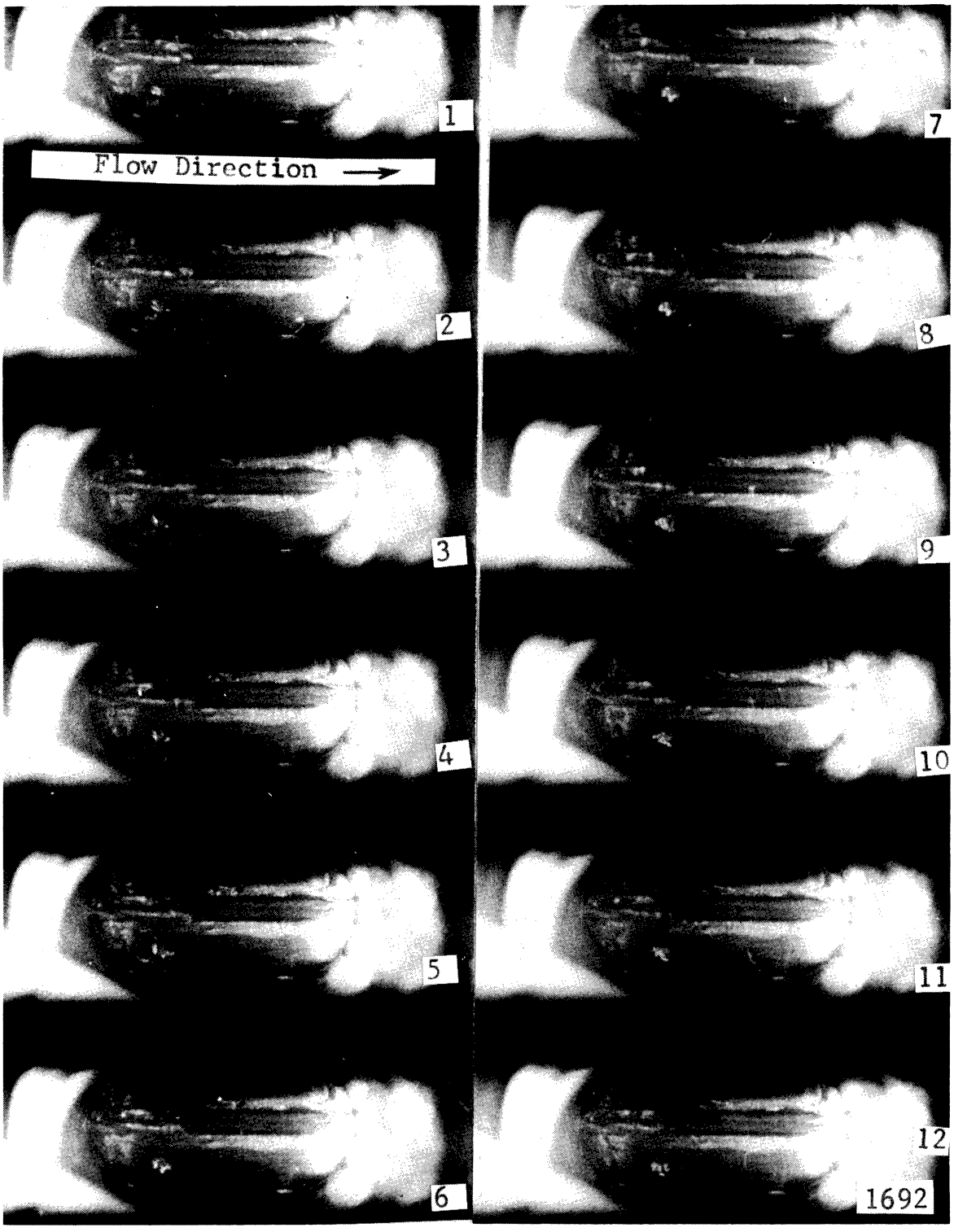

Fig. 38.--Typical sequence of frames of cavitating flow on specimen surface in mercury at 34 ft./sec., exposure time per frame = 25 microseconds, time between frames = 76 microseconds (13,200 pps), Reel #19, for two specimen symmetrical arrangement, "standard cavitation."

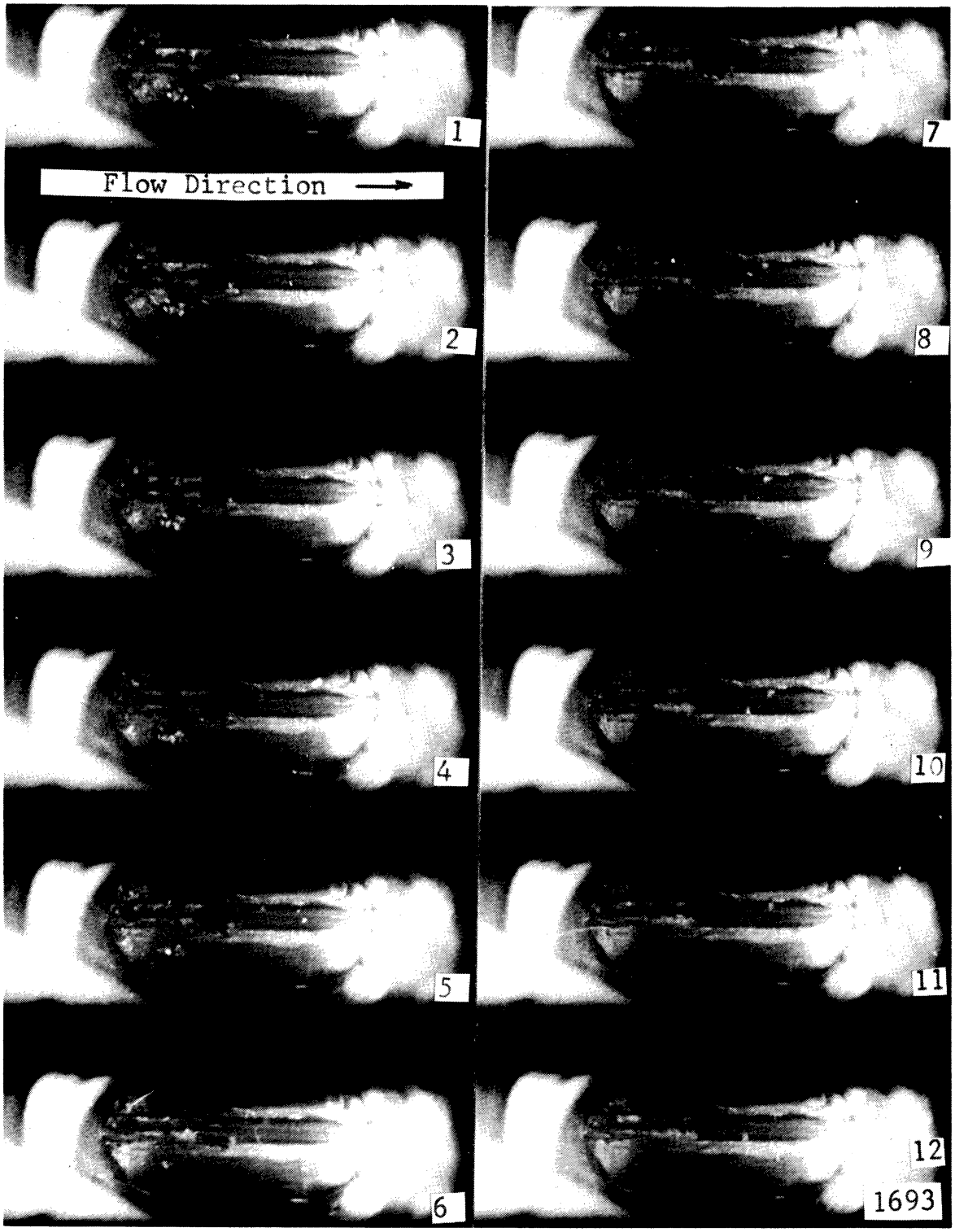

Fig. 39.--Typical sequence of frames of cavitating flow on specimen surface in mercury at 34 ft./sec., exposure time per frame = 25 microseconds, time between frames = 74 microseconds (13,450 pps), Reel #19, for two specimen symmetrical arrangement, "standard cavitation."

and on the sides perpendicular to this. (See Figures 57 and 58.)

Figure 40, for the same flow conditions as Figures 36 through 39, with the exception that only one test specimen was in place in the venturi, shows a more uniform cloud on the surface and relatively more bubbles on the surface.

In several bubble sequences from this Figure, bubbles along the side of the specimen (actually in the corner formed by the side of the specimen and the venturi wall) appear to transform from an oblong to a spherical shape during collapse (Figure 40, frames 7 to 12 and 15 to 27). This observation appears inconsistent with the nonspherical collapse model already discussed. However, the depth of view in the photographs is not clear and the influence of the corner is uncertain. In all bubble sequences observed on the surface, the bubbles retain their circular form during collapse to as small a diameter as can be observed, but to what smaller radius they remain hemispherical cannot be ascertained. A relatively stationary void at the nose of the specimen is indicated, and is confirmed by the electrode specimen tests discussed later. The existence of more bubbles and a steeper pressure gradient on the surface (Figure 34) for this condition than for the two specimen case, indicates that it should be a more damaging condition, although this has not yet been verified.

Figure 41 shows the flow condition for the three specimen symmetrical arrangement in water at a throat velocity of 97 feet per second for "standard cavitation." In this case "back-lighting" was used to silhouette the cloud, which is possible for a transparent fluid. There

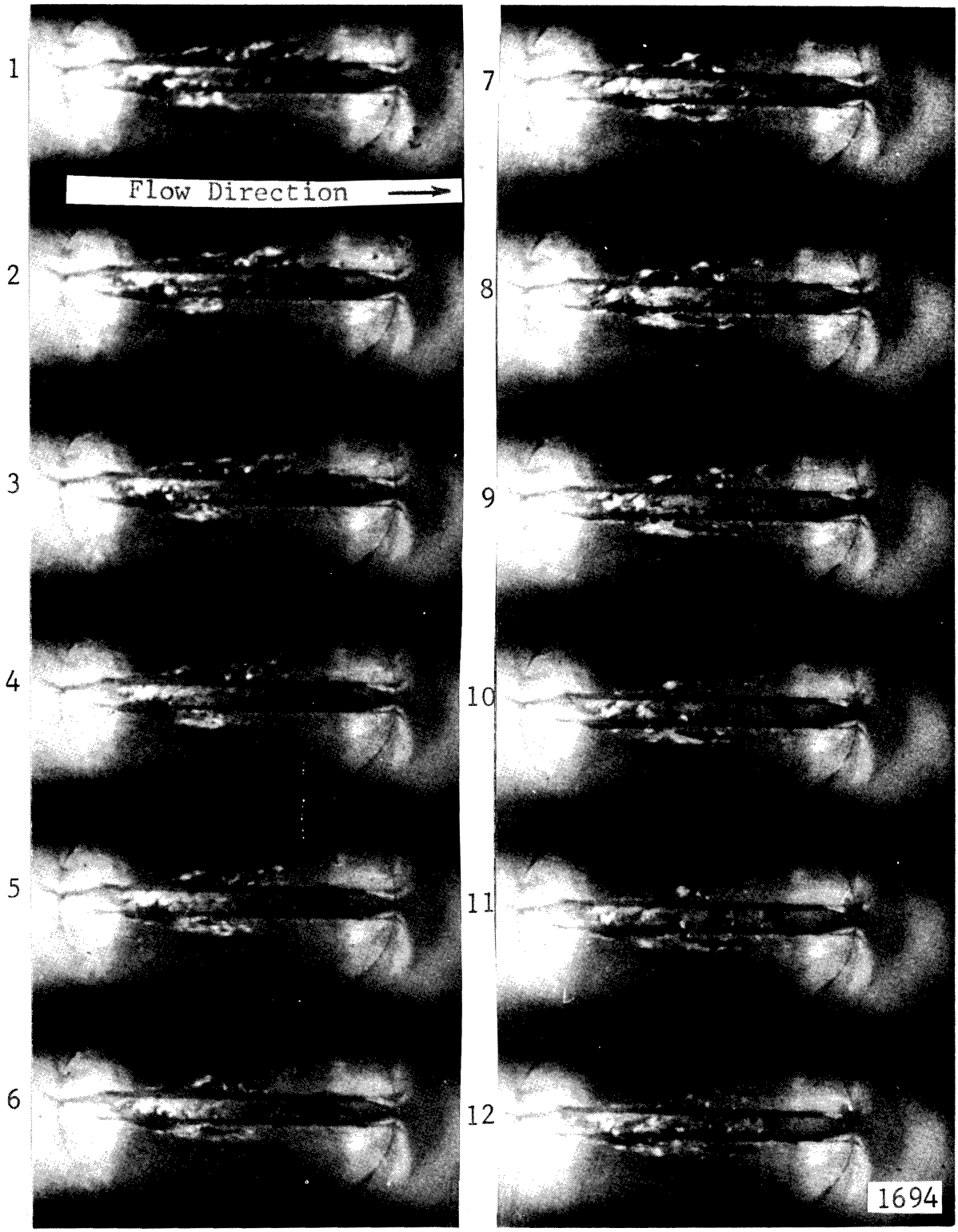

Fig. 40.--Typical sequence of frames of cavitating flow on specimen surface in mercury at 34 ft./sec., exposure time per frame = 30 microseconds, time between frames = 90.5 microseconds (11,100 pps), Reel #2, for single specimen arrangement, "standard cavitation."

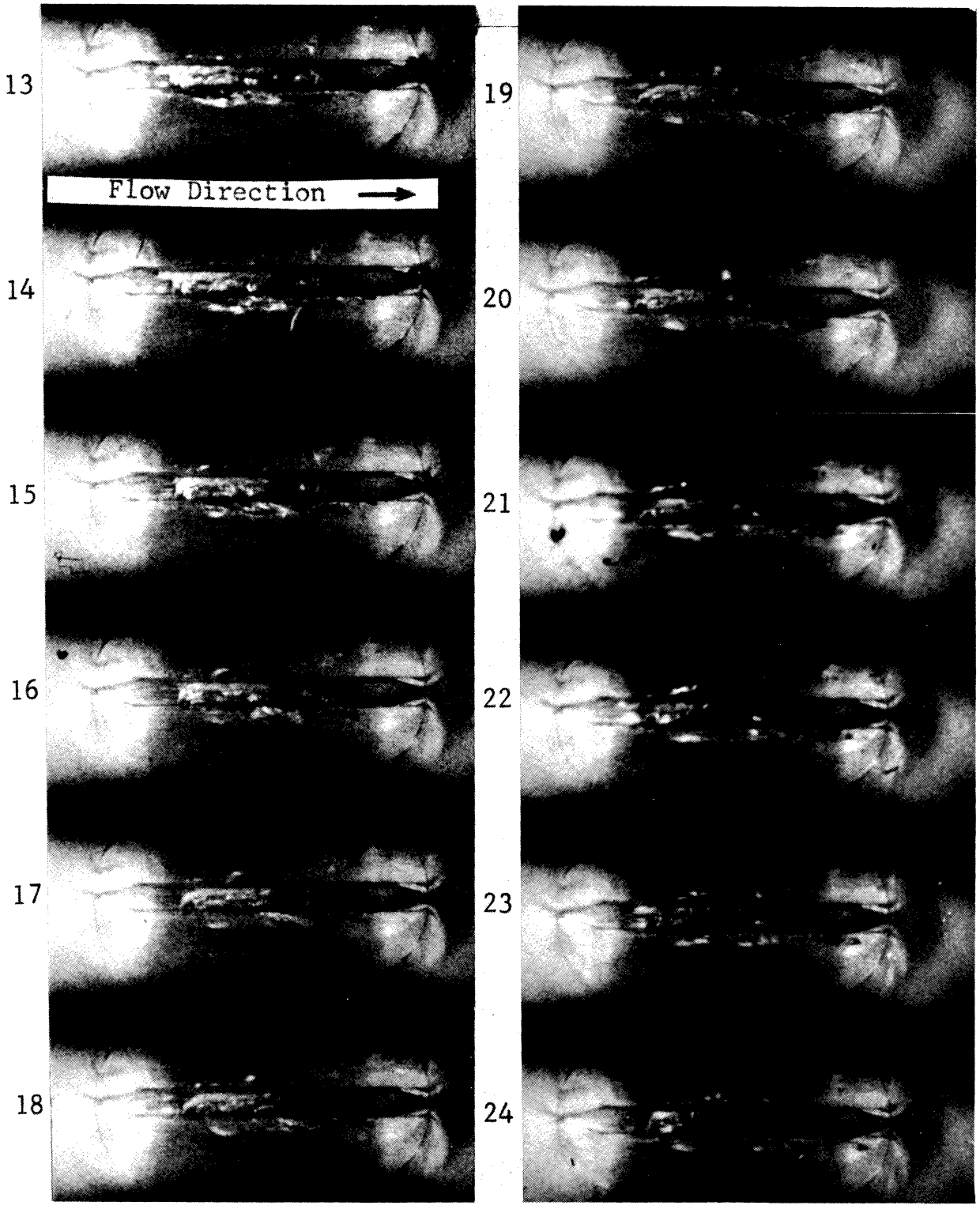

1694(cont'd 1)

Fig. 40.--(Continued)

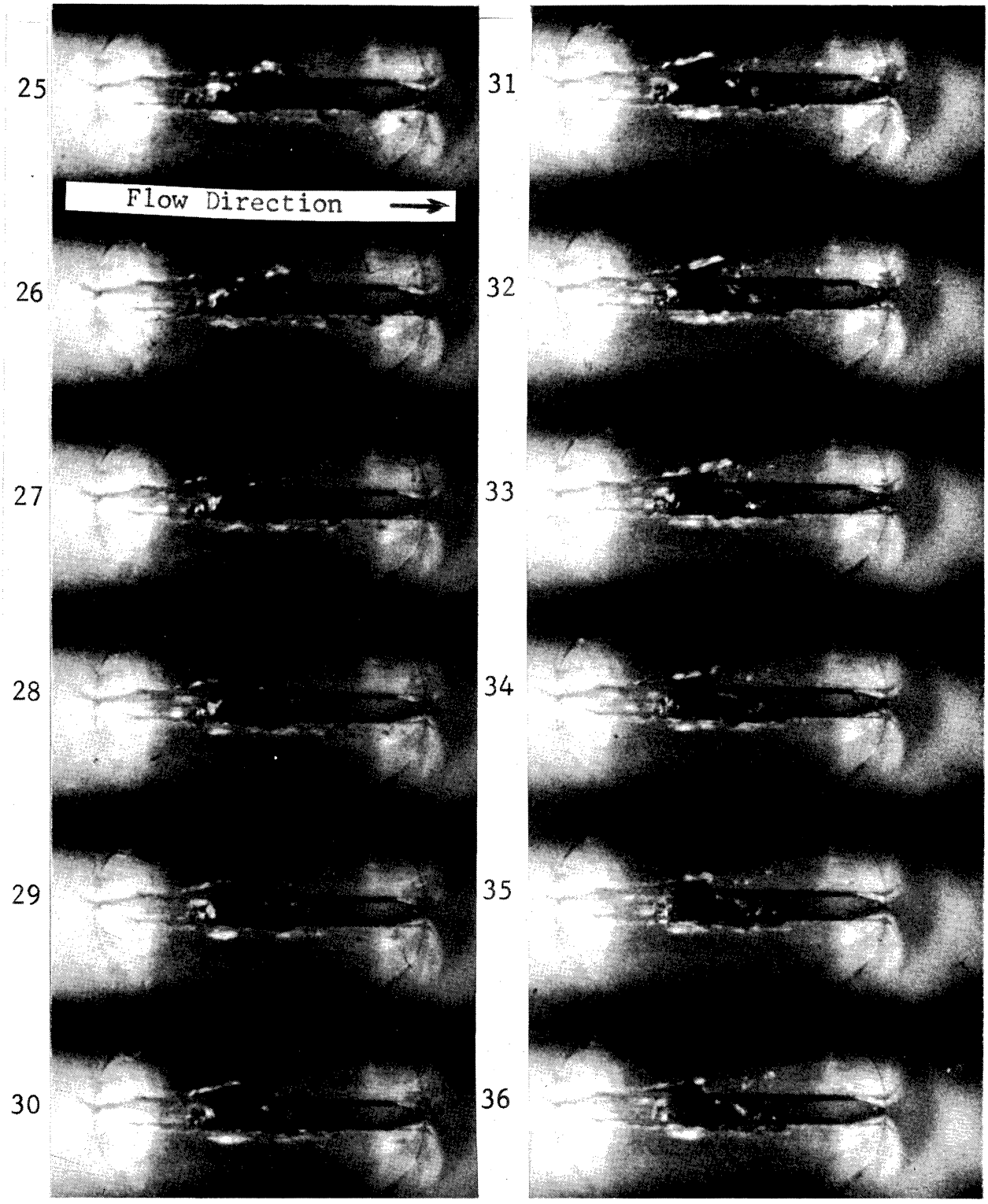

1694(cont'd 2)

Fig. 40.--(Continued)

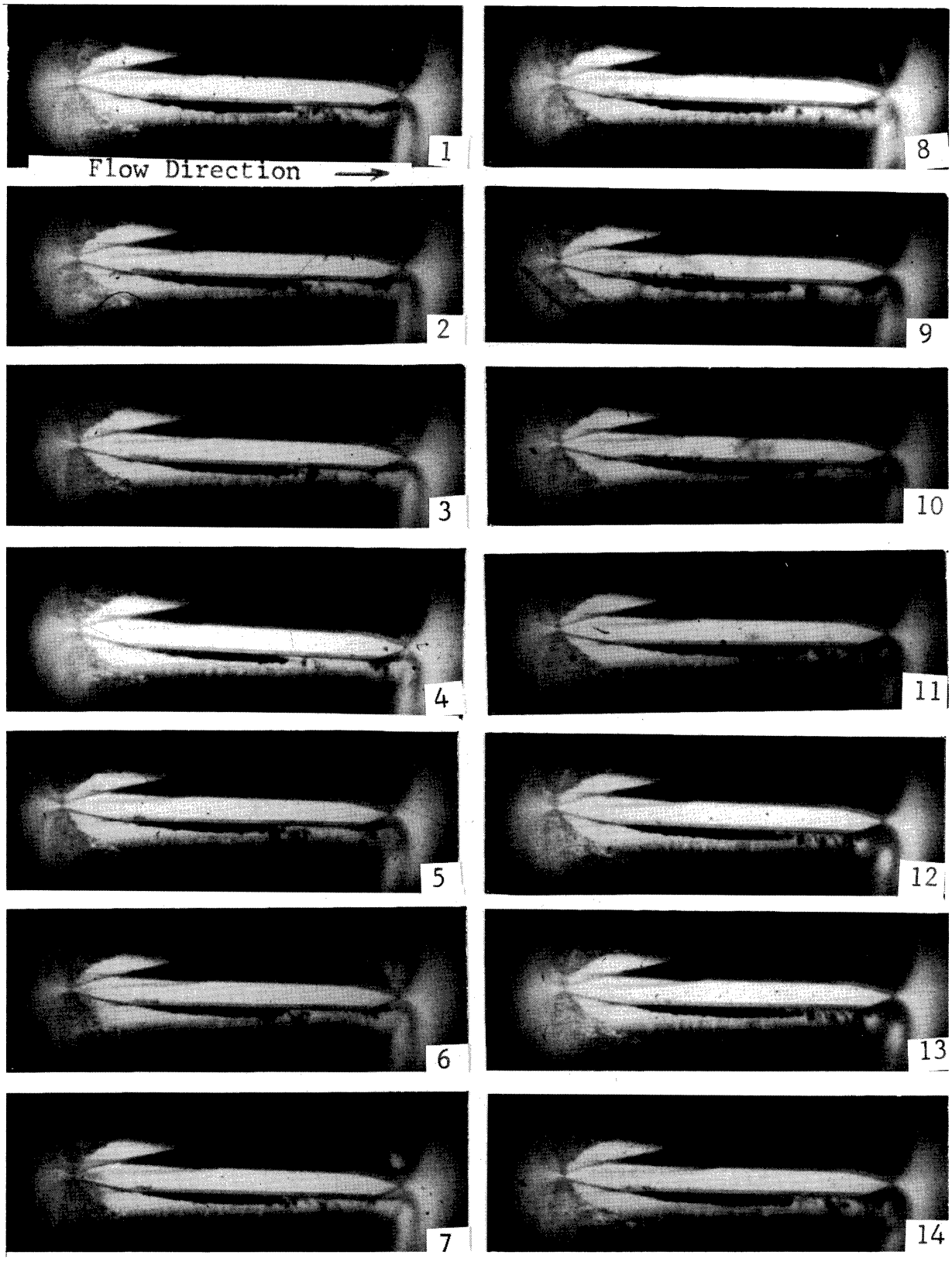

Fig. 41.--Typical sequence of frames of cavitating flow on specimen surface in water at 97 ft./sec., exposure time per frame = 1.2 microseconds, time between frames = 160 microseconds (16,250 pps), Reel #223, three specimen symmetrical arrangement, "standard cavitation."

are two wakes along the edge of the polished surface, as in the mercury case, extending downstream from the nose. There are also heavy cavitation wake formations along the radial sides of the specimen. Of particular interest is the appearance of cavitation bubbles beyond the surface (i.e., further into the fluid) in frames 8 through 11. Since the focal plane of the camera was adjusted to the fluid-specimen interface, and since the depth of focus with this lens system is very shallow, it can be concluded that these bubbles are removed from the surface a distance of about 1/16 to 1/8 of an inch. The small bubbles that are evident near the ends of the surface wakes are on the surface, but no bubbles are noted on the downstream portion of the surface. Typical damage patterns for this flow condition (Figures 63, 65, e.g., presented later) show that the pitting distribution is heaviest on that portion of the surface where no bubbles were observed. The following conclusions can be made with reference to the above observations:

1. Since no bubbles are observed on the surface in the downstream area for an observation time of about 0.1 seconds, it can be assumed that the time interval between bubbles is at least 0.1 seconds. Since the pitting rate in this area has been established as 0.3×10^{-2} pits per second (i.e., $\sim 10^{3}$ pits in 100 hours), Figure 91, the ratio between bubbles and pits could be as large as 3×10^{3}:1. This would be in agreement with the ratio of 10^{4}:1 as reported by Plesset[54] recently for an ultrasonic test.

2. Since no bubbles appear on the surface during this observation time of 0.1 seconds, but one group was observed in the background, perhaps these are the damaging ones which are drawn toward the surface during collapse as has been suggested on a theoretical basis recently.[19,44,45]

All of the aforementioned photographs of the flow have been taken through the transparent specimen-holder apparatus. However, with water, it was possible to photograph the flow from the side, through the venturi wall. The field of view was enlarged to include the complete vertical height of the venturi and the throat exit. Figure 42 shows this view in the water system for the same flow conditions as Figure 41. The detail is not optimum, but still bubbles can be observed near the throat exit, which disappear into the overall cloud in the venturi further downstream. The significance of the cavitation induced by the specimens themselves is made evident in these pictures. The side wakes are clearly shown, in addition to individual bubbles in the immediate wake behind the specimens. The elapsed time between frames is too large in all of these pictures, due to equipment limitations, to allow the following of individual bubbles at the higher velocities.

4. Quantitative Observations

From the high-speed photographs in the mercury system a number distribution of bubbles versus axial position on the specimen has been estimated on the basis of about one hundred frames (Figure 43), as well as the maximum and minimum bubble diameters observed on the surface. The upstream one-third of the specimen appears to be under an almost

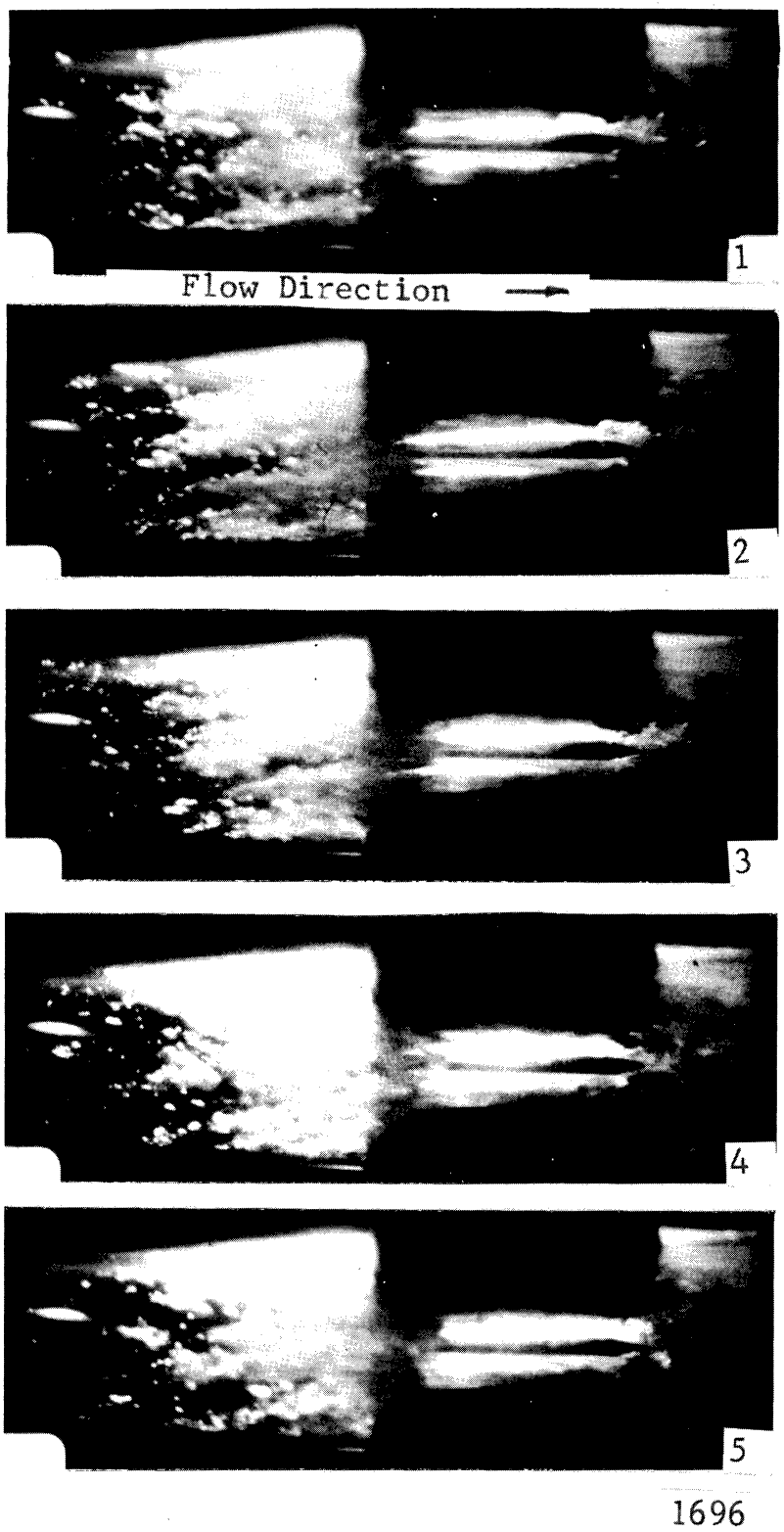

Fig. 42.--Typical sequence of frames of cavitating flow from side in water at 97 ft./sec., exposure time per frame = 1.2 microseconds, time between frames = 181 microseconds (5,500 pps), Reel #226, three specimen symmetrical arrangement, "standard cavitation."

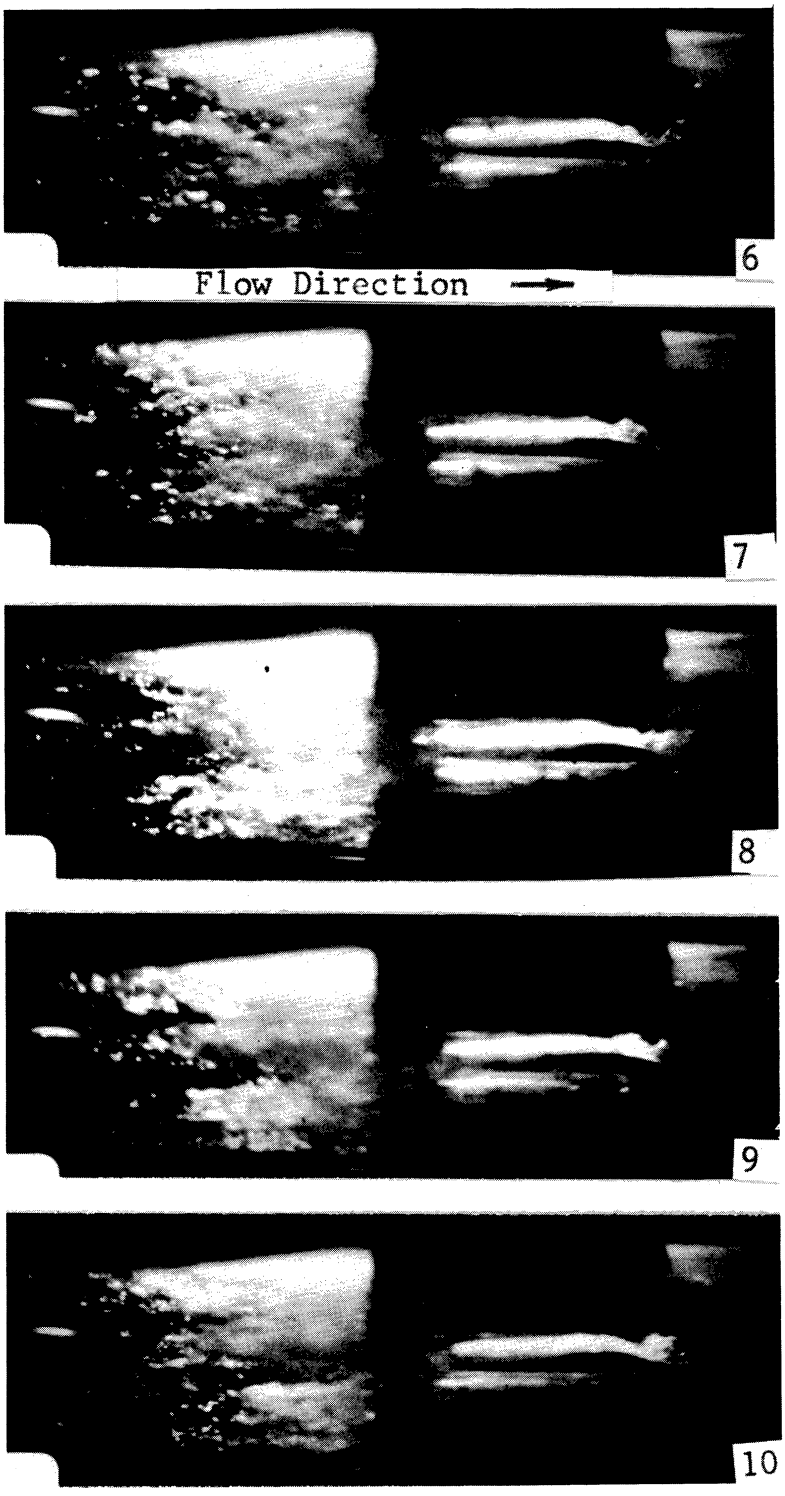

1696(cont'd 1)

Fig. 42.--(Continued)

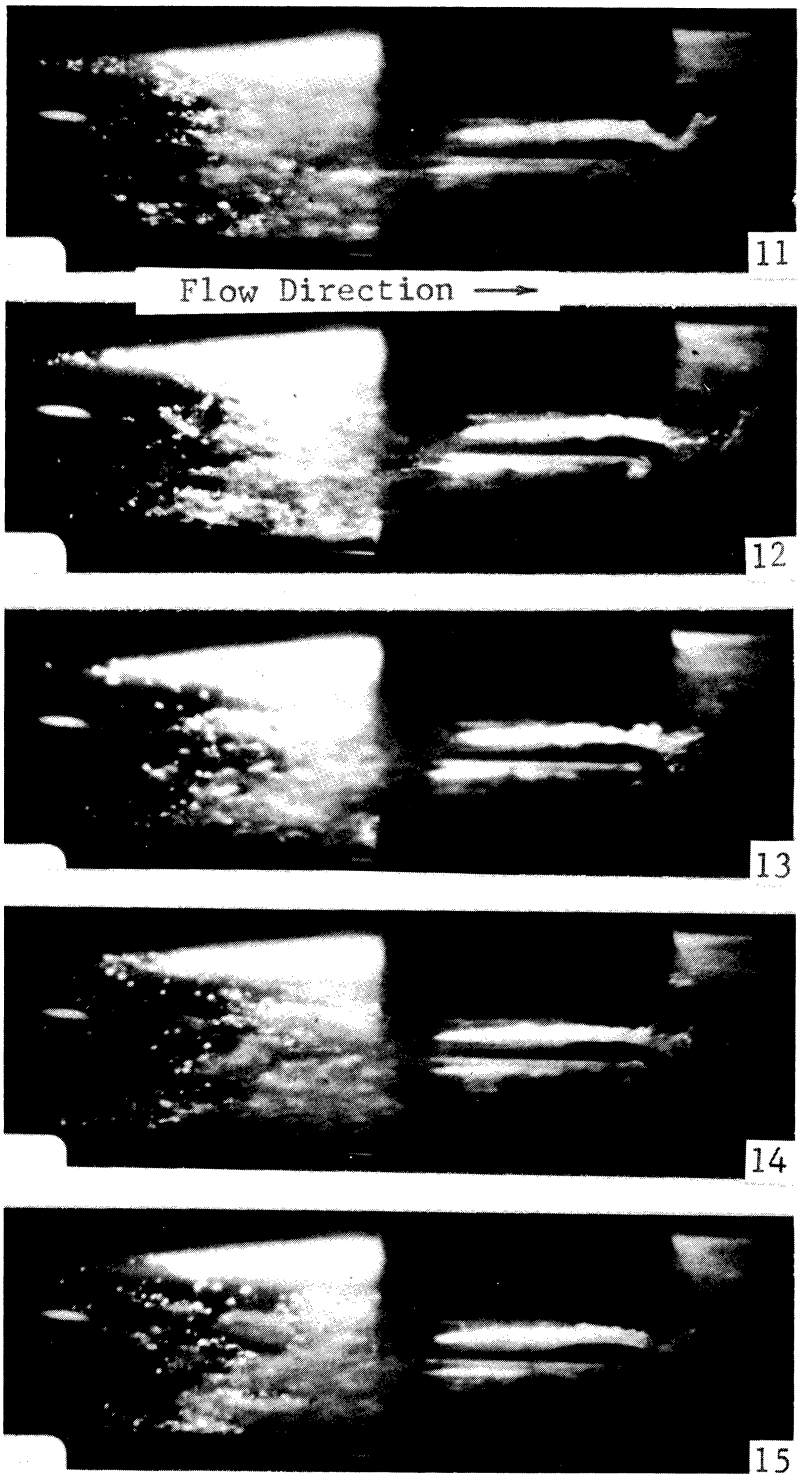

1696(cont'd 2)

Fig. 42.--(Continued)

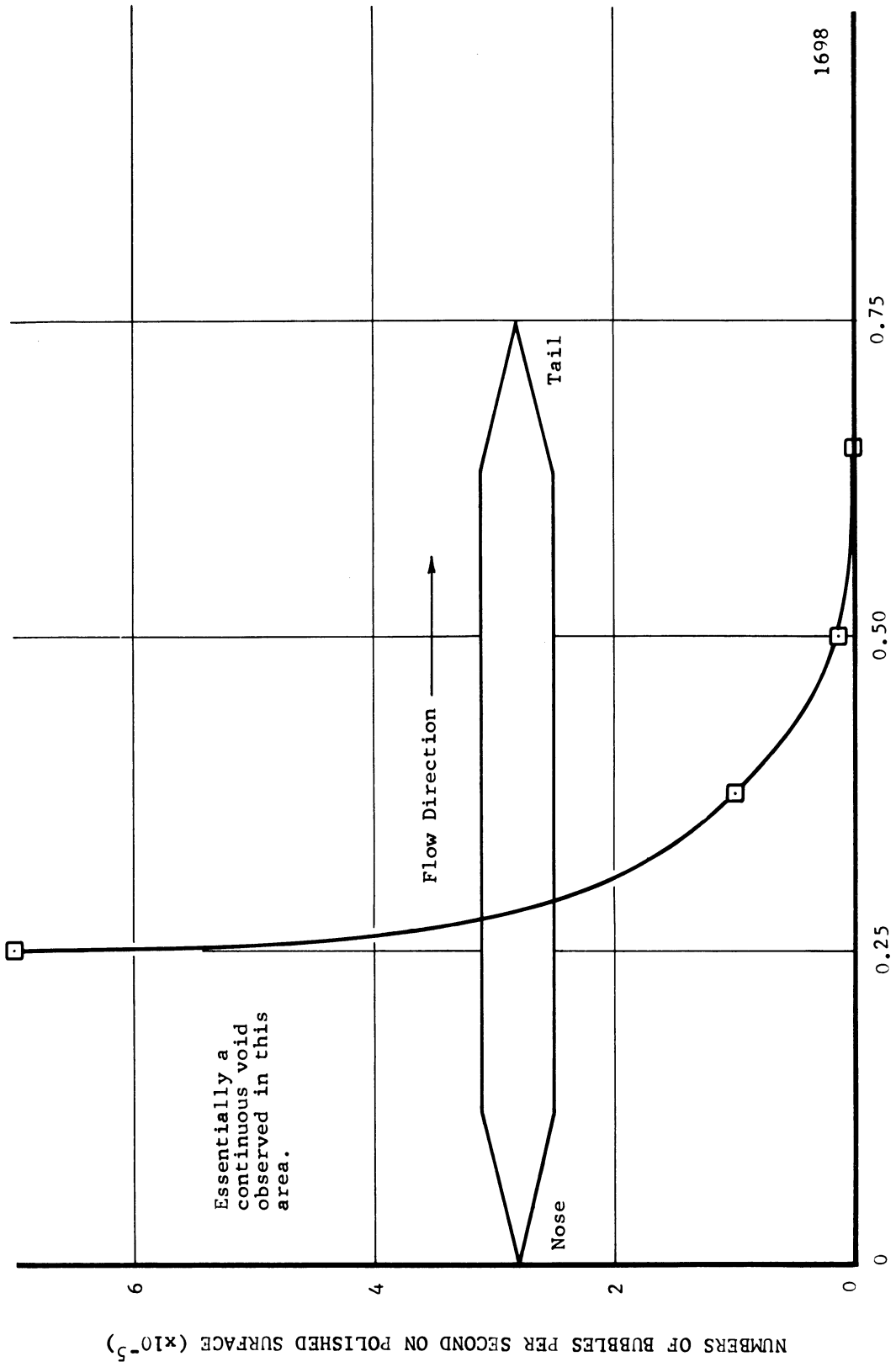

Fig. 43.--Bubble number distribution vs. axial position on test specimen surface in mercury at 34 ft./sec., for two specimen symmetrical arrangement, "standard cavitation," Reel #19.

continuous void, as confirmed by the electrode specimen tests discussed later. Downstream of the void region the number density of bubbles decreases very rapidly. However, the actual numbers of bubbles per second is very large with respect to the numbers of pits per second which occurred, being larger by a factor of about $\sim 10^5$ at the center of the specimen and $\sim 10^3$ near its tail, discussed in greater detail later.

The observed bubbles ranged between $\sim$ 30 and $\sim$ 5 mils diameter, the lower cut-off being due primarily to the limited resolution of the photographs. Also, due to the limited framing rate of the available equipment, it is not possible to determine the relation between a given bubble observation and the stage in its life history, at which it has been observed. Hence, one can only say that bubbles with a maximum diameter of at least 30 mils exist adjacent to the specimen and in very large numbers compared to the number of pits, most of which were less than 0.1 mil diameter. It is thus clear that to photograph a pit being formed in this type of system where the event is not triggered (as with spark-induced bubbles) would require extreme good fortune in sampling the very small applicable portion of the total time, and also very large photographic magnification and resolution. The limitations of photographic technology are such that this goal does not appear presently attainable.

For typical mercury samples (Figure 57 and 58), numerous small pits are observed on the upstream portions of the specimen and relatively smaller numbers of larger pits on the downstream portion, where the pressure is higher. This pitting distribution and its relation to the measured fluid pressures is discussed in greater detail later.

However, since, in general, a larger bubble requires a longer time to collapse, it will penetrate further downstream before collapsing, and as analyses[42,e.g.] show, there will then be larger pressures imposed by it on adjacent structures.

This hypothesized pattern of events is fully substantiated by the observed pitting patterns. In general, the high-speed photographs show very few bubbles on the downstream portions of the specimen polished surface where the maximum numbers of large pits are observed, and very little damage, if any, is observed on the upstream portions of the surface where the relatively stationary void is attached, however, the static pressure is close to vapor pressure, and hence does not provide the required driving force for a violent collapse in the void region.

The existence of a large ratio between observed numbers of bubbles and resulting pits on surfaces exposed to cavitation regimes, as experienced here and elsewhere, is thought to be an area of basic interest to the overall understanding of the cavitation phenomenon. In this particular investigation it has been observed that this enormous ratio increases with distance in an upstream direction where the mean static pressures on the surface are lower. Considering the presently most likely mechanism of damage as being the unsymmetrical collapse of a bubble with a resultant fluid jet of high velocity at the end of collapse impinging on the surface, this large ratio can be explained. It was observed in our own venturi tests[42] that the resultant fluid jet is formed in a direction parallel to the fluid streamlines which, in the case of the venturi, is also normal to the pressure gradient. To cause

damage to a surface oriented parallel to the fluid streamline, as in the present case, it is necessary that the bubble be reoriented during collapse so that the resultant jet is directed towards the surface. Conceivably this could be somehow accomplished by the influence of the adjacent wall. However, in the present case, this reorientation might also be provided by the cavity oscillation as it moves upstream on the specimen surface. When the cavity retreats upstream, a nonspherical bubble sufficiently close to the surface might be tipped by the drag forces on its side nearest the specimen surface, so that the resultant fluid jet would be directed towards the surface. Consequently, only those bubbles that are located at the precise distance from the wall and are at the proper point of collapse at the moment the oscillation occurs, would be able to damage the surface. From another viewpoint, the bubble must be at the proper distance from the surface, so that it will migrate towards the wall during collapse and be at the proper distance from the wall for the fluid jet to be effective, when it is formed, and the bubble reoriented as discussed above, as suggested by Benjamin and Ellis.[19] This clearly would be a very selective process and could indeed explain the large ratio of bubbles to pits formed. This rather complicated process seems capable of providing the required forces for damage, as opposed to the spherical collapse, and in addition explains the anomaly of the bubble to pit ratio.

Conceivably a pit so formed would have unique characteristics indicating its method of formation. In general, for those specimens traced in the direction of flow for the mercury system, a raised rim is

present around the crater, which is sometimes uniform and more often than not higher on the downstream side. This is consistent with the proposed mechanism as one would expect the reorientation to be incomplete at times, so that the resultant jet would be tipped towards the downstream end of the specimen. Detailed examinations of the damage from the water facility (Figures 85 and 88 e.g.) in general indicate an elongated pit in the flow direction, with a predominant ridge on the downstream end and rather uniform ridges at both sides. This can also be explained by the above damage hypothesis. In this case, the velocity is much higher and consequently the reorientation of the resultant jet towards the surface could not be expected to be as complete, thus giving rise to jets oriented generally towards the surface, but predominantly tipped downstream. That the velocity can be an important factor in the degree of reorientation of the jet is shown in Figure 44, where typical photomicrographs of the damage on the high heat treat copper nickel alloy at a duration of 1 hour are compared at three different velocities. Very little damage is evident at the lowest velocity of 64 feet/second, but the damage present consists of small pits that are essentially round. In the next highest velocity of 97 feet/second the damage is somewhat triangular in shape with the base on the upstream side, as if the force were applied to the surface at about a 45° angle in the direction of flow. At the highest velocity of 200 feet/second the pits are in the form of elongated grooves, noted in all the examinations of damage at this velocity, indicating a force aligned at a smaller angle to the surface and in the direction of flow. Consequently, this would

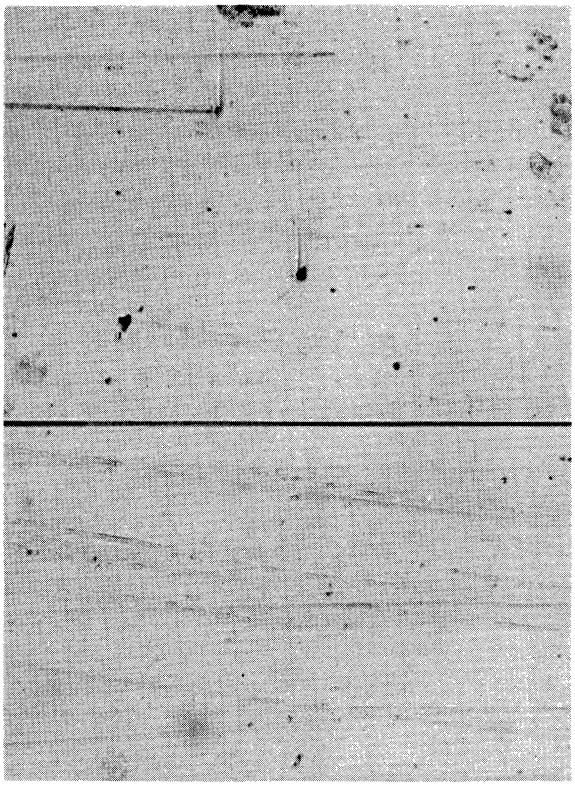

(a)

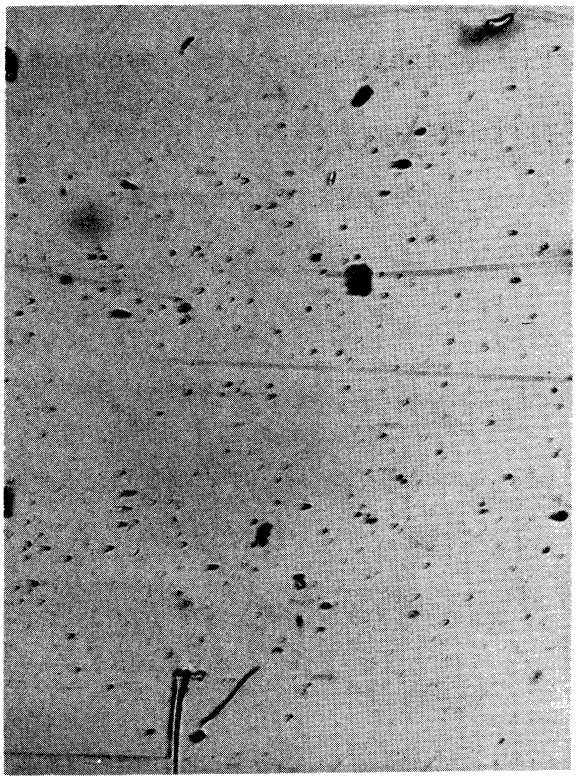

(b)

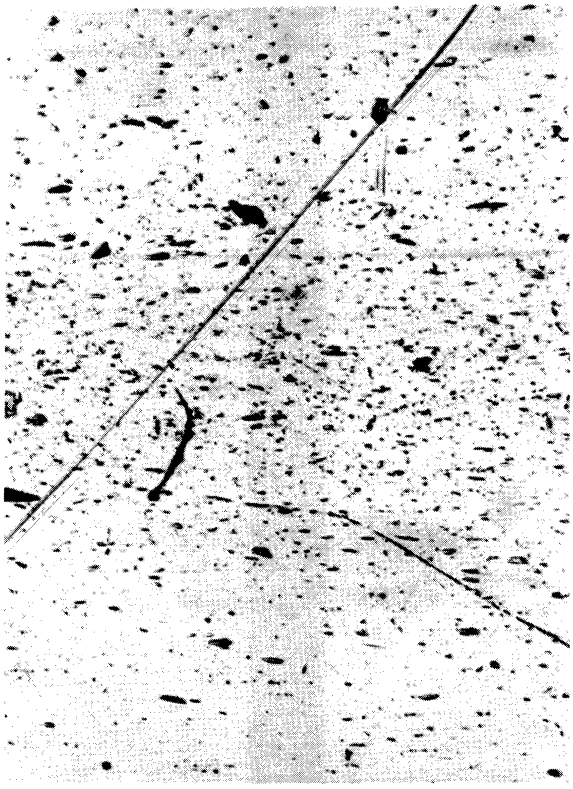

(c)

Fig. 44.--Photomicrographs of cavitation damage on copper-nickel alloy (H.H.Trt), for "standard cavitation" in water at one hour duration, (a) 65 ft./sec., (b) 97 ft./sec., (c) 199 ft./sec.

tend to explain the difference in the basic damage appearance between the water and mercury tests as the velocities were 200 and 34 feet per second, respectively.

It has often been observed that trailing vortices from pump impeller vanes,[48] for instance, are much more damaging to the surfaces on which they impinge than to the initiating vane. This important observation can be explained nicely in light of the above hypothesis. In this case, the bubbles are already moving toward the surface rather than parallel to it as in the venturi, so there may be no requirement for bubble reorientation to the surface. Those bubbles that collapse in close proximity to the surface then need only be at the proper distance from the surface. On the other hand, the initiating surface compares closely to the present specimens. Thus reorientation is required, resulting in fewer damaging bubble collapses.

C. Specimen-Fluid Contact Measurements During Cavitation

1. General-Motivation

During the analysis of the high-speed photographs taken of the mercury flow, it was noted that the fluid seemed to lift clear of the specimen at the nose or initiation point and to recontact the surface at some point downstream on the surface. This seemed to indicate that, for the more advanced cavitation conditions such as "standard" to which the present study applies, there was a continuous void attached to the nose of the test specimen, and consequently, as was actually observed and expected, no damage was observed in this region. Thus the electrode specimen equipment described earlier was developed and used to explore

the relationship between the various degrees of cavitation and velocities, and the duration and amount of contact between the mercury and the specimen surface versus axial position.

Since there were trace amounts of water in the mercury, some question arose as to whether water might preferentially wet the surface, and thus prevent good contact. Simple static tests in a beaker showed that there was no problem in this regard.

2. Data Reduction and Analysis

After determining optimum oscilloscope settings, the vertical sensitivity was set at 2 volts/cm and the sweep rate at 200 milliseconds/cm, and the magnifier at normal (1x). Then a second photo of the same condition was taken with the magnifier at 5x so that one-fifth of the trace was obtained at a sweep rate of 4 milliseconds/cm which has the effect of spreading out one-fifth of the trace to the full screen and "magnifies" the breaks in the circuit. For each photo the camera shutter was opened and a single sweep initiated via the scope manual single sweep switch and then the shutter closed. Thus there was no possibility of obtaining an overlap of the trace. Normally, for each cavitation condition and velocity used, four photographs were obtained: (1) comparing the first probe to the middle probe at 1x, (2) comparing the first probe to the middle probe at 5x, (3) comparing the first probe to the last probe at 1x, and (4) comparing the first probe to the last probe at 5x. In all photos the upper beam denotes an open or closed circuit on the first probe and the lower denotes an open or closed circuit on the other probe, either the middle or last. Figure 45 shows representative oscilloscope traces of the data.

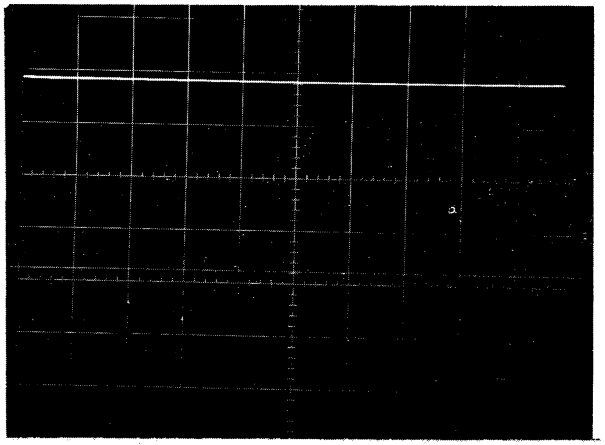

Photo No. 8, Zero Cavitation, Sweep: 20 ms/cm
Mag. X1, 34 ft/sec, Stainless Steel Venturi,
Upper traces:Probe 1(100%),Lower:Probe 2(100%)

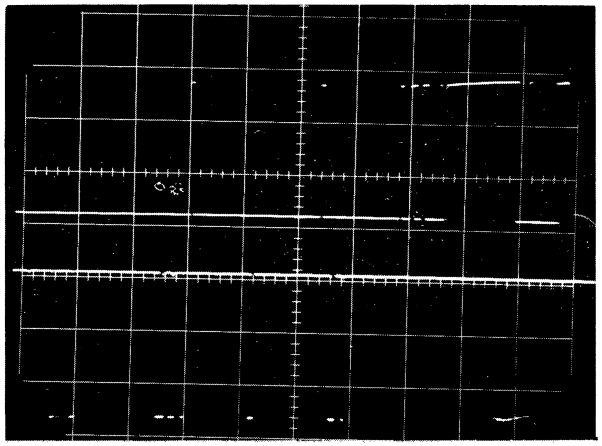

Photo No. 27, Std. Cavitation, Sweep: 20 ms/cm
Mag. X1, 34 ft/sec, Stainless Steel Venturi,
Upper traces:Probe 1(20%),Lower:Probe 2(91%)

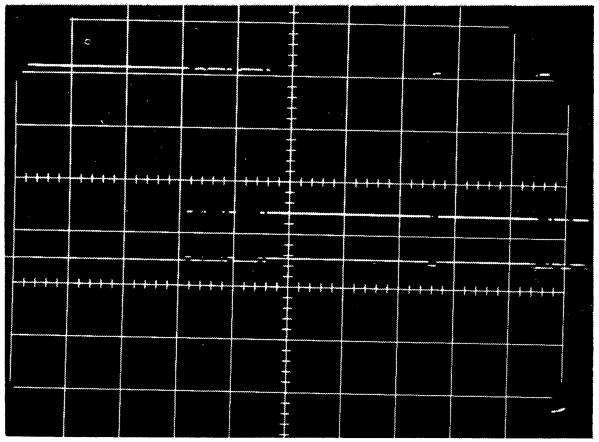

Photo No. 10, Vis. Cavitation,Sweep:20 ms/cm,
Mag. X5, 34 ft/sec, Stainless Steel Venturi,
Upper traces:Probe 1(45%),Lower:Probe 2(100%)

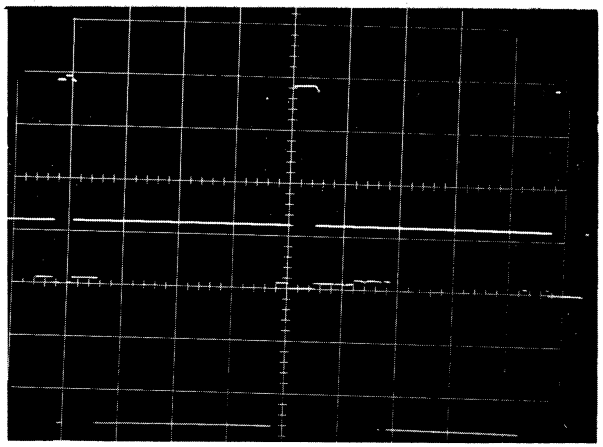

Photo No. 12, Cavitation to Back,Sweep:20 ms/cm
Mag. X5, 34 ft/sec, Stainless Steel Venturi,
Upper traces:Probe 1(8%),Lower:Probe 2(28%)

1642

Fig. 45.--Typical oscilloscope traces of signal from electrode specimen.

Photo number 8 was taken at zero cavitation, with full voltage (closed circuit) on all probes in order to make sure that all photographs taken later were observed in the proper orientation.

Thus, in all photos, a line on the upper trace of one particular beam indicates a closed circuit, i.e , mercury in contact with the surface, while a line on the lower trace of the beam indicates an open circuit, i.e , no mercury contact with the surface at that probe position. From the traces, the percentage of time the mercury spends in contact with the surface can be determined versus axial position on the specimen. All of this data is tabulated from 59 photographs, in Table 2. Representative photographs only are included in Figure 45.

The measurements taken with the electrode test specimen confirm the fact, as presumed from the high-speed movies, that the mercury actually does lift clear of the test specimen surface at the nose and rejoins it at some point downstream. At intermediate points between, the mercury comes in and out of contact with the specimen surface. No fixed frequency of the motion was noted.

In Figure 46, the percentage of time the mercury is in contact with the surface as a function of axial position is compared in mercury for various cavitation conditions at two velocities. Two specimens were placed in the venturi at an orientation of 180°. The curves which show some time out of contact show most at probe position 1, with an increase of in-contact time in the downstream direction. The same trend, an increase of in-contact time in the downstream direction, is indicated as the cavitation condition is decreased at constant velocity and as the

TABLE 2

PERCENT OF TIME MERCURY IS IN CONTACT WITH SURFACE

Photo No.	Cav. Cond. "Degree"	Vel. fps	Sweep Rate ms/cm	Mag.	% of Time Hg in-Contact Probe 1	Probe 2	Probe 3
9	Visible	34	20	5	100	100	
10	"	"	"	"	45	100	
24	"	"	"	"	100	100	
25	"	"	"	"	100	100	
avg.	VISIBLE	34	20	5	86	100	100*
1	Standard	34	20	1	80	100	
2	"	"	"	"	16	90	
3	"	"	"	5	100	100	
4	"	"	"	"	100	100	
5	"	"	"	"	24	90	
6	"	"	"	"	90		100
7	"	"	"	"	100		100
19	"	"	"	"	3	76	
20	"	"	"	"	70	100	
21	"	"	"	"	48		100
22	"	"	"	"	68		100
23	"	"	"	"	5		100
26	"	"	"	1	47	98	
27	"	"	"	"	20	91	
28	"	"	"	"	16		100
29	"	"	"	"	4		100
avg.	STANDARD	34	20	1/5	49.5	94	100
12	Back	34	20	5	8	28	
13	"	"	"	"	10		54
14	"	"	"	"		36	50
15	"	"	"	"	5	50	
16	"	"	"	"	20	42	
17	"	"	"	"	4		86
18	"	"	"	"	7		80
avg.	BACK	34	20	5	9	39	67.5
8	ZERO	34	20	1	100	100*	100
38	Visible	22	20	1	100	100	
39	"	"	"	"	100	100	
avg.	VISIBLE	22	20	1	100	100	100*
30	Standard	22	20	1	100	100	
31	"	"	"	"	88	100	
32	"	"	"	"	100		100
33	"	"	"	"	70		100
avg.	STANDARD	22	20	1	89.5	100	100

TABLE 2--Continued

Photo No.	Cav. Cond. "Degree"	Vel. fps	Sweep Rate ms/cm	Mag.	% of Time Hg in-Contact Probe 1	Probe 2	Probe 3
34	Back	22	20	1	3	57	
35	"	"	"	5	7	59	
36	"	"	"	1	51		94
37	"	"	"	5	8		92
avg.	BACK	22	20	1/5	17.3	58	93
Note: Above values are for two specimens in stainless steel venturi. Following values are for one specimen in stainless steel venturi.							
49	Visible	22	20	1	84	100	
50	"	"	"	5	100	100	
51	"	"	"	1	100		100
avg.	VISIBLE	22	20	1/5	94.7	100	100
45	Standard	22	20	1	74	100	
46	"	"	"	5	62	100	
47	"	"	"	1	95		100
48	"	"	"	5	100		100
avg.	STANDARD	22	20	1/5	82.8	100	100
40	Back	22	20	1	0	71	
41	"	"	"	5	0	69	
42	"	"	"	1	2		85
43	"	"	"	5	5		100
44	"	"	"	5	0		97
avg.	BACK	22	20	1/5	1.4	70	94
52	Standard	34	20	1	26	94	
53	"	"	"	5	8	90	
54	"	"	"	1	10		100
55	"	"	"	5	5		100
avg.	STANDARD	34	20	1/5	12.3	92	100
56	Back	34	20	1	15	84	
57	"	"	"	5	23	75	
58	"	"	"	1	12		100
59	"	"	"	5	23		100
avg.	BACK	34	20	1/5	18.3	79.5	100

*Extrapolated, no data.

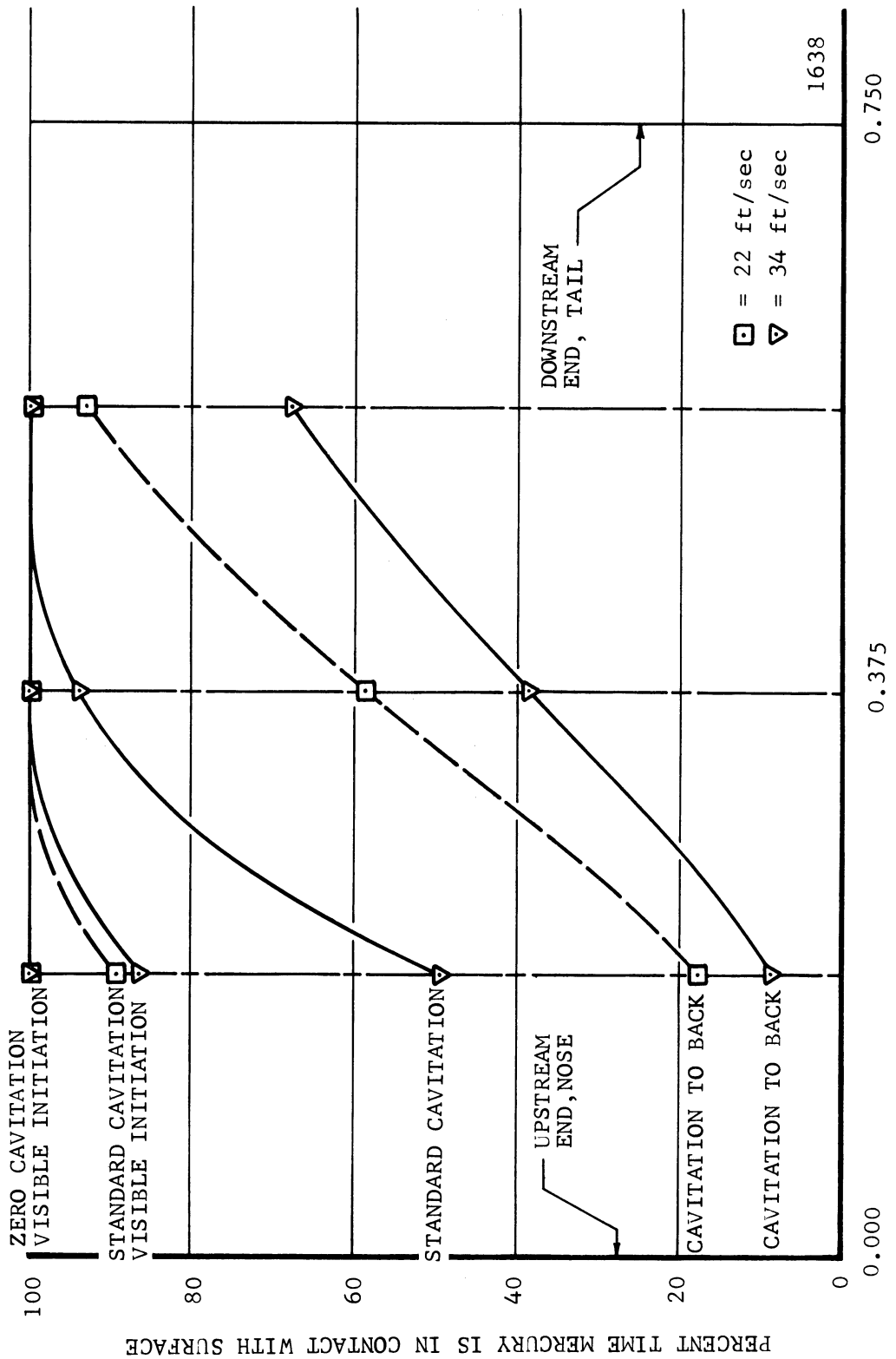

Fig. 46.- Percent contact time of mercury to surface vs. axial position on surface for various cavitation conditions in mercury at two velocities for the two specimen symmetrical arrangement in the SS venturi.

velocity is decreased at constant cavitation condition. The same type of data is shown in Figure 47 for the case of one specimen in the venturi. Again, it is evident that the percentage in-contact time at any probe position decreases as the cavitation condition is increased. The same trend is shown for velocity and axial position as was for the two specimen case. Comparing Figures 46 and 47, the rate of increase of in-contact time with axial position is greater for the one specimen case than for the two specimen case. Figures 48 and 49 show the data replotted for constant cavitation condition, with a comparison of one specimen versus two specimens at two velocities. Figure 48 is for standard cavitation and shows that in the one specimen case the mercury is out of contact for a larger percentage of the time at the upstream end of the specimen, and the in-contact time increases to about the same value at the downstream end as compared to the two specimen case. This results in a larger rate of increase of in-contact time versus axial distance on the test specimen surface for the one specimen as opposed to the two specimen case. This holds true for both of the velocities investigated. The same general trends are shown in Figure 49 for visible initiation at 22 feet/second and cavitation to back at 22 feet/second. The only exception is for cavitation to back at 34 feet/second, where the one specimen case shows more time in-contact than the two, although still showing a larger rate of increase of in-contact time with axial position. This one exception is probably due to the visible setting of the cavitation termination point being farther downstream than it should have been for the two specimen case. Since the cavitation was

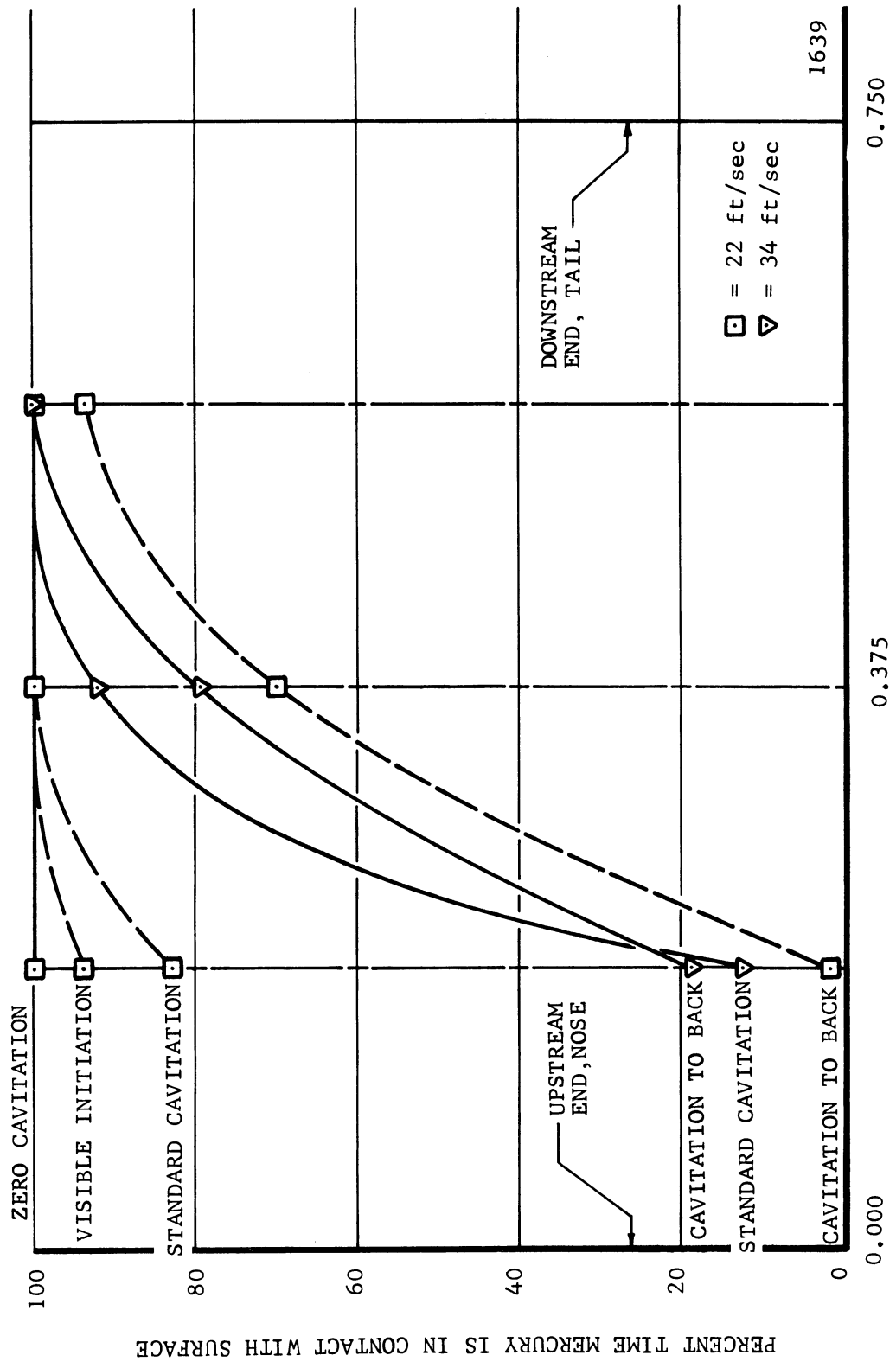

Fig. 47.--Percent contact time of mercury to surface vs. axial position on surface for various cavitation conditions in mercury at two velocities for the one specimen arrangement in the SS venturi.

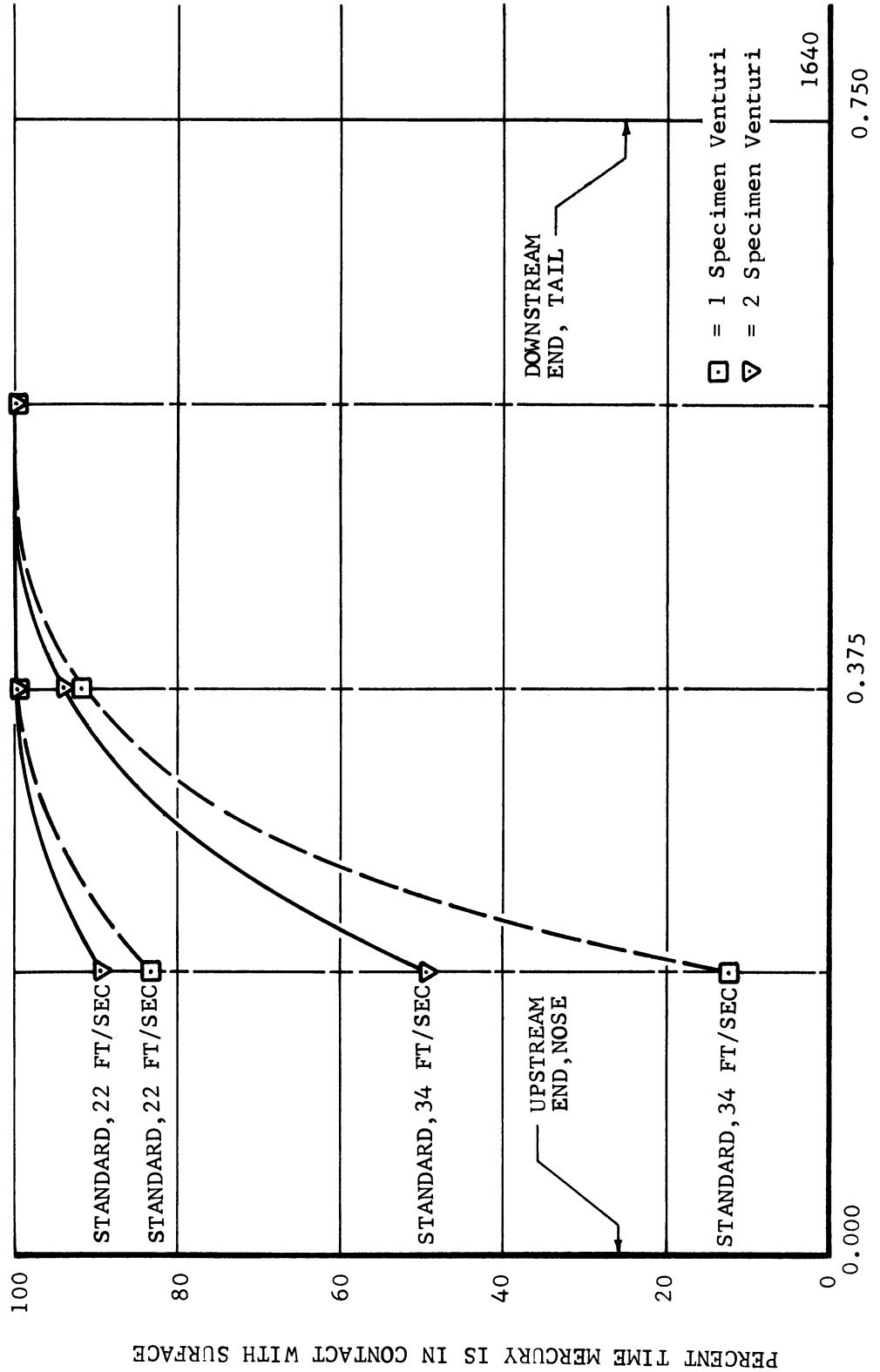

Fig. 48.--Percent contact time of mercury to surface vs. axial position on surface for "standard cavitation" in mercury at two velocities comparing one specimen vs. two.

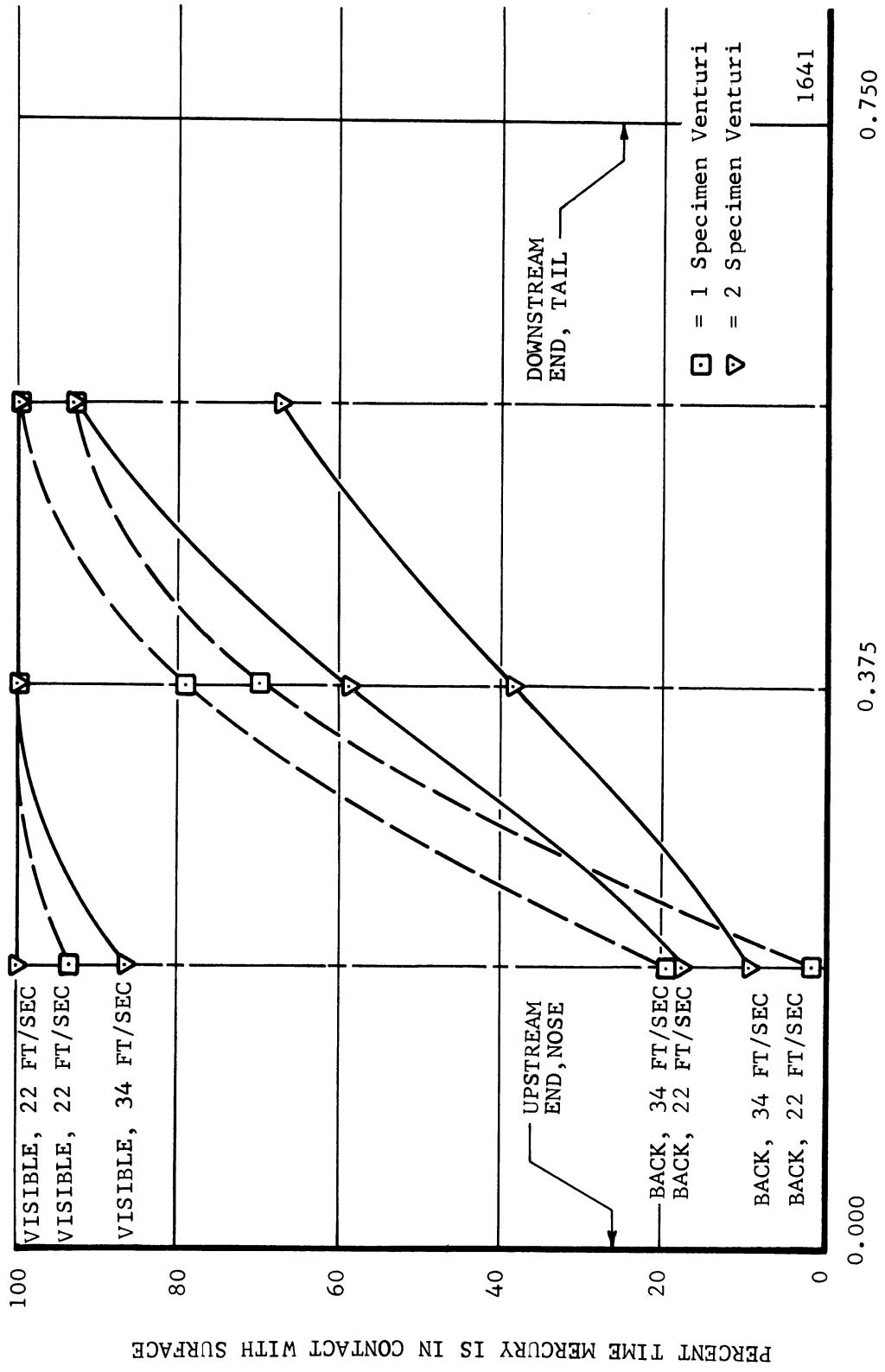

Fig. 49.--Percent contact time of mercury to surface vs. axial position on surface for various cavitation conditions in mercury at two velocities comparing one specimen vs. two.

adjusted visually and the downstream end of the cavitation cloud was set at the downstream end of the specimen in this case (visibility beyond this point being limited by venturi opaqueness), it is conceivable that some overshoot could have occurred. If the whole curve were shifted upwards in accordance with a correction for overshoot of the cloud termination point until the probe 3 values matched, then there would be no discrepancy in the trends.

3. Discussion

This technique provides an independent means of determining quantitatively the extent of the cavitating void in the venturi on local obstructions such as the cavitation damage test specimens. It could be used in any type of two phase system where the fluid phase has an electrical conductivity appreciably higher than the gaseous phase for determining fluid-surface contact time or amount.

The data indicates, as expected, that more voids appear on the surface as the degree of cavitation is increased. A somewhat surprising fact is that the average contact time of fluid to surface never falls below about 50% even when the specimen is completely immersed in a highly turbulent, cavitating flow regime. This fact could be of importance for various direct conversion MHD concepts. The electrical current path for such a system might well be made through a region of substantial void, thus avoiding the necessity of completely separating the fluid and vapor phases.

Comparing the voids measured by the electrode specimen technique, with the pressure profile data taken earlier, it is observed that for "visible initiation" the mean static pressures on the surface at the

same three axial locations are well above vapor pressure, while the mercury loses contact with the surface at 34 feet per second (Figure 46), about 10-15% of the time at the upstream position.

For "standard cavitation," the pressure on the surface at the center position is well above vapor pressure, while the mercury loses contact with the surface only a small portion of the time. It should be pointed out that the pressures are time mean values while the contact time technique can show instantaneous fluctuations. For "cavitation to back," the pressure profile measurements show that the entire surface is under a very low pressure slightly above vapor pressure, while the contact time as recorded in this investigation still averages about 50%, ranging from 15% at the upstream position to about 80% at the downstream position. From the observed damage patterns on the specimens for these conditions, it appears that the pitting occurs in a region where the mercury has a contact time approaching 100%, and where the pressures are considerably above vapor pressure.

The same statements apply for the visible initiation data for only one specimen in both cases. The standard cavitation, one specimen, 34 feet per second data shows essentially vapor pressure existing at the first two probe positions and a higher pressure at the third, while the mercury contact data shows about 15%, 80% and 100%, respectively. This also tends to confirm that the most intense damage occurs in regions of essentially 100% contact and high pressure, as the damaged surfaces from this condition show very heavy damage on the rear one-third of the specimen. (See Figures 57 through 61.)

If it had been shown that very little contact existed between the mercury and test specimen surface in the zones of heavy damage, then the assumption that damage was primarily caused by an impingement effect would be somewhat strengthened. However, since the data indicates approximately 100% contact with the surface in the damage region, there is still the possibility of both the central jet impingement model and the shock wave model.

The major conclusions that can be drawn from this phase of the investigation are:

1. The technique described for measuring the mercury to surface contact time is feasible and could be applied to many other two-phase and/or two component fluid flow regimes.
2. The mercury to surface contact time decreases as the degree or amount of cavitation on the surface is increased.
3. The mercury to surface contact time decreases as the number of specimens is decreased from 2 to 1.
4. The most intense cavitation damage occurs on a region of the test specimen surface where the mercury is in contact with the surface essentially 100% of the time.
5. The mercury contact time increases with distance from the specimen leading edge, but does not increase at the same rate as the increase of pressure along the surface in the axial direction.
6. The mercury contact time averages about 50% even when the entire surface is completely immersed in a highly turbulent cavitating flow regime.

CHAPTER IV

CAVITATION TEST SPECIMEN DATA ANALYSIS

A. General

The normal procedure that each test specimen is subjected to has already been described in an earlier section. In this section are presented the details of the test specimen preparation and mechanical properties measurements needed as correlation data for the subsequent data correlation.

B. Mechanical Property Measurements

As previously mentioned, it is necessary to determine the exact mechanical properties for the materials tested. This requires that mechanical property and cavitation specimens be made from the same stock, thus exhibiting the same heat treat and cold work properties.

Table 3 is a listing of the measured mechanical properties to be used in correlating the damage data. All but a few of these items have been measured in this laboratory from the same stock as the specimens. In this table are listed two values for strain energy to failure, i.e., "engineering strain energy" which is based on the "approximate" or engineering stress-strain curve and is equal to the area under this curve, and "true strain energy," which is based on the true stress-strain curve, which takes into account necking of the specimen,

TABLE 3

MECHANICAL PROPERTIES OF TEST SPECIMEN MATERIALS

Material	Tensile Strength	Yield Strength	Engr. Strain Energy	True Strain Energy	True Brkng. Stress	Hard-ness (BHN)	Elastic Modulus	% Elong.	% Red. Area
304 SS	95,200	44,000	44,800	74,500	172,800	133.5	28×10^6	54.4	50.9
1008 CS	50,000	30,000	15,500	23,000	55,200	91.5	28×10^6	40.0	71.0
Tenelon	131,800	82,000	54,500	94,800	220,900	218.0	28×10^6	44.2	46.6
Cb-1Zr Annealed	29,300	14,600	6,000	25,000	30,000	115.0	12×10^6	42.5	92.8
Cb-1Zr C-Wrked	56,000	52,500	2,900	10,000	80,000	124.0	12×10^6	6.0	84.0
Ta-10W	80,900	72,800	16,800	91,300	117,100	163.0	29×10^6	21.0	63.3
Ta-8W-2Hf	89,300	80,400	20,800	96,000	135,600	175.0	29×10^6	22.0	59.6
Mo-1/2Ti	94,700	89,600	15,000	83,000	120,000	216.0	37×10^6	30.7	54.7
1100-0 Aluminum	14,300	10,500	7,500	52,000	35,600	23.0	10×10^6	36.3	89.3
2024-T351 Aluminum	70,300	56,000	14,400	36,000	102,500	120.0	10×10^6	21.3	35.1
6061-T651 Aluminum	45,000	41,000	10,300	40,800	86,800	95.0	10×10^6	19.0	48.1
Copper-Zinc As Rec'd.	93,900	82,000	4,700	55,400	137,000	168.0	16×10^6	5.3	40.7
Copper-Zinc (L.H.Trt)	47,600	20,000	28,600	57,000	119,500	65.0	16×10^6	62.6	60.9
Copper-Zinc (H.H.Trt)	40,400	11,000	15,300	33,000	79,500	29.0	16×10^6	58.9	51.7

TABLE 3--Continued

Material	Tensile Strength	Yield Strength	Engr. Strain Energy	True Strain Energy	True Brkng. Stress	Hard-ness (BHN)	Elastic Modulus	% Elong.	% Red. Area
Copper-Nickel (As Rec'd.)	87,300	77,000	6,100	13,200	87,400	162.0	22×10^6	4.5	15.4
Copper-Nickel (L.H.Trt)	57,900	20,000	3,100	36,200	85,900	76.0	22×10^6	34.9	43.5
Copper-Nickel (H.H.Trt)	53,300	18,000	16,300	21,800	70,500	56.0	22×10^6	34.4	34.4
Copper OFHC (As Rec'd.)	53,400	49,500	3,100	11,800	85,600	104.0	17×10^6	6.2	19.8
Copper OFHC (L.H.Trt)	31,500	9,500	13,900	26,900	54,300	66.0	17×10^6	51.3	48.5
Copper OFHC (H.H.Trt)	30,700	5,000	6,100	11,800	43,200	15.0	17×10^6	32.5	33.2
Nickel (As Rec'd.)	93,100	82,000	3,200	8,300	99,100	173.0	30×10^6	3.9	10.2
Nickel (L.H.Trt)	50,500	13,000	18,300	48,300	92,700	55.0	30×10^6	43.8	51.6
Nickel (H.H.Trt)	48,700	7,000	16,100	40,500	79,500	45.0	30×10^6	41.8	49.7

reduction in area after plastic deformation begins and the resulting higher values for the true breaking stress and strain. If it is assumed that the volume of the necked section remains constant, then for non-uniform strain:[39]

$$\varepsilon_t = \ln \frac{l}{l_o} = \ln (V/A)/(V/A_o) = \ln \frac{A_o}{A}$$

which can be written for a circular cross section as:

$$\varepsilon_t = 2 \ln \frac{d_o}{d}$$

Similarly, the exact definition for the true stress, based on the actual area A rather than the original area A_o must be used to take into account the necking phenomena:

$$\sigma_t = P/A$$

The rest of the values listed in Table 3 are rather commonly reported values and need no further explanatory remarks. Typical grain structure photomicrographs and chemical compositions are already listed elsewhere.[39]

C. Specimen Preparation

The test specimens are milled from sheet stock and then the 0.060" x 0.750" surface to be exposed to the cavitation regime is metallographically polished. Figures 50 to 56 show typical roughness profiles of the surfaces before exposure to cavitation and serve as

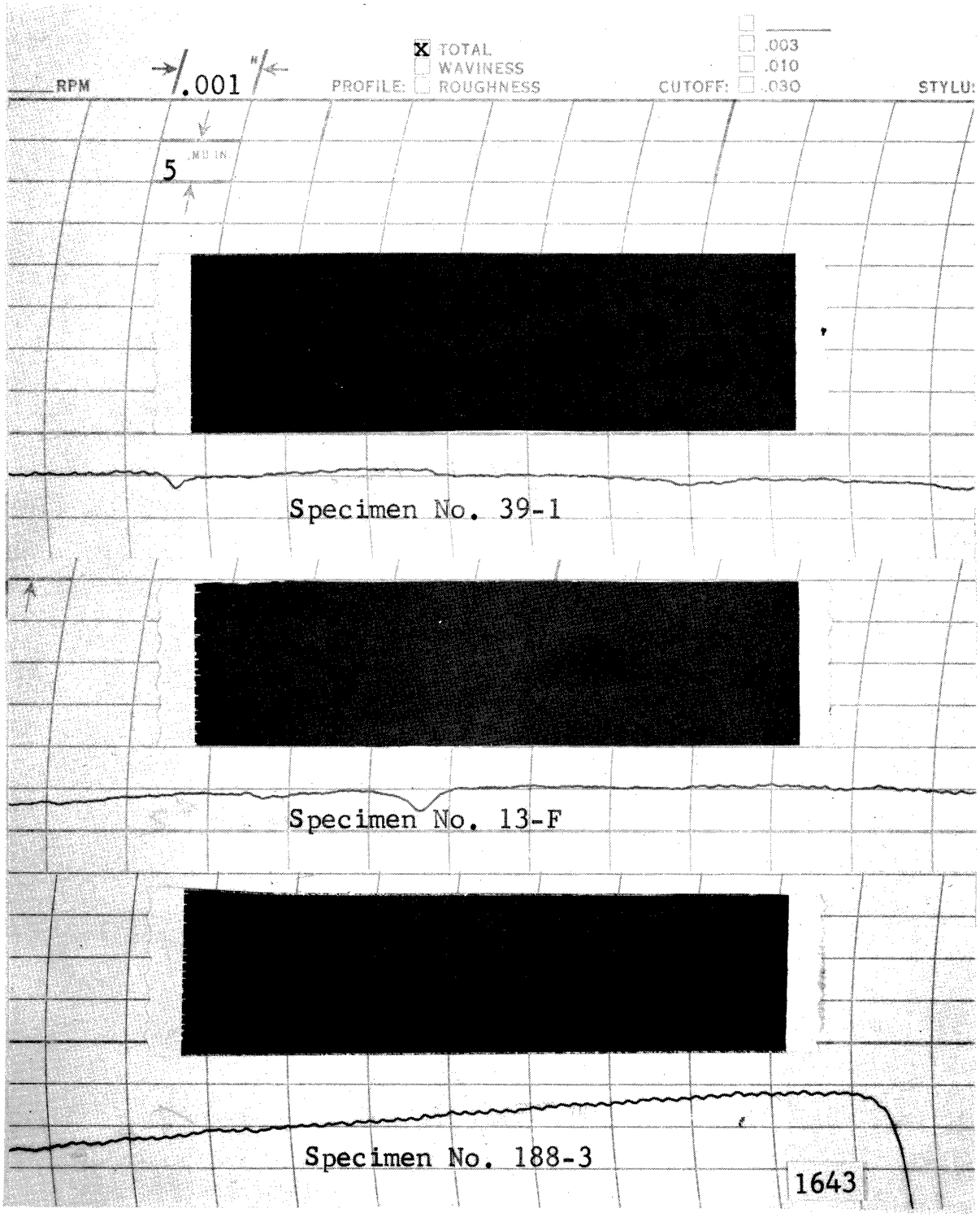

Fig. 50.--Photomicrographs and proficorder traces of original surface characteristics of specimen Nos. 39-1 (1008 carbon steel), 13-F (Tenelon), and 188-3 (304 stainless steel).

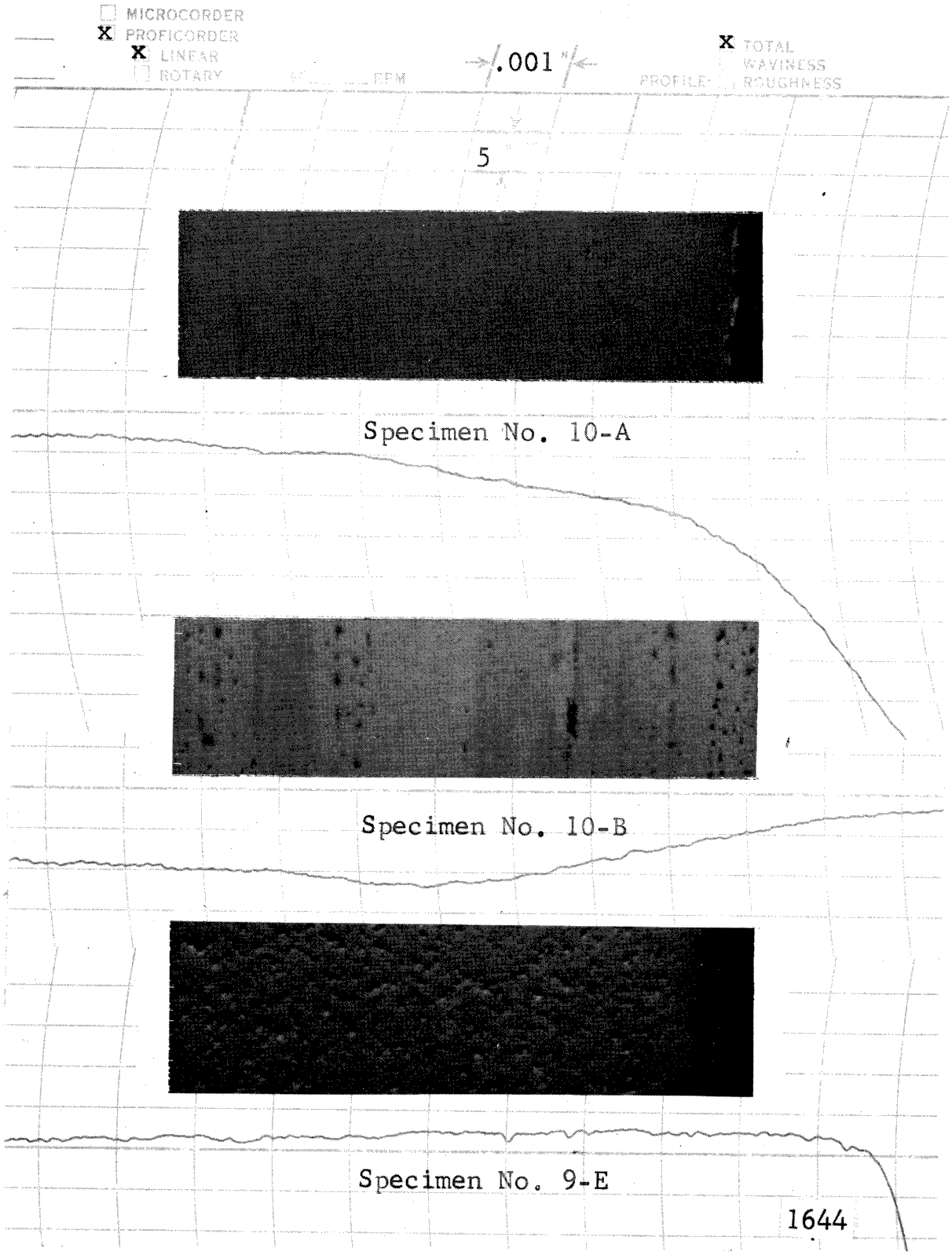

Fig. 51.--Photomicrographs and proficorder traces of original surface characteristics of specimen Nos. 10-A (Ta-10W), 10-B (Ta-8W-2Hf), and 9-E (Mo-1/2Ti).

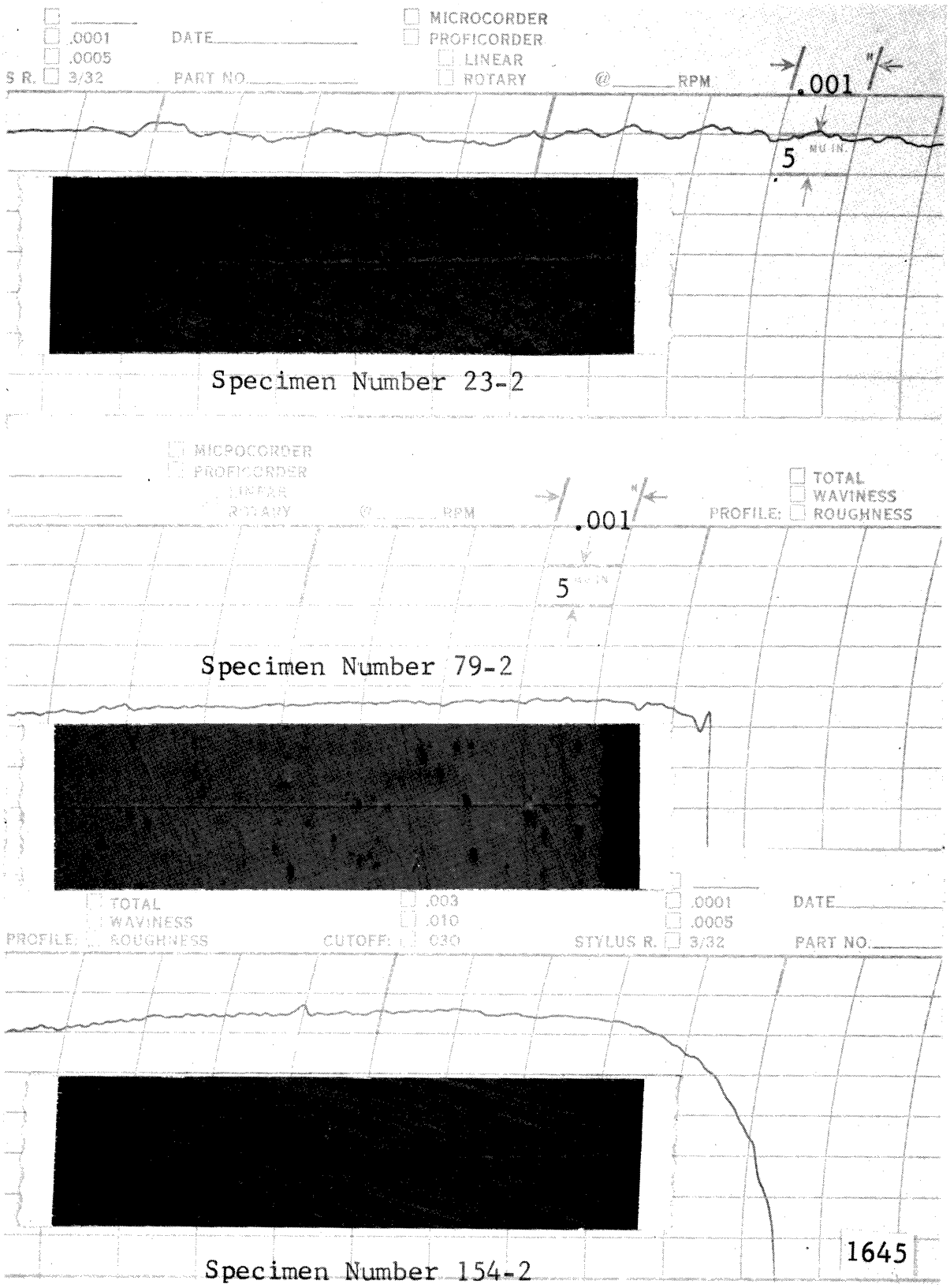

Fig. 52.--Photomicrographs and proficorder traces of original surface characteristics of specimen Nos. 23-2 (1100-0 Aluminum), 79-2 (2024-T351 Aluminum), 154-2 (6061-T651 Aluminum).

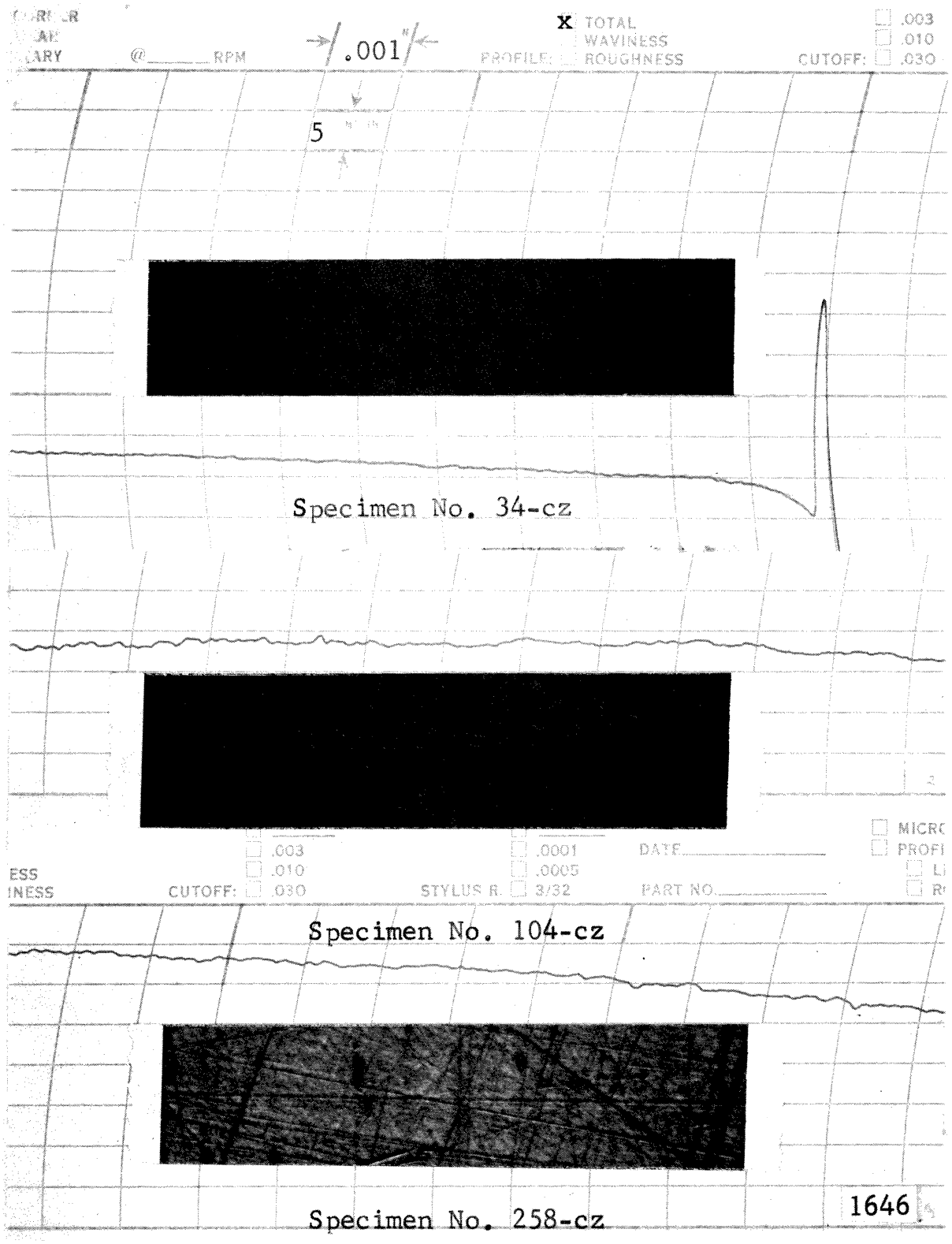

Fig. 53.--Photomicrographs and proficorder traces of original surface characteristics of specimen Nos. 34-cz (as rec'd brass), 104-cz (low heat tr. brass), 258-cz (hi. ht. trt. brass).

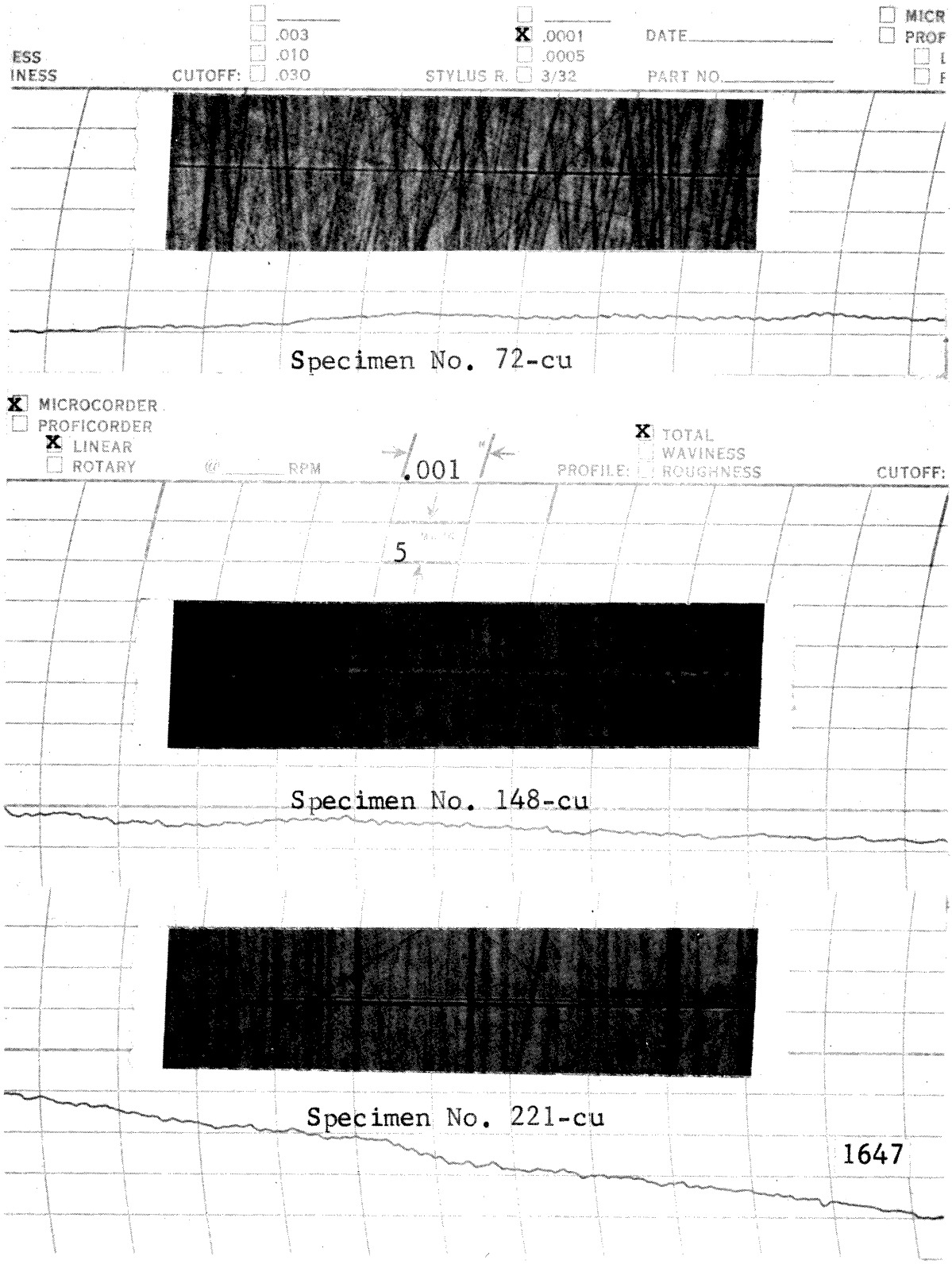

Fig. 54.--Photomicrographs and proficorder traces of original surface characteristics of specimen Nos. 72-cu (as rec'd copper), 148-cu (low ht. trt. copper), 221-cu (hi. ht. trt. copper).

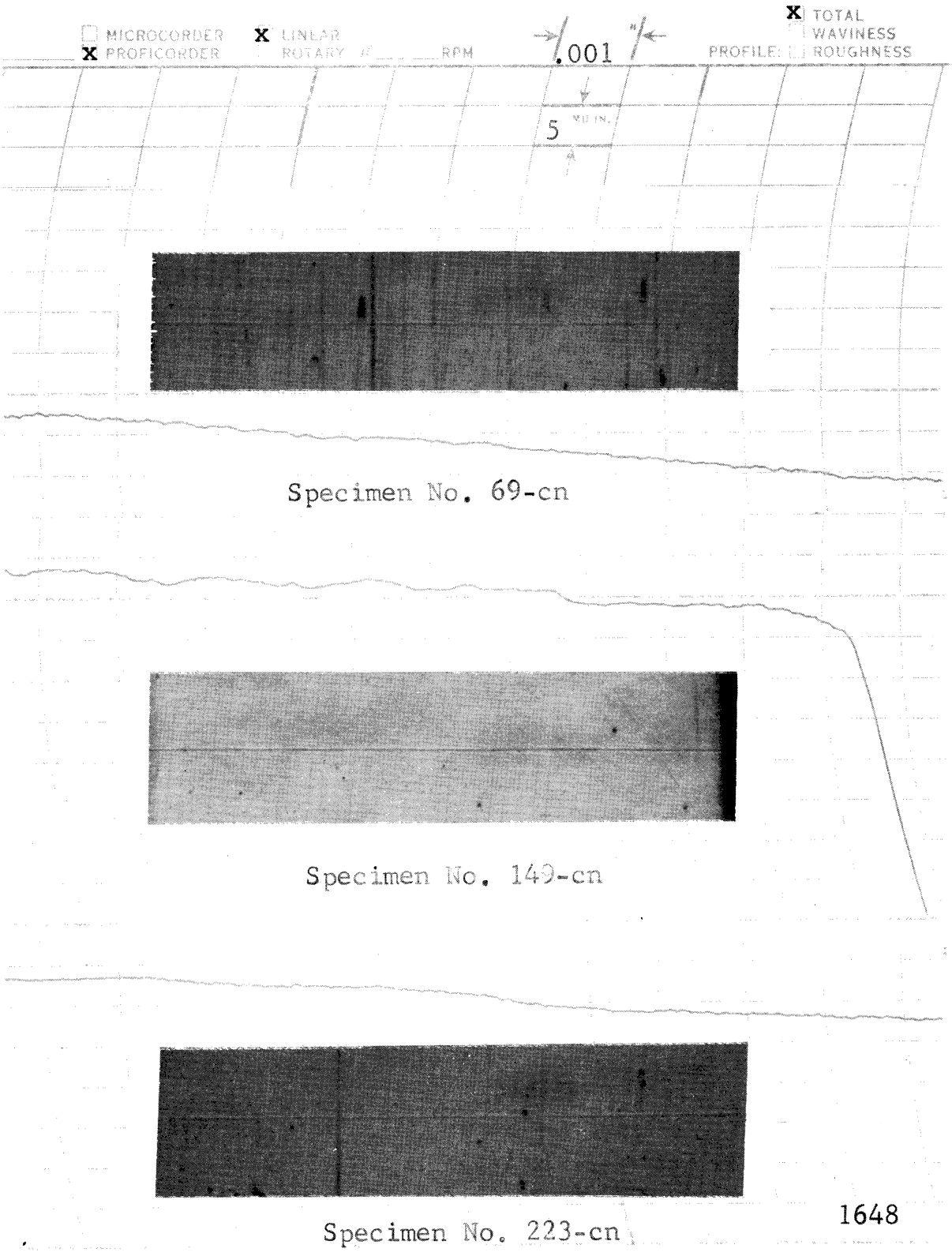

Fig. 55.--Photomicrographs and proficorder traces of original surface characteristics of specimen Nos. 69-cn (as rec'd copper-nickel), 149-cn and 223-cn (low and high heat trt. copper-nickel).

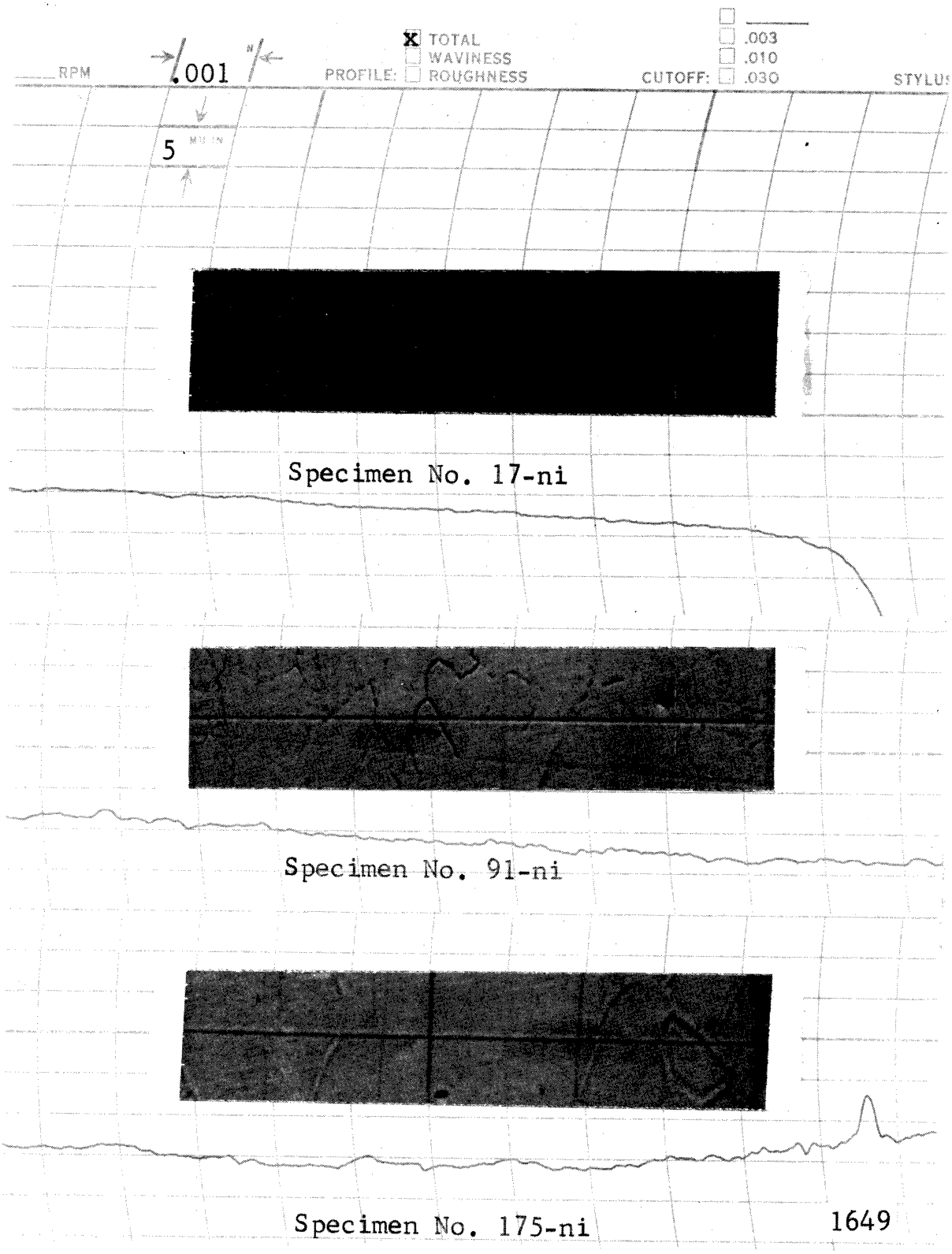

Fig. 56.--Photomicrographs and proficorder traces of original surface characteristics of specimen Nos. 17-ni (as rec'd nickel), 91-ni (low ht. trt. nickel), 175-ni (hi. ht. trt. nickel).

reference surfaces for the detailed proficorder measurements after damage, discussed later.

D. Typical Damage to Specimens in Mercury Facility

Full surface photomicrographs of specimens representing all the materials tested were taken at a magnification of 40X to determine the pitting distribution for comparison with the high-speed motion pictures. Typical photomicrographs for several materials are included (Figures 57 through 61), illustrating the general pitting pattern on the polished (labeled in Figure 6-a) surface after exposure to "standard cavitation" in mercury in the two-specimen symmetrical (180° separation) stainless steel venturi for which the damage correlation was made. The polished surface is only about one-eighth of the total wetted area of the specimen so that the weight loss derives from an area eight times larger than this. However, the other surfaces are not as suitable to photographic studies or metallographic polishing, and hence surface traces have been limited to the polished surface. Figure 57 for Cb-1Zr shows the typical damage pattern for this case at three stages in the damage runs. The larger pits and the more intensely damaged area is on the rear fourth of the specimen where the high-speed photographs and electrode specimen investigations indicated essentially a pure fluid environment on the surface. In the limited time samples taken there was no indication of vapor or bubbles in contact with this portion of the surface. However, from an extrapolation of the data from the motion pictures (Figure 43), it would be estimated that there were still on the order of 10^3 times

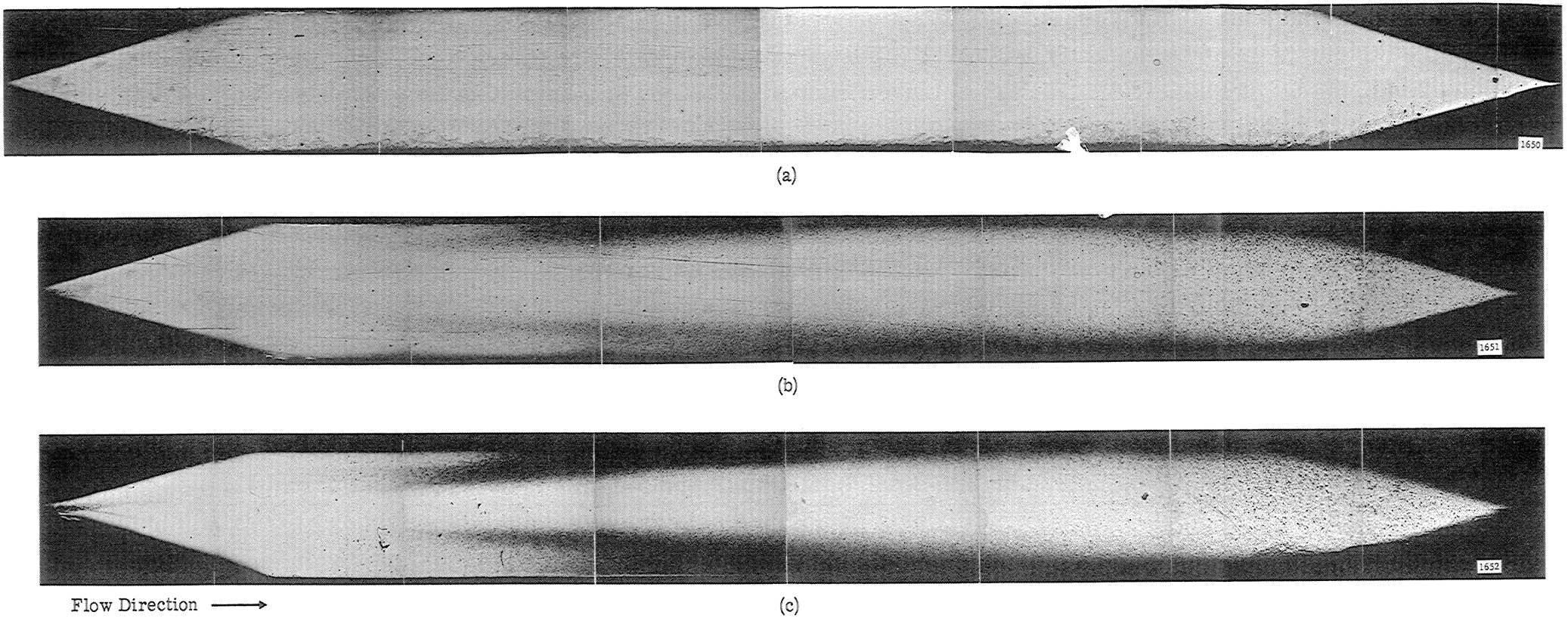

Fig. 57.--Full surface photomicrographs of the polished surface at various stages in the mercury cavitation damage test of (a) spec. No. 10-Cb-1Zr at 0 hours, (b) 10-Cb-1Zr at 10 hours, (c) 3-Cb-1Zr at 50 hours.

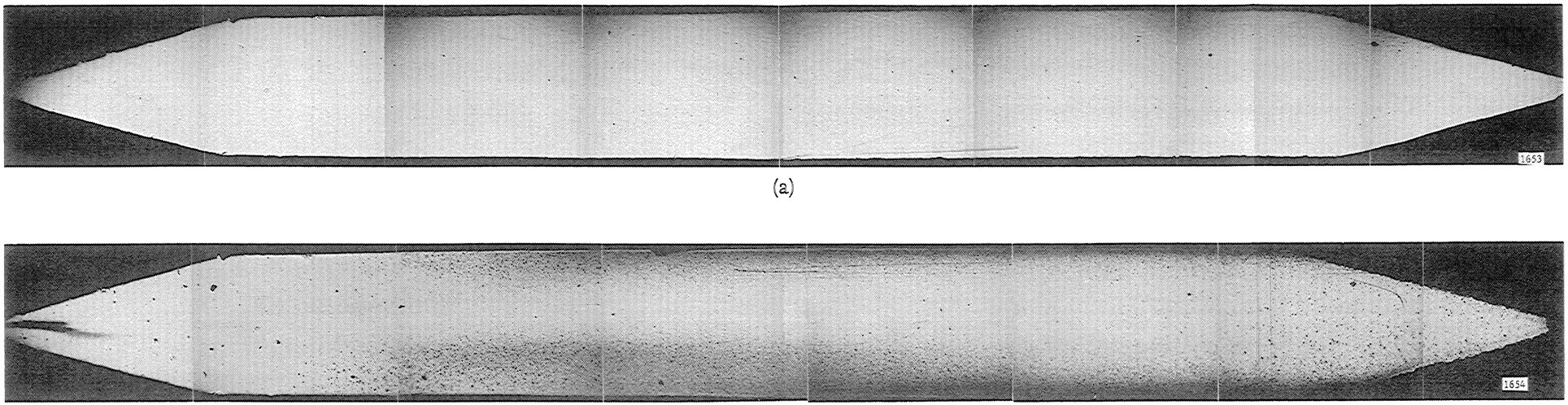

Fig. 58.--Full surface photomicrographs of the polished surface at various stages in the mercury cavitation damage test of (a) spec. No. 37-1, carbon steel, at 0 hours, (b) 37-1 at 10 hours.

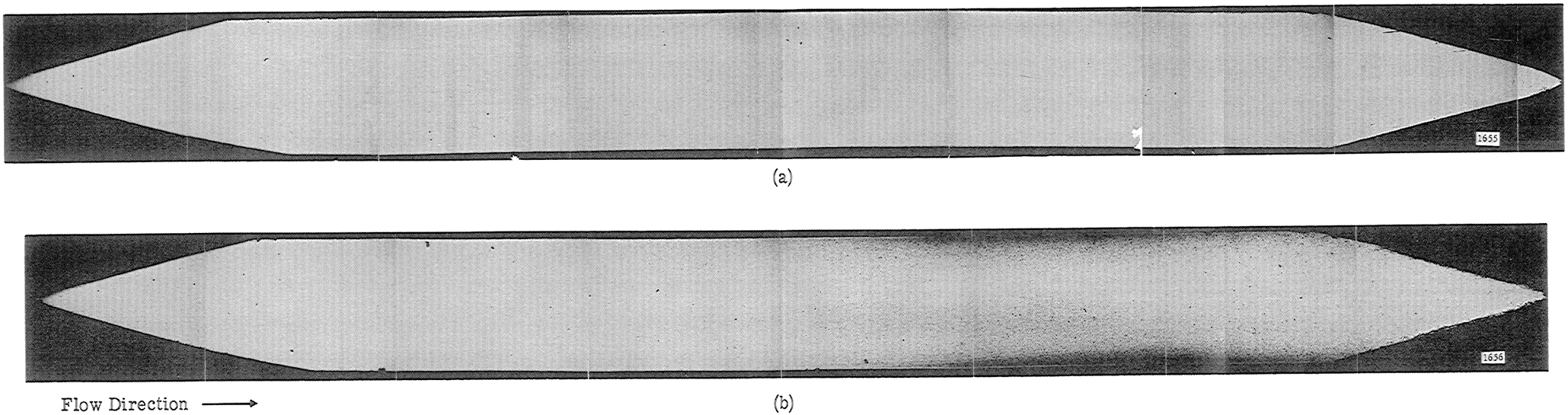

Fig. 59.--Full surface photomicrographs of the polished surface at various stages in the mercury cavitation damage test of (a) 177-3, 304 SS at 0 hours, (b) 177-3 at 10 hours.

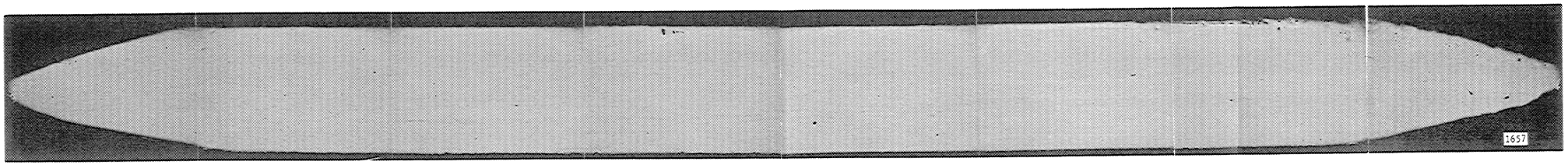

(a)

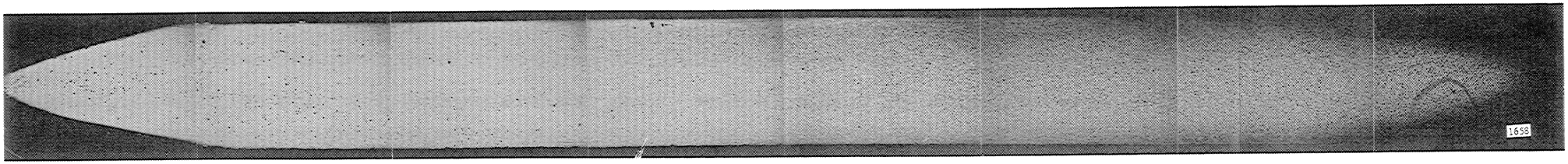

Flow Direction ⟶

(b)

Fig. 60.--Full surface photomicrographs of the polished surface at various stages in the mercury cavitation damage test of spec. No. 8-B, Ta-8W-2Hf, (a) 0 hours, (b) 10 hours.

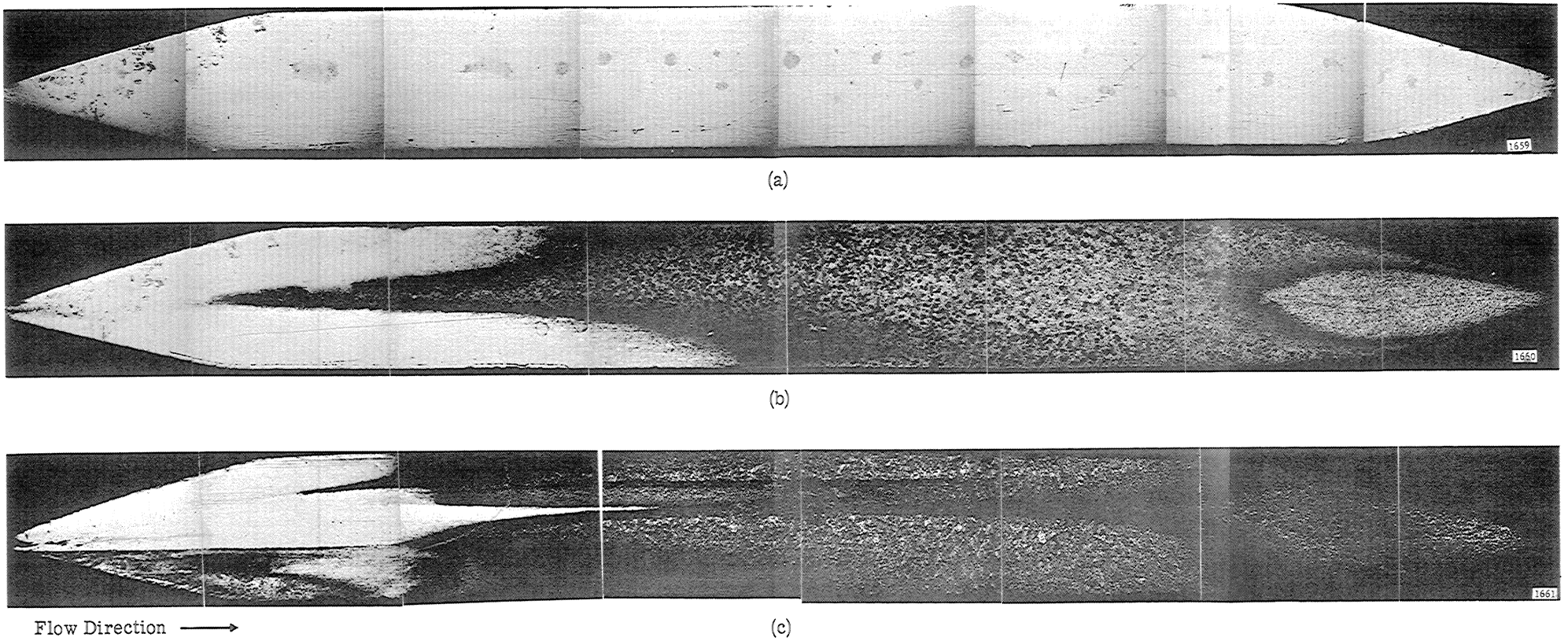

Fig. 61.--Full surface photomicrographs of the polished surface at various stages in the mercury cavitation damage test of (a) spec. No. 89-ni, low ht. trt. nickel, at 0 hours, (b) 89-ni at 10 hours, and (c) 85-ni at 50 hours.

as many bubbles adjacent to the surface in this region as there are pits.

The row of smaller pits along each side of the polished surface is typical. This is in the region where a cavitating wake of small bubbles was observed on the surface (Figures 36 to 39). It has been previously noted in many cavitating tests in turbomachinery[48] and rotating disks,[49] for example, that flows involving considerable vorticity, as this "wake" from the corner of the specimen are much more damaging than translatory flows. This is confirmed by the present observation since the wake, even though it exists in a low pressure region, does create considerable damage. Figures 58, 59, and 60, typical for carbon steel, stainless steel, and Ta-8W-2Hf, respectively, also show the same pattern. These photomicrographs are for a duration for which the damage consists of individual pits, i.e., prior to significant overlapping, so that the formation of individual pits and craters could be investigated. As pointed out in an earlier paper from this laboratory,[40] the evidence is very strong that these are single-event failures, randomly located. Their shape and appearance does not change with additional exposure until overlapping becomes predominant.

Pure nickel in three different heat treats were also tested in the mercury facility. Figure 61 shows the resultant damage. The visible appearance and the fact that these specimens exhibited large weight gains after exposure, comparable to the weight loss exhibited after baking under vacuum, indicate that corrosion was closely coupled with mechanical cavitation damage for this material in mercury. Since this

is not the case for the other materials, it is not reasonable to include the Hg-nickel data in the mechanical properties correlations to be considered later.

E. Typical Damage to Specimens in Water Facility

While some full-surface photomicrographs have been taken of the water-facility specimens, generally smaller areas in regions of probable maximum damage, have been photographed at larger magnification. This reduced photographic coverage was necessitated by the very large numbers of test specimens used in the water test program. Figures 62 and 63 show the propagation of damage on the polished surface for tenelon and Cb-1Zr respectively, up to a duration of 100 hours, Figure 64 shows the respective damage at 100 hours on the three heats of nickel, and Figure 65 the 100 hour condition of stainless steel, Mo-1/2Ti, and the copper-nickel alloy in the "as received" condition.

Individual photomicrographs of the pitting damage in both mercury and water are presented in the next section at much larger magnification, along with the proficorder trace data, and comments regarding the individual pits will be reserved to that section.

F. Comparison of Damage Pattern to Pressure Profiles

Referring to Table 1, the suppression pressures (i.e., pressure above vapor pressure) are tabulated for the conditions corresponding to the photomicrographs previously described for mercury and water. It is noted that the actual suppression pressure gradient is almost identical

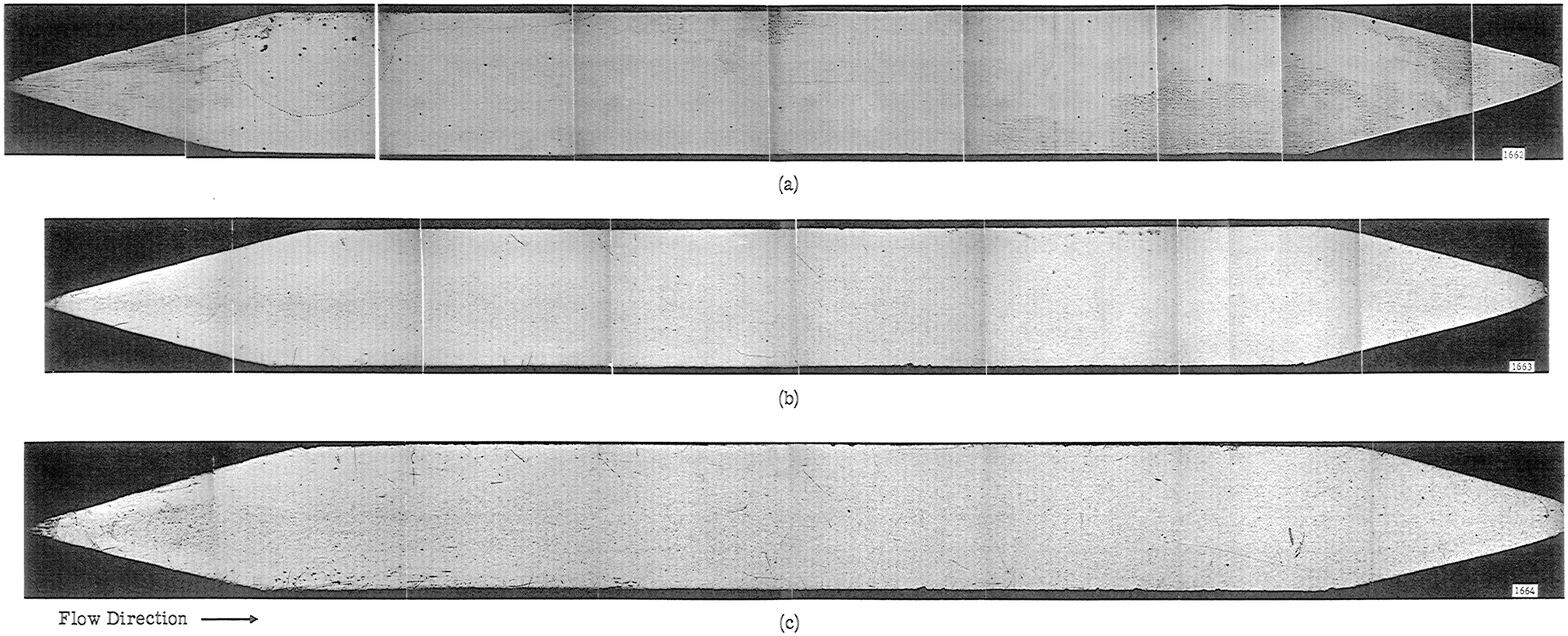

Fig. 62.--Full surface photomicrographs of the polished surface at various stages in the water cavitation damage test of spec. No. 1-F, Tenelon, (a) at 0 hours, (b) at 1 hour, and (c) at 100 hours.

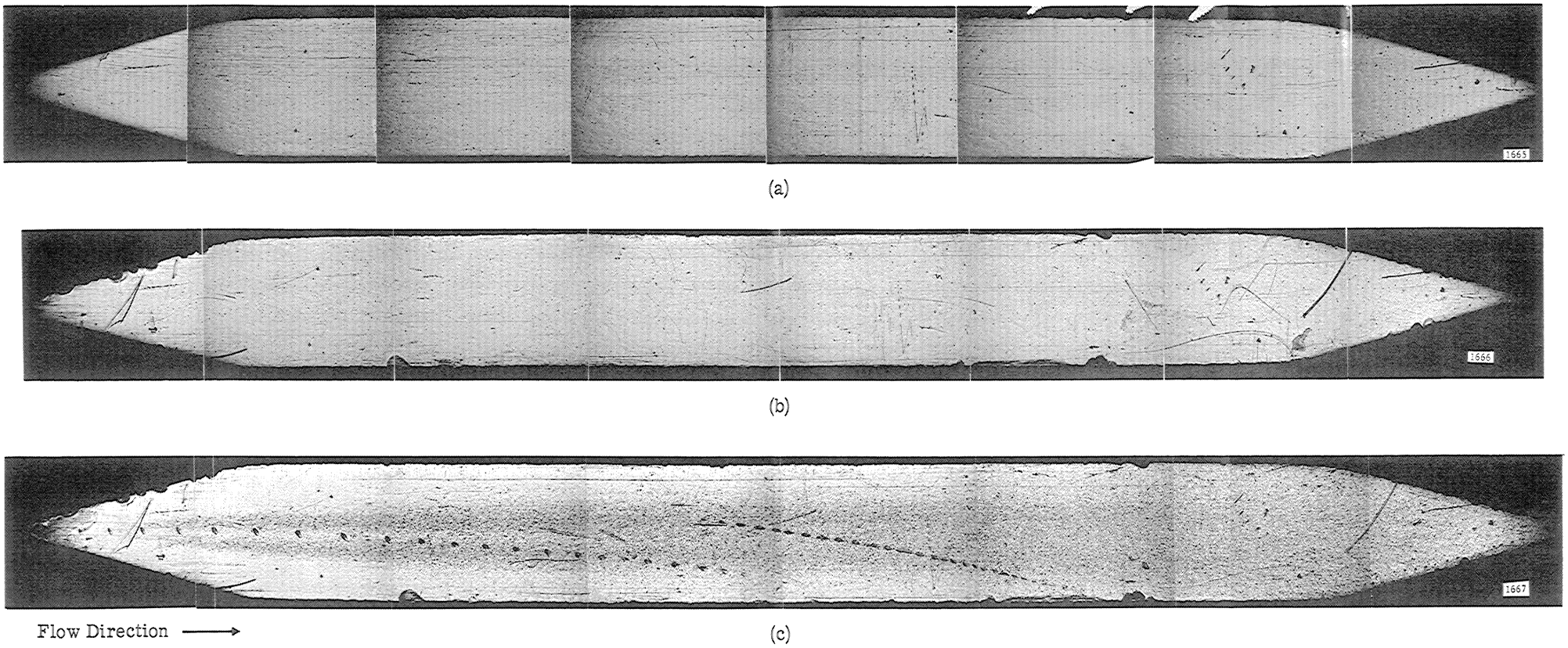

Fig. 63.--Full surface photomicrographs of the polished surface at various stages in the water cavitation damage test of spec. No. 2-Cb-1Zr at (a) 0 hours, (b) 1 hour, and (c) 100 hours.

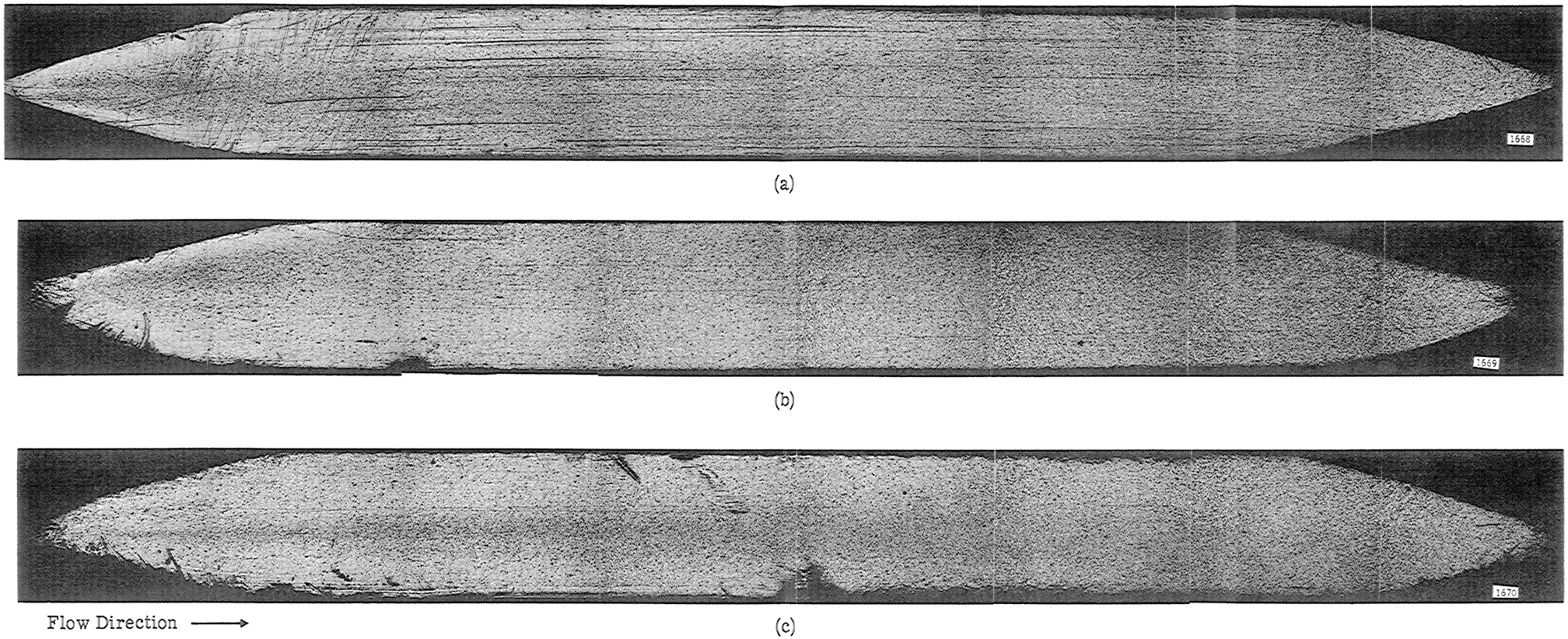

Fig. 64.--Full surface photomicrographs of the polished surface at various stages in the water cavitation damage test of spec. No. (a) 10-ni at 100 hours, (b) 83-ni at 100 hours, (c) 170-ni at 100 hours.

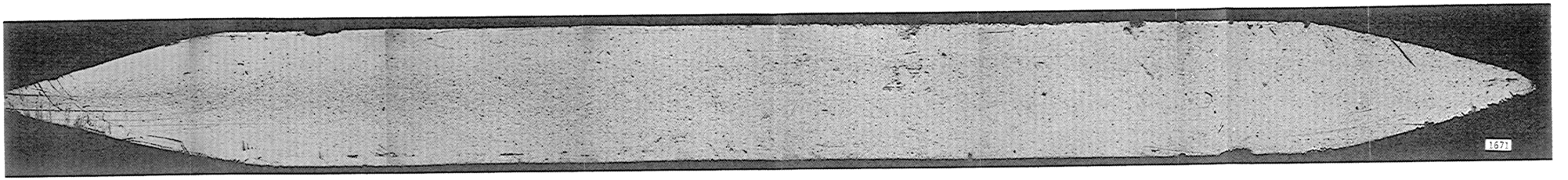

(a)

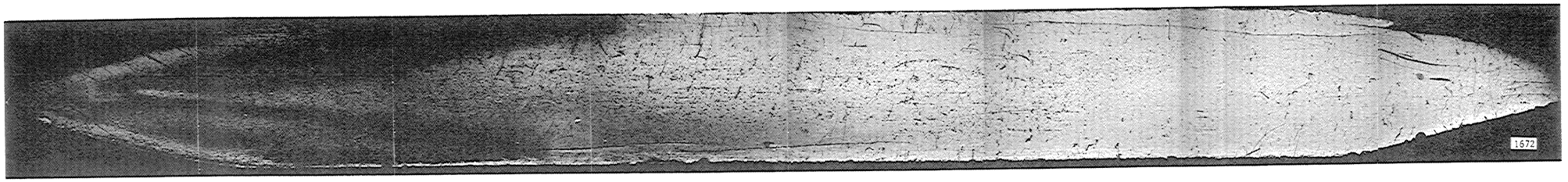

(b)

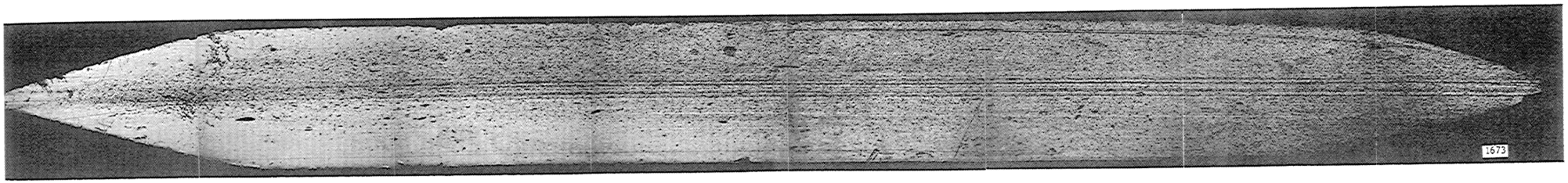

Flow Direction ⟶

(c)

Fig. 65.--Full surface photomicrographs of the polished surface at various stages in the water cavitation damage test of spec. No. (a) 139-3, 304 SS, (b) 1-E, Mo-1/2Ti, and (c) 8-cn, all at 100 hours.

for the three specimen symmetrical arrangement in water at 200 ft./sec., and for the two specimen symmetrical arrangement in mercury at 34 ft./sec. However, the gradient for the two specimen unsymmetrical arrangement in mercury for the same flow conditions is much steeper, as shown earlier by the pressure profile figures, and later in Table 5, and the actual pressures on the downstream portion of the specimen thus are higher. This latter case has been found earlier to be considerably more damaging than the symmetrical arrangement as used herein, indicating that minor flow geometry changes can result in major changes in damage rate.

Although the pressure distribution on the specimen surface is similar for the two symmetrical arrangements in water and mercury, it is not possible with the present state of knowledge to draw any conclusions concerning the expected damage. Theoretical analyses[2,42] show that the same collapse velocities would result if the driving head were the same, i.e., $(p-p_v)/\rho$, neglecting for the moment the relatively minor affects of vicosity, compressibility, surface tension, etc. Hence, for these conditions, the collapse velocities for water should be greater by roughly a factor of 3.5 (proportional to square root of density ratio). In addition, for the same collapse velocities and equally compressible fluids,* the force exerted on the adjacent structure would be proportional to the density ratio, being a factor of 13.6

---

*This is an approximately valid comparison for water and mercury, since the sonic velocities are about the same in the two fluids, and hence, for equal collapse velocities, Mach Numbers would be the same.

greater for mercury. Thus, with this simple approach, one would expect forces applied to specimens in the mercury system to be about 3.5 times as great as in the water system under these conditions. What this would mean in terms of volume loss to the specimens is not easily determinable. Actual across the board comparisons of damage on five materials tested in both systems for the specified conditions shows the damage in mercury to be slightly less than that in water (Table 4). This does not evidently agree with the simple theoretical approach presented above, indicating that a much more complicated situation exists.

In the water venturi the visible cavitation cloud extends to the rear of the specimen for this condition, while in mercury it ends at the center of the specimen. The difference in appearance are at least partially due to the slightly different geometries (2 versus 3 specimens), and the fact that only the boundary layer is observed in the opaque mercury. These two conditions with their similar pressure gradients are the most damaging respectively in the two systems (Figure 27). Comparable data exists for water at two lower velocities, and these are also presented in Table 4, where the comparison is made to mercury. There is a small velocity effect in the water system, showing a damage increase by a factor of about 1.75 with a range in velocity of about 3, i.e., 65 ft./sec. to 200 ft./sec. This is in agreement with earlier results from this laboratory[40] which indicated very little effect of velocity on damage in this system for this cavitation condition. It was reported in this earlier work that there was a factor of about 100 greater damage produced in mercury than in water. This observation was based on a

TABLE 4

COMPARISON OF MERCURY AND WATER DATA

Material	Hg Damage MDP(mils) at 50 Hrs. (34 fps) 2-spec.	H_2O Damage MDP(mils) at 50 Hrs. (200 fps) 3-spec.	H_2O Damage /Hg Damage Ratio
Stainless Steel	0.277×10^{-2}(6)*	0.527×10^{-2}(27)	1.90
Ta-10W	0.17×10^{-1}(2)	0.111×10^{-1}(3)	0.65
Ta-8W-2Hf	0.847×10^{-2}(2)	0.762×10^{-2}(3)	0.90
Cb-1Zr	0.179×10^{-1}(2)	0.203×10^{-1}(3)	1.13
Mo-1/2Ti	0.210×10^{-1}(2)	0.997×10^{-1}(6)	4.75
Tenelon (USS)	0.186×10^{-2}(2)	0.220×10^{-2}(6)	1.18
		Overall Average	1.75

Material	Hg Damage (34 fps)	H_2O Damage (97 fps)	Ratio
Stainless Steel	0.277×10^{-2}(6)	0.377×10^{-2}(3)	1.35

Material	Hg Damage (34 fps)	H_2O Damage (65 fps)	Ratio
Stainless Steel	0.277×10^{-2}(6)	0.277×10^{-2}(6)	1.00

*Numbers in brackets after damage value indicate number of test specimens for which damage value is averaged.

different test specimen arrangement than currently used for the mercury tests. The two-specimen unsymmetrical arrangement was used for these tests, and in addition the mercury contained trace amounts of water. Evidence exists that the "wet" mercury is somewhat more damaging than "dry" mercury.[50] The current investigation was conducted in dry mercury for a two-specimen symmetrical arrangement. The wet mercury two-specimen unsymmetrical arrangement was analyzed in terms of the pressures on the specimen surface during the current investigation, and the comparison made with the current arrangement. The results are shown in Table 5, where it is observed that the suppression pressure (pressure above vapor) axial gradient is very much steeper for the earlier system. This indicates that more damage would be expected since the available head for bubble collapse is much higher, particularly at the rear of the specimen, thus giving rise to more energetic bubble collapses. In addition, a crosswise pitting pattern was observed, indicating local cavitation as the flow crossed the specimen edge, due presumably to the nonsymmetrical arrangement. Thus, for this system, bubbles are carried into the high pressure region and very violent collapses afforded. This does not occur in the symmetrical arrangement because if the pressure is raised to the same levels, no bubbles are present on the damaged face.

The present comparison does not mean that identical degrees of cavitation with the same velocities in identical systems, in one case using water and in another mercury, would produce approximately the

TABLE 5

ACTUAL PRESSURE ABOVE VAPOR PRESSURE ON TEST SPECIMEN SURFACE FOR STANDARD CAVITATION IN MERCURY FOR TWO SPECIMEN SYMMETRICAL VERSUS UNSYMMETRICAL ARRANGEMENTS

Fluid	Velocity ft./sec.	No. of Specs.	Spec. Tap No.	Pressure above vapor pressure Run No.1	Run No.2	Run No.3
"Dry" Mercury 75°F	34	2 (symm.)	1	1.7	1.7	
			2	4.9	1.7	
			3	9.5	5.3	
"Wet" Mercury 75°F	34	2 (unsymm.)	1	2.2	2.1	2.0
			2	12.3	16.8	19.3
			3	41.3	39.8	40.8

same damage, but merely that in this particular case, about the same suppression pressures between water and mercury on the polished surface, but with a considerably greater velocity in water, have produced about the same damage. Since the pressures are not known on the sides of the specimen (which provide about 88% of the exposed area), and since the geometries in the water and mercury venturis are not identical (3 versus 2 test specimens), the present data cannot be regarded as a generalized comparison between water and mercury damaging capabilities anymore, in retrospect, than the previous tests[40] which indicated a factor of about 100 between mercury and water. Unfortunately, the physical limitations of the systems are such that a direct experimental comparison cannot be made. Eventually, however, such data should be provided by the vibratory facility tests also being conducted in this laboratory. Ideally,

if the cavitation condition, velocity, geometry, and suppression head are identical between the two systems then, assuming that the compressibilities of the two fluids are also similar, the forces exerted on adjacent solids should be proportional to the density ratio (13.5), so that the damage from mercury should be much greater. At the present, there is no real evidence to contradict this expectation. However, it is quite evident at this point that seemingly minor changes in flow geometry can have important effects on damage.

G. Detailed Examinations of Damage

1. Mercury Specimens

Typical areas from the heavily pitted regions of each material were traced with a precision profilometer ("Linear Proficorder"),* at a horizontal sensitivity of 1000:1 and at a vertical sensitivity of 50,000:1. For each specimen several crosswise and longitudinal (in the direction of flow) traces were made at intervals of about 0.5 mils. Due to the extreme sensitivity used, very precise leveling of the surface was required if the trace curve were to remain on scale. This was accomplished by a built-in adjustment on the machine, and the specimen was incremented by a micrometer table adjustment made especially for this purpose. After tracing, the specimens were examined with a metallographic microscope at 500X and photomicrographs taken of the area

---

*Micrometrical Division, The Bendix Corporation, Ann Arbor, Michigan.

traced. The trace marks left by the diamond-tipped stylus were visible, with the use of oblique lighting techniques, very clearly in some cases though not so in others, depending on the hardness of the material. The edge of the specimen is a good reference point, clearly indicated by the dropping of the stylus, which facilitates the location of a particular pit on the photomicrograph. Also, it was possible to visually observe where the stylus had passed through a pit (by the trace mark) with reference to the pit centerline. Figure 66 shows the procedure in complete detail for matching the traces with the corresponding photomicrographs. In general, it was not necessary to photograph the entire length of the traced area, as only those areas of interest could be located. This was accomplished by a micrometer adjustment on the metallograph by which the specimen could be indexed by .001 inch increments. Thus, once the end of the proficorder trace was located (the end where it dropped off the edge), it was only necessary to index back along the trace by the amount measured from the end of the trace to the pit from the proficorder trace. Due to the size of the pits examined, the sensitivities used and the random location of the pits, roughly ten to twenty feet of chart paper were required per successful pit trace. Figure 66 shows six transverse traces, spaced apart by either 0.5 or 1.0 mils, and covering almost the full width of the specimen for carbon steel tested in mercury. Since the stylus had to be started on the surface, the full width of the specimen is not covered by the traces. The corresponding photomicrograph is at slightly smaller magnification than the trace, so that the arrows are necessary to indicate the correspondence

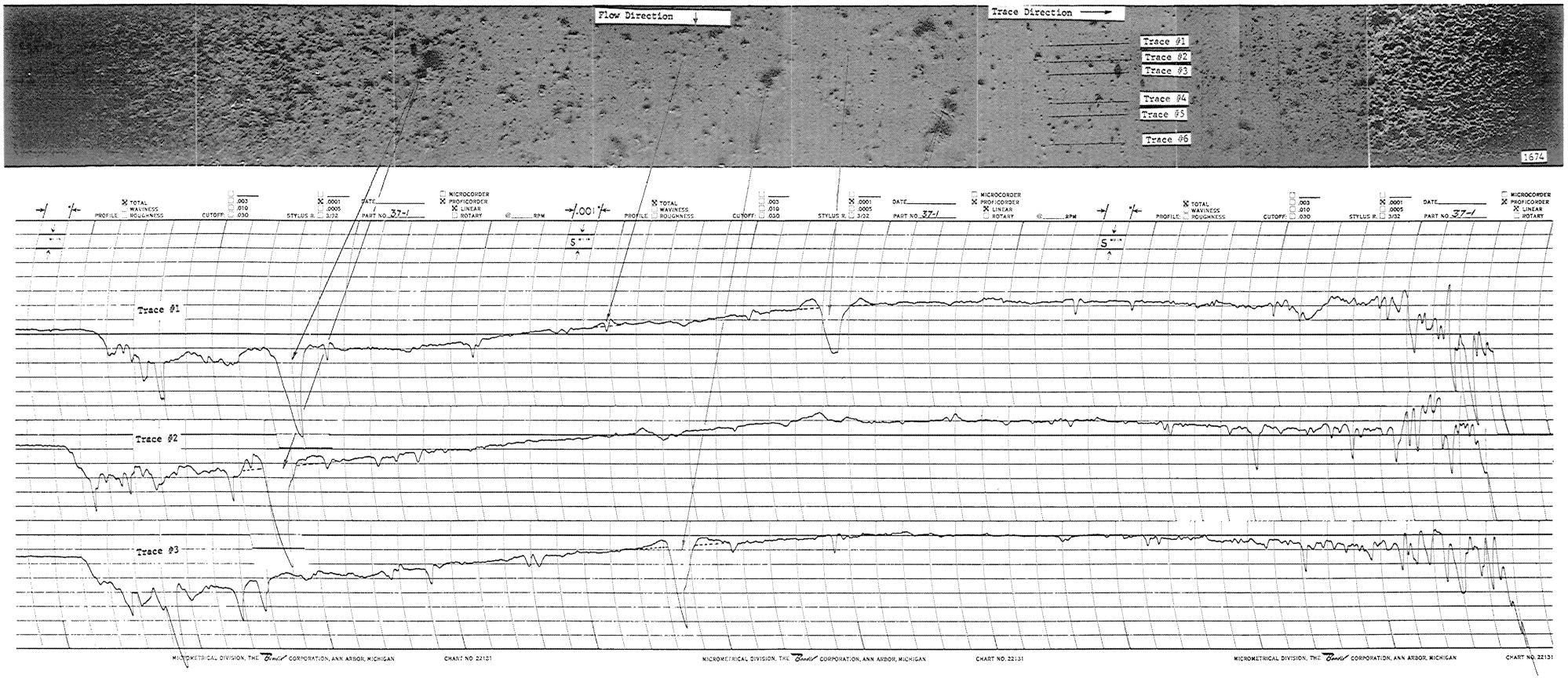

Fig. 66.--Photomicrograph and corresponding proficorder traces of surface of specimen 39-1 (carbon steel), after 10 hours exposure to "standard cavitation" in mercury at a throat velocity of 34 feet per second.

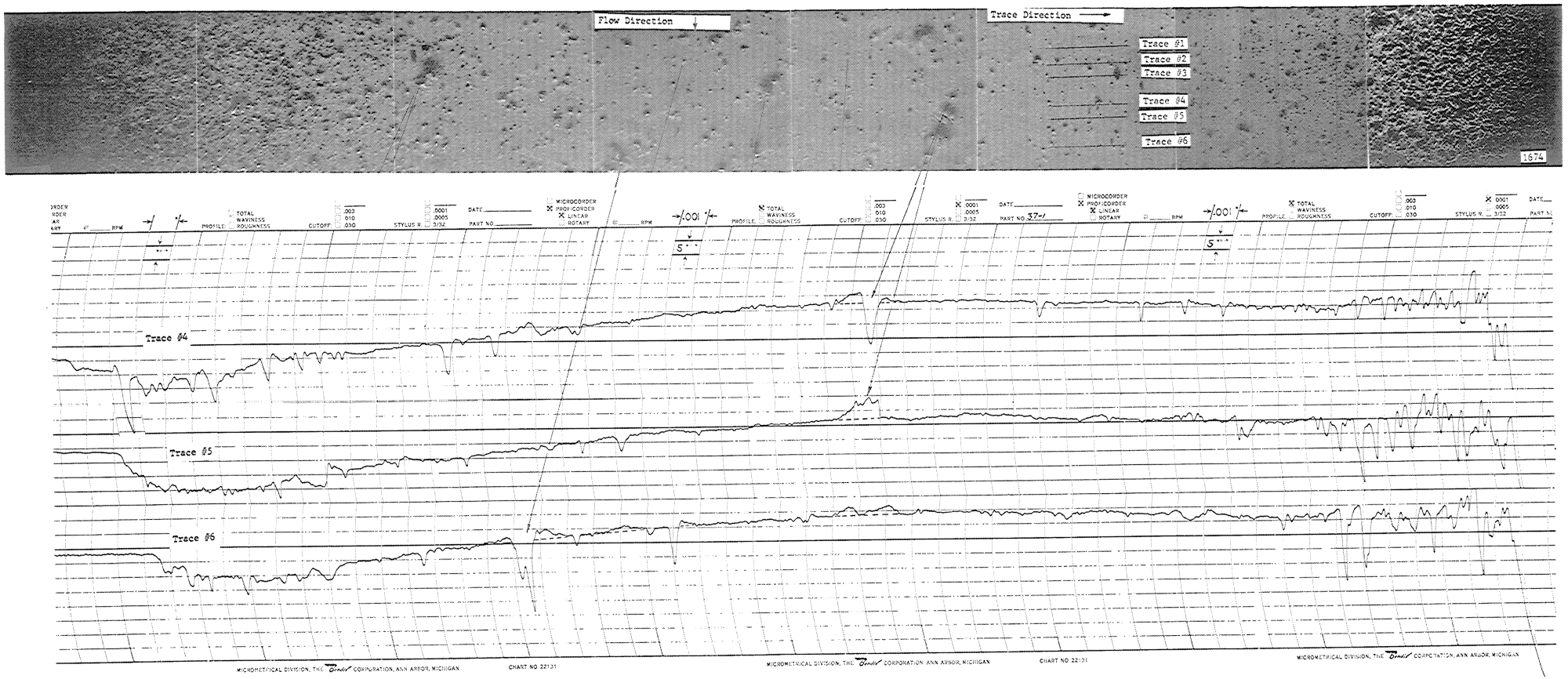

Fig. 66.--Photomicrograph and corresponding proficorder traces of surface of specimen 39-1 (carbon steel), after 10 hours exposure to "standard cavitation" in mercury at a throat velocity of 34 feet per second.

between pit and pit trace. However, in the following figures in this section, each of which cover only about 8 mils in length, the correspondence between pit and trace is obvious since there is only a very small difference in magnification and the width of the area covered is small.

Figure 67 shows the areas on the polished surface covered by the proficorder traces. To compare pit sizes and shapes between materials it was necessary to trace all specimens in corresponding areas so that regions which had been exposed to the same cavitation flow regime would be compared. Figures 68 through 81 are photomicrographs ($\sim$ 500X), with the corresponding proficorder traces for the mercury specimens. A careful inspection of all of these figures indicates that generally the individual pits are very symmetrical and are surrounded by raised rims, i.e., they are "craters." No preferred orientation has been observed for the raised rim formation, i.e., it occurs on all sides, upstream and downstream, as often as not. In Figure 69, e.g., the surface area around the individual pits clearly is raised into the form of a rim, as would be expected from a central load in excess of the yield strength of the material. This type of pit formation, presumably due by its symmetry to a single bubble implosion, is very prominent in this investigation in mercury, although sometimes obscured by the damage in adjacent areas. In only one case (Figure 77) was a fatigue-type failure observed, i.e., grossly nonsymmetrical failure, presumably due to many blows of reduced violence. The "fatigue pit" (trace #1) is triangular in shape and has a raised lip on the downstream

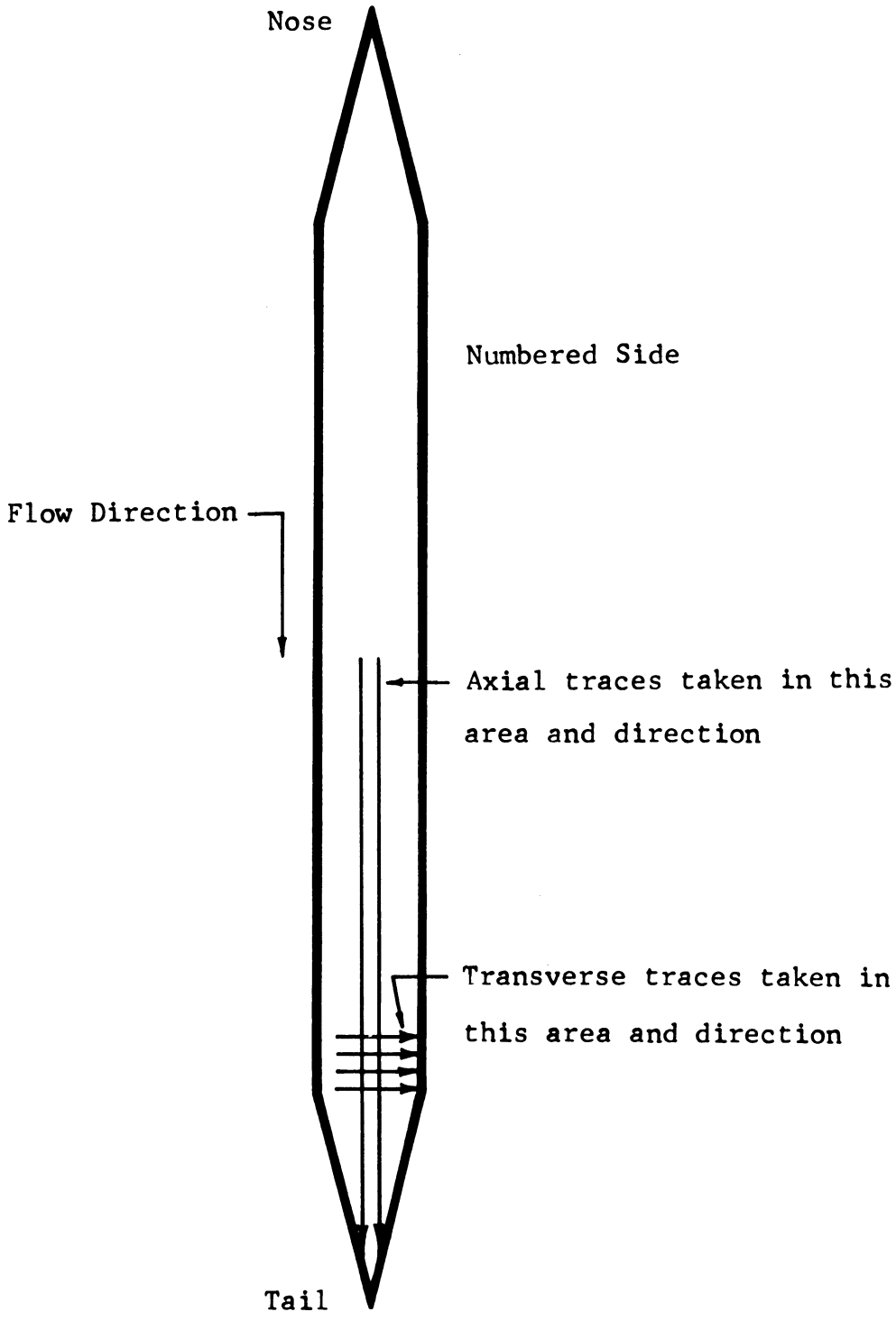

Fig. 67.--Schematic of polished surface showing areas covered by transverse and longitudinal traces.

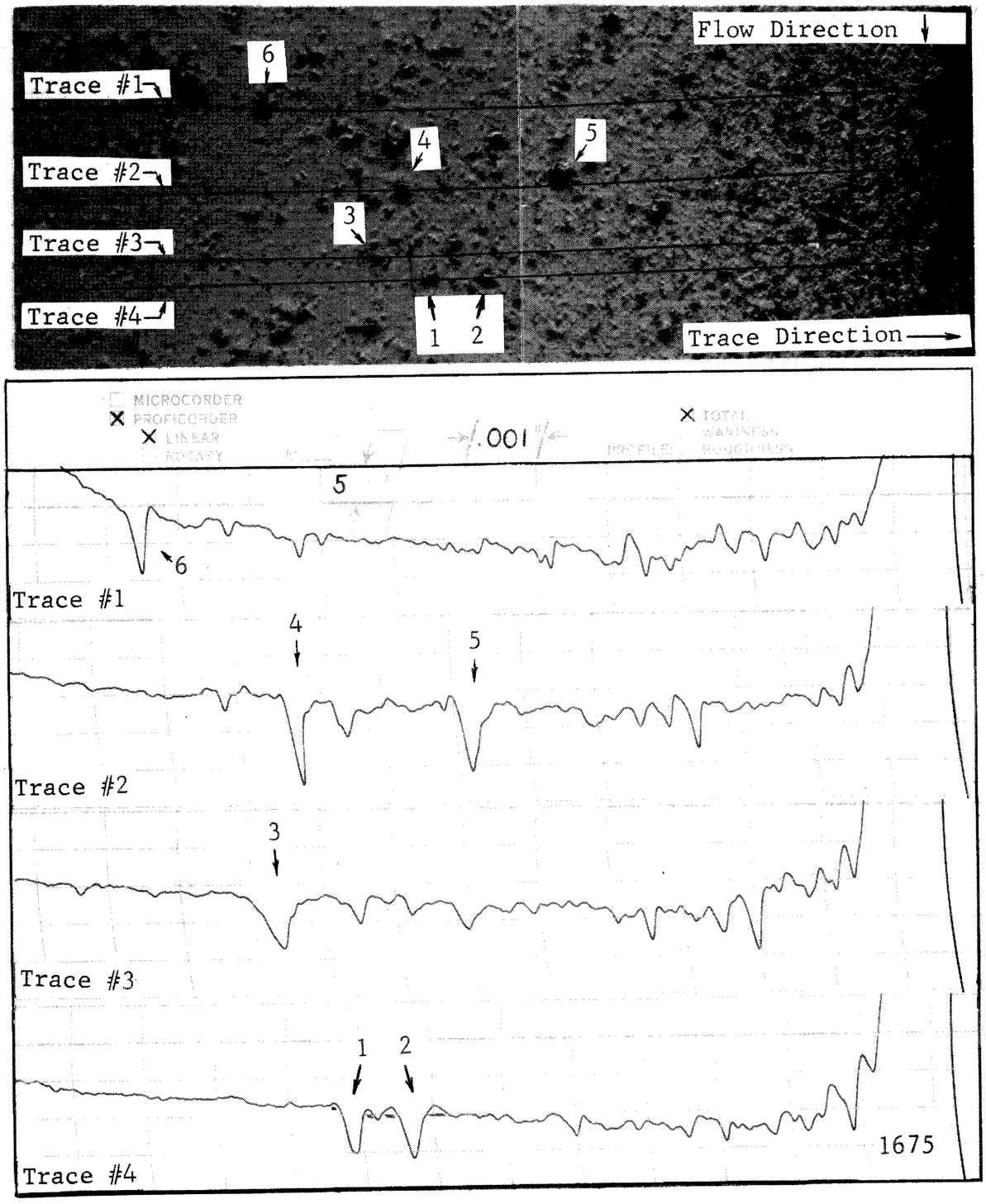

Fig. 68.--Photomicrograph and corresponding proficorder traces of surface of specimen 11-F (Tenelon), after 10 hours exposure to "standard cavitation" in mercury at a throat velocity of 34 feet per second.

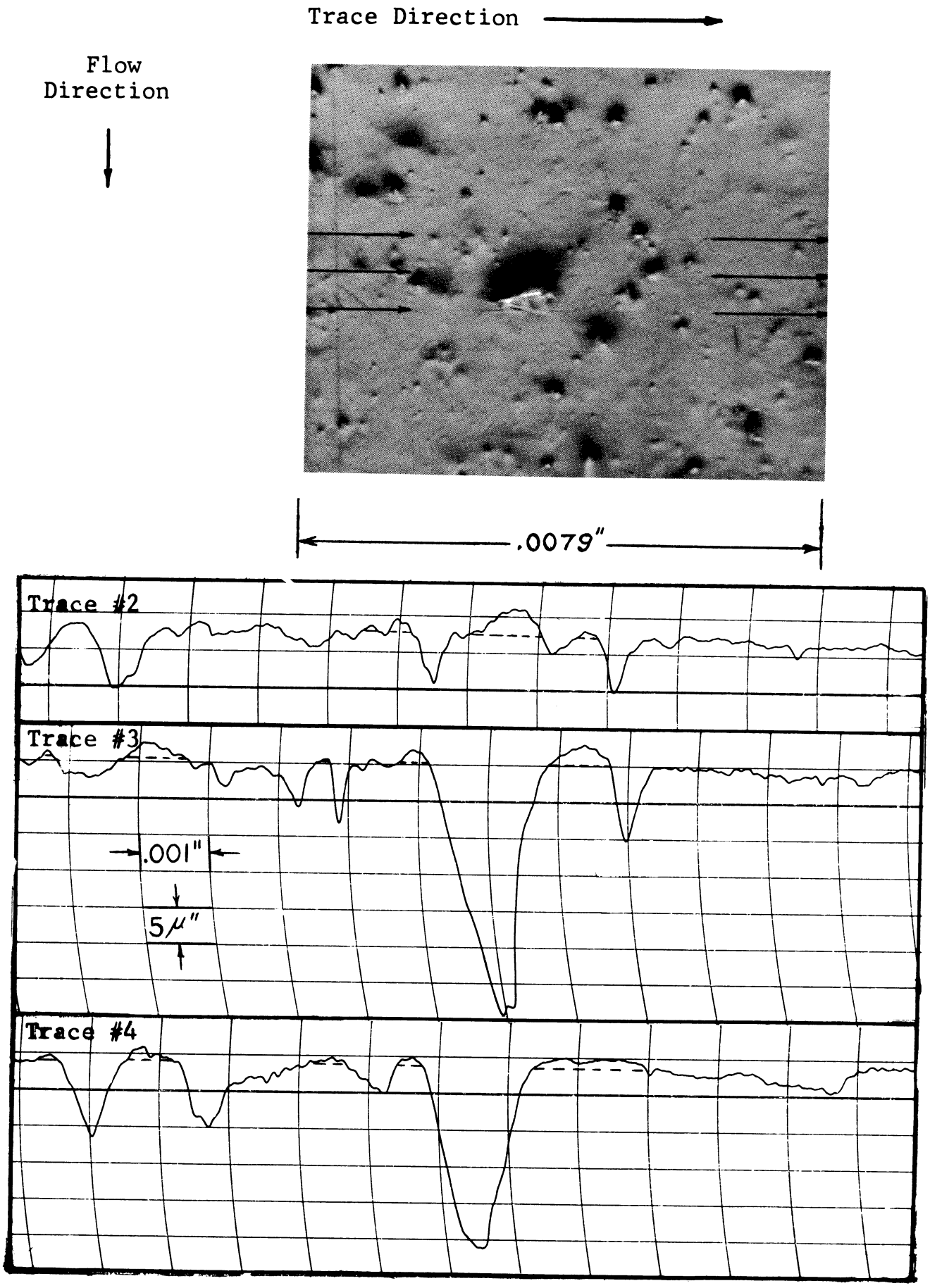

Fig. 69.--Photomicrograph and corresponding proficorder traces of surface of specimen 22-SS (304 stainless steel), after 10 hours exposure to "standard cavitation" in mercury at a throat velocity of 34 feet per second.

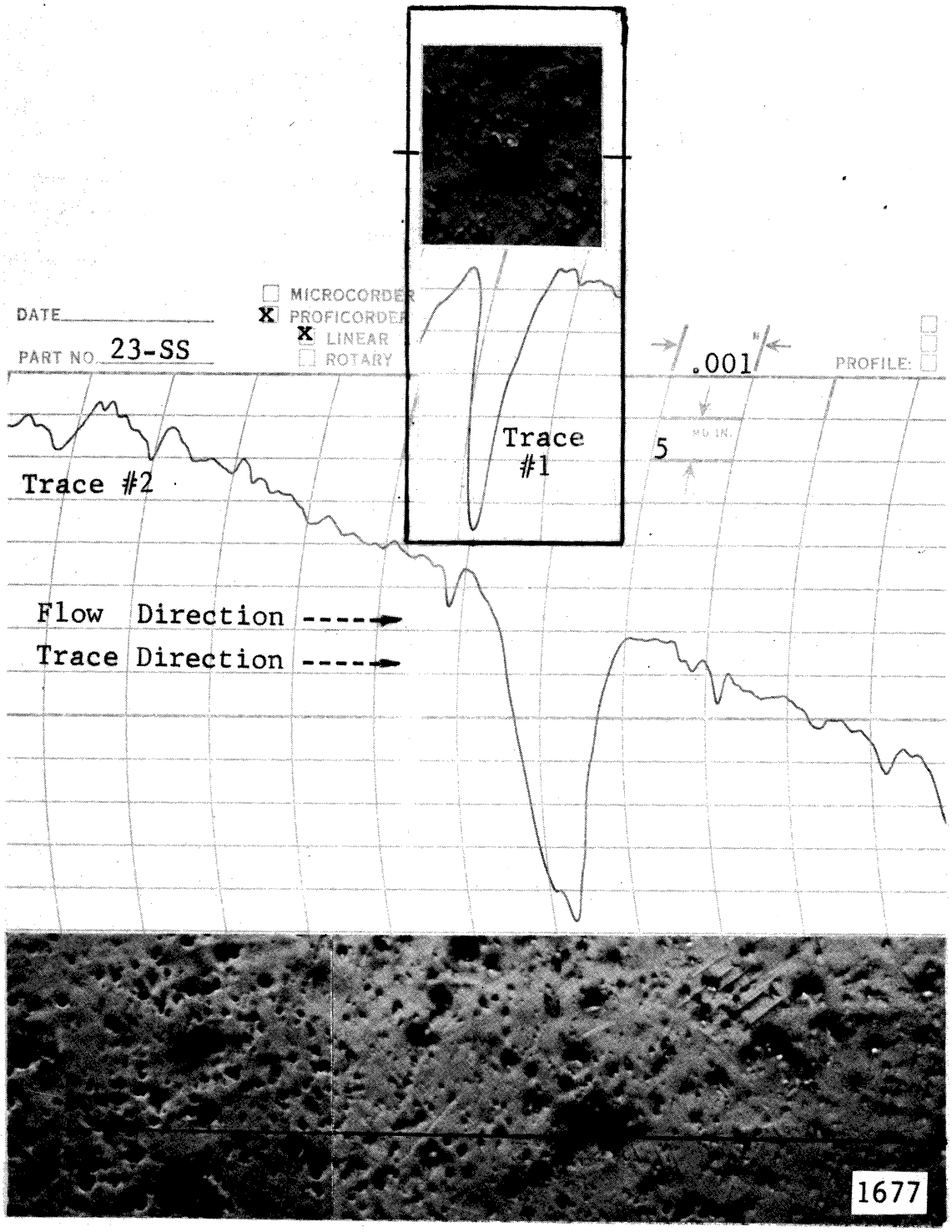

Fig. 70.--Photomicrograph and corresponding proficorder traces of surface of specimen 23-SS (stainless steel), after 10 hours exposure to "standard cavitation" in mercury at a throat velocity of 34 feet per second.

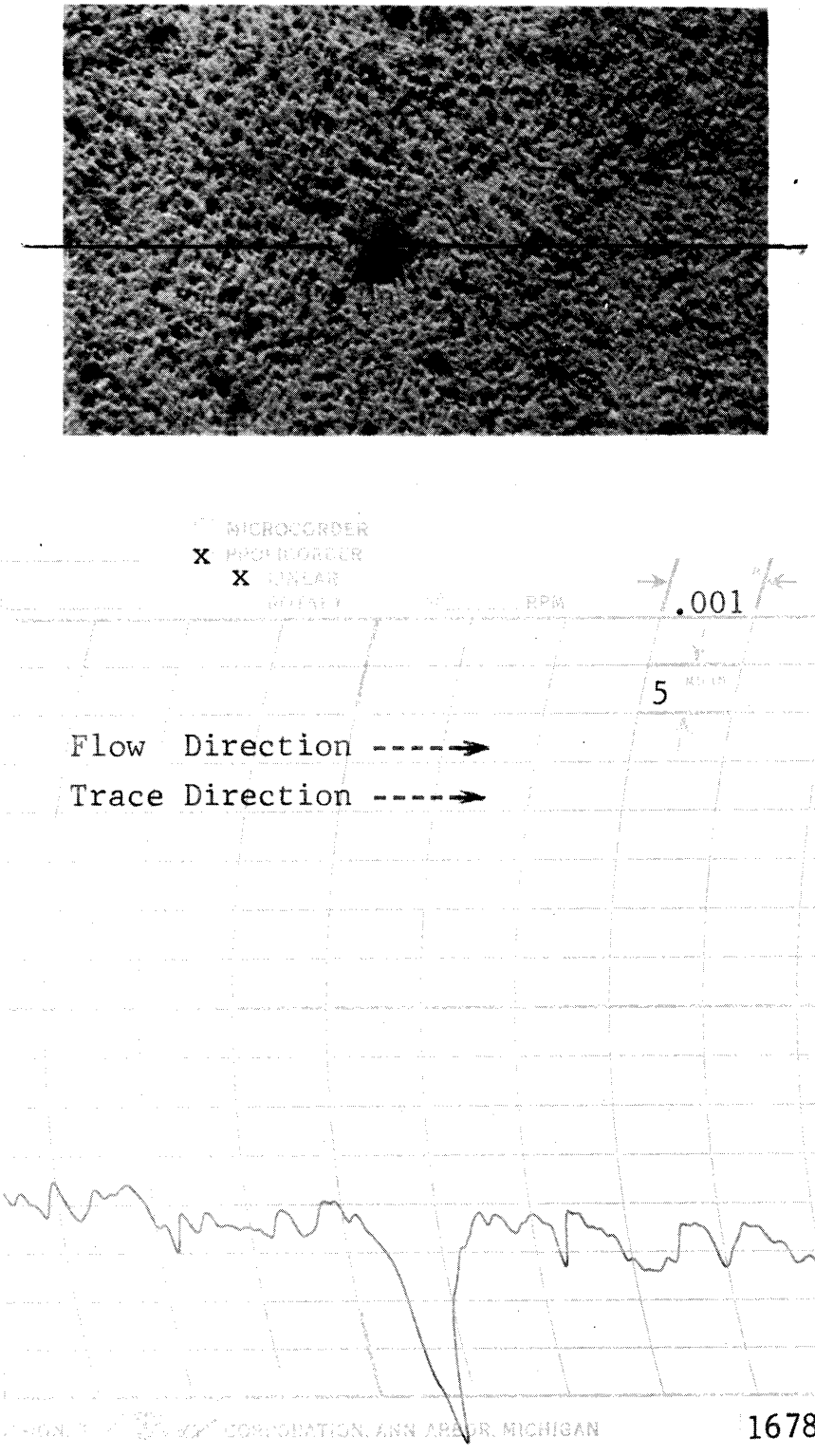

Fig. 71.--Photomicrograph and corresponding proficorder traces of surface of specimen 4-Cb-1Zr, after 50 hours exposure to "standard cavitation" in mercury at a throat velocity of 34 feet per second.

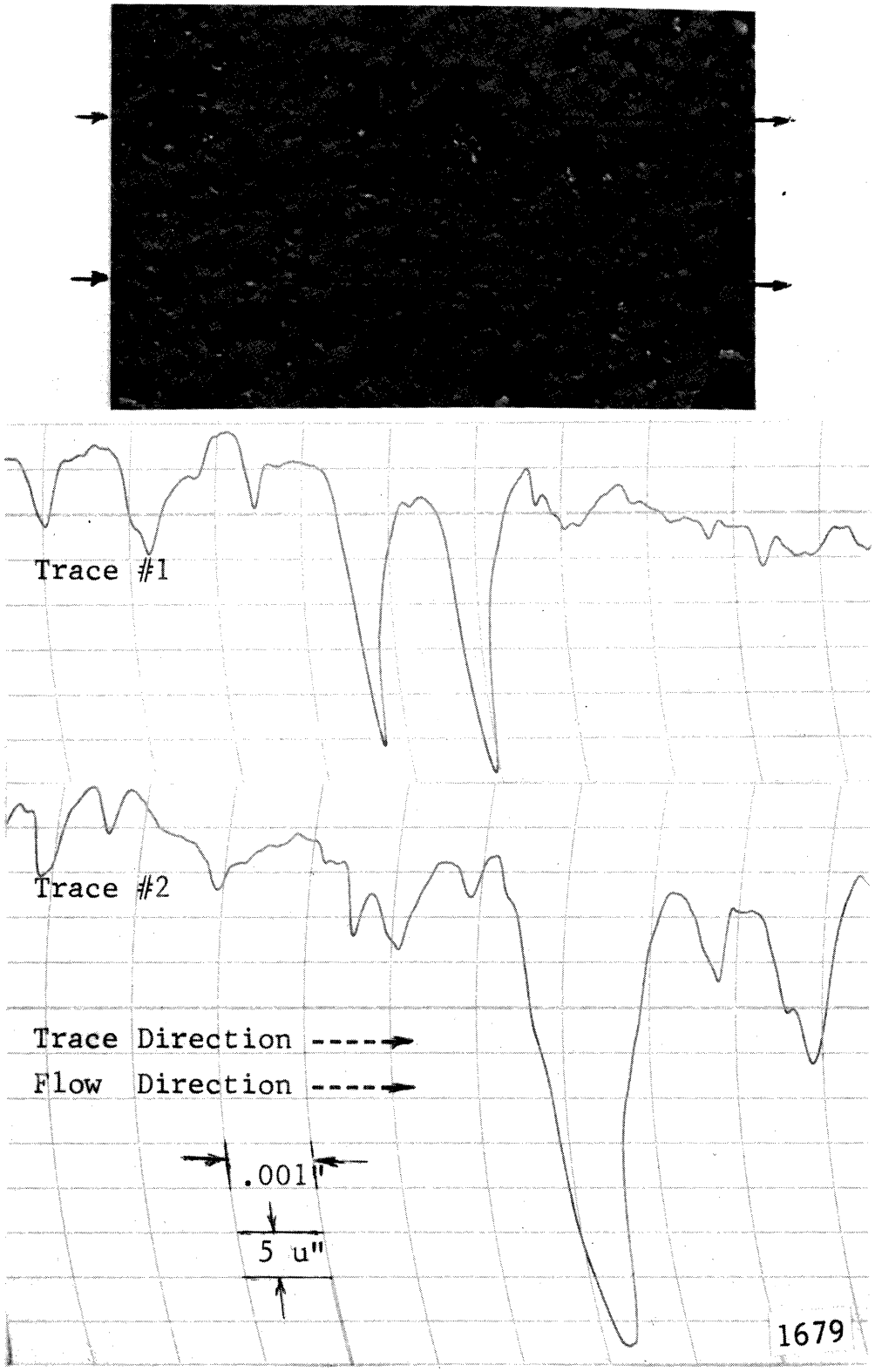

Fig. 72.--Photomicrograph and corresponding proficorder traces of surface of specimen 10-Cb-1Zr, after 10 hours exposure to "standard cavitation" in mercury at a throat velocity of 34 feet per second.

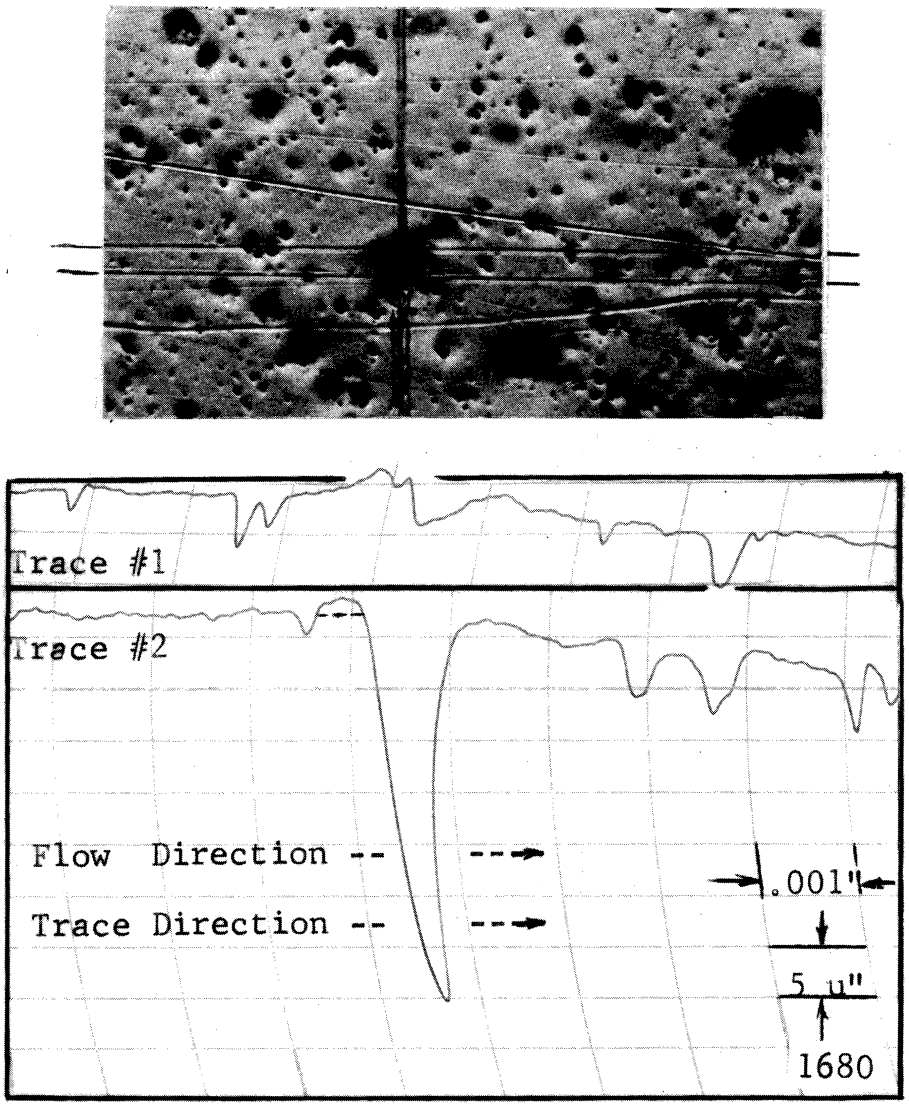

Fig. 73.--Photomicrograph and corresponding proficorder traces of surface of specimen 10-Cb-1Zr, after 10 hours exposure to "standard cavitation" in mercury at a throat velocity of 34 feet per second.

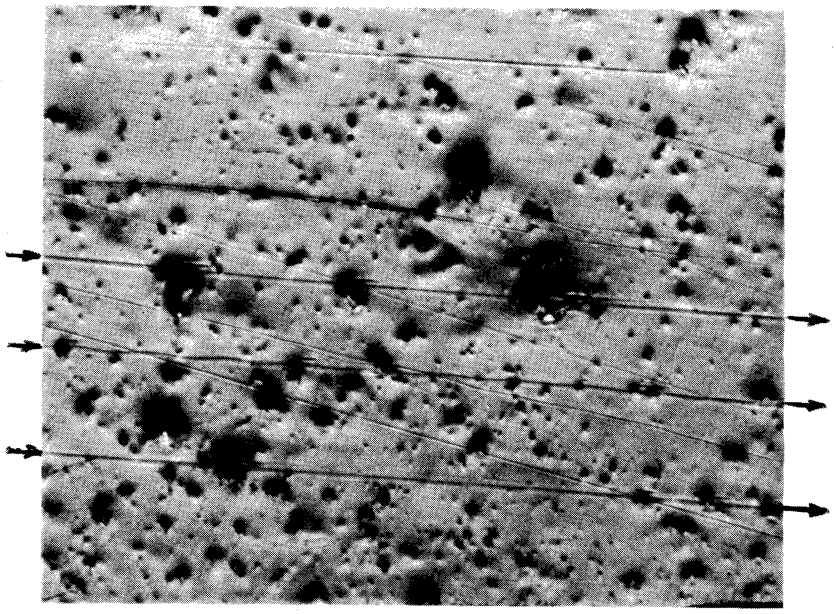

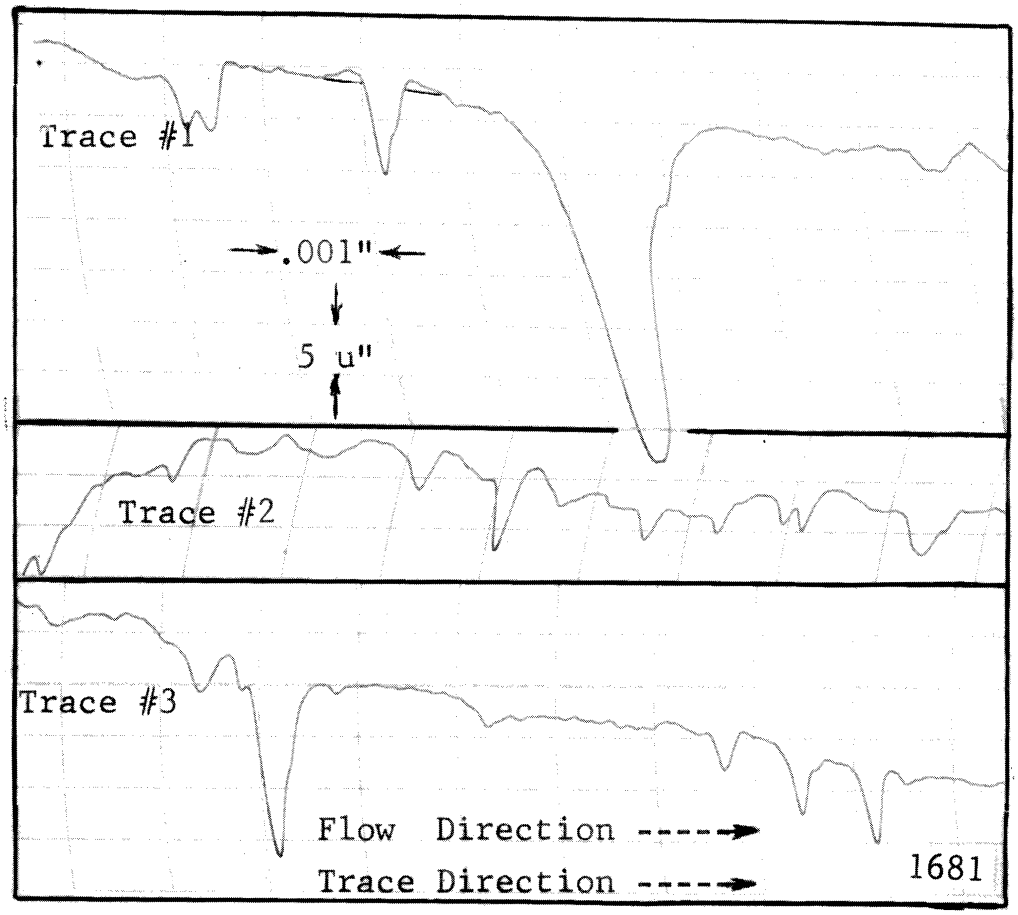

Fig. 74.--Photomicrograph and corresponding proficorder traces of surface of specimen 10-Cb-1Zr, after 10 hours exposure to "standard cavitation" in mercury at a throat velocity of 34 feet per second.

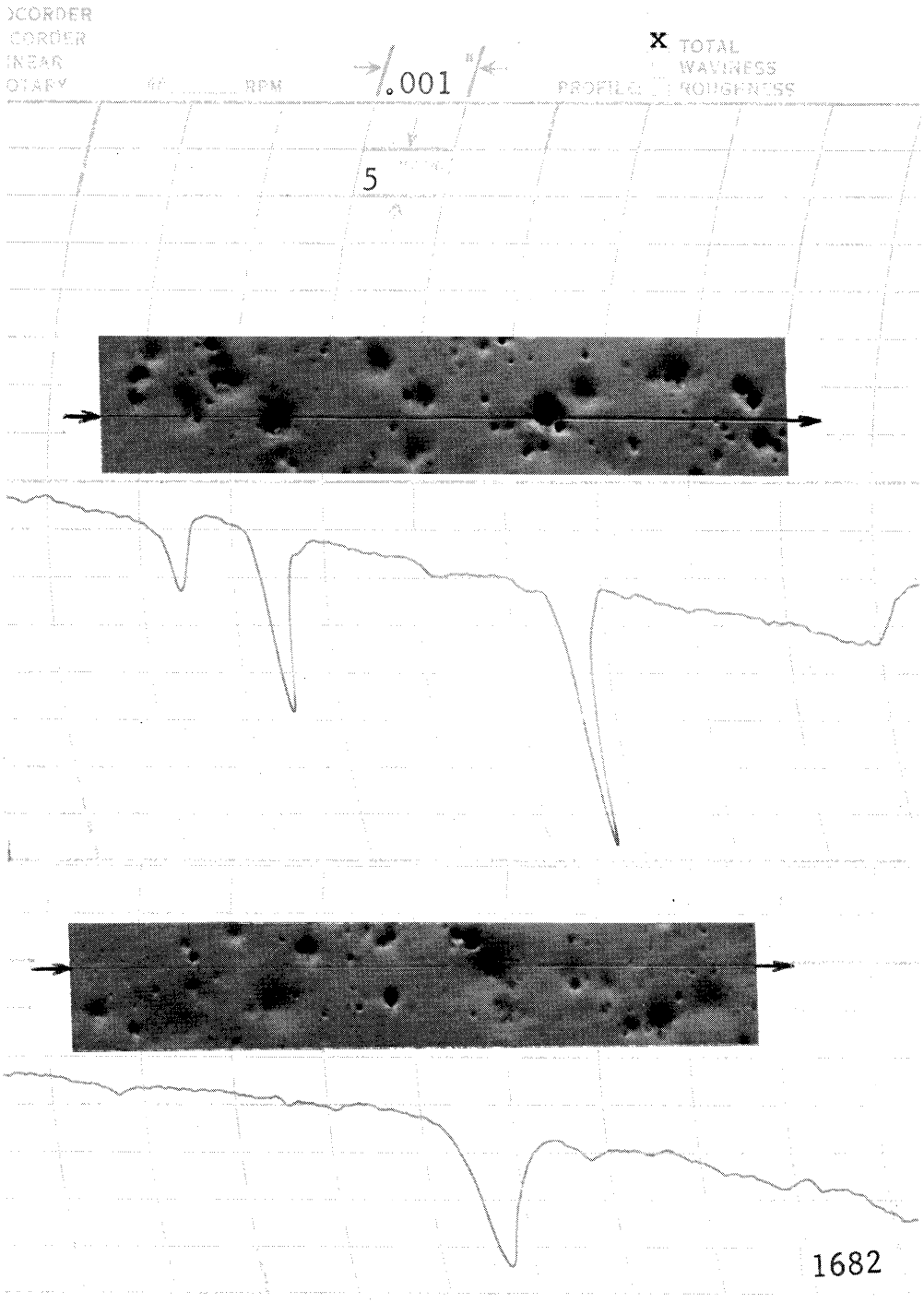

Fig. 75.--Photomicrograph and corresponding proficorder traces of surface of specimen 9-A (Ta-10W), after 10 hours exposure to "standard cavitation" in mercury at a throat velocity of 34 feet per second.

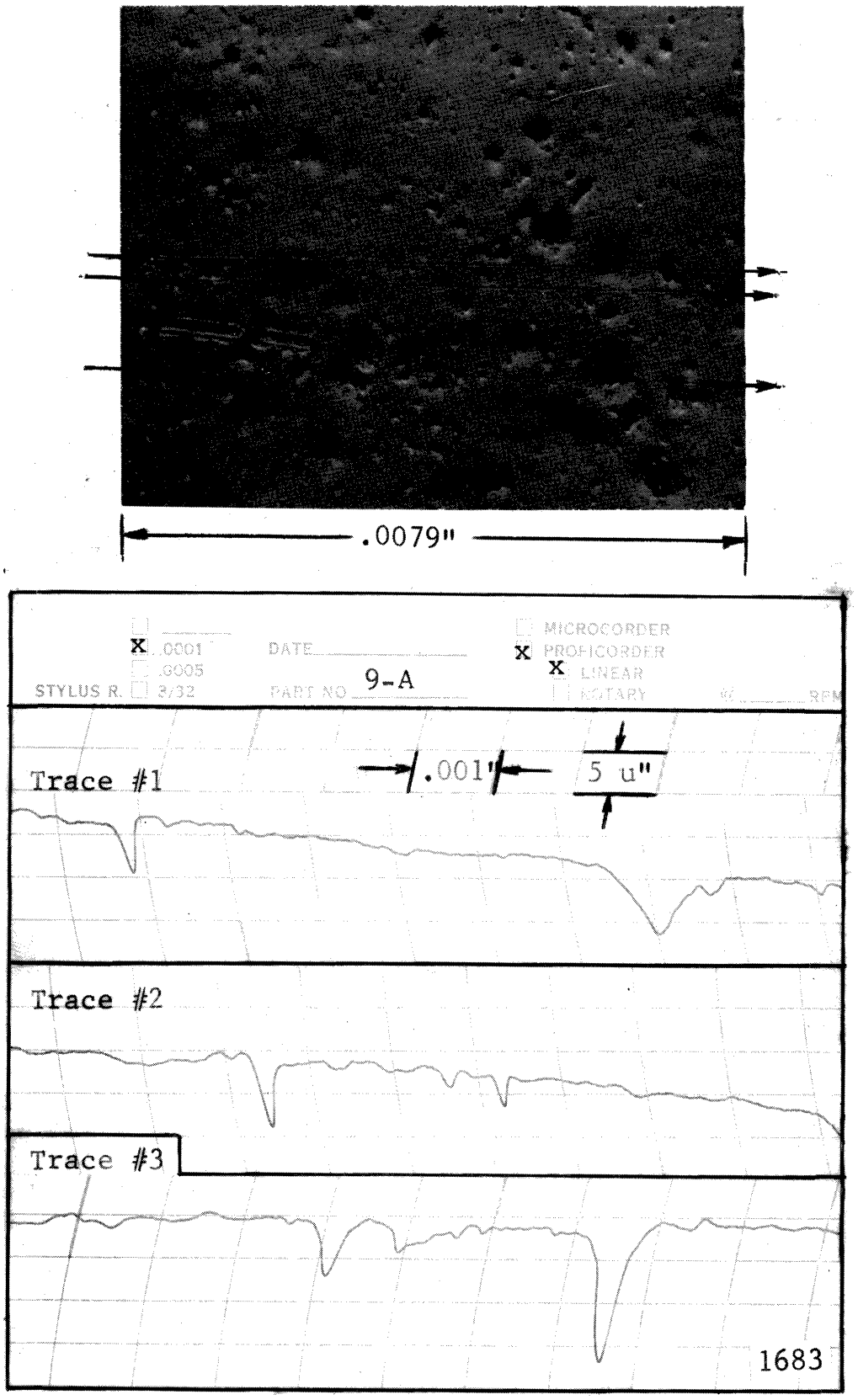

Fig. 76.--Photomicrograph and corresponding proficorder traces of surface of specimen 9-A (Ta-10W), after 10 hours exposure to "standard cavitation" in mercury at a throat velocity of 34 feet per second.

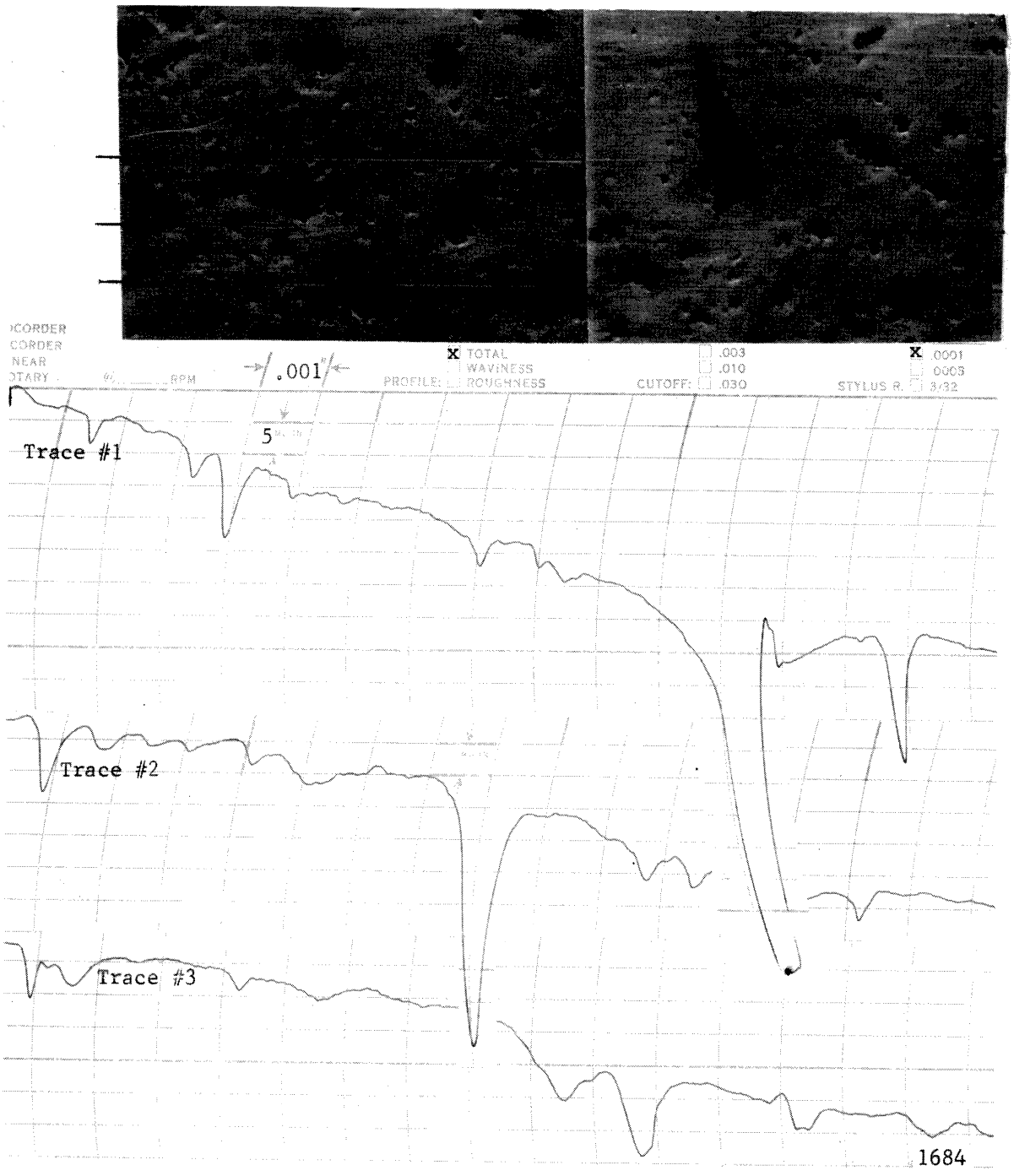

Fig. 77.--Photomicrograph and corresponding proficorder traces of surface of specimen 9-A (Ta-10W), after 10 hours exposure to "standard cavitation" in mercury at a throat velocity of 34 feet per second.

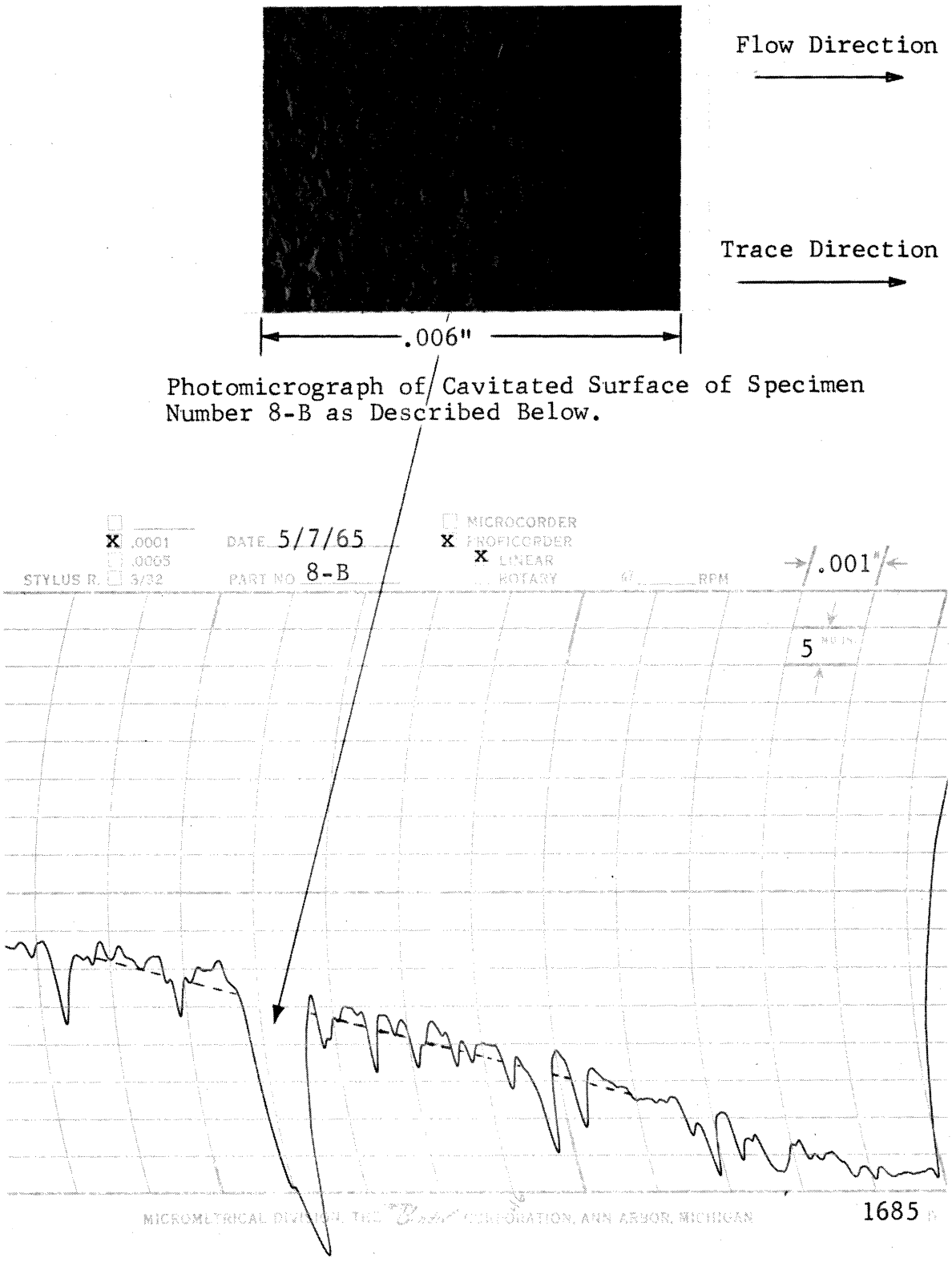

Fig. 78.--Photomicrograph and corresponding proficorder traces of surface of specimen 8-B (Ta-8W-2Hf), after 10 hours exposure to "standard cavitation" in mercury at a throat velocity of 34 feet per second.

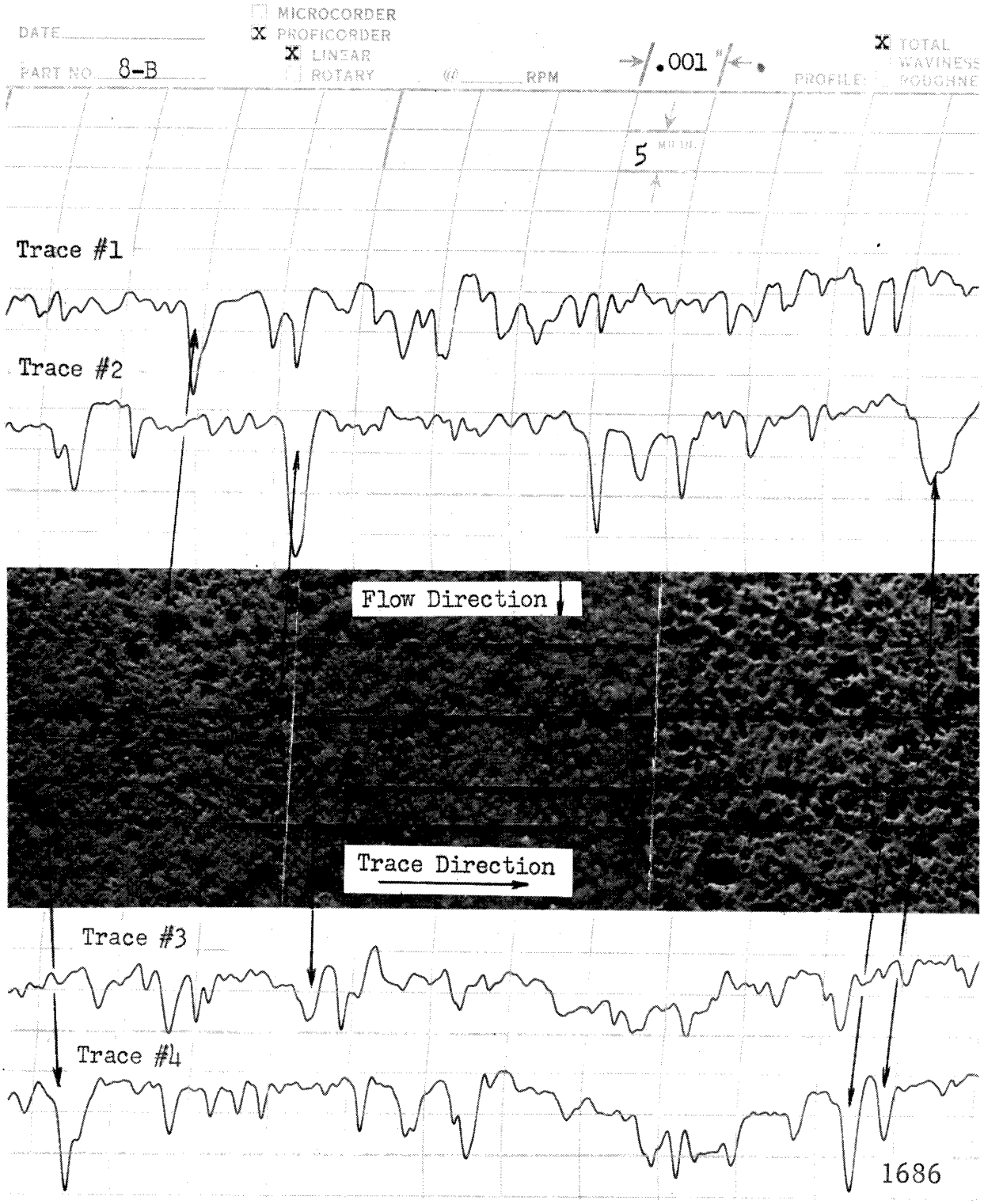

Fig. 79.--Photomicrograph and corresponding proficorder traces of surface of specimen 8-B (Ta-8W-2Hf), after 10 hours exposure to "standard cavitation" in mercury at a throat velocity of 34 feet per second.

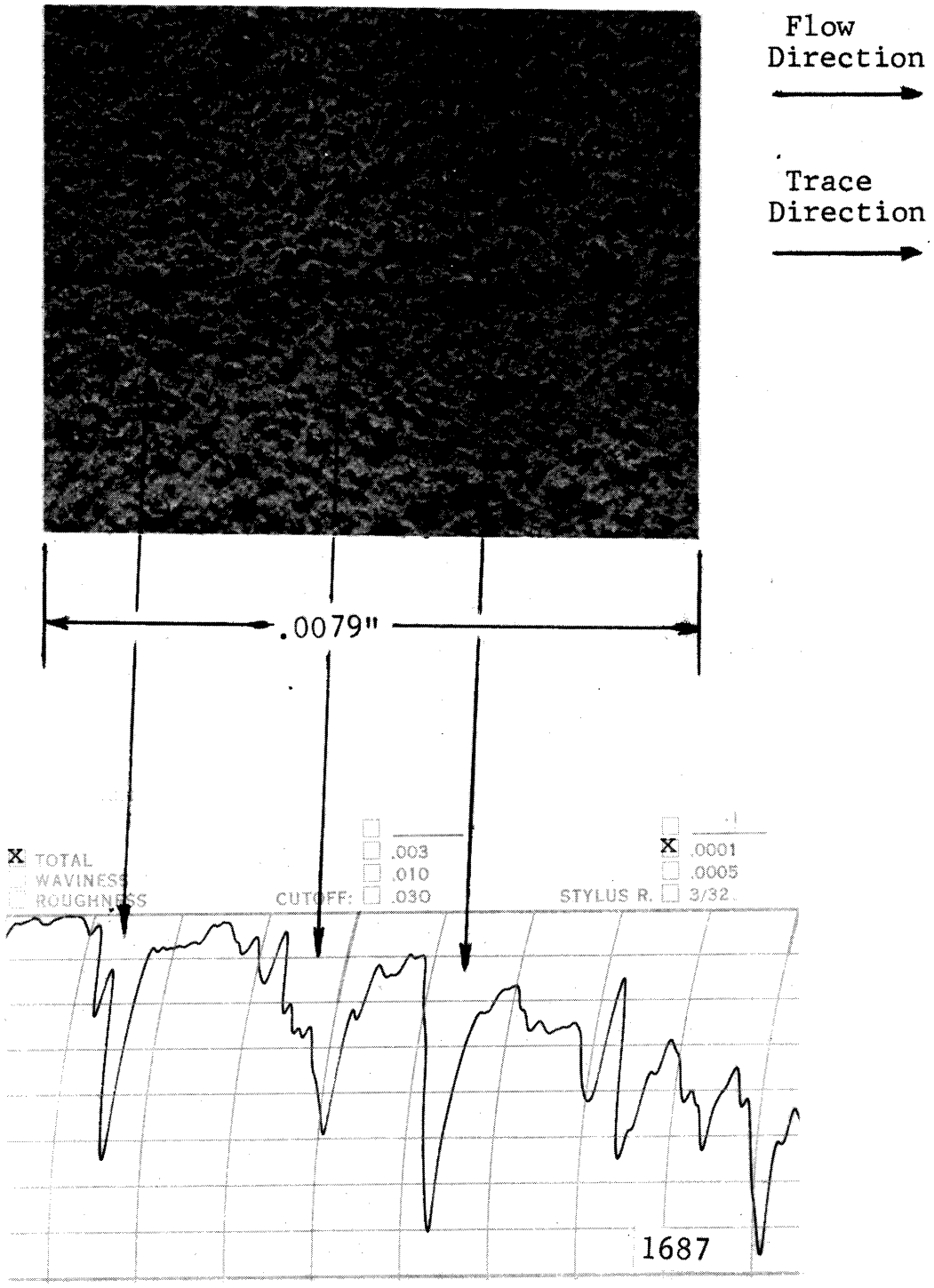

Fig. 80.--Photomicrograph and corresponding proficorder traces of surface of specimen 8-B (Ta-8W-2Hf), after 10 hours exposure to "standard cavitation" in mercury at a throat velocity of 34 feet per second.

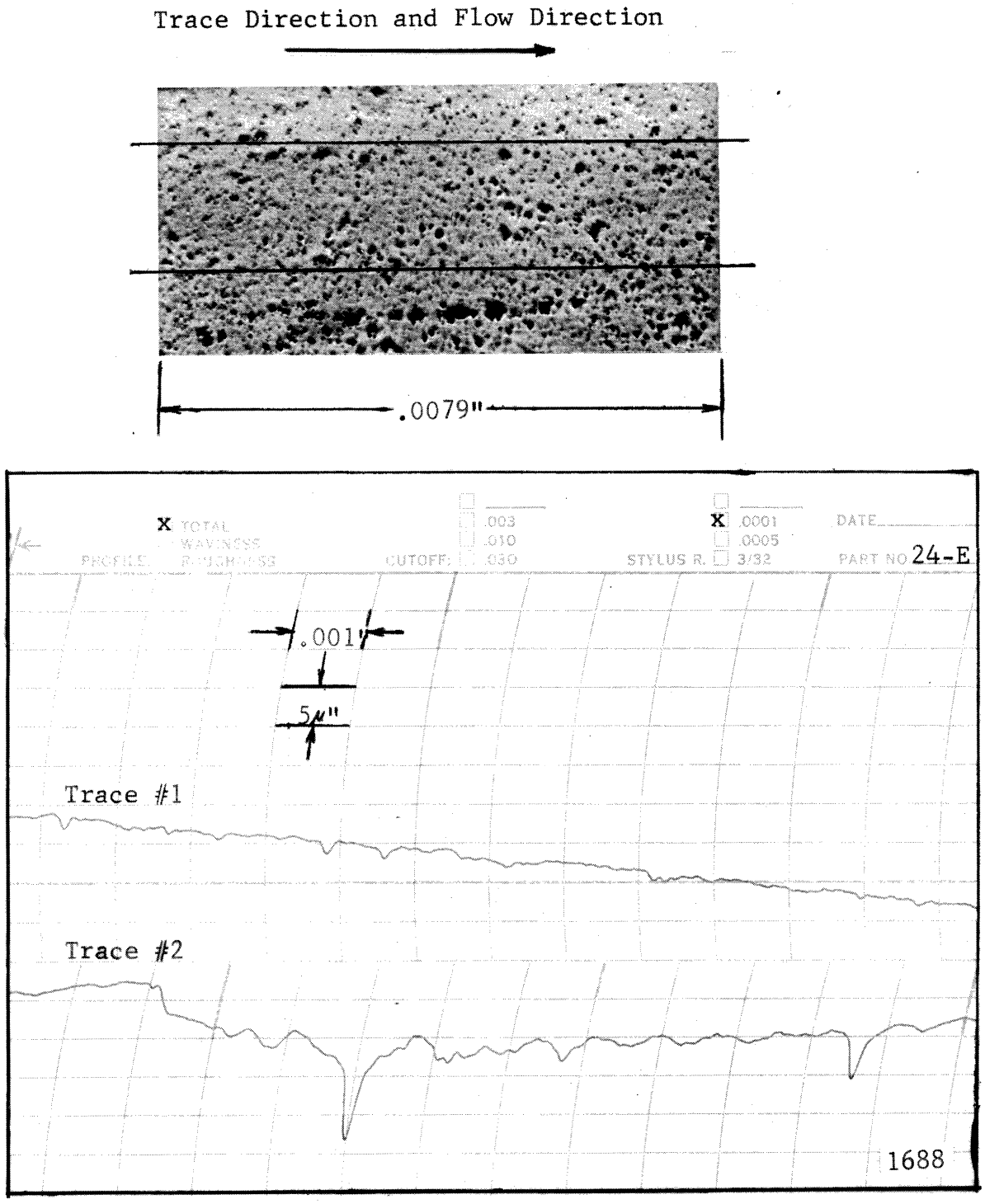

Fig. 81.--Photomicrograph and corresponding proficorder traces of surface of specimen 24-E (Mo-1/2Ti), after 10 hours exposure to "standard cavitation" in mercury at a throat velocity of 34 feet per second.

side. This is believed to indicate a surface failure produced by fatigue action, which has loosened a slab, conceivably along grain boundaries, and subsequently the slab was torn away by the flowing mercury, leaving a raised lip on the downstream side. This type of failure was previously observed and described in tests conducted several years ago in this laboratory.[40] This fatigue type of failure has been observed only rarely for the mercury specimens. In many instances, Figure 76, e.g., the damage has the form of very shallow craters, as perhaps first discussed by Knapp,[24] for aluminum, and is thought to be the result of a single blow from a bubble collapse, which was not sufficiently strong enough to cause material removal. On the other hand, the other craters, which appear dark in the center and show a greater depth to diameter ratio on the traces, are thought to be the result of a single blow which was strong enough to cause material removal.

In an earlier investigation,[46] where a few proficorder traces of this type were compared with microsections through the traced pits, it appeared that material was actually removed from such pits (contrary to Knapp's guess),[24] in that the volume of the depression exceeded that of the raised rim. However, the margin of error for such measurements was considerable. Since, on many specimens, this is essentially the only type of damage observed, and a measurable weight loss exists, it is further substantiated that material removal occurs in this type of damage. As already mentioned, this type of damage appears to result from a single blow to the surface, since the size and shape of these pits does not change with additional exposure, while numerous other pits appear in

adjacent areas. In the present study it has been observed that many times smaller pits will appear on the rim of larger ones, and even within the larger ones (Figures 69, 73, 75, 77, etc.). It is thus verified, as also previously reported,[40] that the formation of pits in the initial stages of cavitation damage is a locally random process, and that gross material removal from cavitation damage, at least in the present mercury tests, is the result of many superimposed individual craters of this single blow type. The transition of this type of pitting to the gross damage often found in prototype equipment can be seen in Figures 78, 79, 80, and 81, where the craters are so close together that even at 500X, the distinction of individual pits is hard to make. To the unaided eye, this type of damage looks like a fog on the polished surface.

Figure 82, typical of the nickel specimens, illustrates the interplay between mechanical cavitation damage and the associated chemical attack, which may be enhanced by cavitation. The shape of the damaged areas is about the same as the mechanical damage areas of the specimens already discussed, where there was very little, if any, chemical attack. The individual pits of the nickel are very much deeper than those previously discussed. However, there is no visible attack on the surface, other than in those areas where it was indicated by the previously discussed specimens that cavitation damage would be expected. Thus it appears that the chemical attack is accelerated by the mechanical pounding due to cavitation, and the amount of damage is greatly increased by the combined action of these interconnected phenomena.

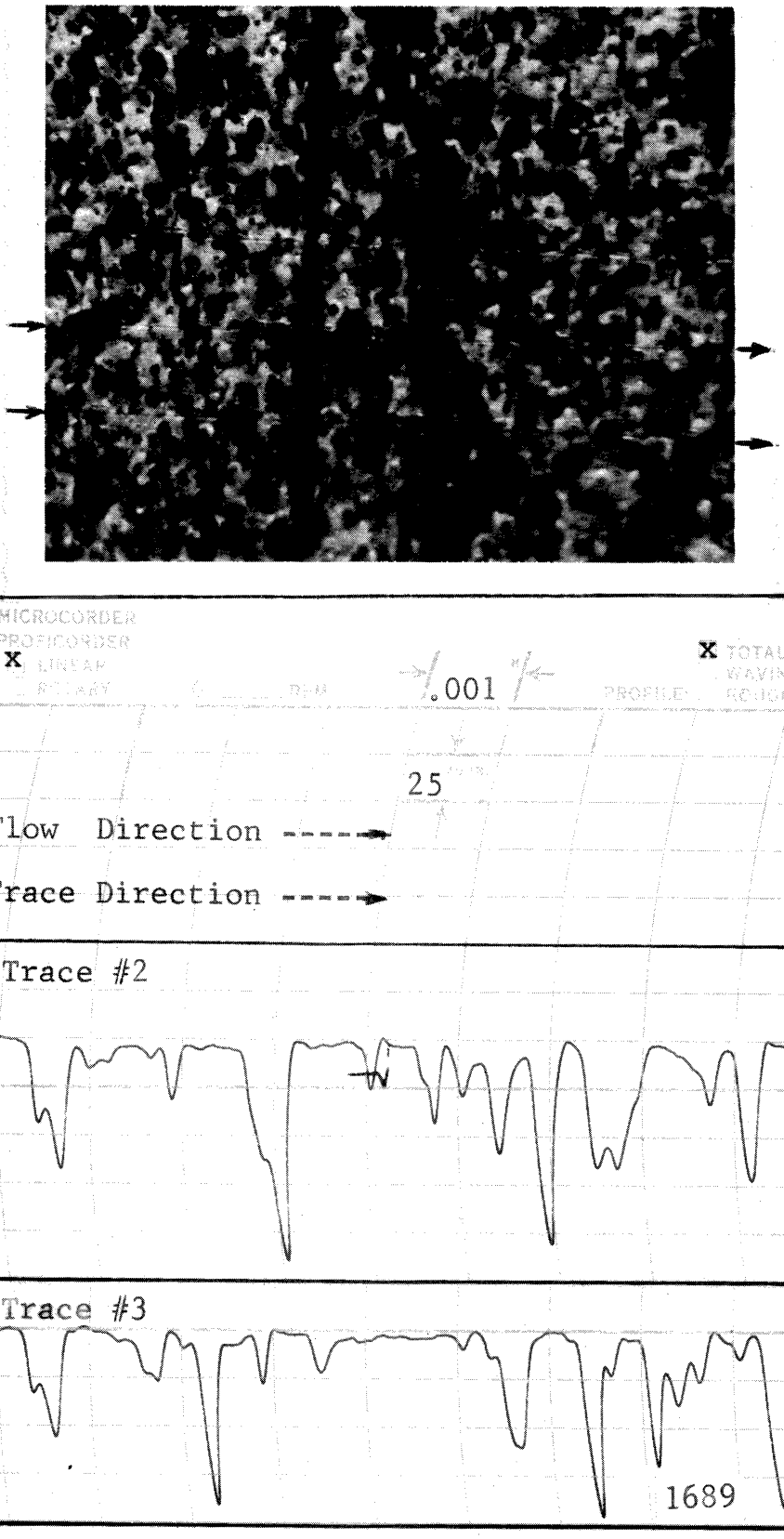

Fig. 82.--Photomicrograph and corresponding proficorder traces of surface of specimen 13-ni (as rec'd nickel), after 10 hours exposure to "standard cavitation" in mercury at a throat velocity of 34 feet per second.

That the combined damage from corrosion and cavitation is considerably greater than the summation which would be caused by the two mechanisms working separately was clearly demonstrated by Plesset[53] in a vibratory facility. This general phenomenon appears to be very similar to stress corrosion as encountered in many fields.

The depth to diameter ratios for all of the proficorder observations for which the tracer tip passed through the center of the pit are listed in Table 6. These ratios do not depend very substantially on type of material, being of the order 0.015 to 0.06 for most materials, and ranging as high as 0.09 for one particular material, Mo-1/2Ti. This lack of strong dependence on the material may be reasonable in that the variation of mechanical properties between the materials tested in mercury is not excessive. Presumably, if a very weak material could be included (or one weakened by a high temperature environment), the depth to diameter ratio would be markedly larger. This has been observed in fact in high temperature cavitation tests with potassium on stainless steel[48] and in certain particle or droplet impact tests where the depth to diameter ratio increases with impact velocity.[51] The larger depth to diameter ratios for nickel are presumed due to the combined cavitation-corrosion effects previously mentioned. It is again noted that the pits on the nickel are roughly of the same diameter as those on the other materials, indicating enhancement of corrosion in the area where craters were formed.

The number distribution of pits versus pit diameter was also examined on two materials tested in mercury, stainless steel and carbon

TABLE 6

DEPTH TO DIAMETER RATIO FOR MERCURY CAVITATION PITS

Material	Pit Diameter (mils)	Pit Depth (mils)	Depth/ Diameter
Tenelon (USS)	0.3	0.009	0.03
	0.5	0.010	0.02
	0.4	0.012	0.03
	0.3	0.006	0.02
	0.4	0.007	0.018
		Average =	0.024
304 SS	1.8	0.035	0.02
	1.0	0.012	0.012
	1.0	0.027	0.027
	1.5	0.034	0.023
	1.0	0.025	0.025
		Average =	0.021
Cb-1Zr (10)	0.8	0.037	0.046
	1.5	0.035	0.023
	0.5	0.017	0.034
		Average =	0.034
Cb-1Zr (4)	0.8	0.027	0.034
	0.7	0.030	0.043
	1.5	0.050	0.044
		Average =	0.040
Ta-10W (9-A)	0.3	0.018	0.06
	0.6	0.027	0.045
	0.8	0.015	0.02
	0.25	0.007	0.003
	1.0	0.009	0.009
	0.3	0.008	0.027
	0.6	0.015	0.025
	0.8	0.013	0.017
	1.2	0.037	0.03
	0.5	0.019	0.038
		Average =	0.027

TABLE 6--Continued

Material	Pit Diameter (mils)	Pit Depth (mils)		Depth/ Diameter
Ta-8W-2Hf (8-B)	1.0	0.032		0.032
	0.4	0.017		0.043
	0.2	0.012		0.06
	0.4	0.023		0.058
	0.5	0.025		0.05
			Average =	0.049
Mo-1/2Ti (24-E)	0.3	0.010		0.093
	0.25	0.006		0.024
			Average =	0.055
As Rec'd Nickel (13-ni)	0.5	0.115		0.23
	0.3	0.085		0.28
	0.25	0.075		0.15
	0.3	0.090		0.30
			Average =	0.22

steel, in considerable detail. Figures 83 and 84 show the results of this study, made at 500X.

The maximum number density lies in the size range of 0.025 to 0.25 mils. As already indicated, the diameter of bubbles in contact with the surface ranged from $\sim$ 5 to $\sim$ 30 mils, showing that the pits are about 10^{-2} times as small as the bubbles. It is thus indicated, as expected theoretically, that the bubbles collapse to very small sizes before the damage is produced, or that the central jet produced from a nonsymmetrical collapse covers a very small area compared with the initial bubble size.

2. Water Facility Damage Specimens

The general areas traced by the proficorder for the following specimens tested in the water facility and the general procedure followed is the same as that listed in the previous section for the mercury facility. However, one additional difficulty was encountered in the course of the specimen examination, in that the tracemarks of the stylus tip were not visible on most materials. Thus it is not possible to obtain photomicrographs of the exact areas traced in most cases. Typical photomicrographs at $\sim$ 500X and typical proficorder traces are presented of the damage in water for comparison to those for mercury.

The difficulty in locating the tracemarks on the surface of the water specimens is believed due to the following: The surfaces may be harder due either to additional coldworking of the surface layers in water by the cavitation which takes the form of larger numbers of less energetic bubbles so that the surface layer is more resistant to marking

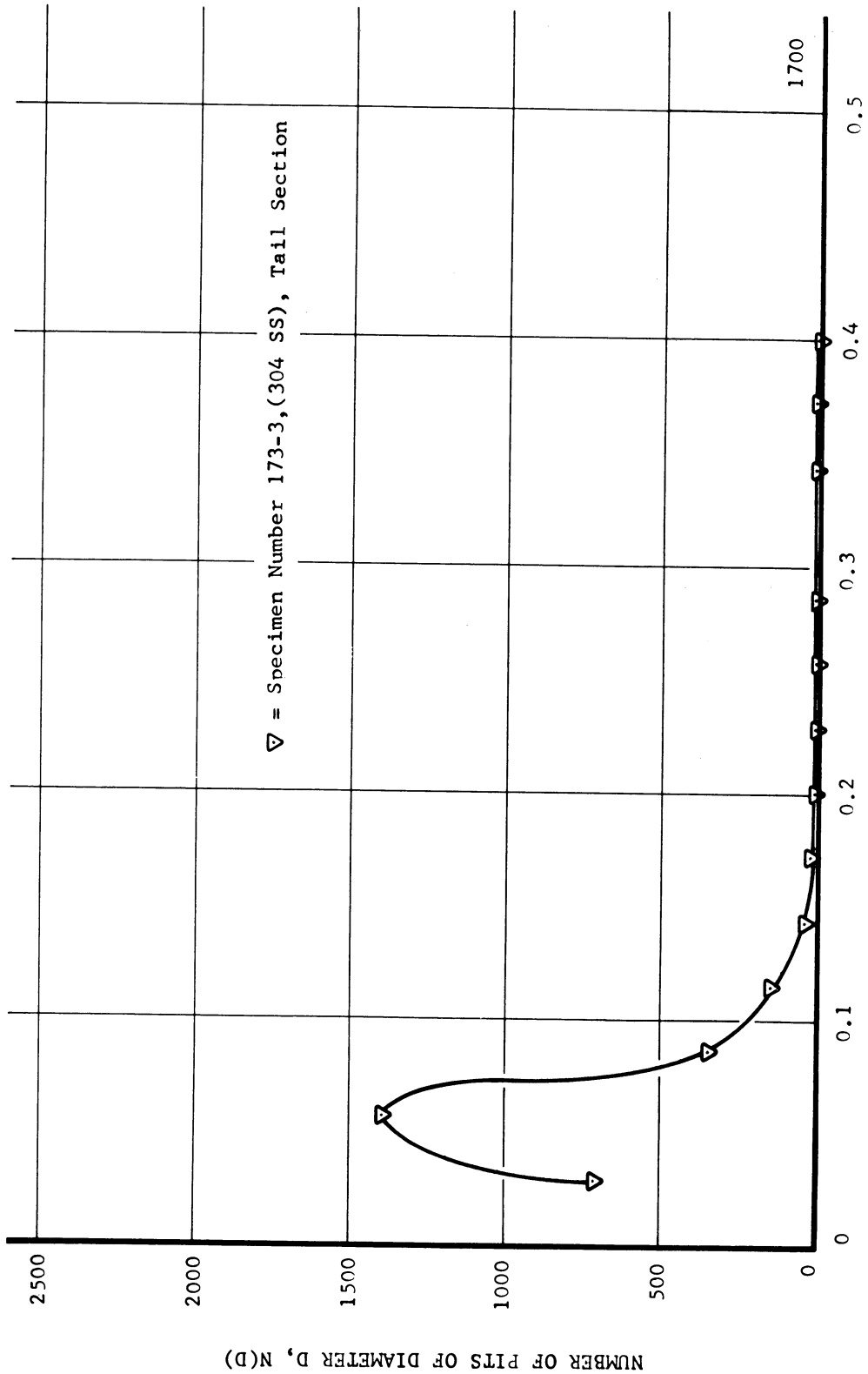

Fig. 83.--Pit size density vs. pit diameter for stainless steel tested at "standard cavitation" in mercury at 34 ft./sec.

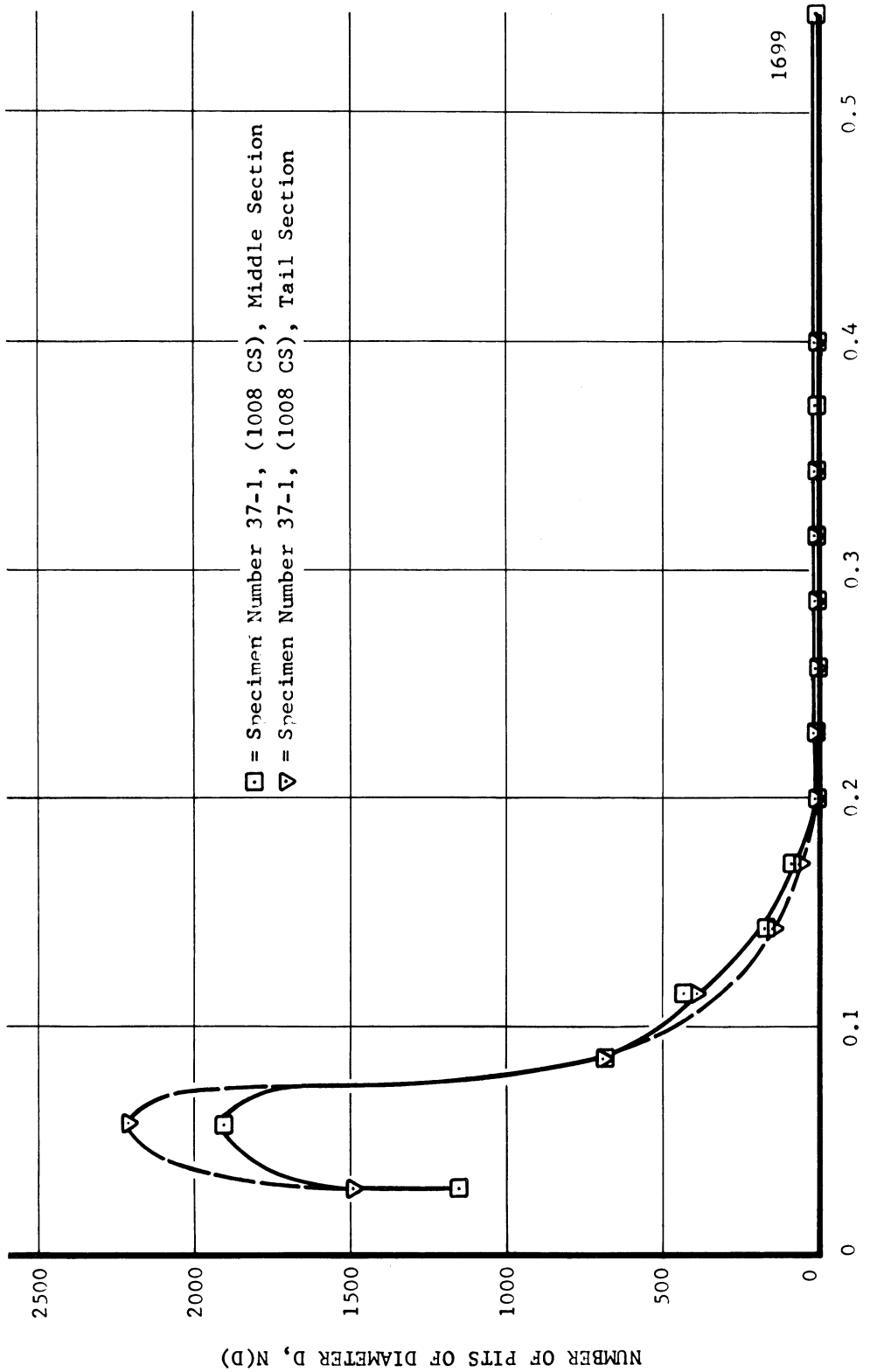

Fig. 84.--Pit size density vs. pit diameter for carbon steel tested in mercury at "standard cavitation" at 34 ft./sec.

by the stylus (evidence of such an increase in surface hardness has been observed in this laboratory). Also, in general, the pits are more numerous and the surface correspondingly more roughened, making location of the traces more difficult. In mercury, individual pits are more predominant in a rather flat surface.

Figures 85 through 90 are photomicrographs and proficorder traces of typical damage areas on several materials from the water facility. As mentioned earlier, the damage consists of pits which are elongated in the direction of flow on almost all of the materials. Also, in general, there is a predominant lip on the downstream side of the pit, due presumably to the application of a force slanted in the downstream direction. In addition, it was observed (Fig. 88, e.g.) that transverse traces exhibit no preferential location of the rim, i.e., the transverse traces show predominantly that a rim is present either on both sides of the pit or on one side or the other in essentially equal numbers, thus eliminating the possibility that the rim indications are due to peculiarities of the tracing mechanism. These observations are consistent with the earlier discussed damage mechanism consisting of an unsymmetrical bubble collapse with the formation of a jet, oriented by the flow into a partially downstream direction.

The depth to diameter ratio for the water cavitation pits has also been tabulated from the proficorder trace data, although it was not possible to determine whether the stylus had passed through the pit centerline or not, due to reasons presented earlier. However, enough pits have been examined to give a good statistical indication of the

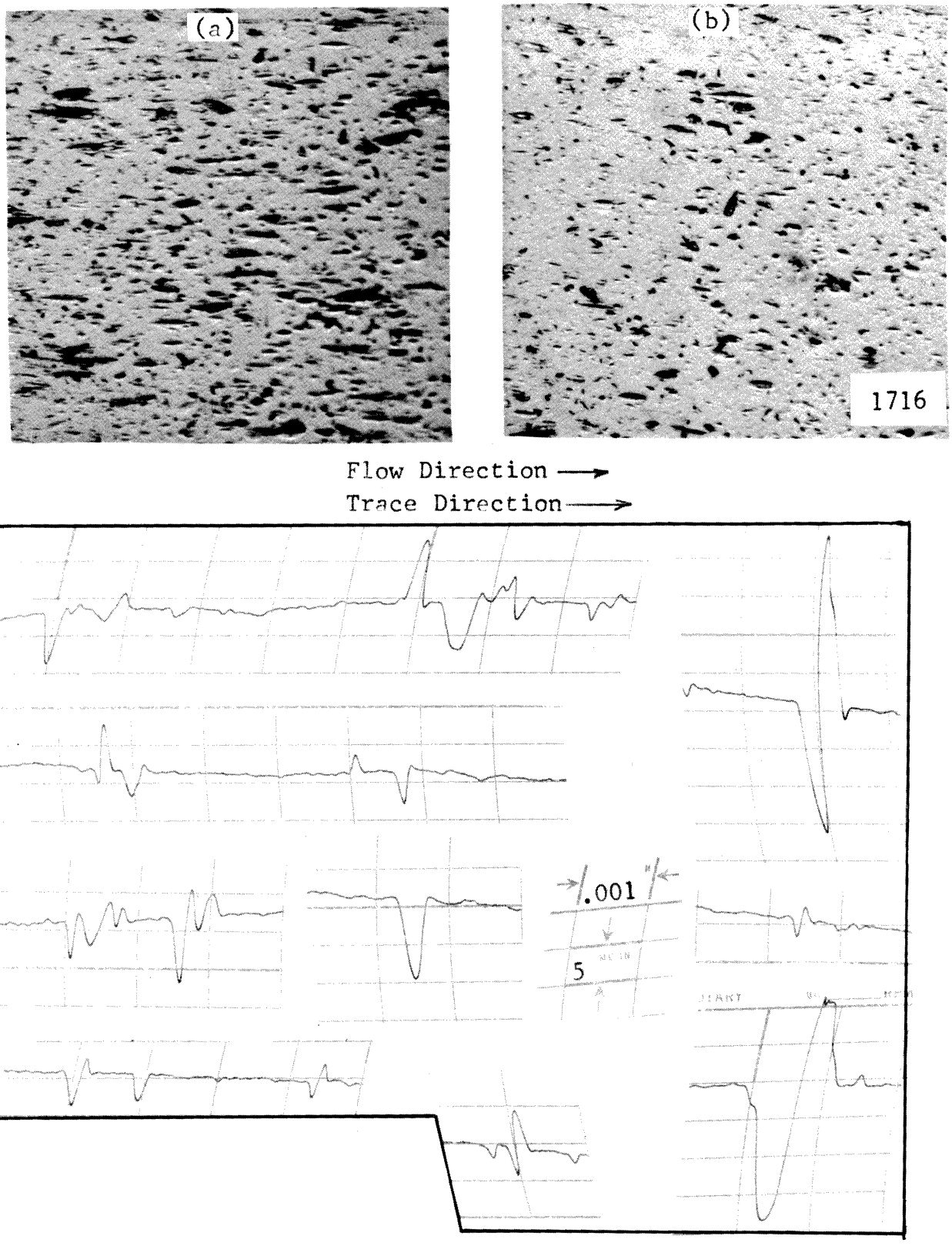

Fig. 85.--Typical photomicrographs and typical axial proficorder traces of cavitated surface of specimen No. 139-3 (304 SS) after 100 hours in water at a throat velocity of 200 ft./sec. for "standard cavitation" (a) nose area, (b) tail area.

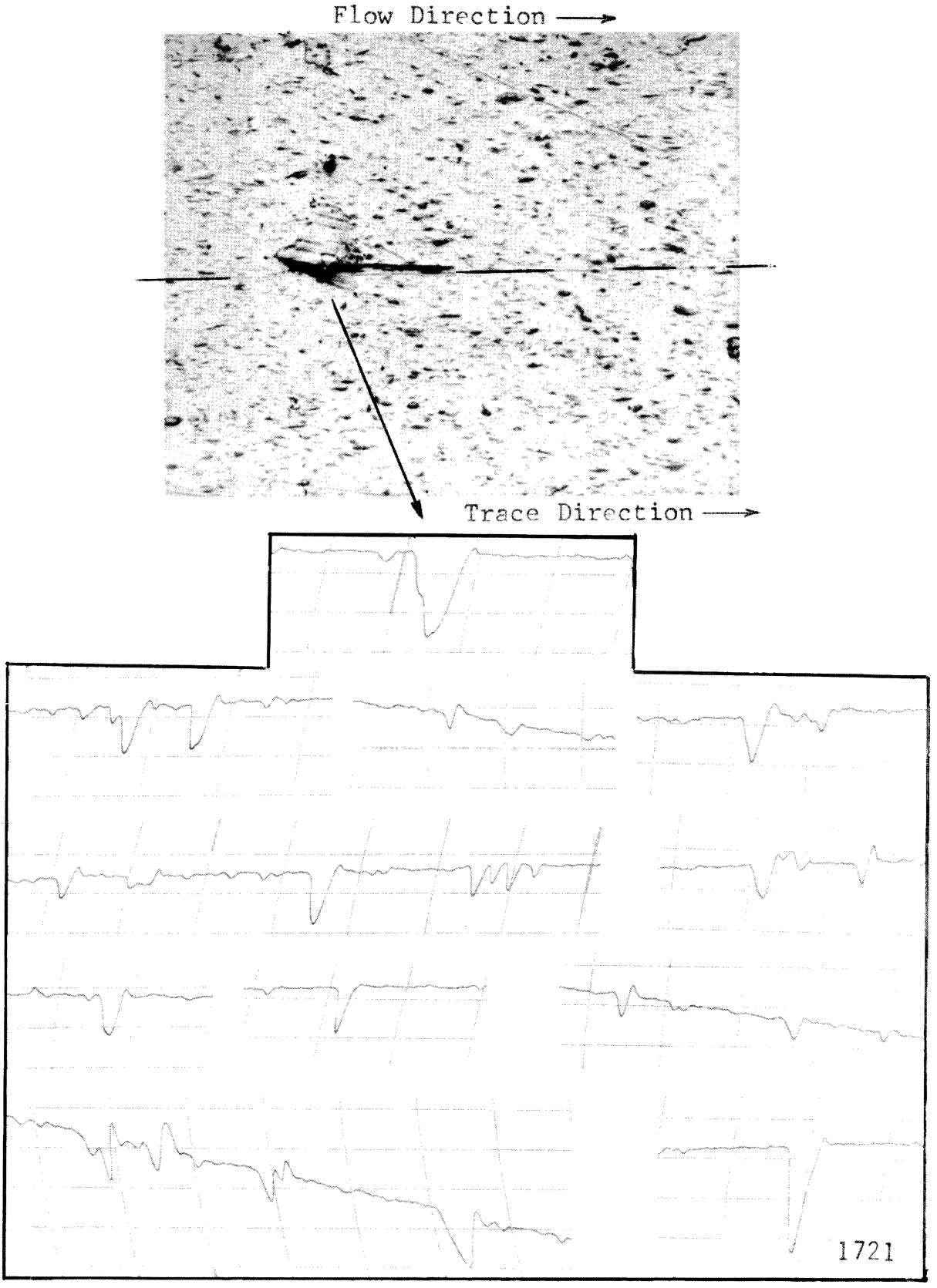

Fig. 86.--Typical photomicrographs and typical axial proficorder traces of cavitated surface of specimen No. 1-F (Tenelon) after 100 hours in water at a throat velocity of 200 ft./sec. for "standard cavitation."

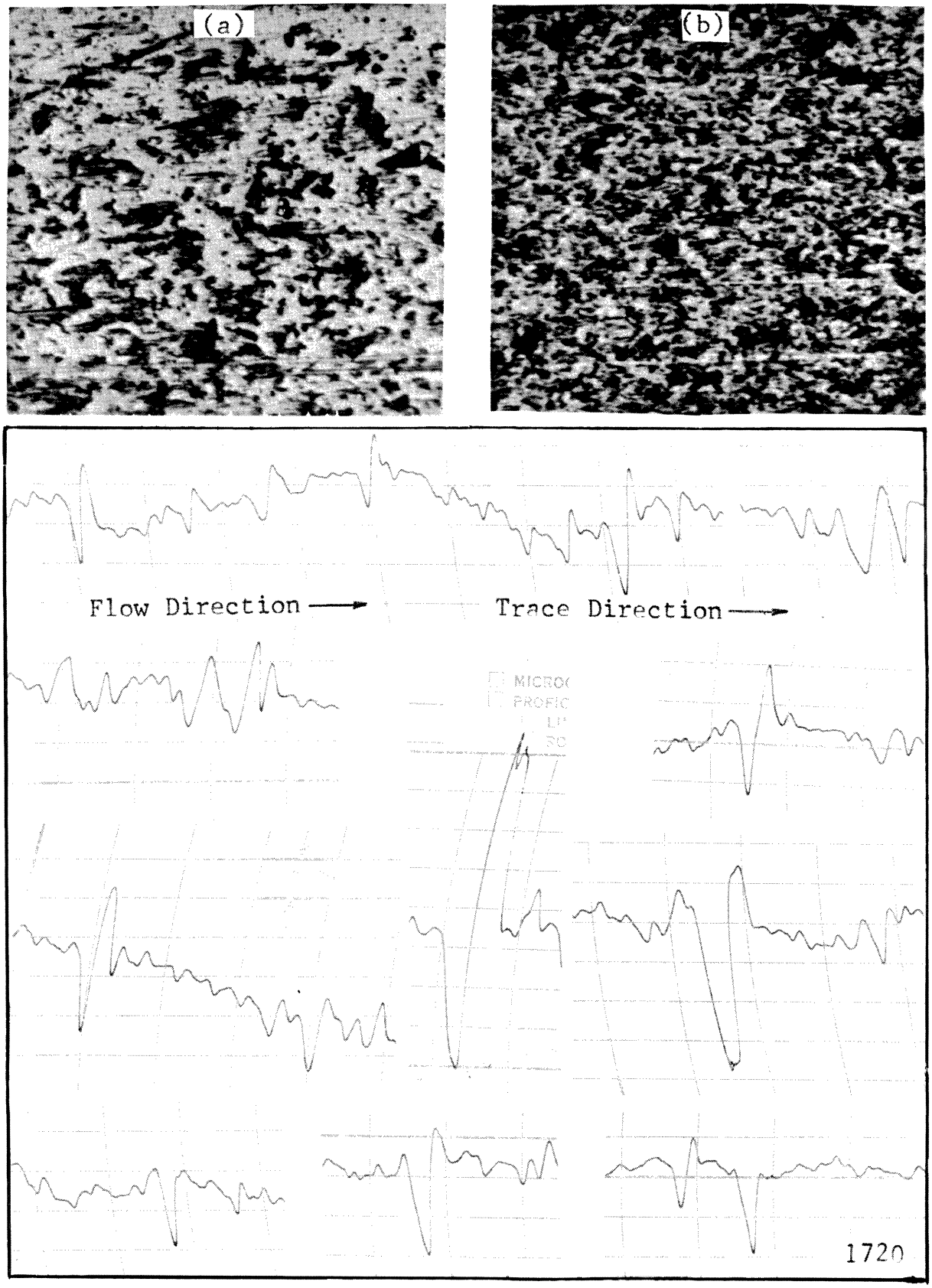

Fig. 87.--Typical photomicrographs and typical axial proficorder traces of cavitated surface of specimen No. 2-Cb-1Zr (Columbium-1% Zirconium) after 100 hours in water at a throat velocity of 200 ft./sec. for "standard cavitation" (a) nose area, (b) tail area.

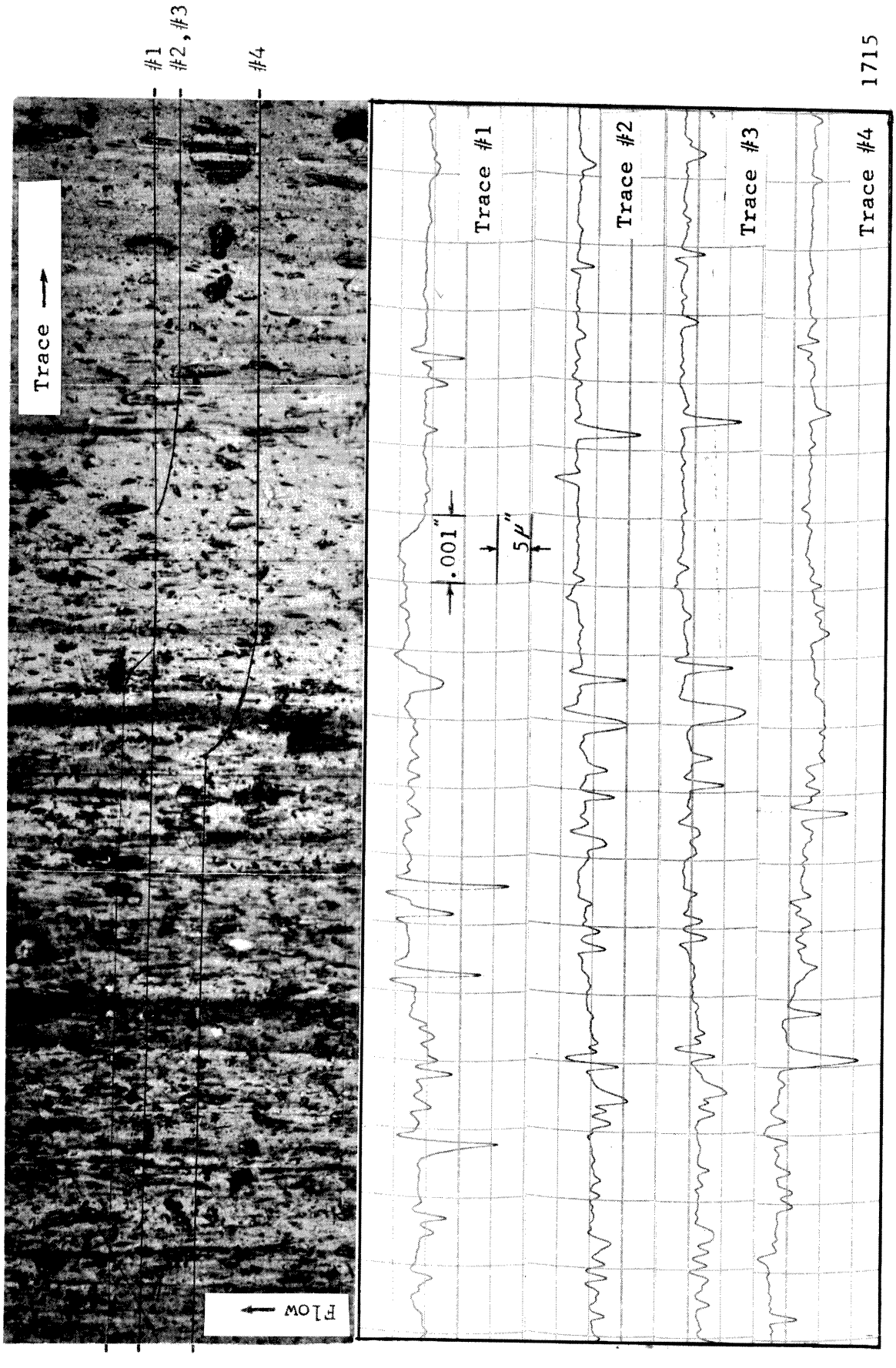

Fig. 88.--Typical photomicrographs and corresponding transverse proficorder traces of cavitated surface of specimen No. 8-cn (as rec'd copper-nickel) after 100 hours in water at a throat velocity of 200 ft./sec. for "standard cavitation."

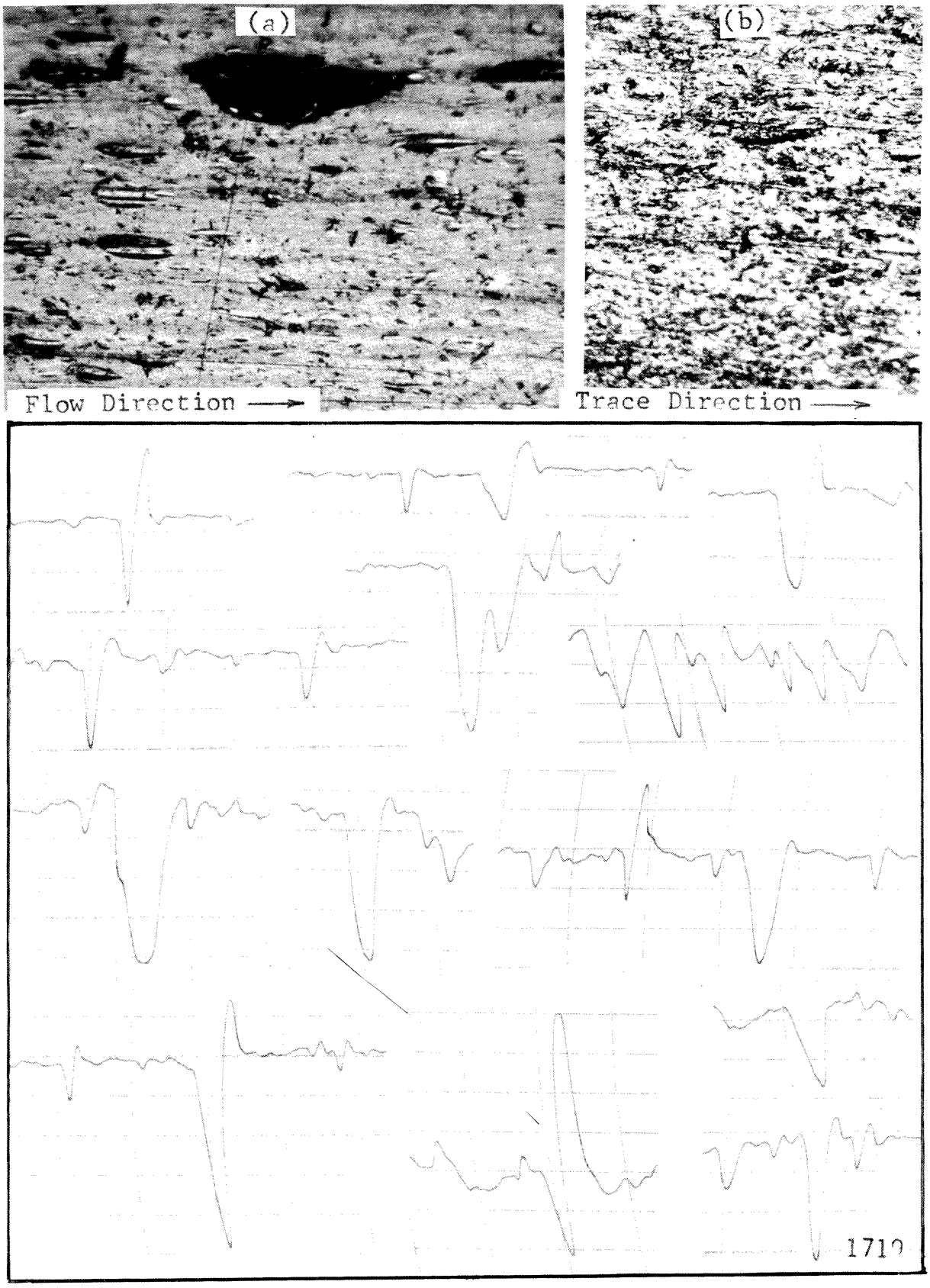

Fig. 89.- Typical photomicrographs and typical axial proficorder traces of cavitated surface of specimen No. 8-cn (as rec'd copper-nickel) after 100 hours in water at a throat velocity of 200 ft./sec. for "standard cavitation" (a) nose area, (b) tail area.

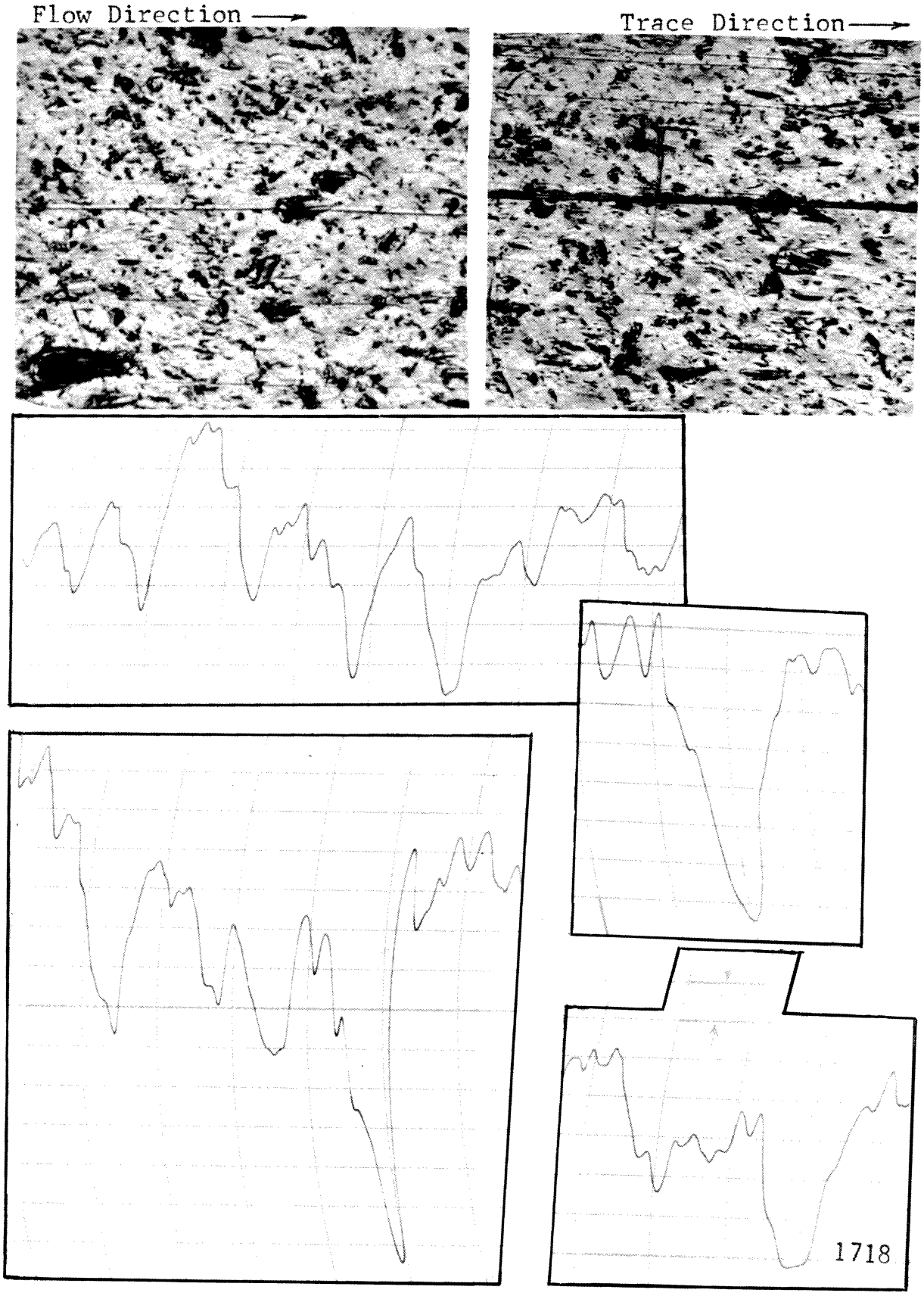

Fig. 90.--Typical photomicrographs and typical axial proficorder traces of cavitated surface of specimen No. 85-ni (low ht. trt. nickel) after 100 hours in water at a throat velocity of 200 ft./sec. for "standard cavitation."

actual situation. The general range of values for this ratio (Table 7) compares quite closely with the mercury data presented earlier. Maximum and minimum values are 0.06 and 0.01 respectively. It is indicated in general that pits in the weaker materials show a greater depth to diameter ratio from similar blows, as stated in the discussion of the mercury data. The measured diameter data (taken as the length of depression from the proficorder trace) could be misleading, considering the elongated shape of the pits, since the direction of trace compared to the orientation of the pit is not precisely known in most cases.

A detailed pit size distribution was made for stainless steel tested in water and is presented in Figure 91, where it is observed that the majority of pits on this material are in the size range below 0.1 mils, with no apparent lower limit. Thus, in addition to the overall volume loss being about the same for this particular combination of conditions in mercury and water, the individual pit sizes are also about the same and are distributed in similar size ranges. This would seem to indicate that the same type of bubble collapses are present in these two fluids, and that cavitation damage in general is not dependent on type of fluid other than as the choice of fluid results in different fluid dynamic situations during bubble collapse (assuming chemical effects are negligible). Such a change in fluid dynamic regimes would be expected in the present case between mercury and water under identical flow situations where, for instance, the suppression pressures present for bubble collapse would be higher in mercury if the same velocity were maintained due to the density difference, and the damage in mercury would presumably be greater.

TABLE 7

DEPTH TO DIAMETER RATIO FOR WATER CAVITATION PITS

Material	Pit Diameter (mils)	Pit Depth (mils)	Depth/ Diameter
304 SS (139-3)	0.3	0.007	0.023
	0.5	0.007	0.014
	0.2	0.003	0.015
	0.2	0.002	0.010
	0.3	0.018	0.060
	0.1	0.003	0.030
	0.2	0.004	0.020
	0.1	0.002	0.020
	0.2	0.004	0.020
	0.4	0.010	0.025
	0.2	0.008	0.040
	0.1	0.005	0.050
	0.2	0.004	0.020
	0.2	0.003	0.015
	0.1	0.003	0.030
	0.1	0.004	0.040
	0.6	0.018	0.030
		Average =	0.027
Cb-1Zr (2)	0.4	0.011	0.028
	0.4	0.007	0.018
	0.2	0.008	0.040
	0.3	0.009	0.030
	0.5	0.007	0.014
	0.3	0.010	0.033
	0.5	0.022	0.044
	0.4	0.017	0.043
	0.2	0.010	0.050
	0.2	0.009	0.045
	0.3	0.013	0.043
	0.2	0.006	0.030
	0.3	0.010	0.033
		Average =	0.035

TABLE 7--Continued

Material	Pit Diameter (mils)	Pit Depth (mils)	Depth/ Diameter
Tenelon (USS)	0.2	0.005	0.025
(1-F)	0.2	0.005	0.025
	0.1	0.003	0.030
	0.3	0.007	0.023
	0.2	0.005	0.025
	0.1	0.003	0.030
	0.3	0.008	0.027
	0.25	0.006	0.024
	0.2	0.005	0.025
	0.2	0.003	0.015
	0.2	0.003	0.015
	0.1	0.002	0.020
	0.2	0.002	0.020
	0.25	0.003	0.012
	0.4	0.008	0.020
	0.4	0.018	0.045
		Average =	0.022
Copper-Nickel	0.2	0.018	0.090
(As Rec'd.)	0.3	0.015	0.050
(8-cn)	0.2	0.005	0.025
	0.3	0.008	0.027
	0.5	0.008	0.016
	0.4	0.008	0.020
	0.2	0.006	0.030
	0.6	0.022	0.037
	0.4	0.024	0.060
	0.5	0.015	0.030
	0.3	0.010	0.033
	0.4	0.022	0.055
	0.2	0.011	0.055
	0.4	0.010	0.025
	0.4	0.018	0.045
	0.4	0.012	0.030
		Average =	0.039

TABLE 7--Continued

Material	Pit Diameter (mils)	Pit Depth (mils)	Depth/ Diameter
Nickel	1.2	0.019	0.016
(L. Ht. Trt.)	0.7	0.015	0.021
(85-ni)	0.5	0.012	0.024
	1.8	0.037	0.021
	0.3	0.007	0.023
	0.4	0.007	0.018
	1.0	0.024	0.024
	0.8	0.016	0.020
	1.0	0.042	0.042
	1.2	0.018	0.015
		Average =	0.022

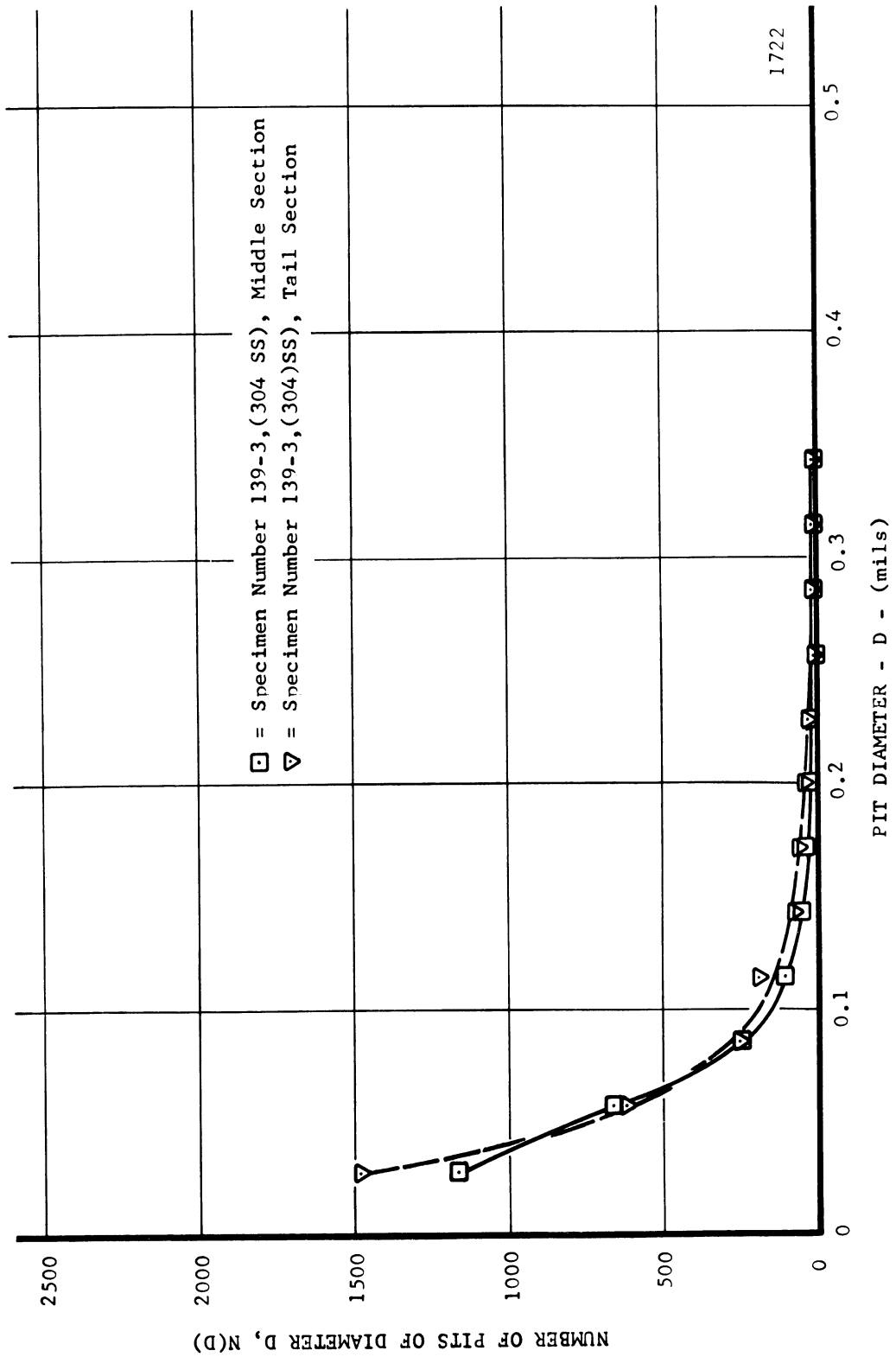

Fig. 91.--Pit size distribution for stainless steel tested in water at 200 ft./sec. for "standard cavitation."

If one considers the unsymmetrical bubble collapse and resultant fluid jet as the major damage mechanism, as it is observed in this investigation, then it should be possible to draw some confirming conclusions from analogous droplet impact tests. An examination of several pertinent reports from this type of study reveals that in general the type of damage sustained due to droplet impact forces is quite similar to the damage observed in this investigation. In particular, damage consisting of individual pits with raised rims are reported by Engel[51] where the fluid and material used were mercury and copper respectively. It was noted that the craters produced in this case are dependent on the size of droplet and the velocity of impact. It is also noted that the depth to diameter ratio, scaled from figures presented, is 0.60, 0.286 and 0.083 for velocities of 2445, 1200 and 695 feet per second. The lowest of these is comparable to the range of values observed in the present investigation, indicating an impact velocity of $\sim$ 600 feet per second for the cavitation craters. It is apparent that the larger depth to diameter ratios reported for the mercury impact pits result for the larger droplet velocities, which are presumably larger than occurring in the cavitation case. It is encouraging to note that the ratio decreases with decreasing droplet velocity, indicating that it is not unrealistic to expect, with jets from bubbles of the size observed, that this shallower cavitation damage is indeed the result of this hypothesized mechanism, but with jet velocities lower than used in the impact tests. Cavitation pits in stainless steel from high temperature potassium have been reported[48] which have the same shape as the higher velocity impact pits reported above,[51] further confirming the hypothesized mechanism of impact in the cavitation case.

CHAPTER V

CAVITATION DAMAGE DATA CORRELATIONS

A. Mercury Damage Data Analysis Versus Mechanical Properties

1. General

To obtain a better understanding of the damage mechanisms, it is useful to attempt to correlate the damage data with the mechanical properties of the test materials. Unfortunately, only the data from the present tests can be used appropriately, since systematic tests wherein the presently required material mechanical properties have been measured do not as yet exist in the literature. The use of nominal handbook values for standard materials listed in previous investigations has been found far too inaccurate to be useful.

A digital computer program which was available,[47] consisting of a relatively sophisticated least mean square fit regression analysis incorporating simple learning techniques, was employed for the data correlation. The general description and unique operational features of the program are described in Appendix D. Ten applicable properties of the test materials and/or fluids were selected either because previous investigators had attempted correlations with respect to them, or because they were involved in hypothesized damage mechanisms. These

independent variables were utilized in the program with ten allowed exponents, ±1, ±2, ±1/2, ±3, ±1/3. The selected variables are listed in Table 8, and their precise definitions are found in Chapter II.

2. Single Property Correlations

The first analysis of the damage data was performed with respect to each property individually to determine the relative importance of each alone with respect to the observed cavitation damage. The ten variables considered, along with the best predicting equation generated by the program for each variable and the corresponding coefficient of determination and standard error, which indicate the degree of correlation and the degree of fit or data scatter around the mean respectively, obtained between the best fit curve and the data, are listed in Table 8-A. No good single property correlation of the mercury data is obtained. However, true breaking stress exhibits the best fit. The rest of the variables are listed in order of significance of the fit obtained with the data. In the following tabulations of this type, no predicting equation will be listed if the coefficient of determination values are less than 0.5, as a value of 0.95 or better is indicative of a good correlation, and a predicting equation for anything less than 0.5 would be misleading.

3. Multiple Property Correlation

Next, the relation between the damage data and a combination of all ten variables, raised to the ten above-mentioned exponents, was examined. The resultant best predicting equation is shown in Table 8-B. The data correlates best with a combination of true breaking stress and

TABLE 8

A. TERM BY TERM ANALYSIS OF HG CAVITATION DAMAGE DATA VS. MECHANICAL PROPERTIES

Property*	Correlating Equation	F Level	Std. Error	Coef D.
1. True Breaking Stress	$MDP = 0.025 - 0.63\times10^{-12}(TBS)^{2}$	12.90	0.008	0.85
2. Engineering Strain Energy	$MDP = 0.028 - 0.54\times10^{-6}(ESE)$	10.60	0.009	0.83
3. Percent Elongation	$MDP = 0.029 - 0.24\times10^{-1}(\%El.)^{1/2}$	9.20	0.009	0.82
4. True Strain Energy	$MDP = 0.008 + 0.24\times10^{12}(TSE)^{-3}$	8.00	0 009	0.80
5. Tensile Strength	$MDP = 0.034 - 0.25\times10^{-6}(TS)$	5.80	0.01	0.77
6. Percent Reduction Area	$MDP = 0.022 - 0.11\times10^{-6}(\%RA)^{3}$	2.86	0.011	0.70
7. Brinell Hardness	$MDP = 0.007 + 0.10\times10^{5}(BHN)^{-3}$	2.60	0.012	0.69
8. Yield Strength	$MDP = 0.009 + 0.17\times10^{+3}(YS)^{-1}$	0.415	0.013	0.604
9. Elastic Modulus	$MDP = 0.013 + 0.85\times10^{19}(E)^{-3}$	0.11	0.013	0.59
10. Acoustic Impedance	$MDP = 0.024 - 0.64\times10^{-2}(AcI)^{1/3}$	0.21	0.013	0.59

*Precise definitions of properties given in Chapter II.

TABLE 8

B. BEST CORRELATION WITH ALL TEN PROPERTIES CONSIDERED

$$MDP = -0.064 + 0.34\times10^{2}(TBS)^{-1/2} - 0.17\times10^{9}(TS)^{-2} + 0.74\times10^{8}(TBS)^{-2}$$

Coefficient of Determination	=	0.994
Standard Error	=	0.00188
Maximum Absolute Deviation	=	0.0034
Maximum Percent Deviation	=	44.56%

tensile strength. This is a reasonable result. The type of damage observed on these materials, i.e., crater-type pitting, indicates that cavitation damage resistance would likely be a function of the ultimate strength of the material and a property associated with the plastic flow of the material at stresses above the proportional limit, as e.g., true breaking stress. The degree of fit of the data to this predicting equation is shown in Figure 92, which also serves as an illustrative example of the degree of fit and amount of data scatter indicated by particular values of the coefficient of determination and the standard error as reported later.

B. Water Damage Data Analysis Versus Mechanical Properties

1. General

The procedure already described for mercury was followed in the analysis of the water damage data. In addition to the full data analysis, since many more materials were tested in water than in mercury, an analysis was also performed using only those data for which comparable mercury data existed. Next, the remaining data was treated alone. Thus a direct comparison between water and mercury effects are afforded using precisely the same test materials for each fluid. In these two particular systems, and at the chosen test conditions, the water and mercury damage is very similar, as already mentioned, both in amount and type. The carbon steel water cavitation damage data has been deleted from this analysis since significant corrosion effects exist in water for this material.

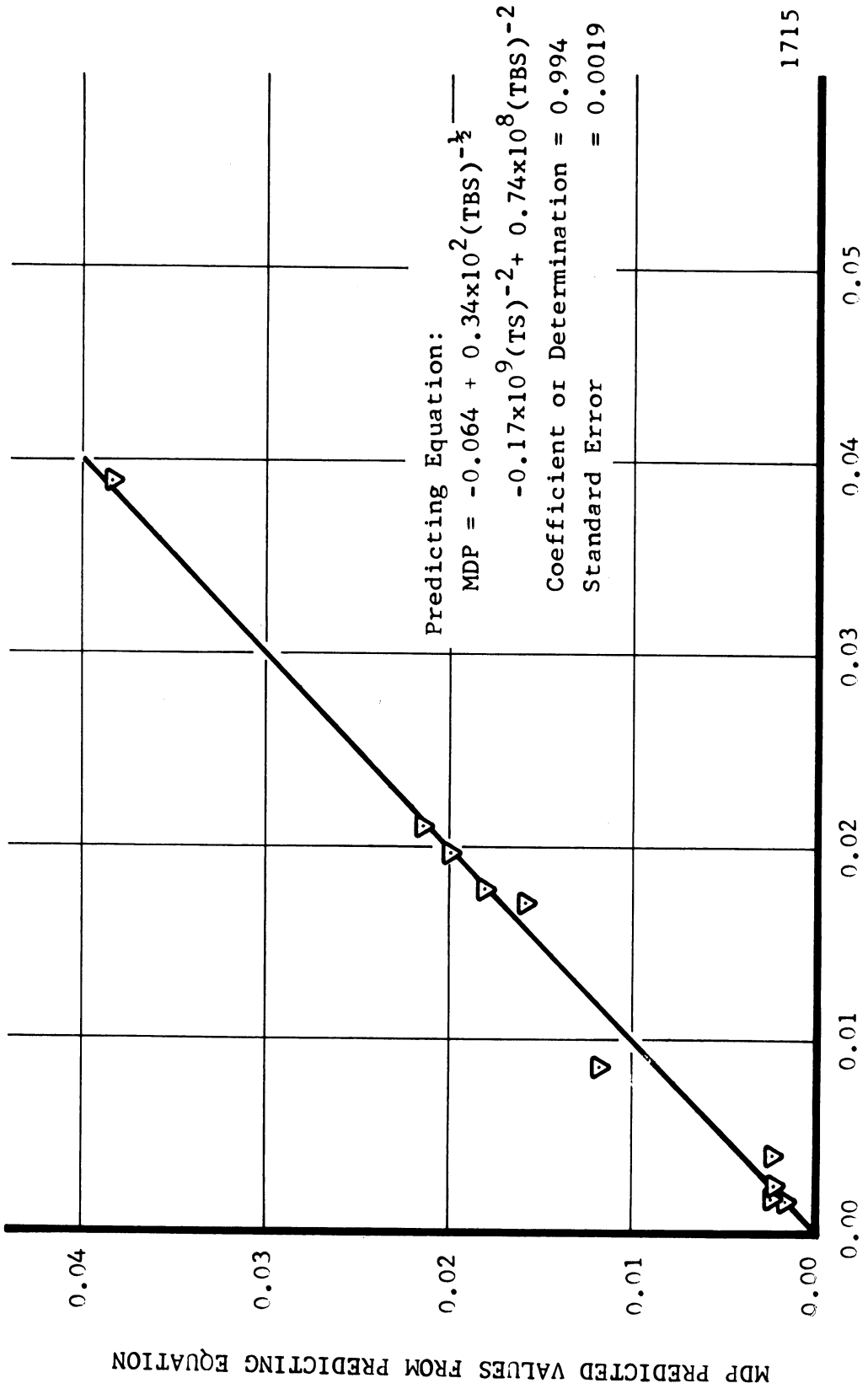

Fig. 92.--Comparisons of predicted values of MDP from the prediction equation listed to the actual values observed in mercury for all materials tested.

2. Single Property Correlations

The relative importance of each mechanical property considering the full set of water data was examined as with mercury. They are listed in Table 9-A, in their relative order of significance. The best fit is obtained with the acoustic impedance ratio between material and fluid.* However, nearly as good a fit is obtained with elastic modulus, indicating that this term which appears in the definition of the acoustic impedance (see Appendix D) may be of primary importance as compared to the other terms in the acoustic impedance ratio. A set of single property correlations (Table 9-B) for the water data on materials also tested in mercury shows that again a very good fit is obtained with elastic modulus and also with percent reduction of area, although the fit with acoustic impedance for these materials is quite poor, as it was in mercury. The analysis of the remainder of the water data (i.e., those materials tested in water only--Table 9-C) shows that the correlation with elastic modulus and acoustic impedance again is very good. However, there is no reasonably good correlation with any other single property.

3. Multiple Property Correlations

The excellent fit of the acoustic impedance parameter was overriding in the multiple property analysis, and in view of the close comparison of this parameter to the elastic modulus, it was decided to

---

*Chosen as a coupling parameter between fluid and material, and related to the ratio of reflected to transmitted energy as liquid shock waves or jets impinge on the solid.

TABLE 9-A

SINGLE VARIABLE CORRELATIONS FOR FULL SET OF WATER DATA EXCEPT CARBON STEEL

Rank	Property*	Correlating Equation	Std.Err.	Coef.D.
1	Acoustic Impedance	$MDP = 0.095+4.75(AcImp)^{3}-0.239(AcImp)^{-1/3}$	0.107	0.970
2	Elastic Modulus	$MDP = -31.23+0.639\times10^{22}(E)^{-3}-0.134\times10^{17}(E)^{-2}$	0.117	0.966
3	Percent Elongation	$MDP = 0.010 + 0.173\times10^{-1}(\%E1)^{-2}$	0.411	0.542
4	Tensile Strength	$MDP = 0.070 + 0.673\times10^{13}(TS)^{-3}$	0.428	0.503
5	True Breaking Stress		0.551	0.179
6	Percent Reduction Area	(No more correlating equations listed	0.562	0.145
7	Engineering Strain Energy	since the data does not show	0.564	0.138
8	Brinell Hardness	sufficient correlation.)	0.565	0.135
9	True Strain Energy		0.569	0.123
10	Yield Strength		0.573	0.110

*Ibid., Table 8.

TABLE 9-B

SINGLE VARIABLE CORRELATIONS FOR WATER DATA SUBSET OF MATERIALS AS USED IN MERCURY

Rank	Property*	Correlating Equation	Std.Err.	Coef.D.
1	Elastic Modulus	$MDP = 0.0536+0.105\times10^{-22}(E)^3-0.357\times10^{-15}(E)^2$	0.0016	0.998
2	Percent Reduction Area	$MDP = -1.72-0.109\times10^{4}(\%RA)^{-2}+0.864\times10^{2}(\%RA)^{-1}+0.172\times10^{-3}(\%RA)^2$	0.010	0.946
3	Yield Strength	$MDP = 0.054-0.616\times10^{-10}(YS)^2+0.714\times10^{-15}(YS)^3$	0.020	0.765
4	Engineering Stress Energy	$MDP = -0.146-0.275\times10^{11}(ESE)^{-3}+0.249\times10^{4/3}(ESE)^{-1/3}$	0.023	0.692
5	Brinell Hardness	(No more correlating equations listed since the data does not show sufficient correlation.)	0.028	0.497
6	True Breaking Stress		0.030	0.438
7	Percent Elongation		0.033	0.321
8	Acoustic Impedance		0.033	0.300
9	Tensile Strength		0.034	0.275
10	True Strain Energy		0.034	0.255

*Ibid., Table 8.

TABLE 9-C

SINGLE VARIABLE CORRELATIONS FOR WATER DATA SUBSET OF MATERIALS
AS TESTED IN WATER ONLY

Rank	Property*	Correlating Equation	Std.Err.	Coef.D.
1	Elastic Modulus	$MDP = 56.63+0.476\times10^{23}(E)^{-3}-0.690\times10^{16}(E)^{-2}$ $-0.106\times10^{-1}(E)^{1/2}+0.273\times10^{-21}(E)^{3}$	0.156	0.971
2	Acoustic Impedance	$MDP = -0.119+0.248\times10^{1}(AcImp)^{3}$	0.149	0.970
3	Percent Elongation	$MDP = 0.0105 + 0.167\times10^{-2}(\%El)^{-3}$	0.562	0.547
4	Tensile Strength	$MDP = 0.131 + 0.656\times10^{13}(TS)^{-3}$	0.577	0.521
5	True Breaking Stress	(No more correlation equations listed	0.683	0.330
6	True Strain Energy		0.719	0.258
7	Engineering Strain Energy	since the data does not show	0.743	0.208
8	Percent Reduction Area	sufficient correlation.)	0.747	0.200
9	Yield Strength		0.761	0.169
10	Brinell Hardness		0.763	0.165

*Ibid., Table 8.

examine the correlation with only the other nine variables, all of which are actual mechanical properties of the specimens, not involving fluid properties. Considering the full set of water data, the resulting best fit predicting equation is:

$$MDP = -27.75 + 0.563\times10^{22}(E)^{-3} - 0.118\times10^{17}(E)^{-2} + 0.885\times10^{9}(E)^{-1} + 0.316\times10^{-6}(E) + 0.186\times10^{9}(TS)^{-2} - 0.849\times10^{2}(TBS)^{-1/2}$$

where

Standard Error	= 0.0547
Coef. Determination	= 0.993
Maximum Absolute Deviation	= 0.176
Maximum Absolute % Deviation	= 1111.9

A correlation was also determined for the two subsets of water data, i.e., those for which comparable mercury data existed, and those remaining. The best correlation for the former is:

$$MDP = 0.887\times10^{-23}(E)^{3} - 0.274\times10^{-15}(E)^{2} + 0.70\times10^{1}(TSE)^{-1/2}$$

where

Coefficient of Determination	= 0.9993
Standard Error	= 0.00108
Maximum Absolute Deviation	= 0.00276
Maximum Absolute % Deviation	= 105.7

The other subset of water data, consisting of those materials tested only in water, produces the following predicting equation:

$$MDP = 0.273 + 0.239\times10^{1}(AcImp)^{3} - 0.104\times10^{7}(TBS)^{-2} + 0.217\times10^{13}(TS)^{-3} - 0.169\times10^{4}(E)^{-1/2}$$

where

Coefficient of Determination	=	0.9949
Standard Error	=	0.0651
Maximum Absolute Deviation	=	0.1735
Maximum Absolute % Deviation	=	604.3

C. Discussion and Conclusions

It was found that no good correlation existed between any single mechanical property and cavitation damage in the mercury tests. In the water tests the elastic modulus did correlate very well with the observed damage. The resultant multiterm predicting equation also is dominated by terms involving the elastic modulus, and shows that MDP decreases as E increases. This correlation with E may indicate that the damaging mechanism is very local in nature. Thus a material capable of substantial deflection under load without permanent deformation would not be damaged. This suggests the possible influence of a rigidity parameter, in addition to E alone, as the ratio of yield strength to elastic modulus which is the maximum possible nonpermanent deformation for the material. However, a check of this parameter as a single correlating parameter produced a coefficient of determination of only 0.18 for the full water data set and 0.69 for the mercury data set. However, the local nature of the damaging mechanism is consistent with the already discussed hypothesized damage mechanism wherein a central jet

along the axis of symmetry of a nonspherical collapsing bubble impinges upon the surface to be damaged, in that the penetrating range of such a microjet at full strength is very small.

E did not appear in the multiterm predicting equation for mercury, perhaps because it does not vary significantly between the materials tested in mercury, and also perhaps because the data used for E for the refractory alloys may not be sufficiently precise to allow a good correlation with E, if it did exist, over the narrow range of variation available.

In the full set and one of the subsets of water data, a good correlation was obtained with acoustic impedance ratio, showing that as this increased, damage also increased. This is consistent with the variation of damage with elastic modulus, since E appears in the denominator of the acoustic impedance ratio. For a given material, the predicting equation for acoustic impedance indicates that damage should be greater with mercury than water, other things being equal, which is probably the case. However, it does not explain the qualitative observation previously made in these tests[40] that plexiglas is relatively resistant to damage in water (as compared with the metals), but comparatively nonresistant in mercury. In any case, it is indicated that further understanding might be achieved by tests in which elastic modulus and acoustic impedance were varied singly over large ranges. This could be a key approach for future investigations after the present study.

Since no good physical explanation of the apparent correlation with elastic modulus can be advanced at present, and since the amount

of variation in this parameter is relatively small as compared to the other variables, the data was further analyzed with neither acoustic impedance or elastic modulus allowed as a variable. In this case, a best fit curve was generated as follows:

$$MDP = 2.706 - 0.189\times10^{10/3}(TS)^{-1/3} + 0.209\times10^{4}(TS)^{-1/2} - 0.116\times10^{3}(YS)^{-1/2}$$

where

Coefficient of Determination	=	0.560 (i.e., essentially no meaningful degree of correlation)
Standard Error	=	0.415
Maximum Absolute Deviation	=	0.145
Maximum Absolute % Deviation	=	10,698.9%

It is thus not possible to correlate the water data with any function of the other eight variables when elastic modulus and acoustic impedance were dissallowed. This could indicate that some mechanical property not yet considered is significant. As an example, properties difficult to include quantitatively as ability to be cold worked, or corrodibility may be important.

From a consideration of the types of damage observed it was anticipated,[26] in connection with the present study, that two or more properties in combination would be required to predict the damage, and that these would include a strength and an energy property. As already mentioned, the mercury damage data correlates well as a function of tensile strength and true breaking stress. This is consistent with the argument presented above, since true breaking stress involves strength and ductility, and hence, is related to failure energy.

The subset of water data for materials not tested in mercury includes the weaker materials for which, in some cases, three heat treats were utilized. For many of these materials the tensile strength increases as the strain energy is decreased, according to the different heat treatments, although the steels and refractory alloys, tested both in mercury and water, behave in the opposite manner. The material subset not tested in mercury was chosen partially to allow a selection between the strength and energy property effects. As it results, the best fit equation for these materials includes, in relative order of importance: acoustic impedance, true breaking stress, tensile strength, and elastic modulus. Again, the correlation was possible only with a combination of strength and energy properties, as true breaking stress and tensile strength, which were also involved in the mercury correlation. However, the surprisingly predominant effect of elastic modulus and acoustic impedance is still not clearly understood. The full set of water data correlated similarly as a function of elastic modulus, tensile strength and true breaking stress, although in this case acoustic impedance did not appear.

Several conclusions can be stated as a result of the foregoing analysis:

1. No single mechanical property correlates well with the mercury damage data. However, elastic modulus correlates well with both water subsets and with the full set, and acoustic impedance with the full set and one of the subsets. Acoustic impedance does not correlate for that subset of materials for which strain energy increased as strength increased.

2. Fairly good correlations are possible for a combination of tensile strength and true breaking stress in mercury, and of tensile strength, true breaking stress and elastic modulus in water.
3. The correlation is best in both fluids for those materials that have the highest strength properties. An examination of the standard errors for the predicted results shows that there is more scatter in the data for the weaker materials. Since these are more susceptible to handling damage, it is conceived that errors introduced in this fashion may be significant.
4. The absence of certain mechanical properties in the correlations is significant, i.e., yield strength (which is generally proportional to fatigue limit) does not occur, further substantiating the conclusion that single-blow craters, rather than multi-blow fatigue failures, are predominant in these tests.

   Hardness also does not appear, although in general increasing hardness indicates increasing cavitation damage resistance. Apparently the numerical hardness values within a given range and the various hardness scales are not sufficiently rationally related.
5. Since cavitation-induced loading is of a highly transient nature, it is not surprising that some difficulty is encountered when attempting to correlate cavitation damage with the semi-statically determined mechanical properties. However, in

general, suitable dynamically measured property values are very difficult to obtain. Nevertheless, investigations such as the present one can assist in the selection of properties for which dynamic values might be obtained in a future investigation.

CHAPTER VI

CONCLUSIONS

Many detailed conclusions have been drawn throughout the body of the report; however, the major conclusions from the overall investigation are summarized below.

A. Pressure Profiles

The measurements of pressures on the test specimen surfaces have shown that in general the venturi wall pressure profile measurements can be adequately assumed to represent the pressure profile along the venturi and on the test specimens. A very much larger axial pressure gradient has been measured on the test specimen surface for an unsymmetrical two-specimen arrangement than for a symmetrical two-specimen arrangement in the same venturi in mercury and for the same apparent termination of the cavitation cloud. This observation tends to explain the larger amount of damage, observed in earlier tests in this laboratory using this equipment, than was obtained in the present series.

It has been observed that similar pressures above vapor in water and mercury on the test specimen surfaces result in similar quantities of damage, as might be expected. However, the velocities to

produce these pressures were of course far different and, as it happens, the system specimen geometry differed to some extent. Very approximate theoretical treatments indicate that more damage should occur in the mercury system, under identical velocity and geometry conditions; this is not contradicted in the present case.

Minor geometrical changes can apparently result in major changes in local flow parameters affecting bubble collapse during

B. High-Speed Motion Pictures

In the mercury system, it has been observed from the high-speed pictures that there exist on the order of 10^3 to 10^4 bubbles adjacent to the specimen surface per pit formed, and similar observations have been made by other investigators[52] using other test systems. Thus a damaging bubble collapse must involve a highly selective process separating the very large number of nondamaging bubbles from the very few which produce damage.

It has further been observed in the mercury that some bubbles detach from the relatively steady-state void at the nose of the specimen, travel along the corner formed by the test specimen radial sides and the venturi wall, and transform from a nonsymmetrical to a circular shape as they collapse at a slight distance from the test specimen. Since the bubbles observed in mercury must be in contact with the viewing surface, only their contact area can be viewed, and it is not possible to determine their behavior in the dimension normal to the viewing surface. All bubbles that were observed to collapse on the polished

surface of the test specimen were observed to retain a circular shape during collapse to as small a diameter as was visually observable. However, the technique of observation did not allow a determination of the retention of symmetry to critically small diameters where nonsymmetries might conceivably occur.

In the water tests, no bubbles were observed to contact the polished surface in the area of maximum damage during the short time sample available (less than 1/20 second per 100 foot roll of Fastax film). However, an estimate of the probable numbers of bubbles in the area, by extrapolating from regions where bubbles were observed, confirms the large bubble to pit ratio observed in the mercury tests.

C. Specimen-Fluid Contact Measurements

The unique technique employed to observe the amount and location of contact between the specimen surface and the fluid in the mercury system confirmed the observations from the motion picture analysis that there exists very little, if any, contact between the fluid and specimen near the nose where the motion pictures indicated essentially a continuous void. Also, this technique indicated almost continuous contact between the specimen and fluid at the tail of the specimen where the motion pictures indicated very few bubbles in contact with the surface.

D. Typical and Detailed Analysis of Damage to Specimens

It was found that the type of damage inflicted was very similar in the two different fluid systems. The damage appeared as craters

with raised rims, as have also been observed in many droplet and particle impact tests by other investigators. Due to the symmetry of the craters, and the fact that they do not change in any way if exposed to further cavitation,[40] it must be concluded that the damage is the result of single blows. A rim predominantly on the downstream side of the craters was observed in the present series of water tests as it had been in a previous study in this laboratory.[40] The nonsymmetrical location of the rim lends support to the unsymmetrical bubble collapse with resultant fluid jet damage hypothesis, as opposed to the shock wave impingement hypothesis. The similarity in amount and type of damage due to two different fluids leads to the conclusion that the effect on damage from different fluids, chemical effects excluded, stems from the different flow regime which may be afforded, and the resultant driving pressures for bubble collapse.

The size range of pits (predominantly less than 0.1 mils diameter), compared to the observed bubble sizes, confirms the belief that damage is produced in the very final stage of bubble collapse which is, of course, the most difficult portion to observe.

Comparison of the depth to diameter ratios for the two fluids with those from impact type tests[51] leads to the conclusion that the damage is produced by an impact mechanism in the later stages of bubble collapse, and that probable velocities of impact in mercury are on the order of 600 ft./sec. Assuming the "water hammer equation" to give a first approximation to pressure exerted by an impacting drop on a solid surface, then since the velocity of sound in water and mercury is about

the same, a water velocity necessary to create the same force would be scaled up in proportion, i.e., about 8000 ft./sec.

A recent article from water jet impact tests[54] with velocities in the 2500 to 3500 ft./sec. range reports damage of an almost identical type to that observed in the present investigation. The profiles of pits reported[54] are strikingly similar to those presented herein which fact lends very strong support to the unsymmetrical bubble collapse with a resultant fluid jet damage hypothesis being the contributing factor in the cavitation damage case as subscribed to in this investigation.

E. Damage Data Versus Mechanical Property Correlations

The analysis of the mercury damage data showed that it was not possible to correlate the observed damage with any single mechanical property. In the water damage data analysis, it was found that either elastic modulus or acoustic impedance correlated well with the full set of materials. A fairly good correlation was found in terms of a function of tensile strength and true breaking stress in mercury, and as a function of tensile strength, true breaking stress and elastic modulus in water. Accelerated corrosion effects were noted for three nickel alloys in mercury and for carbon steel in water, attributed to the interplay of mechanical forces applied to the surfaces from the cavitating flow regime and ordinary corrosive action. The fit of the acoustic impedance parameter in two of the three water data sets, and elastic modulus in three, indicates that further studies where these two parameters were singly varied over larger ranges would be rewarding in determining whether such a correlation exists over a larger range of different materials.

APPENDIX A

DEFINITION OF CAVITATION CONDITIONS

The degree of cavitation as defined in the overall damage investigations in this laboratory and in this particular investigation differ between mercury and water. In the mercury venturi, where only two specimens are used, cavitation initiates at the throat outlet for all velocities used thus far, and the degree of cavitation applied to the mercury tests describes the extent of the cavitation cloud starting at the throat outlet and extending downstream to the point indicated, i.e., "cavitation to nose" is self explanatory. However, in the case of water, where three specimens are used, thus presenting more blockage to the venturi, the cavitation cloud initiates on the nose of the specimens and extends downstream to some point arbitrarily labeled by the degree of cavitation terminology. The first visible manifestation of cavitation occurs on the nose of the test specimen, and thus the term "visible initiation" was applied in this case. Then, succeeding degrees of more fully developed cavitation followed the old progression, regardless of the termination point on the specimen. The following are the definitions of the degrees of cavitation as used in this investigation:

Mercury

Visible Initiation - continuous ring of cavitation at the throat outlet, about 1/8" long.

Cavitation to Nose - cavitation cloud extends from throat outlet to termination at the nose of the specimen.

Standard Cavitation - cavitation cloud extends from throat outlet to termination at the middle of the specimen.

Cavitation to Back - cavitation cloud extends from throat outlet to termination at the rear of the specimen.

Water

Visible Initiation - cavitation cloud extends from nose of specimen to a point downstream on specimen about 1/8" long.

Cavitation to Nose - cavitation cloud extends from nose of specimen to termination at the middle of the specimen.

Standard Cavitation - cavitation cloud extends from nose of specimen to termination at the rear of the specimen.

From the pressure profile data in this report, the correspondence between water and mercury from a standpoint of degree of cavitation is as follows:

Mercury Condition (2 spec.)	corresponds to	Water Condition (3 spec.)
Cavitation to Nose	--	Visible Initiation
Standard Cavitation	--	Cavitation to Nose
Cavitation to Back	--	Standard Cavitation

This would result in the pressure gradients on the surfaces and the termination points on the surfaces being approximately the same for corresponding conditions from water to mercury.

APPENDIX B

COMPUTER ANALYSIS OF PRESSURE PROFILE DATA

The computer program used to reduce the raw pressure data taken during the venturi pressure profile portion of this examination is listed below. The program is based on earlier work in this laboratory,[40] another thesis investigation currently under way,[35] and several modifications incorporated for the present investigation. A typical set of pressures and the resulting computer output is also presented below.

```
$COMPILE MAD,EXECUTE,I/O DUMP,PRINT OBJECT,PUNCH OBJECT
         R
         R  PRESSURE PROFILE DATA REDUCTION PROGRAM  MJR THESIS
         R
          INTEGER COND,NRD,NPT,NRS,RPM,FL,I,J,K,L,M,N,DEX,TOTAL,REPEAT,
        1SHTNO,SPEC,CORR,TPC1,TPC2
          REPEAT = 1
          V'S X(1)=-2.000,0.100,1.226,2.271,2.979,2.784,3.166,3.354,
        13.166,3.540,4.131,6.000
BEGIN     READ DATA TOTAL
BEGIN1    DEX = 1
START     READ FORMAT IN1,COND,SPEC,HB,HC,NRD,NPT,NRS,TEMP,INCH,GPM,
        1FL,RPM,SHTNO,DT
          V'S IN1 = $2I3,2F8.4,3I3,3F7.3, I3,I5,I8,F7.4*$
          PRINT FORMAT HEAD
          V'S HEAD =$1H1,S50,33HPRESSURE PROFILE RUNS, MJR THESIS*$
          W'R FL .E. 1
          PRINT FORMAT LIQ1
          V'S LIQ1 = $1H0,S10,19HTEST FLUID IS WATER*$
          O'E
          PRINT FORMAT LIQ2
          V'S LIQ2 = $1H0,S10,21HTEST FLUID IS MERCURY*$
          E'L
          TRANSFER TO CON(COND)
CON(1)    PRINT FORMAT ZERO
          V'S ZERO = $1H0,S10,38HCAVITATION CONDITION = ZERO CAVITATION
        1*$
          TRANSFER TO SPN(SPEC)
CON(2)    PRINT FORMAT VIS
          V'S VIS = $1H0,S10,41HCAVITATION CONDITION = VISIBLE INITIATI
        1ON*$
          TRANSFER TO SPN(SPEC)
CON(3)    PRINT FORMAT NOSE
          V'S NOSE = $1H0,S10,41HCAVITATION CONDITION = CAVITATION TO N
        1OSE*$
          TRANSFER TO SPN(SPEC)
CON(4)    PRINT FORMAT STD
          V'S STD = $1H0,S10,42HCAVITATION CONDITION = STANDARD CAVITAT
        1ION*$
          TRANSFER TO SPN(SPEC)
CON(5)    PRINT FORMAT BACK
          V'S BACK=$1H0,S10,41HCAVITATION CONDITION = CAVITATION TO BAC
        1K*$
          TRANSFER TO SPN(SPEC)
SPN(1)    PRINT FORMAT ONE
          V'S ONE = $1H0,S10,42HNUMBER OF TEST SPECIMENS IN VENTURI =
        1ONE*$
          TRANSFER TO INFO
SPN(2)    PRINT FORMAT TWO
          V'S TWO = $1H0,S10,42HNUMBER OF TEST SPECIMENS IN VENTURI =
        1TWO*$
          TRANSFER TO INFO
SPN(3)    PRINT FORMAT TRE
          V'S TRE = $1H0,S10,44HNUMBER OF TEST SPECIMENS IN VENTURI =
        1THREE*$
INFO      PRINT FORMAT CONDS,TEMP,HB,HC,INCH,GPM,RPM,SHTNO
          V'S CONDS=$1H0,S14,22HTEMPERATURE          = F7.3,2H F/1H ,S14
        1,22HBAROMETRIC PRESSURE = F8.4,8H MM  HG./1H ,S14,22HHEIGHT C
        2ORRECTION    = F8.4,10H MM  FLUID/1H ,S14,22HFLOW RATE
```

```
          3    =  F7.3,14H IN. FLUID OR F7.3,4H GPM/1H ,S14,22HPUMP SPEED
          4          = I5,4H RPM/1H ,S14,26HORIGINAL DATA ON SHEET NO.I8
          5*$
           V1(2) = NPT
           V2(2) = NPT
           PRINT FORMAT TAPS
           V'S TAPS = $1H0,S25,4HV-IN,S4,4HP-00,S3,3HP-0,S4,3HP-1,S4,3HS
          1-1,S4,3HP-2,S4,3HS-2,S4,3HS-3,S4,3HP-3,S4,3HP-4,S4,3HP-5,S3,
          25HV-OUT*$
           READ FORMAT IN2,PTD(1,1)...PTD(NRD,NPT)
           V'S IN2 = $(6F7.2/6F7.2)*$
           PRINT FORMAT OPTD1
           V'S OPTD1 = $1H0,S43,26HORIGINAL PRESSURE TAP DATA*$
           PRINT FORMAT OPTD2,PTD(1,1)...PTD(NRD,NPT)
           V'S OPTD2 = $1H0,S23,12F7.2/(S24,12F7.2)*$
           AT = 3.1416*(DT.P.2.0)/576.0
           B = 0.002228/AT
           W'R FL .E. 1
             TRANSFER TO BETA1A
           O'E
             TRANSFER TO BETA2
           E'L
BETA1A     DEN = 1.0409*62.3689/TEMP.P.0.01089
           W'R TEMP .LE. 113.
             LNVP = 2.303 + 0.03175*(TEMP - 50.0)
           O'E
             LNVP = 4.290 + 0.0261*(TEMP - 113.0)
           E'L
           VAP = EXP.(LNVP)*(14.7/760.)
           TRANSFER TO GAMMA
BETA2      DEN = (13.5708-0.001448*(TEMP-50.))*62.3689
           WHENEVER TEMP .LE. 158.
             VAP = 0.0
             TRANSFER TO GAMMA
             OR WHENEVER TEMP .G. 158.
             TRANSFER TO ERROR 1
           END OF CONDITIONAL
GAMMA      PC = HB*(14.7/760) + HC*DEN/1728.
           VT = GPM*B
           KE = (VT.P.2.)/64.4
           THROUGH DELTA, FOR I=1,1,I.G.NRD
           THROUGH DELTA, FOR J=1,1,J.G.NPT
           NPSH(I,J) = (PTD(I,J) + PC - VAP)*144.*1./DEN
DELTA      NRMPR(I,J) = NPSH(I,J)/KE
           PRINT FORMAT INFO2
           V'S INFO2=$1H0,S32,36HTHE UNCORRECTED NORMALIZED PRESSURES*$
           PRINT FORMAT OUT2, NRMPR(1,1)...NRMPR(NRD,NPT)
           V'S OUT2=$1H0,S23,12F7.4/(S24,12F7.4)*$
           PRINT FORMAT OUT3, VT
           V'S OUT3=$1H0,S14,18HTHROAT VELOCITY = F7.2,7H FT/SEC*$
           READ FORMAT IN3,CORR,TPC1,TPC2,LTH1,LTH2,MULT
           V'S IN3 =$(3I5,3F7.4)*$
           W'R CORR .E. 2
           T'O ZETA
           O'E
             PRINT FORMAT INFO2A
           V'S INFO2A=$1H0,S14,43HNO CORRECTIONS MADE TO NORMALIZED PRES
          1SURES*$
           T'O THETA
```

```
          F'L
ZETA      T'H ZETA1, FOR N=1,1,N.G.NRD
          DELP(N) = (NRMPR(N,2) - NRMPR(N,3))/LTH1
          CALNPR(N) = NRMPR(N,3) - (DELP(N)*LTH2*MULT)
ZETA1     FACTOR(N) = NRMPR(N,4) - CALNPR(N)
          T'H ZETA2,FOR J=1,1,J.G.NRD
          T'H ZETA2, FOR I= TPC1,1,I.G.TPC2
ZETA2     NRMPR(J,I) = NRMPR(J,I) - FACTOR(J)
ETA       P'T INFO3
          V'S INFO3=$1H0,S33,34HTHE CORRECTED NORMALIZED PRESSURES*$
          P'T OUT2,NRMPR(1,1)...NRMPR(NRD,NPT)
THETA     THROUGH THETA2, FOR I=1,1,I.G.NPT
          SUM(DEX,I) = 0.0
          THROUGH THETA1, FOR J=1,1,J.G.NRD
THETA1    SUM(DEX,I) = SUM(DEX,I) + NRMPR(J,I)
THETA2    AVGNP(DEX,I) = SUM(DEX,I)/NRD
            LOSC(DEX) = AVGNP(DEX,1) - AVGNP(DEX,NPT)
IOTA      THROUGH IOTA1, FOR M=1,1,M.G.NRD
          THROUGH IOTA1, FOR L=1,1,L.G.NPT
          DEVNP(M,L) = NRMPR(M,L) - AVGNP(DEX,L)
IOTA1     SQDEV(M,L) = DEVNP(M,L).P.2.
          THROUGH IOTA3, FOR I=1,1,I.G.NPT
          SUMSQ(DEX,I) = 0.0
          THROUGH IOTA2, FOR J=1,1,J.G.NRD
IOTA2     SUMSQ(DEX,I) = SUMSQ(DEX,I) + SQDEV(J,I)
          VAR(DEX,I) = SUMSQ(DEX,I)/NRD
          STDDEV(DEX,I) = VAR(DEX,I).P.0.50
IOTA3     COVAR(DEX,I) = (.ABS.STDDEV(DEX,I)*100.)/(.ABS.AVGNP(DEX,I))
KAPPA     PRINT FORMAT INFO4
          V'S INFO4=$1H0,S42,32HTHE AVERAGE NORMALIZED PRESSURES*$
          PRINT FORMAT OUT4, AVGNP(DEX,1)...AVGNP(DEX,NPT)
          V'S OUT4=$1H0,(S23,12F7.4)*$
            PRINT FORMAT OUT4A, LOSC(DEX)
          V'S OUT4A=$1H0,S14,23HTHE LOSS COEFFICIENT = F8.4*$
KAPPA1    PRINT FORMAT INFO5
          V'S INFO5=$1H0,S40,37HTHE VARIANCES IN NORMALIZED PRESSURES*$
          PRINT FORMAT OUT5, VAR(DEX,1)...VAR(DEX,NPT)
          V'S OUT5=$1H0,(S23,12F7.4)*$
          PRINT FORMAT INFO6
          V'S INFO6=$1H0,S40,36HTHE STANDARD DEVIATIONS*$
          PRINT FORMAT OUT6, STDDEV(DEX,1)...STDDEV(DEX,NPT)
          V'S OUT6=$1H0,(S23,12F7.4)*$
          PRINT FORMAT INFO7
          V'S INFO7=$1H0,S43,29HTHE COEFFICIENTS OF VARIATION*$
          PRINT FORMAT OUT7, COVAR(DEX,1)...COVAR(DEX,NPT)
          V'S OUT7=$1H0,(S23,12F7.4)*$
LAMBDA    CAVN(DEX) = AVGNP(DEX,1)
          THROUGH LOA1, FOR K=2,1,K.G.NPT
          WHENEVER AVGNP(DEX,K) .L. CAVN(DEX)
          CAVN(DEX) = AVGNP(DEX,K)
LOA1      END OF CONDITIONAL
MU        PRINT FORMAT OUT8, CAVN(DEX)
          V'S OUT8=$1H0,S14,24HTHE CAVITATION NUMBER = F8.4*$
NU        WHENEVER DEX .L. NRS
            DEX = DEX + 1
            TRANSFER TO START
            OR WHENEVER DEX .E. 1 .AND. TOTAL .E. 1
            TRANSFER TO BEGIN
            OTHERWISE
```

```
              TRANSFER TO PI
             END OF CONDITIONAL
PI           THROUGH PI2, FOR I=1,1,I.G.NPT
             SUMAVG(I) = 0.0
             THROUGH PI1, FOR J=1,1,J.G.NRS
PI1          SUMAVG(I) = SUMAVG(I) + AVGNP(J,I)
             MEAVG(I) = SUMAVG(I)/NRS
PI2          Y(I) = MEAVG(I)
             THROUGH PI3, FOR L=1,1,L.G.NRS
             THROUGH PI3, FOR M=1,1,M.G.NPT
             DEVME(L,M) = AVGNP(L,M) - MEAVG(M)
PI3          SQDME(L,M) = DEVME(L,M).P.2.
             THROUGH PI5, FOR J=1,1,J.G.NPT
             SQSUME(J) = 0.0
             THROUGH PI4, FOR I=1,1,I.G.NRS
PI4          SQSUME(J) = SQSUME(J) + SQDME(I,J)
             VARM(J) = SQSUME(J)/NRS
             STDEM(J) = VARM(J).P.0.5
PI5          COVRM(J) = (.ABS.STDEM(J)*100.)/(.ABS.MEAVG(J))
             PRINT FORMAT HEAD
RHO          PRINT FORMAT INFO8, NRS
             V'S INFO8=$1H0,S14,16HMEAN VALUES FOR I3,48HSETS AT SAME FLOW
            1, RPM, AND CAVITATION CONDITION*$
             PRINT FORMAT INFO9,GPM,RPM
             V'S INFO9=$1H0,S14,12HFLOW RATE = F7.3,4H GPM/1H ,S14,13HPUMP
            1 SPEED = I5,4H RPM*$
             TRANSFER TO RH(COND)
RH(1)        PRINT FORMAT ZERO
             TRANSFER TO SP(SPEC)
RH(2)        PRINT FORMAT VIS
             TRANSFER TO SP(SPEC)
RH(3)        PRINT FORMAT NOSE
             TRANSFER TO SP(SPEC)
RH(4)        PRINT FORMAT STD
             TRANSFER TO SP(SPEC)
RH(5)        PRINT FORMAT BACK
             TRANSFER TO SP(SPEC)
SP(1)        PRINT FORMAT ONE
             TRANSFER TO AGN
SP(2)        PRINT FORMAT TWO
             TRANSFER TO AGN
SP(3)        PRINT FORMAT TRE
AGN          PRINT FORMAT OUT3,VT
             PRINT FORMAT TAPS
             PRINT FORMAT INFO4
             PRINT FORMAT OUT9, MEAVG(1)...MEAVG(NPT)
             V'S OUT9=$1H0,(S23,12F7.4)*$
             PRINT FORMAT INFO5
             PRINT FORMAT OUT10, VARM(1)...VARM(NPT)
             V'S OUT10=$1H0,(S23,12F7.4)*$
             PRINT FORMAT INFO6
             PRINT FORMAT OUT11, STDEM(1)...STDEM(NPT)
             V'S OUT11=$1H0,(S23,12F7.4)*$
             PRINT FORMAT INFO7
             PRINT FORMAT OUT12, COVRM(1)...COVRM(NPT)
             V'S OUT12=$1H0,(S23,12F7.2)*$
TAU          MECAV = MEAVG(1)
             THROUGH TAU1, FOR J=2,1,J.G.NPT
             WHENEVER MEAVG(J) .LE. MECAV
```

```
            MECAV = MEAVG(J)
TAU1        END OF CONDITIONAL
            PRINT FORMAT OUT13, MECAV
            V'S OUT13=$1H0,S14,29HTHE MEAN CAVITATION NUMBER = F6.4*$
            PRINT FORMAT TITLE
            V'S TITLE =$1H1,S50,34HPRESSURE PROFILE PLOTS, MJR THESIS*$
            EXECUTE PLOT1.(NSCALE,5,10,5,20)
            V'S NSCALE = 1.0,3.0,3
            EXECUTE PLOT2.(IMAGE,6.000,-2.000,1.600,-0.400)
            EXECUTE PLOT3.(5*$,X(1),Y(1),NPT)
            EXECUTE PLOT4.(44,ORD)
            V'S ORD=$                    AVERAGE NORMALIZED PRESSURE $
            PRINT FORMAT BOTTOM
            V'S BOTTOM=$1H ,S11,1HV,S25,1HP,S12,1HP,S14,1HP,S6,1HP,S1,
           12HSS,S3,3HS P,S5,1HP,S23,1HV/1H ,S75,1HP/1H0,S51,59H DISTANCE
           2 OF TAP FROM VENTURI ENTRANCE      ---     (INCHES) *$
            DIMENSION Y(16),X(16),IMAGE(1000)
OMEGA       WHENEVER REPEAT .L. TOTAL
              REPEAT = REPEAT + 1
              TRANSFER TO BEGIN1
              OTHERWISE
              TRANSFER TO BEGIN
            END OF CONDITIONAL
            TRANSFER TO START
ERROR1      PRINT FORMAT ERR1
            VECTOR VALUES ERR1=$1H0,S10,25HTEMPERATURE LIMIT EXCEEDED*$
            TRANSFER TO BEGIN
            DIMENSION PTD(160,V1),NPSH(160,V1),NRMPR(160,V1),DELP(10),
           1CALNPR(10),FACTOR(10),SUM(80,V2),AVGNP(80,V2),DEVNP(160,V1),
           2SUMSQ(96,V2),VAR(80,V2),STDDEV(80,V2),COVAR(80,V2),CAVN(5),
           3SUMAVG(16),MEAVG(16),DEVME(80,V2),SQDME(80,V2),SQSUME(16),
           4VARM(16),STDEM(16),COVRM(16),SQDEV(160,V1),LOSC(10)
            VECTOR VALUES V1 = 2,1,16
            VECTOR VALUES V2 = 2,1,16
            END OF PROGRAM
```

PRESSURE PROFILE RUNS, MJR THESIS

TEST FLUID IS MERCURY

CAVITATION CONDITION = STANDARD CAVITATION

NUMBER OF TEST SPECIMENS IN VENTURI = THREE

TEMPERATURE = 88.000 F
BAROMETRIC PRESSURE = 735.6000 IN. HG.
HEIGHT CORRECTION = .0000 IN. FLUID
FLOW RATE = 2.500 IN. FLUID OR 21.100 GPM
PUMP SPEED = 1490 RPM
ORIGINAL DATA ON SHEET NO. 198350

V-IN	P-CO	P-0	P-1	S-1	P-2	S-2	S-3	P-3	P-4	P-5	V-OUT

ORIGINAL PRESSURE TAP DATA

112.00	-3.95	-5.95	-8.95	-9.00	4.25	-2.75	4.80	-8.60	29.00	45.50	76.00

THE UNCORRECTED NORMALIZED PRESSURES

1.2646	.1030	.0829	.0529	.0524	.1851	.1150	.1906	.0564	.4331	.5984	.9039

THROAT VELOCITY = 33.14 FT/SEC

NO CORRECTIONS MADE TO NORMALIZED PRESSURES

THE AVERAGE NORMALIZED PRESSURES

1.2646	.1030	.0829	.0529	.0524	.1851	.1150	.1906	.0564	.4331	.5984	.9039

THE LOSS COEFFICIENT = .3606

THE VARIANCES IN NORMALIZED PRESSURES

.0000	.0000	.0000	.0000	.0000	.0000	.0000	.0000	.0000	.0000	.0000	.0000

THE STANDARD DEVIATIONS

.0000	.0000	.0000	.0000	.0000	.0000	.0000	.0000	.0000	.0000	.0000	.0000

THE COEFFICIENTS OF VARIATION

.00	.00	.00	.00	.00	.00	.00	.00	.00	.00	.00	.00

THE CAVITATION NUMBER = .0524

PRESSURE PROFILE RUNS, MJR THESIS

TEST FLUID IS MERCURY

CAVITATION CONDITION = STANDARD CAVITATION

NUMBER OF TEST SPECIMENS IN VENTURI = THREE

TEMPERATURE = 88.000 F
BAROMETRIC PRESSURE = 735.3000 IN. HG.
HEIGHT CORRECTION = .0000 IN. FLUID
FLOW RATE = 2.500 IN. FLUID OR 21.100 GPM
PUMP SPEED = 1492 RPM
ORIGINAL DATA ON SHEET NO. 198350

V-IN	P-00	P-0	P-1	S-1	P-2	S-2	S-3	P-3	P-4	P-5	V-OUT
ORIGINAL PRESSURE TAP DATA											
112.00	-2.95	-4.75	-8.65	-7.30	3.30	3.20	15.00	.50	31.50	47.50	77.00
THE UNCORRECTED NORMALIZED PRESSURES											
1.2645	.1129	.0949	.0558	.0693	.1755	.1745	.2927	.1475	.4580	.6183	.9139

THROAT VELOCITY = 33.14 FT/SEC

NO CORRECTIONS MADE TO NORMALIZED PRESSURES

THE AVERAGE NORMALIZED PRESSURES											
1.2645	.1129	.0949	.0558	.0693	.1755	.1745	.2927	.1475	.4580	.6183	.9139

THE LOSS COEFFICIENT = .3506

THE VARIANCES IN NORMALIZED PRESSURES											
.0000	.0000	.0000	.0000	.0000	.0000	.0000	.0000	.0000	.0000	.0000	.0000
THE STANDARD DEVIATIONS											
.0000	.0000	.0000	.0000	.0000	.0000	.0000	.0000	.0000	.0000	.0000	.0000
THE COEFFICIENTS OF VARIATION											
.00	.00	.00	.00	.00	.00	.00	.00	.00	.00	.00	.00

THE CAVITATION NUMBER = .0558

PRESSURE PROFILE RUNS, MJR THESIS

TEST FLUID IS MERCURY

CAVITATION CONDITION = STANDARD CAVITATION

NUMBER OF TEST SPECIMENS IN VENTURI = THREE

TEMPERATURE = 88.000 F
BAROMETRIC PRESSURE = 737.3000 IN. HG.
HEIGHT CORRECTION = .0000 IN. FLUID
FLOW RATE = 2.500 IN. FLUID OR 21.100 GPM
PUMP SPEED = 1496 RPM
ORIGINAL DATA ON SHEET NO. 198353

V-IN	P-00	P-0	P-1	S-1	P-2	S-2	S-3	P-3	P-4	P-5	V-OUT
ORIGINAL PRESSURE TAP DATA											
112.00	-2.95	-5.05	-8.80	-7.80	4.05	-.50	11.20	-3.95	30.50	47.00	76.00
THE UNCORRECTED NORMALIZED PRESSURES											
1.2649	.1133	.0923	.0547	.0647	.1834	.1379	.2551	.1033	.4484	.6137	.9042

THROAT VELOCITY = 33.14 FT/SEC

NO CORRECTIONS MADE TO NORMALIZED PRESSURES

THE AVERAGE NORMALIZED PRESSURES											
1.2649	.1133	.0923	.0547	.0647	.1834	.1379	.2551	.1033	.4484	.6137	.9042

THE LOSS COEFFICIENT = .3606

THE VARIANCES IN NORMALIZED PRESSURES											
.0000	.0000	.0000	.0000	.0000	.0000	.0000	.0000	.0000	.0000	.0000	.0000
THE STANDARD DEVIATIONS											
.0000	.0000	.0000	.0000	.0000	.0000	.0000	.0000	.0000	.0000	.0000	.0000
THE COEFFICIENTS OF VARIATION											
.00	.00	.00	.00	.00	.00	.00	.00	.00	.00	.00	.00

THE CAVITATION NUMBER = .0547

PRESSURE PROFILE RUNS, MJR THESIS

MEAN VALUES FOR 3SETS AT SAME FLOW, RPM, AND CAVITATION CONDITION

FLOW RATE = 21.100 GPM
PUMP SPEED = 1496 RPM

CAVITATION CONDITION = STANDARD CAVITATION

NUMBER OF TEST SPECIMENS IN VENTURI = THREE

THROAT VELOCITY = 33.14 FT/SEC

V-IN	P-00	P-0	P-1	S-1	P-2	S-2	S-3	P-3	P-4	P-5	V-OUT
THE AVERAGE NORMALIZED PRESSURES											
1.2646	.1097	.0900	.0545	.0621	.1814	.1425	.2461	.1024	.4465	.6101	.9073
THE VARIANCES IN NORMALIZED PRESSURES											
.0000	.0000	.0000	.0000	.0001	.0000	.0006	.0018	.0014	.0001	.0001	.0000
THE STANDARD DEVIATIONS											
.0002	.0048	.0051	.0012	.0072	.0042	.0245	.0422	.0372	.0103	.0085	.0046
THE COEFFICIENTS OF VARIATION											
.01	4.36	5.70	2.23	11.53	2.30	17.22	17.13	36.33	2.30	1.40	.51

THE MEAN CAVITATION NUMBER = .0545

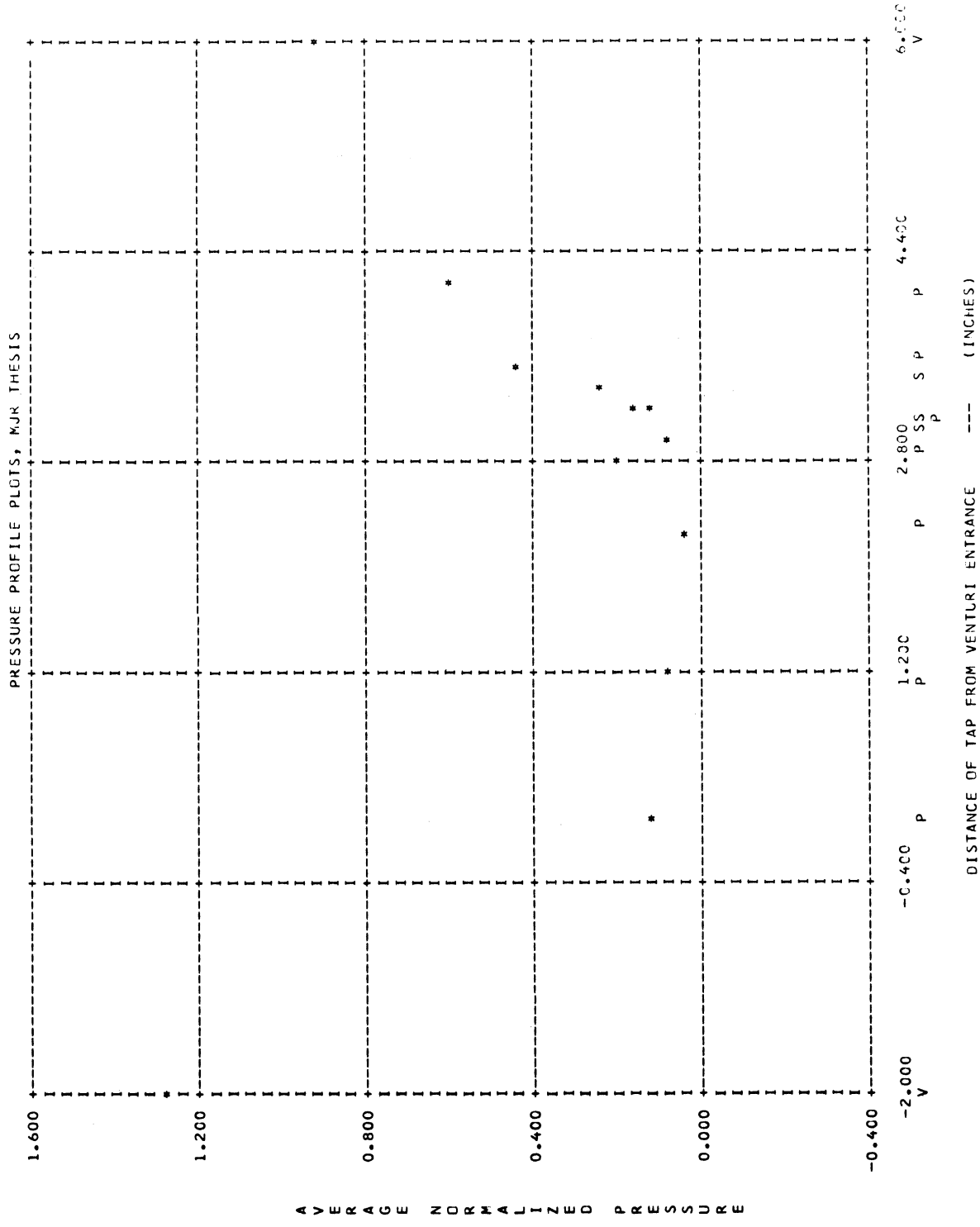
PRESSURE PROFILE PLOTS, MJR THESIS
AVERAGE NORMALIZED PRESSURE
1.600
1.200
0.800
0.400
0.000
-0.400
-2.000
-0.400
1.200
2.800
4.400
6.000
DISTANCE OF TAP FROM VENTURI ENTRANCE --- (INCHES)

APPENDIX C

COMPUTER ANALYSIS OF CAVITATION DAMAGE DATA

The computer program used to compute the mean depth of penetration, both from the pit count data and the weight loss measurements, is listed on the following pages. Included also is a page of typical output showing the numbers calculated, etc.

```
$COMPILE MAD,EXECUTE,DUMP,PUNCH OBJECT
          R                              PROGRAM A
          R                 REVISED AS OF FEB 23, 1965.
          R
           Z=Z
           READ DATA FLUID
           PRINT FORMAT TABLE
           PRINT FORMAT TITLE, FLUID
           J=0
           K=1
START      READ FORMAT REMT,MATL,NO,VEL,CAV
           MDPR = 0
           AMDPR = 0
           MDP2 = 0
           AMDP2 = 0
           H2 = 0
           I=0
AGAIN      READ DATA HRS,N1,N2,N3,N4,AWL
           WHENEVER Z.E.3
           PRINT COMMENT $0                                          NEXT SAMP
          1LE DATA WERE OBTAINED IN THE OLD WATER LOOP$
           J = J + 1
           Z = 1
           OR WHENEVER Z.E.4
           PRINT COMMENT $0                                          NEXT SAMP
          1LE DATA WERE OBTAINED IN DRY MERCURY $
           J = J + 1
           Z = 2
           END OF CONDITIONAL
           WHENEVER J.E.25
           K = K + 1
           PRINT FORMAT PAGE, K
           PRINT FORMAT TITLE, FLUID
           J = 0
           END OF CONDITIONAL
           WHENEVER HRS.L.0, TRANSFER TO START
           WHENEVER I.E.0
           FLAG = HRS
           N10=N1
           N20=N2
           N30=N3
           N40=N4
           I=1
           END OF CONDITIONAL
           WHENEVER Z.E.2
           N1 = 0
           N2 = 0
           N3 = 0
           N4 = 0
           OTHERWISE
           N1=N1-N10
           N2=N2-N20
           N3=N3-N30
           N4=N4-N40
           END OF CONDITIONAL
           WHENEVER MATL.E.$SS$.OR.MATL.E.$CS$
           RO = 7.85
           OR WHENEVER MATL.E.$PLEX$
           RO = 1.23
```

```
OR WHENEVER MATL.F.$CBZR$
RO = 8.72
OR WHENEVER MATL.F.$AL$
RO = 2.77
OR WHENEVER MATL .E.$CZ$
RO = 8.616
OR WHENEVER MATL.F.$A$.OR.MATL.E.$B$
RO = 17.655
OR WHENEVER MATL.F.$CU$
RO = 9.0248
OR WHENEVER MATL.F.$CN$
RO = 9.040
OR WHENEVER MATL.F.$NI$
RO = 8.973
OR WHENEVER  MATL .E.$SS1$
RO = 7.994
OR WHENEVER MATL.E.$F$
RO = 7.810
OR WHENEVER MATL.F.$D$
RO = 9.832
OR WHENEVER MATL.E.$G$
RO = 4.52
OR WHENEVER MATL.F.$E$
RO = 10.215
END OF CONDITIONAL
AUX1  =            .5216*N1+6.0363*N2+71.1547*N3+334.4513*N4
KO = 7.346E-3
KP = 1.172
KS = 3.601
WLPS = 1.642E-8*RO*KO*KP.P.3*AUX1
WL = KS * WLPS
APS = 3.72E4
AT = 3.362E5
MDPPS = KO * KP.P.3 * AUX1 /APS
MDP = KO * KP.P.3 * KS *AUX1/AT
AUX2 =     .6480*N1 + 3.1525*N2 + 16.4799*N3 + 46.6233 * N4
PDAPS = 25.*3.14159 * KP.P.2 *AUX2/APS
PDA = 25.*3.14159*KP.P.2 *KS *AUX2/AT
AMDP = AWL/(AT * 1.642E-8 * RO)
WHENEVER  WL.E.0
APDA = 0
OTHERWISE
APDA = PDA * AWL / WL
END OF CONDITIONAL
WHENEVER HRS.F.0
MDPR = 0
AMDPR = 0
MDP2 = 0
AMDP2 = 0
H2 = 0
OTHERWISE
H1 = H2
MDP1 = MDP2
AMDP1 = AMDP2
H2 = HRS
MDP2 = MDP
AMDP2 = AMDP
MDPR = (MDP2 - MDP1)/(H2-H1)
AMDPR = (AMDP2 -AMDP1)/(H2-H1)
```

```
 END OF CONDITIONAL
 WHENEVER HRS.G.FLAG
 WHENEVER Z.E.1
 PRINT FORMAT PFMT1,HRS,N1,N2,N3,N4,MDP,PDA,MDPR,AMDP,APDA,
1 AMDPR,AWL
 OR WHENEVER Z.E.0
 PRINT FORMAT PFMT1,HRS,N1,N2,N3,N4,MDP,PDA,MDPR
 OR WHENEVER Z.E.2
 PRINT FORMAT PFMT2,HRS,AMDP,      AMDPR,AWL
 END OF CONDITIONAL
 OTHERWISE
 PRINT FORMAT PFMT,MATL,NO,VEL,CAV,HRS,N1,N2,N3,N4,MDP,PDA,
1 MDPR,AMDP,APDA,AMDPR,AWL
 END OF CONDITIONAL
 J=J+1
 WHENEVER J.E.25
 K=K+1
 PRINT FORMAT PAGE,K
 PRINT FORMAT TITLE, FLUID
 J=0
 END OF CONDITIONAL
 TRANSFER TO AGAIN
 FORMAT VARIABLE Z
 INTEGER MATL,NO,N1,N2,N3,N4,J,K,I,Z,FLUID, CAV
R
R               FORMAT VALUES
R
 VECTOR VALUES TABLE=$1H1,S63,8HTABLE    *$
 VECTOR VALUES TITLE=$1HO,S50,30HCAVITATION  DAMAGE  DATA  IN
1 ,C6//S10,103H         WL = WEIGHT LOSS,  MDP = MEAN DEPTH OF
2PENETRATION,  PDA = PERCENT DAMAGED AREA,  R = RATE      ///S9
3,119HTHROAT  CAV. HOURS  PIT COUNT DATA      ---- CALCULATED
4VALUES ----          ----- ACTUAL (OR MEASURED) VALUES -----
5  /129HMATL NO. VEL-FPS COND  RUN    N1  N2  N3 N4    MDP-MIL
6S   PDA-PERCENT MDPR-MILS/HR MDP-MILS   PDA-PERCENT MDPR-MILS
7/HR   WL-GRAMS *$
 VECTOR VALUES PAGE=$1H1,S63,5HPAGE ,I2*$
 VECTOR VALUES RFMT=$C4,S6,I3,S7,F5.1,S5,C4*$
 VECTOR VALUES PFMT=$1HO,C4,   I3,S2,F5.1,S2,C4,S1,F5.1,S1,I4,
1S1,I3,S2,I2,S1,I2,S3,1PE10.3,S2,1PE10.3,S2,1PE10.3,S2,1PE10.3
2,S2,1PF10.3,S2,1PE10.3,S2,1PE10.3*$
 VECTOR VALUES PFMT1=$1HO,S21,                          F5.1,S1,I4,
1S1,I3,S2,I2,S1,I2,S3,1PF10.3,S2,1PE10.3,S2,1PF10.3,S2,1PE10.3
2,S2,1PF10.3,S2,1PF10.3,S2,1PE10.3*$
 VECTOR VALUES PFMT2 = $1HO,S21,F5.1,55H        ---- PIT COUNT
1ING WAS NOT POSSIBLE ----         ,1PE10.3,S14,          1PE10
2.3,S2,1PF10.3*$
 END OF PROGRAM
```

CAVITATION DAMAGE DATA IN WATER

WL = WEIGHT LOSS, MDP = MEAN DEPTH OF PENETRATION, PDA = PERCENT DAMAGED AREA, R = RATE

MAIL	NO.	THROAT VEL-FPS	CAV. COND	HOURS RUN	PIT COUNT DATA N1	N2	N3	N4	---- CALCULATED VALUES ---- MDP-MILS	PDA-PERCENT	MDPR-MILS/HR	----- ACTUAL (OR MEASURED) VALUES ----- MDP-MILS	PDA-PERCENT	MDPR-MILS/HR	WL-GRAMS
CU	84	200.0	STND	.0	0	0	0	0	.000E 00	.000E 00	.000E 00	.000E 00	.000E 00	.000E 00	.000E 00
				1.0	51	8	0	0	9.486E-06	6.733E-02	9.486E-06	3.212E-03	2.279E 01	3.212E-03	1.600E-04
				4.0	53	36	1	3	1.671E-04	3.515E-01	5.255E-05	5.219E-03	1.098E 01	6.691E-04	2.600E-04
				10.0	120	54	2	6	3.214E-04	6.479E-01	2.572E-05	9.635E-03	1.942E 01	7.360E-04	4.800E-04
				20.0	161	50	3	3	2.030E-04	5.214E-01	-1.184E-05	1.285E-02	3.300E 01	3.212E-04	6.400E-04
				30.0	293	64	7	4	3.008E-04	8.013E-01	9.784E-06	1.806E-02	4.812E 01	5.219E-04	9.000E-04
				40.0	643	124	11	9	6.177E-04	1.627E 00	3.169E-05	2.328E-02	6.135E 01	5.219E-04	1.160E-03
				50.0					---- PIT COUNTING WAS NOT POSSIBLE ----			2.509E-02		1.806E-04	1.250E-03
				75.0					---- PIT COUNTING WAS NOT POSSIBLE ----			3.352E-02		3.372E-04	1.670E-03
				100.0					---- PIT COUNTING WAS NOT POSSIBLE ----			5.600E-02		8.992E-04	2.790E-03
CU	157	200.0	STND	.0	0	0	0	0	.000E 00	.000E 00	.000E 00	.000E 00	.000E 00	.000E 00	.000E 00
				1.0	44	6	2	1	6.788E-05	1.468E-01	6.788E-05	3.412E-03	7.377E 00	3.412E-03	1.700E-04
				4.0	107	30	4	2	1.508E-04	3.733E-01	2.763E-05	6.423E-03	1.590E 01	1.004E-03	3.200E-04
				10.0	193	59	11	7	4.535E-04	9.460E-01	5.046E-05	1.285E-02	2.679E 01	1.071E-03	6.400E-04
				20.0	242	56	11	6	4.121E-04	9.179E-01	-4.142E-06	1.465E-02	3.263E 01	1.806E-04	7.300E-04
				30.0	381	67	12	7	4.811E-04	1.135E 00	6.897E-06	1.827E-02	4.309E 01	3.613E-04	9.100E-04
				40.0	1521	160	14	13	8.997E-04	2.689E 00	4.186E-05	2.108E-02	6.298E 01	2.810E-04	1.050E-03
				50.0					---- PIT COUNTING WAS NOT POSSIBLE ----			2.148E-02		4.014E-05	1.070E-03
				75.0					---- PIT COUNTING WAS NOT POSSIBLE ----			3.593E-02		5.781E-04	1.790E-03
				100.0					---- PIT COUNTING WAS NOT POSSIBLE ----			7.025E-02		1.373E-03	3.500E-03
CU	158	200.0	STND	.0	0	0	0	0	.000E 00	.000E 00	.000E 00	.000E 00	.000E 00	.000E 00	.000E 00
				1.0	0	0	1	1	5.138E-05	7.292E-02	5.138E-05	3.212E-03	4.558E 00	3.212E-03	1.600E-04
				4.0	0	1	5	4	2.153E-04	3.143E-01	5.464E-05	5.419E-03	7.913E 00	7.360E-04	2.700E-04
				10.0	139	27	5	6	3.291E-04	6.209E-01	1.897E-05	9.835E-03	1.856E 01	7.360E-04	4.900E-04
				20.0	179	31	5	4	2.500E-04	5.577E-01	-7.903E-06	5.821E-03	1.298E 01	-4.014E-04	2.900E-04

APPENDIX D

COMPUTER REGRESSION ANALYSIS OF DAMAGE DATA VERSUS MECHANICAL PROPERTIES

Due to the length and complexity of the regression program it is not reproduced in detail here as it appears in the original reference.[47] However, it is desirable to describe in general the characteristics and unique operational features of the program in order to better understand the predictions resulting from the use of it with respect to the damage data.

The program is in essence a least mean square fit regression analysis. It is capable of handling 59 independent variables, one dependent variable, 36 terms per variable, i.e., 36 powers per independent variable, and third order interactions of terms, i.e., a term of this latter type would be $X(1)^{a}X(2)^{b}X(3)^{c}$. Due to the tremendous number of possible terms available if the program is utilized to full capacity, it has incorporated into it a process of learning. The program selects a subset of up to 59 terms for a single pass out of the possible large number of terms generated for the entire number of variables considered to their different powers and interaction orders, e.g., for 8 variables, 10 terms per variable, there are 80 possible terms to analyze. However, if second order interactions are permitted, the total number of possible terms becomes 2880. Thus, it is soon obvious that it would take a long

time to examine all possible terms in this manner. The simple learning technique incorporated in this program consists of a weighting of the terms in the matrix, such that the probability of selecting terms of the type that have been selected in a previous pass as good fits are increased, and vice versa, for the terms of a type that have not been shown to have a good fit in a previous pass. Thus, the program is able to converge more rapidly on a statistically good fit of the observed data points with a function of the independent variables that were presented to it. The regression analysis is terminated when either of three criterion are satisfied: (1) The probability of inserting another term or removing a term from the current predicting equation is such that the chance of getting a bad term in or of taking a good term out is greater than the control value specified, (2) the total number of possible terms is exhausted and there are none left to insert, (3) the total number of trial passes specified is exceeded.

The sequence of analysis events occurs as follows:

The program reads in the specified control information and data sets, sets up a labeling system for the total possible number of terms, and then randomly picks out a subset of up to 59 of these for the first pass. It then computes individual correlation coefficients for each term with respect to the observed data values listed. The term with the highest correlation coefficient is selected to be entered into the equation and the least mean squares analysis is used to generate the coefficients for an equation of the following form:

$$Y = a_o + a_1 X_1$$

and the statistical information regarding the fit of this equation to the data is computed. The program then computes an importance factor for the test of the terms not in the equation with regard to how each will best account for the deviations between the actual data and the predicted values. The best term in this respect is entered into the equation if the test for the probability of insertion and deletion error is passed. If not, the regression is terminated. This process is continued until the best fit predicting equation possible with the first subset of terms is achieved. This completes a standard trial. Then, still working with the same subset of terms, a random trial is performed. The above process is repeated through the entering of the first term. The second term in this case is chosen randomly from the remaining terms of the subset with respect to the importance factors. This process is continued as for the standard trial until the regression is terminated for one of the three reasons mentioned previously. Several random trials are possible per pass, and in some cases result in a better predicting equation than the standard trial due to the combination of several terms that did not have as high of importance factors being better than another single term with the highest importance factor as selected in the standard trial.

At this point, the learning technique is employed by increasing the probability of picking terms of the type that got into the equation in the last pass and decreasing the probability of picking those types of terms that did not get in. The terms that are in the equation from the last pass are entered in the subset for the next pass and a random

process of selection, with respect to the changed probabilities of term selection, is employed to select enough other terms from the total possible to fill out the subset to its normal value. Another pass as described above is then initiated and carried out. At the end of the prescribed number of passes, the best trial of the best pass is indicated and the statistics of degree of fit to the data are generated and printed out along with the predicted equation. A typical pass and set of trials for this pass are included for the data and control parameters as used in this investigation for clarification of the above statements.

Control parameters used for following pass:

Prescribed Coefficient of Determination	=	0.97
Prescribed Standard Error of Y	=	0.00
Probability of insertion error	=	0.01
Probability of deletion error	=	0.01
Number of independent variables	=	10
Number of terms per variable	=	10
Interaction order	=	1
Number of terms per pass	=	40

Thus the total possible terms is 100.

TYPICAL PASS FOR MERCURY REGRESSION ANALYSIS

In the following program, the mechanical properties were read in as follows, i.e., as dependent variables:

X(1) = Tensile Strength

X(2) = Yield Strength

X(3) = Engineering Strain Energy

X(4) = Elastic Modulus

X(5) = Brinell Hardness

X(6) = Acoustic Impedance = $\frac{(\rho (E/\rho)^{1/2})_{\text{fluid}}}{(\rho (E/\rho)^{1/2})_{\text{material}}}$ =

$$\frac{(\text{Density x Sonic Velocity})_{\text{fluid}}}{(\text{Density x Sonic Velocity})_{\text{material}}}$$

X(7) = True Breaking Stress

X(8) = True Strain Energy

X(9) = % Elongation

X(10) = % Reduction of Area

X(11) = MDP (Independent Variable)

- FIRST ORDER INTERACTION - HG AVERAGED DATA W/O NICKEL

POSSIBLE TERMS= 100

STARTER PROGRAM

PROBLEM NO. 5

RAW DATA

OBSERVATION NO. 29 WEIGHT = 1.00000
X(1) = .9520000E 01 X(2) = .3700000E 01 X(3) = .4480000E 01 X(4) = .2800000E 02
X(5) = .1250000E 03 X(6) = .4320000E 01 X(7) = .1728000E 02 X(8) = .7450000E 01
X(9) = .5440000E 02 X(10) = .5090000E 02 X(11) = .2430000E-02 X(

OBSERVATION NO. 30 WEIGHT = 1.00000
X(1) = .9520000E 01 X(2) = .3700000E 01 X(3) = .4480000E 01 X(4) = .2800000E 02
X(5) = .1325000E 03 X(6) = .4320000E 01 X(7) = .1728000E 02 X(8) = .7450000E 01
X(9) = .5440000E 02 X(10) = .5090000E 02 X(11) = .1850000E-02 X(

OBSERVATION NO. 31 WEIGHT = 1.00000
X(1) = .9523000E 01 X(2) = .3700000E 01 X(3) = .4480000E 01 X(4) = .2800000E 02
X(5) = .1325000E 03 X(6) = .4320000E 01 X(7) = .1728000E 02 X(8) = .7450000E 01
X(9) = .5443000E 02 X(10) = .5090000E 02 X(11) = .4040000E-02 X(

OBSERVATION NO. 32 WEIGHT = 1.00000
X(1) = .5000000E 01 X(2) = .3000000E 01 X(3) = .1550000E 01 X(4) = .2800000E 02
X(5) = .9150000E 02 X(6) = .4320000E 01 X(7) = .5520000E 01 X(8) = .2300000E 01
X(9) = .4000000E 02 X(10) = .7100000E 02 X(11) = .3900000E-01 X(

OBSERVATION NO. 33 WEIGHT = 1.00000
X(1) = .4440000E 01 X(2) = .3400000E 01 X(3) = .1550000E 01 X(4) = .2800000E 02
X(5) = .7900000E 02 X(6) = .4320000E 01 X(7) = .5520000E 01 X(8) = .2300000E 01
X(9) = .4000000E 02 X(10) = .7100000E 02 X(11) = .1973000E-01 X(

OBSERVATION NO. 34 WEIGHT = 1.00000
X(1) = .8000000E 01 X(2) = .7280000E 01 X(3) = .1680000E 01 X(4) = .2900000E 02
X(5) = .1630000E 03 X(6) = .1340000E 01 X(7) = .1171000E 02 X(8) = .9130000E 01
X(9) = .2160000E 02 X(10) = .6330000E 02 X(11) = .1709000E-01 X(

OBSERVATION NO. 35 WEIGHT = 1.00000
X(1) = .8930000E 01 X(2) = .8040000E 01 X(3) = .2030000E 01 X(4) = .2900000E 02
X(5) = .1750000E 03 X(6) = .1334000E 02 X(7) = .1356000E 02 X(8) = .9600000E 01
X(9) = .2200000E 02 X(10) = .5960000E 02 X(11) = .8470000E-02 X(

OBSERVATION NO. 36 WEIGHT = 1.00000

```
      X(  1) =    .2930000E 01        X(  2) =    .1460000E 01        X(  3) =    .6000000E 00        X(  4) =    .1200000E 02
      X(  5) =    .1150000E 03        X(  6) =    .6280000E 01        X(  7) =    .3000000E 01        X(  8) =    .2500000E 01
      X(  9) =    .4250000E 02        X( 10) =    .9280000E 02        X( 11) =    .1787000E-01        X(

OBSERVATION NO.    40   WEIGHT =    1.00000
      X(  1) =    .9470000E 01        X(  2) =    .8960000E 01        X(  3) =    .1500000E 01        X(  4) =    .3710000E 02
      X(  5) =    .2160000E 03        X(  6) =    .3270000E 01        X(  7) =    .1200000E 02        X(  8) =    .2500000E 01
      X(  9) =    .3070000E 02        X( 10) =    .5470000E 02        X( 11) =    .2102000E-01        X(

OBSERVATION NO.    41   WEIGHT =    1.00000
      X(  1) =    .1375000E 02        X(  2) =    .8200000E 01        X(  3) =    .5450000E 01        X(  4) =    .2900000E 02
      X(  5) =    .2190000E 03        X(  6) =    .4320000E 01        X(  7) =    .2209000E 02        X(  8) =    .9480000E 01
      X(  9) =    .4420000E 02        X( 10) =    .4660000E 02        X( 11) =    .1860000E-02        X(
```

```
EDITOR PROGRAM


PROBLEM NO.     5
SO  TION PASS NO.     2
NO. OF INDEPENDENT VARIABLES =    10
NO. OF TRIAL TERMS =    40


TRIAL TERM DEFINITIONS FOR PASS NO.     2

TERM( 1) = 1.0, CONSTANT TERM.

TERM( 2) = INTERACTION OF ORDER  1, WHERE THE COMPONENTS ARE DEFINED TO BE --
         COMPONENT( 1) = X( 7)

TERM( 3) = INTERACTION OF ORDER  1, WHERE THE COMPONENTS ARE DEFINED TO BE --
         COMPONENT( 1) = X( 5) .P.     -.33333

TERM( 4) = INTERACTION OF ORDER  1, WHERE THE COMPONENTS ARE DEFINED TO BE --
         COMPONENT( 1) = X( 7) .P.     3.00000

TERM( 5) = INTERACTION OF ORDER  1, WHERE THE COMPONENTS ARE DEFINED TO BE --
         COMPONENT( 1) = X( 1) .P.      .50000

TERM( 6) = INTERACTION OF ORDER  1, WHERE THE COMPONENTS ARE DEFINED TO BE --
         COMPONENT( 1) = X(10) .P.    -2.00000

TERM( 7) = INTERACTION OF ORDER  1, WHERE THE COMPONENTS ARE DEFINED TO BE --
         COMPONENT( 1) = X( 2) .P.      .33333

TERM( 8) = INTERACTION OF ORDER  1, WHERE THE COMPONENTS ARE DEFINED TO BE --
         COMPONENT( 1) = X( 5)

TERM( 9) = INTERACTION OF ORDER  1, WHERE THE COMPONENTS ARE DEFINED TO BE --
         COMPONENT( 1) = X( 9) .P.    -2.00000

TERM(10) = INTERACTION OF ORDER  1, WHERE THE COMPONENTS ARE DEFINED TO BE --
         COMPONENT( 1) = X( 3) .P.      .50000

TERM(11) = INTERACTION OF ORDER  1, WHERE THE COMPONENTS ARE DEFINED TO BE --
         COMPONENT( 1) = X( 4) .P.     3.00000

TERM(12) = INTERACTION OF ORDER  1, WHERE THE COMPONENTS ARE DEFINED TO BE --
         COMPONENT( 1) = X(10) .P.      .50000

TERM(13) = INTERACTION OF ORDER  1, WHERE THE COMPONENTS ARE DEFINED TO BE --
         COMPONENT( 1) = X( 4) .P.      .33333

TERM(14) = INTERACTION OF ORDER  1, WHERE THE COMPONENTS ARE DEFINED TO BE --
         COMPONENT( 1) = X( 4) .P.    -2.00000

TERM(15) = INTERACTION OF ORDER  1, WHERE THE COMPONENTS ARE DEFINED TO BE --
         COMPONENT( 1) = X( 4) .P.     2.00000

TE   (16) = INTERACTION OF ORDER  1, WHERE THE COMPONENTS ARE DEFINED TO BE --
         COMPONENT( 1) = X( 9) .P.    -3.00000

TERM(17) = INTERACTION OF ORDER  1, WHERE THE COMPONENTS ARE DEFINED TO BE --
         COMPONENT( 1) = X( 8) .P.     2.00000
```

```
TERM(18) = INTERACTION OF ORDER  1, WHERE THE COMPONENTS ARE DEFINED TO BE --
         COMPONENT( 1) = X( 3) .P.    -1.00000

TERM(19) = INTERACTION OF ORDER  1, WHERE THE COMPONENTS ARE DEFINED TO BE --
         COMPONENT( 1) = X( 4) .P.      .50000

TERM(20) = INTERACTION OF ORDER  1, WHERE THE COMPONENTS ARE DEFINED TO BE --
         COMPONENT( 1) = X( 1) .P.    -2.00000

TERM(21) = INTERACTION OF ORDER  1, WHERE THE COMPONENTS ARE DEFINED TO BE --
         COMPONENT( 1) = X(10)

TERM(22) = INTERACTION OF ORDER  1, WHERE THE COMPONENTS ARE DEFINED TO BE --
         COMPONENT( 1) = X( 3) .P.    -1.00000

TERM(23) = INTERACTION OF ORDER  1, WHERE THE COMPONENTS ARE DEFINED TO BE --
         COMPONENT( 1) = X(10) .P.     2.00000

TERM(24) = INTERACTION OF ORDER  1, WHERE THE COMPONENTS ARE DEFINED TO BE --
         COMPONENT( 1) = X( 4) .P.     -.33333

TERM(25) = INTERACTION OF ORDER  1, WHERE THE COMPONENTS ARE DEFINED TO BE --
         COMPONENT( 1) = X( 3) .P.    -3.00000

TERM(26) = INTERACTION OF ORDER  1, WHERE THE COMPONENTS ARE DEFINED TO BE --
         COMPONENT( 1) = X( 7) .P.     -.50000

TERM(27) = INTERACTION OF ORDER  1, WHERE THE COMPONENTS ARE DEFINED TO BE --
         COMPONENT( 1) = X(10) .P.     3.00000

TE. (28) = INTERACTION OF ORDER  1, WHERE THE COMPONENTS ARE DEFINED TO BE --
         COMPONENT( 1) = X( 5) .P.    -3.00000

TERM(29) = INTERACTION OF ORDER  1, WHERE THE COMPONENTS ARE DEFINED TO BE --
         COMPONENT( 1) = X( 5) .P.     -.50000

TERM(30) = INTERACTION OF ORDER  1, WHERE THE COMPONENTS ARE DEFINED TO BE --
         COMPONENT( 1) = X( 7) .P.    -1.00000

TERM(31) = INTERACTION OF ORDER  1, WHERE THE COMPONENTS ARE DEFINED TO BE --
         COMPONENT( 1) = X( 8) .P.    -2.00000

TERM(32) = INTERACTION OF ORDER  1, WHERE THE COMPONENTS ARE DEFINED TO BE --
         COMPONENT( 1) = X( 5) .P.     3.00000

TERM(33) = INTERACTION OF ORDER  1, WHERE THE COMPONENTS ARE DEFINED TO BE --
         COMPONENT( 1) = X( 5) .P.      .50000

TERM(34) = INTERACTION OF ORDER  1, WHERE THE COMPONENTS ARE DEFINED TO BE --
         COMPONENT( 1) = X( 5) .P.    -2.00000

TERM(35) = INTERACTION OF ORDER  1, WHERE THE COMPONENTS ARE DEFINED TO BE --
         COMPONENT( 1) = X( 9) .P.      .50000

TERM(36) = INTERACTION OF ORDER  1, WHERE THE COMPONENTS ARE DEFINED TO BE --
         COMPONENT( 1) = X( 5) .P.    -1.00000

TERM(37) = INTERACTION OF ORDER  1, WHERE THE COMPONENTS ARE DEFINED TO BE --
         COMPONENT( 1) = X( 7) .P.    -2.00000
```

```
TERM(38) = INTERACTION OF ORDER  1, WHERE THE COMPONENTS ARE DEFINED TO BE --
         COMPONENT( 1) = X( 7) .P.     -3.00000

TERM(39) = INTERACTION OF ORDER  1, WHERE THE COMPONENTS ARE DEFINED TO BE --
         COMPONENT( 1) = X( 2) .P.       .50000

TERM(40) = INTERACTION OF ORDER  1, WHERE THE COMPONENTS ARE DEFINED TO BE --
         COMPONENT( 1) = X( 2) .P.      -.50000

TERM(41) = X(11), DEPENDENT VARIABLE.
```

STEPWISE REGRESSION

PROBLEM NO. 5

NO. OF DATA SETS = 10

NO. OF TERM CHOICES = 40

PROBABILITY OF
1) ERROR IN ENTERING TERM = 1.0000 0/0
2) ERROR IN DELETING TERM = 1.0000 0/0

WEIGHTED DEGREES OF FREEDOM = 10.00

PASS NO. 2 STANDARD TRIAL.

STANDARD ERROR OF Y = .184522433E-01

STEP NO. 1
TERM ENTERED 1
F LEVEL = .000000000E 00
STANDARD ERROR OF Y = .126781249E-01
COEFF OF DETERMINATION = .580377102E 00
MULTIPLE CORLTN COEFF = .761824846E 00

CONSTANT TERM = .000000000E 00

TERM NO.	COEFFICIENT	STD ERR OF COEFF	F LEVEL
TERM- 1	.133359993E-01	.400917511E-02	-.968164429E 01

PREDICTED RESULTS VERSUS DATA POINTS

OBS. NO.	PREDICTIONS Y - SIGMA	PREDICTIONS Y	PREDICTIONS Y + SIGMA	DATA POINTS	DEVIATIONS (DATA - Y)	DEVIATIONS PERCENT
29	.65787439E-03	.13335999E-01	.26014124E-01	.24300000E-02	-.10905999E-01	-448.807
30	.65787439E-03	.13335999E-01	.26014124E-01	.18500000E-02	-.11485999E-01	-620.865
31	.65787439E-03	.13335999E-01	.26014124E-01	.40400000E-02	-.92959993E-02	-230.099
32	.65787439E-03	.13335999E-01	.26014124E-01	.39000000E-01	.25664000E-01	65.805
33	.65787439E-03	.13335999E-01	.26014124E-01	.19730000E-01	.63940004E-02	32.408
34	.65787439E-03	.13335999E-01	.26014124E-01	.17090000E-01	.37540006E-02	21.966
35	.65787439E-03	.13335999E-01	.26014124E-01	.84699999E-02	-.48659994E-02	-57.450
36	.65787439E-03	.13335999E-01	.26014124E-01	.17870000E-01	.45340005E-02	25.372
40	.65787439E-03	.13335999E-01	.26014124E-01	.21020000E-01	.76840005E-02	36.556
41	.65787439E-03	.13335999E-01	.26014124E-01	.18600000E-02	-.11475999E-01	-616.989

MAXIMUM ABSOLUTE DEVIATION = .2566400E-01,(SEE OBS. NO. 32, LINE NO. 4)

MAXIMUM ABSOLUTE PERCENT DEVIATION = 620.865,(SEE OBS. NO. 30, LINE NO. 2)

STEP NO. 2
TERM ENTERED 2
F LEVEL = .129055079E 02
STANDARD ERROR OF Y = .803735927E-02
COEFF OF DETERMINATION = .952434799E 00
MULTIPLE CORLTN COEFF = .923273958E 00

CONSTANT TERM = .000000000E 00

TERM NO.	COEFFICIENT	STD ERR OF COEFF	F LEVEL
TERM- 1	.326596148E-01	.594924043E-02	-.258316576E 02
TERM- 2	-.154292699E-02	.423494713E-03	-.110613639E 02

PREDICTED RESULTS VERSUS DATA POINTS

OBS. NO.	PREDICTIONS			DATA	DEVIATIONS	
	Y - SIGMA	Y	Y + SIGMA	POINTS	(DATA - Y)	PERCENT
29	-.20395205E-02	.59978387E-02	.14035198E-01	.24300000E-02	-.35678387E-02	-148.825
30	-.20395206E-02	.59978387E-02	.14035198E-01	.18500000E-02	-.41478387E-02	-224.207
31	-.20395206E-02	.59978387E-02	.14035198E-01	.40400000E-02	-.19578387E-02	-48.461
32	.16105299E-01	.24142658E-01	.32180017E-01	.39000000E-01	.14857342E-01	38.095
33	.16105299E-01	.24142658E-01	.32180017E-01	.19730000E-01	-.44126585E-02	-22.365
34	.65545813E-02	.14591941E-01	.22629300E-01	.17090000E-01	.24980593E-02	14.617
35	.37001673E-02	.11737527E-01	.19774886E-01	.84699999E-02	-.32675267E-02	-38.578
36	.19993474E-01	.28030834E-01	.36068193E-01	.17870000E-01	-.10160834E-01	-56.860
40	.61071325E-02	.14144492E-01	.22181851E-01	.21020000E-01	.68755080E-02	32.709
41	-.94609971E-02	-.14236378E-02	.66137215E-02	.18600000E-02	.32836378E-02	176.540

MAXIMUM ABSOLUTE DEVIATION = .1495734E-01,(SEE OBS. NO. 32, LINE NO. 4)

MAXIMUM ABSOLUTE PERCENT DEVIATION = 224.207,(SEE OBS. NO. 30, LINE NO. 2)

REGRESSION TERMINATED AFTER 2 STEPS.

DIAGONAL ELEMENTS

VAR. NO.	VALUE
1	.547893651E 01
2	.547893651E 01
3	.670395739E-02
4	.753390677E-01
5	.310583644E-02
6	.564924158E-02
7	.218209295E-01
8	.575747900E-01
9	.372760940E 00
10	.132635543E-01
11	.173221907E 00
12	.133868573E-02
13	.548915111E-02
14	.354802053E 00
15	.955615543E-01
16	.568901233E 00
17	.114405777E 00
18	.840869285E-01
19	.112671576E-01
20	.201670785E 00
21	.691714600E-02
22	.116608379E 00
23	.402577454E-01
24	.791389525E-02
25	.542865485E 00
26	.144841103E-01
27	.108746253E 00
28	.287460446E 00
29	.148276282E-01
30	.816887427E-01
31	.162732925E 00

32	.3179105D0E 00
33	.1320830D8E-01
34	.1714558435 00
35	.2226637265-01
36	.5481190235-01
37	.2917420755 00
38	.4478505485 00
39	.4684526625-01
40	.4988640535-01

POSTULATED CRITERIA

STANDARD ERROR OF Y = .CCCCCCCE 00
COEFF OF DETERMINATION = .9700000E 00

FITTED CURVE PROPERTIES

STANDARD ERROR OF Y = .8037359E-02
COEFF OF DETERMINATION = .8524348E 00

PASS NO. 2 WILL BE EXECUTED 2 TIMES, USING RANDOM SELECTION

.SS NUMBER 2 RANDOM TRIAL NUMBER 1

STANDARD ERROR OF Y = .184522433E-01

STEP NO. 1
TERM ENTERED 1
F LEVEL = .000000000E 00
STANDARD ERROR OF Y = .129781249E-01
COEFF OF DETERMINATION = .5803771025 00
MULTIPLE CORLTN COEFF = .7618240465 00

CONSTANT TERM = .000000000E 00

TERM NO.	COEFFICIENT	STD ERR OF COEFF	F LEVEL
TERM- 1	.133359993E-01	.4009175115-02	-.9681644295 01

PREDICTED RESULTS VERSUS DATA POINTS

OBS. NO.	PREDICTIONS Y - SIGMA	PREDICTIONS Y	PREDICTIONS Y + SIGMA	DATA POINTS	DEVIATIONS (DATA - Y)	DEVIATIONS PERCENT
29	.65787439E-03	.13335999E-01	.26014124E-01	.24300000E-02	-.10905999E-01	-448.807
30	.65787439E-03	.13335999E-01	.26014124E-01	.18500000E-02	-.11485999E-01	-620.755
31	.65787439E-03	.13335999E-01	.26014124E-01	.40400000E-02	-.92959993E-02	-230.099
32	.65787439E-03	.13335999E-01	.26014124E-01	.39000000E-01	.25664000E-01	65.805
33	.65787439E-03	.13335999E-01	.26014124E-01	.19730000E-01	.63940004E-02	32.404
34	.65787439E-03	.13335999E-01	.26014124E-01	.17090000E-01	.37540005E-02	21.966
35	.65787439E-03	.13335999E-01	.26014124E-01	.84699999E-02	-.48659994E-02	-57.450
36	.65787439E-03	.13335999E-01	.26014124E-01	.17870000E-01	.45340005E-02	25.372
40	.65787439E-03	.13335999E-01	.26014124E-01	.21020000E-01	.76840005E-02	36.559
41	.65787439E-03	.13335999E-01	.26014124E-01	.19600000E-02	-.11475999E-01	-614.939

MAXIMUM ABSOLUTE DEVIATION = .2566400E-01,(SEE OBS. NO. 32, LINE NO. 4)

MAXIMUM ABSOLUTE PERCENT DEVIATION = 620.865,(SEE OBS. NO. 30, LINE NO. 2)

P NO. 2
TERM ENTERED 26
F LEVEL = .459425967E 02
STANDARD ERROR OF Y = .102855172E-01
COEFF OF DETERMINATION = .758337393E 00
MULTIPLE CORLTN COEFF = .870825700E 00

CONSTANT TERM = .000000000E 00

TERM NO.	COEFFICIENT	STD ERR OF COEFF	F LEVEL
TERM- 1	-.807051301E-02	.997370318E-02	-.561232217E 00
TERM- 26	.665723443E-01	.293216225E-01	-.441839866E 01

PREDICTED RESULTS VERSUS DATA POINTS

OBS. NO.	PREDICTIONS Y - SIGMA	PREDICTIONS Y	PREDICTIONS Y + SIGMA	DATA POINTS	DEVIATIONS (DATA - Y)	DEVIATIONS PERCENT
29	-.23412124E-02	.79443048E-02	.18229822E-01	.24300000E-02	-.55143048E-02	-226.926
30	-.23412124E-02	.79443048E-02	.18229822E-01	.18500000E-02	-.6094304BE-02	-329.422
31	-.23412124E-02	.79443048E-02	.18229822E-01	.40400000E-02	-.39043048E-02	-96.641
32	.99790417E-02	.20264559E-01	.30550076E-01	.39000000E-01	.18735441E-01	48.040
33	.99790417E-02	.20264559E-01	.30550076E-01	.19730000E-01	-.53455913E-03	-2.709
34	.10982609E-02	.11383778E-01	.21669295E-01	.17090000E-01	.57062219E-02	33.389
35	-.27746253E-03	.10008055E-01	.20293572E-01	.84699999E-02	-.15330548E-02	-18.159
36	.20079530E-01	.30365047E-01	.40650564E-01	.17870000E-01	-.1249504BE-01	-69.922
40	.86175033E-03	.11147267E-01	.21432785E-01	.21020000E-01	.98727323E-02	46.968
41	-.41917008E-02	.6093816BE-02	.16379333E-01	.18600000E-02	-.42338163E-02	-227.625

MAXIMUM ABSOLUTE DEVIATION = .1873544E-01,(SEE OBS. NO. 32, LINE NO. 4)

MAXIMUM ABSOLUTE PERCENT DEVIATION = 329.422,(SEE OBS. NO. 30, LINE NO. 2)

STEP NO. 3
TERM ENTERED 20
F LEVEL = .190802384E 02
STANDARD ERROR OF Y = .377583772E-02
COEFF OF DETERMINATION = .972085036E 00
MULTIPLE CORLTN COEFF = .985943727E 00

CONSTANT TERM = .000000000E 00

TERM NO.	COEFFICIENT	STD ERR OF COEFF	F LEVEL
TERM- 1	-.621383607E-01	.877700008E-02	-.417682342E 02
TERM- 20	-.974804571E 00	.129063446E 00	-.382854979E 02
TERM- 26	.312137801E 00	.377944969E-01	-.568400346E 02

PREDICTED RESULTS VERSUS DATA POINTS

OBS. NO.	PREDICTIONS Y - SIGMA	PREDICTIONS Y	PREDICTIONS Y + SIGMA	DATA POINTS	DEVIATIONS (DATA - Y)	DEVIATIONS PERCENT
29	-.47795186E-03	.32978659E-02	.70737235E-02	.24300000E-02	-.85788588E-03	-35.715
30	-.47795186E-03	.32978859E-02	.70737235E-02	.18500000E-02	-.14478859E-02	-78.264
31	-.47795186E-03	.32978859E-02	.70737235E-02	.40400000E-02	.74211409E-03	18.369
32	.31948288E-01	.35724126E-01	.39499963E-01	.39000000E-01	.32758741E-02	8.400
33	.22564784E-01	.26340621E-01	.30116459E-01	.19730000E-01	-.66106217E-02	-33.505
34	.11934763E-01	.15710601E-01	.19486438E-01	.17090000E-01	.13793993E-02	8.071
35	.78807566E-02	.11656594E-01	.15432432E-01	.84699999E-02	-.31865945E-02	-37.622
36	.12398257E-01	.16174095E-01	.19949932E-01	.17870000E-01	.16959051E-02	9.490

40	.14437587E-01	.18213425E-01	.21989262E-01	.21020000E-01	.28065750E-02	13.352
41	-.41289626E-02	-.35312492E-03	.34227128E-02	.18600000E-02	.22131249E-02	118.933

MAXIMUM ABSOLUTE DEVIATION = .6610622E-02,(SEE OBS. NO. 33, LINE NO. 5)

MAXIMUM ABSOLUTE PERCENT DEVIATION = 118.933,(SEE OBS. NO. 41, LINE NO. 10)

STEP NO. 4
TERM ENTERED 37
F LEVEL = .000000000E 00
STANDARD ERROR OF Y = .188477034E-02
COEFF OF DETERMINATION = .994203761E 00
MULTIPLE CORLTN COEFF = .997097671E 00

CONSTANT TERM = .000000000E 00

TERM NO.	COEFFICIENT	STD ERR OF COEFF	F LEVEL
TERM- 1	-.641359329E-01	.440498479E-02	-.169591451E 03
TERM- 20	-.171556721E 01	.202973813E 00	-.571512483E 02
TERM- 26	.344175375E 00	.202413429E-01	-.231298167E 03
TERM- 37	.749148796E 00	.171504891E 00	-.152641907E 02

PREDICTED RESULTS VERSUS DATA POINTS

OBS. NO.	PREDICTIONS Y - SIGMA	PREDICTIONS Y	PREDICTIONS Y + SIGMA	DATA POINTS	DEVIATIONS (DATA - Y)	DEVIATIONS PERCENT
29	.35476123E-03	.22395321E-02	.41243029E-02	.24300000E-02	.19046792E-03	7.833
30	.35476123E-03	.22395321E-02	.41243029E-02	.18500000E-02	-.38953308E-03	-21.057
31	.35476123E-03	.22395321E-02	.41243029E-02	.40400000E-02	.18004679E-02	44.566
32	.36433703E-01	.38318474E-01	.40203244E-01	.39000000E-01	.68152603E-03	1.748
33	.18031842E-01	.19916613E-01	.21801384E-01	.19730000E-01	-.18661306E-03	-.947
34	.13307712E-01	.15692483E-01	.17577254E-01	.17090000E-01	.13975166E-02	8.177
35	.10005704E-01	.11690475E-01	.13775246E-01	.84699999E-02	-.34204753E-02	-40.377
36	.16092635E-01	.17977406E-01	.19862177E-01	.17870000E-01	-.10740641E-02	-6.011
40	.19407052E-01	.21291823E-01	.23176593E-01	.21020000E-01	-.27192279E-03	-1.293
41	-.33062427E-03	.16541466E-02	.34389174E-02	.18600000E-02	.30458342E-03	16.444

MAXIMUM ABSOLUTE DEVIATION = .3420475E-02,(SEE OBS. NO. 35, LINE NO. 7)

MAXIMUM ABSOLUTE PERCENT DEVIATION = 44.566,(SEE OBS. NO. 31, LINE NO. 3)

POSTULATED CRITERIA

STANDARD ERROR OF Y = .CCC0000E 00
COEFF OF DETERMINATION = .97C0000E 00

FITTED CURVE PROPERTIES

STANDARD ERROR OF Y = .1C347715E-02
COEFF OF DETERMINATION = .99420384E 00

BEST PREVIOUS FITTED CURVE PROPERTIES

STANDARD ERROR OF Y = .[illegible]E-02
COEFFICIENT OF DETERMINATION = .[illegible]E 00

STANDARD TRIAL REJECTED IN FAVOR OF THE CURRENT TRIAL.

PASS NUMBER 2 RANDOM TRIAL NUMBER 2

STANDARD ERROR OF Y = .184522433E-01

STEP NO. 1
TERM ENTERED 1
F LEVEL = .000000000E 00
STANDARD ERROR OF Y = .126731249E-01
COEFF OF DETERMINATION = .590377102E 00
MULTIPLE CORLTN COEFF = .768182946E 00

CONSTANT TERM = .000000000E 00

TERM NO.	COEFFICIENT	STD ERR OF COEFF	F LEVEL
TERM- 1	.133359993E-01	.400917511E-02	-.968164429E 01

PREDICTED RESULTS VERSUS DATA POINTS

OBS. NO.	PREDICTIONS Y - SIGMA	Y	Y + SIGMA	DATA POINTS	DEVIATIONS (DATA - Y)	PERCENT
29	.657874398-03	.133359998-01	.260141248-01	.243000008-02	-.109059998-01	-448.807
30	.657874398-03	.133359998-01	.260141248-01	.185000008-02	-.114859998-01	-620.865
31	.657874398-03	.133359998-01	.260141248-01	.404000008-02	-.929599988-02	-230.099
32	.657874398-03	.133359998-01	.260141248-01	.390000008-01	.256640008-01	65.855
33	.657874398-03	.133359998-01	.260141248-01	.197300008-01	.639400048-02	32.403
34	.657874398-03	.133359998-01	.260141248-01	.170900008-01	.375400068-02	21.966
35	.657874398-03	.133359998-01	.260141248-01	.846999998-02	-.486599948-02	-57.450
36	.657874398-03	.133359998-01	.260141248-01	.178700008-01	.453400058-02	25.372
40	.657874398-03	.133359998-01	.260141248-01	.210200008-01	.763400058-02	36.316
41	.657874398-03	.133359998-01	.260141248-01	.196000008-02	-.114759998-01	-614.989

MAXIMUM ABSOLUTE DEVIATION = .256643OE-01,(SEE OBS. NO. 32, LINE NO. 4)

MAXIMUM ABSOLUTE PERCENT DEVIATION = 620.865,(SEE OBS. NO. 30, LINE NO. 2)

STEP NO. 2
TERM ENTERED 31
F LEVEL = .000000000E 00
STANDARD ERROR OF Y = .941521563E-02
COEFF OF DETERMINATION = .797503397E 00
MULTIPLE CORLTN COEFF = .893030457E 00

CONSTANT TERM = .000000000E 00

TERM NO.	COEFFICIENT	STD ERR OF COEFF	F LEVEL
TERM- 1	.645091236E-02	.339620267E-02	-.234969981E 01
TERM- 31	.107476410E 00	.392298613E-01	-.643347979E 01

PREDICTED RESULTS VERSUS DATA POINTS

OBS. NO.	PREDICTIONS Y - SIGMA	Y	Y + SIGMA	DATA POINTS	DEVIATIONS (DATA - Y)	PERCENT

29	-.10278786E-02	.83873370E-02	.17902553E-01	.24300000E-02	-.59573371E-02	-245.153
30	-.10278786E-02	.83873370E-02	.17902553E-01	.18500000E-02	-.63273371E-02	-342.579
31	-.10278786E-02	.83873370E-02	.17902553E-01	.40400000E-02	-.43473371E-02	-107.637
32	.17352598E-01	.26767814E-01	.36183030E-01	.39000000E-01	.12232186E-01	31.365
33	.17352598E-01	.26767814E-01	.36183030E-01	.19730000E-01	-.70378144E-02	-35.671
34	-.16749509E-02	.77402648E-02	.17155430E-01	.17090000E-01	.93497352E-02	54.709
35	-.17981095E-02	.76171061E-02	.17032322E-01	.84699999E-02	.85289369E-03	10.070
36	.14231923E-01	.23647138E-01	.33062354E-01	.17870000E-01	-.57771387E-02	-32.329
40	-.14041869E-02	.80110287E-02	.17426244E-01	.21020000E-01	.13008971E-01	61.889
41	-.17683987E-02	.76468169E-02	.17062033E-01	.18600000E-02	-.57868169E-02	-311.119

MAXIMUM ABSOLUTE DEVIATION = .1300897E-01,(SEE OBS. NO. 40, LINE NO. 9)

MAXIMUM ABSOLUTE PERCENT DEVIATION = 353.370,(SEE OBS. NO. 30, LINE NO. 2)

STEP NO. 3
TERM REMOVED 31
F LEVEL = .000000000E 00
STANDARD ERROR OF Y = .146394376E-01
COEFF OF DETERMINATION = .580377102E 00
MULTIPLE CORLTN COEFF = .761824846E 00

CONSTANT TERM = .000000000E 00

TERM NO.	COEFFICIENT	STD ERR OF COEFF	F LEVEL
TERM- 1	.133359993E-01	.462939657E-02	-.691546030E 01

PREDICTED RESULTS VERSUS DATA POINTS

OBS. NO.	PREDICTIONS Y - SIGMA	Y	Y + SIGMA	DATA POINTS	DEVIATIONS (DATA - Y)	PERCENT
29	-.13034383E-02	.13335999E-01	.27975437E-01	.24300000E-02	-.10905999E-01	-448.807
30	-.13034383E-02	.13335999E-01	.27975437E-01	.18500000E-02	-.11485999E-01	-620.865
31	-.13034383E-02	.13335999E-01	.27975437E-01	.40400000E-02	-.92959993E-02	-230.099
32	-.13034383E-02	.13335999E-01	.27975437E-01	.39000000E-01	.25664000E-01	65.805
33	-.13034383E-02	.13335999E-01	.27975437E-01	.19730000E-01	.63940004E-02	32.409
34	-.13034383E-02	.13335999E-01	.27975437E-01	.17090000E-01	.37540006E-02	21.966
35	-.13034383E-02	.13335999E-01	.27975437E-01	.84699999E-02	-.48659994E-02	-57.450
36	-.13034383E-02	.13335999E-01	.27975437E-01	.17870000E-01	.45340005E-02	25.372
40	-.13034383E-02	.13335999E-01	.27975437E-01	.21020000E-01	.76840005E-02	36.556
41	-.13034383E-02	.13335999E-01	.27975437E-01	.18600000E-02	-.11475999E-01	-616.939

MAXIMUM ABSOLUTE DEVIATION = .2566400E-01,(SEE OBS. NO. 32, LINE NO. 4)

MAXIMUM ABSOLUTE PERCENT DEVIATION = 620.865,(SEE OBS. NO. 30, LINE NO. 2)

STEP NO. 4
TERM REMOVED 1
F LEVEL = .000000000E 00
STANDARD ERROR OF Y = .247562820E-01
COEFF OF DETERMINATION = .745058060E-08
MULTIPLE CORLTN COEFF = .863167457E-04

CONSTANT TERM = .000000000E 00

TERM NO.	COEFFICIENT	STD ERR OF COEFF	F LEVEL

TULATED CRITERIA

STANDARD ERROR OF Y = .0000000E 00
COEFF OF DETERMINATION = .9700000E 00

FITTED CURVE PROPERTIES

STANDARD ERROR OF Y = .2475628E-01
COEFF OF DETERMINATION = .7450581E-08

BEST PREVIOUS FITTED CURVE PROPERTIES

STANDARD ERROR OF Y = .1884771E-02
COEFFICIENT OF DETERMINATION = .9942038E 00

CURRENT TRIAL REJECTED IN FAVOR OF RANDOM TRIAL NO. 1.

POSTULATED CRITERIA

STANDARD ERROR OF Y = .0000000E 00
COEFF OF DETERMINATION = .9700000E 00

FITTED CURVE PROPERTIES

STANDARD ERROR OF Y = .1884771E-02
COEFF OF DETERMINATION = .9942038E 00

FITTED CURVE MEETS ONLY COEF. OF DETERMINATION CRITERION.

CURRENT PASS IS THE BEST SO FAR.

PASS NUMBER 3 BEGUN FOR PROBLEM NO. 5
5 TOTAL PASSES ALLOWED.

MAD EXTERNAL FUNCTION STATEMENTS FOR PREDICTING EQUATION PRODUCED BY LAST REGRESSION STEP

```
$ COMPILE MAD
; PUNCH OBJECT
$ PRINT OBJECT
          EXTERNAL FUNCTION(X1,X 2,X 3,X 4,X 5,X 6,X 7,X 8,X 9,X10)
          ENTRY TO  HGMDP.
          INTEGER I
          DIMENSION T( 4)
          T( 1) =    -.64135933E-01
          T( 2) =    -.17155672E 01
          T( 2) = T( 2) *  X 1 .P. ( -2)
          T( 3) =     .34417588E 00
          T( 3) = T( 3) * .ABS. X 7 .P. (  -.500000)
          T( 4) =     .74914879E 00
          T( 4) = T( 4) *  X 7 .P. ( -2)
          T(0) = 0.
          THROUGH SUM, FOR I = 1,1,I .G.  4
      SUM T(0) = T(0) + T(I)
          FUNCTION RETURN T(0)
          END OF FUNCTION

PROBLEM NO.     5 ... NORMAL TERMINATION



**** ALL INPUT DATA HAVE BEEN PROCESSED.
       AT LOCATION 10220
```

REFERENCES

1. Euler, Leonhard, "Theorie plus complete des machines qui sont mises mouvement par la reaction de l'eau" (More complete theory of machines driven by Hydraulic Reaction) Historie de l'Academie Royale, Berline, Germany, 1754.

2. Lord Rayleigh, "On the Pressure Developed in a Liquid During the Collapse of a Spherical Cavity," Phil. Mag. 34 (1917), 94-98.

3. Besant, W., A Treatise on Hydrodynamics, Cambridge University Press, Cambridge (1859), 198.

4. Barnaby, S. W., "On the Formation of Cavities in Water by Screw Propellers at High Speeds," Trans. Inst. Nav. Arch. 39 (1898), 139-144.

5. Parsons, Sir Charles, "The Application of the Compound Steam Turbine to the Purpose of Marine Propulsion," Trans. Inst. Nav. Arch. 38 (1897), 232-42.

6. Wagenbach, W., "Beitrage zur Berechnung und Konstrucktion der Wasserturbinen" (Contribution to the Calculation and Construction of Hydraulic Turbines), Zietschrift fur das Gesamte Turbinenwesen, Vol. 4, 1907, pp. 273-277.

7. Schroter, Hellmut, "Korrosion durch Kavitation in einen Diffusor" (Erosion by Cavitation in a Diffusor), Zietschrift Verein deutscher Ingenieure, Vol. 76, 1932, pp. 511-512.

8. Gaines, N., "A Magnetostriction Oscillator Producing Intense Audible Sound and Some Effects Obtained," Physics 3 (1932).

9. Kerr, S. L., "Determination of the Relative Resistance to Cavitation-Erosion by the Vibratory Method," Trans. ASME, Vol. 59, No. 4 (1937), 373-395.

10. Hobbs, J. M., "Problems of Predicting Cavitation Erosion from Accelerated Tests," ASME Paper No. 61-HYD-19 (1961).

11. Rasmussen, R. E. H., Trans. of the Danish Academy of Technical Science, No. 1, 1949.

12. Boetcher, H. N., "Die Zerstorung von Metallen durch Kavitation" (The Destruction of Metals through Cavitation), Zeitschrift Verein deutscher Ingenieure, Vol. 80, Dec. 12, 1936, pp. 1499-1503.

13. Mousson, J. M., "Pitting Resistance of Metals Under Cavitation Conditions," Trans. ASME, Vol. 59, 1937, pp. 399-408.

14. Knapp, R. T., and Hollander, A., "Laboratory Investigations of Mechanisms of Cavitation," Trans. ASME, Vol. 70, No. 5 (1948), 418-35.

15. DeHaller, P., and Ackeret, J., "Schweizer Archiv fur angewandte Wissenschaft und Technik, Solothurn, 1938, 4, 293.

16. Kornfeld, M., and Suvorov, L., "On the Destructive Action of Cavitation," J. of Applied Physics 15, No. 6 (1944), 495-96.

17. Naude, C. F., and Ellis, A. T., "On the Mechanism of Cavitation Damage by Hemispherical Cavities Collapsing in Contact with a Solid Boundary," Trans. ASME, J. Basic Engr., Series D., Vol. 83, No. 4, Dec., 1961.

18. Shuttler, N. D., and Messler, R. B., "A Photographic Study of the Dynamics and Damage Capabilities of Bubbles Collapsing Near Solid Boundaries," Trans. ASME, J. Basic Engr., Vol. 87, No. 2, June, 1965, 511-17.

19. Benjamin, T. B., and Ellis, A. T., "The Collapse of Cavitation Bubbles and the Pressures Thereby Produced Against Solid Boundaries," Paper presented at Royal Society Discussion, Deformation of Solids Due to Liquid Impact, London, May 27, 1965 (to be published in Proc. Roy. Soc.).

20. Stepanoff, A. J., Trans. ASME, Vol. 67 (1945), 539.

21. Beeching, R., "Resistance to Cavitation Erosion," Trans. Inst. Engr. and Shipbuilders in Scotland, Vol. 85 (1942), 210-76.

22. Richardson, E. G., Endeavor, Vol. 9, No. 35, July, 1950, 149.

23. Burrill, L. C., Trans. of the Inst. of Marine Engrs., Vol. 63, No. 8, 1951.

24. Knapp, R. T., "Recent Investigations of the Mechanisms of Cavitation and Cavitation Damage," Trans. ASME, Vol. 77, 1955, 1045-54.

25. Plessett, M. S., and Ellis, A. T., "On the Mechanism of Cavitation Damage," Trans. ASME, Vol. 77, No. 7, 1955, 1055-64.

26. Hammitt, F. G., et. al., "Initial Phases of Damage to Test Specimens in a Cavitating Venturi as Affected by Fluid and Material Properties and Degree of Cavitation," Trans. ASME, Vol. 87, No. 2, Series D, 1965, 453-464.

27. Petracchi, G., "Investigations of Cavitation Corrosion," La Metallurgia Italiana, Vol. 41, No. 1, 1949, 1-6. Engineering Digest, Vol. 10, No. 9, September, 1949, 314.

28. Eisenberg, P , "On the Mechanism and Prevention of Cavitation," DTMB Report No. 712, July, 1950.

29. McCrary, S. E., ASTM Bulletin No. 186, December, 1952 (TP188), 46.

30. Galtung, E , JASNE, Vol. 65, No. 2, 1953, 389.

31. Wheeler, W. H., "Indentation of Metals by Cavitation," Trans. ASME, J. Basic Engr. (March, 1960), 184-94.

32. Taylor, I., "Cavitation Pitting by Instantaneous Chemical Action from Impacts," ASME Paper No. 54-A-109.

33. Hammitt, F. G., "Cavitation Damage and Performance Research Facilities," ASME Fluids Engr. Conf., Philadelphia, Pa., May, 1964, Symposium on Cavitation Research Facilities and Techniques, 175-184.

34. Hammitt, F. G., "Observation of Cavitation Scale and Thermodynamic Effects in Stationary and Rotating Components," Trans. ASME, Series D, J. Basic Engr., Vol. 85, 1963, 1-16.

35. Ericson, D. M , Jr., "Cavitation Scale Effects Investigation," Ph.D Thesis, Department of Nuclear Engineering, University of Michigan (to be published).

36. Lichtman, J. Z., "Possible Contributions of Reentrant Flow to Cavitation Erosion," ASME Paper No. 62 HYD-3.

37. Hammitt, F. G., Robinson, M. J., Siebert, C. A., and Aydinmakine, F. A., "Cavitation Damage Correlations for Various Fluid-Material Combinations," Department of Nuclear Engineering, Laboratory for Fluid Flow and Heat Transport Phenomena, ORA Report 03424-14-T, University of Michigan.

38. Hammitt, F. G., Smith, W., Lauchlan, I. E. B., Ivany, R. D., and Robinson, M. J., "Void Fraction Measurements in a Cavitating Mercury Venturi," ANS Trans., Vol. 7, No. 1, 1964, 189.

39. Harrison, C. A., Robinson, M. J., Siebert, C. A., Hammitt, F. G., and Lawrence, J., "Complete Mechanical Properties Specifications for Materials as Used in Venturi Cavitation Damage Tests," Department of Nuclear Engineering, Laboratory for Fluid Flow and Heat Transport Phenomena, University of Michigan (to be published).

40. Hammitt, F. G., "Observations of Cavitation Damage in a Flowing System," Trans. ASME, J. Basic Engr., Vol. 85, Sept., 1963, 347-59.

41. Hickling, R., and Plesset, M. S., "Collapse and Rebound of a Spherical Bubble in Water," The Physics of Fluids, Vol. 7, No. 1, Jan., 1964, 7-14.

42. Ivany, R. D., "Collapse of a Cavitation Bubble in Viscous Compressible Liquid-Numerical and Experimental Analyses," Ph.D. Thesis, Department of Nuclear Engineering, University of Michigan, 1965.

43. Ivany, R. D., and Hammitt, F. G., "Cavitation Bubble Collapse in Viscous, Compressible Liquids-Numerical Analyses," Department of Nuclear Engineering, Laboratory for Fluid Flow and Heat Transport Phenomena, ORA Report 03424-24-I, University of Michigan, April, 1965.

44. Herring, C., Theory of the Pulsations of the Gas Bubble Produced by an Underwater Explosion, Report C4-sr20-010 (Columbia Univ., 1941), 67.

45. Cole, R. H., Underwater Explosions (Princeton Univ. Press, 1948).

46. Cramer, V. F., and Hammitt, F. G., "Cavitation Pit Diameter-Depth Observations for Stainless Steel in Water," Department of Nuclear Engineering, Laboratory for Fluid Flow and Heat Transport Phenomena, ORA Report 03424-9-I, University of Michigan, Aug., 1961.

47. Westervelt, F. H., "Automatic System Simulation Programming," Ph.D. Thesis, University of Michigan, November, 1960.

48. Kelley, R. W., Wood, G. M., Kulp, R. S., and Altieri, J. V., "Cavitation Damage of Mechanical Pump Impellers Operating in Liquid Metal Space Power Loops," CNLM-6101, prepared for NASA by Pratt & Whitney Aircraft Div., United Aircraft Corp., December 8, 1964.

49. Kelley, R. W., et. al., "Rotating Disc Approach for Cavitation Damage Studies in High Temperature Liquid Metal," ASME Paper No. 63-AHGT-26.

50. Hammitt, F. G., "Damage to Solids Caused by Cavitation," Paper presented at Royal Society Discussion, Deformation of Solids Due to Liquid Impact, London, May 27, 1965 (to be published in Proc. Roy. Soc.).

51. Engel, O. G., "Pits in Metals Caused by Collision with Liquid Drops and Soft Metal Spheres," J. of Res. of Nat. Bur. Stds., Vol. 62, No. 6, Research Paper No. 2958, June, 1959, 229-246.

52. Plesset, M. S., "Shock Waves from Cavitation Collapse," Paper presented at Royal Society Discussion, Deformation of Solids Due to Liquid Impact, London, May 27, 1965 (to be published in Proc. Roy. Soc.).

53. Plesset, M. S., "Pulsing Techniques for Studying Cavitation Erosion of Metals," Corrosion, May, 1962, 181-188.

54. DeCorso, S. M., "Erosion Tests of Steam Turbine Blade Materials," ASTM Proceedings, Am. Soc. Testing Mats., Vol. 64, pp. 782-796.